

AD-A062 163

GEORGIA INST OF TECH ATLANTA SCHOOL OF PHYSICS
CALCULATION OF ELECTRON IMPACT CROSS SECTIONS FROM METASTABLE S--ETC(U)
AUG 78 M R FLANNERY

F/G 7/4

F33615-74-C-4003

UNCLASSIFIED

1 OF 3
AD
A062163

ACADI -TD-7A-5A

NI



STEFEN

1 OF 3

AD
A062163



AD A062163

AFAPL-TR-78-58

② LEVEL II

CALCULATION OF ELECTRON IMPACT CROSS SECTIONS FROM METASTABLE STATES

M. RAYMOND FLANNERY
SCHOOL OF PHYSICS
GEORGIA INSTITUTE OF TECHNOLOGY
ATLANTA, GEORGIA 30332

AUGUST 1978



TECHNICAL REPORT AFAPL-TR-78-58
Final Technical Report for Period 8 October 1973 - 7 October 1977

Approved for public release; distribution unlimited.

AIR FORCE AERO PROPULSION LABORATORY
AIR FORCE WRIGHT AERONAUTICAL LABORATORIES
AIR FORCE SYSTEMS COMMAND
WRIGHT-PATTERSON AIR FORCE BASE, OHIO 45433

78 12 11 018

DDC FILE COPY

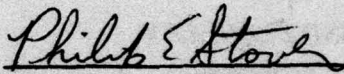
NOTICE

When Government drawings, specifications, or other data are used for any purpose other than in connection with a definitely related Government procurement operation, the United States Government thereby incurs no responsibility nor any obligation whatsoever; and the fact that the government may have formulated, furnished, or in any way supplied the said drawings, specifications, or other data, is not to be regarded by implication or otherwise as in any manner licensing the holder or any other person or corporation, or conveying any rights or permission to manufacture, use, or sell any patented invention that may in any way be related thereto.

This report has been reviewed by the Information Office (OI) and is releasable to the National Technical Information Service (NTIS). At NTIS, it will be available to the general public, including foreign nations.

This technical report has been reviewed and is approved for publication.


ALAN GARSCADDEN
Project Engineer


PHILIP E. STOVER
Chief, High Power Branch

FOR THE COMMANDER


JAMES D. REAMS
Chief, Aerospace Power Division

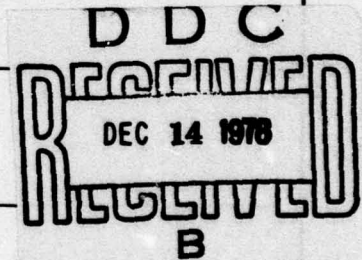
"If your address has changed, if you wish to be removed from our mailing list, or if the addressee is no longer employed by your organization please notify AFAPL/POD-2, W-PAFB, OH 45433 to help us maintain a current mailing list".

Copies of this report should not be returned unless return is required by security considerations, contractual obligations, or notice on a specific document.

Unclassified

SECURITY CLASSIFICATION OF THIS PAGE (When Data Entered)

REPORT DOCUMENTATION PAGE		READ INSTRUCTIONS BEFORE COMPLETING FORM
1. REPORT NUMBER AFAPL TR-78-58	2. GOVT ACCESSION NO.	3. RECIPIENT'S CATALOG NUMBER kept.
4. TITLE (and Subtitle) CALCULATION OF ELECTRON IMPACT CROSS SECTIONS FROM METASTABLE STATES,	5. TYPE OF REPORT & PERIOD COVERED Final 8 October 1973 - 7 October 1977	6. PERFORMING ORG. REPORT NUMBER
7. AUTHOR(s) M. Raymond Flannery	8. CONTRACT OR GRANT NUMBER(s) F-33615-74-C-4003 F-33615-76-C-2003	
9. PERFORMING ORGANIZATION NAME AND ADDRESS School of Physics Georgia Institute of Technology Atlanta, Georgia 30332	10. PROGRAM ELEMENT, PROJECT, TASK AREA & WORK UNIT NUMBERS 2301-52-15	
11. CONTROLLING OFFICE NAME AND ADDRESS Air Force Aero Propulsion Laboratory AFAPL/POD Wright Patterson Air Force Base, OH 45433	12. REPORT DATE August 1978	
14. MONITORING AGENCY NAME & ADDRESS (if different from Controlling Office) 216p.	13. NUMBER OF PAGES 208	
	15. SECURITY CLASS. (of this report) Unclassified	
16. DISTRIBUTION STATEMENT (of this Report) Approved for public release; distribution unlimited.		
17. DISTRIBUTION STATEMENT (of the abstract entered in Block 20, if different from Report)		
18. SUPPLEMENTARY NOTES		
19. KEY WORDS (Continue on reverse side if necessary and identify by block number) Cross sections, excited states, excitation, ionization, metastable rare gases, electron impact, Born, binary encounter multi-channel eikonal theory.		
20. ABSTRACT (Continue on reverse side if necessary and identify by block number) A multi-channel eikonal theoretical treatment of atomic collisions is developed with electron-metastable atom collisions in mind. The treatment is applied to electron-impact excitation of hydrogen and helium atoms in their ground state and of helium initially in its metastable level. Differential integral cross sections are calculated together with the orientation and alignment parameters. Cross sections for ionization of metastable rare-gas atoms and of metastable nitrogen and carbon monoxide molecules by collision with electrons are also calculated as a function of electron impact energy.		



DD FORM 1 JAN 73 1473 EDITION OF 1 NOV 65 IS OBSOLETE

Unclassified
SECURITY CLASSIFICATION OF THIS PAGE (When Data Entered)

404227

JB

PREFACE

This technical report was accomplished under Project 2301, Work Unit 2301-S2-15 "Calculation of Electron Impact Cross Sections from Metastable States in Atomic and Molecular Gases" by the School of Physics, Georgia Institute of Technology. The Air Force Project Monitor was Dr. Alan Garscadden. The research for this work was performed in the period March 1976 through March 1978.

ACCESSION for	
NTIS	White Section <input checked="" type="checkbox"/>
DDC	Buff Section <input type="checkbox"/>
UNANNOUNCED	<input type="checkbox"/>
JUSTIFICATION _____	
BY _____	
DISTRIBUTION/AVAILABILITY CODES	
Dist.	AVAIL. and/or SPECIAL
A	

TABLE OF CONTENTS

SECTION	PAGE
I. INTRODUCTION	1
II. SUMMARY OF WORK PERFORMED	4
2.1 e-He($2^1,3S$) Inelastic Collisions	4
2.2 e-H($1s$) and e-He(1^1S) Inelastic Collisions	4
2.3 e-He($2^1,3S$) Collisional Excitation and Ionization. Figures and Tables	6
2.4 e-Ne*, Ar*, Kr*, Xe* Ionization. Figures and Tables	7
2.5 General Trends	7
2.6 Other Related Work	7
2.7 Ph.D. Theses	8
III. EXCITATION IN ELECTRON-METASTABLE HELIUM COLLISIONS	9
IV. THE MULTICHANNEL EIKONAL TREATMENT OF ATOMIC AND MOLECULAR COLLISIONS	15
4.1 The Multistate Eikonal Treatment of Electron-Atom Collisions	16
4.2 e-H($1s$) Elastic and Inelastic Scattering	20
4.3 The 2^1S and 2^1P Inelastic Scattering of Electrons by Helium	34
4.4 A Pseudostate Multichannel Eikonal Study of e-H($1s$) Inelastic Collisions	43
4.5 A Ten-Channel Eikonal Treatment of Differential and Integral Cross Sections and of the (λ, χ) Parameters for the $n=2$ and 3 Excitations of Helium by Electron Impact	49
V. THE EXCITATION AND IONIZATION OF He($2^1,3S$) BY ELECTRON IMPACT	67
5.1 Ten-Channel Eikonal Treatment of Electron-Metastable Helium Collisions: Differential and Integral Cross Sections for $2^1,3P$ and $n=3$ Excitations from He($2^1,3S$) and the (λ, χ, Π) Parameters	68
5.2 Cross Sections for Excitation and Ionization in e-He($2^1,3$) Collisions	78
VI. CROSS SECTIONS FOR IONIZATION OF METASTABLE RARE-GAS ATOMS (Ne*, Ar*, Kr*, Xe*) AND OF METASTABLE N*, CD* MOLECULES BY ELECTRON IMPACT	93
VII. SYSTEMATIC TRENDS IN THE INELASTIC CROSS SECTIONS AND FROM FACTORS FOR $n'l \rightarrow n'l'$ DIRECT COLLISIONAL TRANSITIONS	104
VIII. FINAL RESULTS: TABLES AND FIGURES OF THE RELEVANT EXCITATION AND IONIZATION CROSS SECTIONS AS A FUNCTION OF IMPACT-ENERGY E	146

TABLE OF CONTENTS (cont'd)

SECTION	PAGE
IX. LIST OF REFEREED RESEARCH PUBLICATIONS RESULTING FROM THIS CONTRACT	166
X. PERSONNEL INVOLVED IN THE CONTRACT	168
XI. RELATED ADDITIONAL WORK PERFORMED UNDER PRESENT CONTRACT	169
<u>Appendix A:</u> A Theoretical Treatment of Atomic Collisions at Intermediate Energies and Highly Excited States	
<u>Appendix B:</u> New Semiclassical Treatments of Rotational and Vibrational Transitions in Heavy-Particle Collisions. I. H-H ₂ and He-H ₂ Collisions	
<u>Appendix C:</u> The Multichannel Eikonal Treatment of Electron-Atom Collisions	

SECTION I

INTRODUCTION

This report describes the development of new theoretical techniques and results obtained in the theoretical investigation of inelastic cross sections for electron-impact excitation and ionization of atoms and molecules initially in their metastable states. The research described here was conducted under the auspices of USAF contracts F33615-74-C-4003 and F33615-76-C-2003. The cross sections to be obtained as a result are of basic significance to kinetic modeling of rare gas-rare gas excimer and rare gas-halide laser systems.

The objectives of these contracts were (a) to assess the suitability of application of any present theoretical treatments of electron-atom scattering to atoms initially in excited states and then (b) to select one or more of these theories for calculation of the cross sections σ for excitation and ionization of metastable atoms (He^* , Ne^* , Ar^* , Kr^* and Xe^*) and molecules (N_2^* , CO^*) by collision with electrons as a function of impact-energy E . This latter step (b) also required the formulation of the selected theory or theories into computer codes which are suitable for CDC-6400 and CDC-6600 computers and which yield, as the end product, the required cross sections σ versus E . The computer programs are fully documented in an accompanying report entitled, "User's Manual."

EXCITATION: However, as the investigation progressed, it soon became apparent that there were not any available methods that were directly suitable for collisional excitation between excited states and that new theoretical treatments were required. The physics of this situation was carefully examined and this effort culminated in the development of a new theoretical method which we named, "The

multichannel eikonal treatment of electron-atom collisions," which was designed with excited states in mind, and which was directly applicable to excitation collisions between electrons and excited rare-gas atoms. The method has since met with considerable success and has received extremely favorable reviews in the scientific literature.

The method is fully described in Sections 4.1-4.5, is fully tested by comparison with other theoretical descriptions and experiments for collisions involving ground-state species in Sections 4.2-4.5 and Appendix C and is then applied to electron-metastable helium collisions in Section 5.1.

Various interesting trends emerged in this investigation, all of which are fully documented in this report. For example, contrary to expectation, the optically forbidden $2^{1,3}S \rightarrow 3^{1,3}D$ transitions in He^* , induced by electron-impact, are much more probable than the optically allowed $2^{1,3}S - 3^{1,3}P$ transitions, except, of course, in the limit of high impact energies when σ for the dipole transitions with their slower varying $E^{-1} \ln E$ dependence eventually dominate.

These unexpected trends were fully investigated and were found to be but particular cases of a more general trend underlying collisions involving atoms in excited states in general. This investigation culminated in new predictions for the preferential population of final states with angular momentum ℓ' in collisions involving atoms initially excited. We named this investigation, "Systematic trends in the inelastic cross sections and form factors for $n\ell \rightarrow n'\ell'$ direct collisional transitions," and is fully described in Section 7.

Here, certain theoretical predictions are presented for the preferential population of final states with angular momentum ℓ' in collisions

involving an atom initially excited. With variation of ℓ' , we find that the maxima of both the inelastic form factors and cross sections for the $n\ell \rightarrow n'\ell'$ transitions in hydrogen, induced by collision with electrons and heavy particles, in general oscillate on a background which rises as ℓ' is increased, until they both attain a pronounced peak at a unique value ℓ'_{\max} which is strongly dependent only on the initial principal quantum number n and which is fairly insensitive to changes in ℓ and n' . An expression for ℓ'_{\max} is derived. For $\ell' > \ell'_{\max}$, the form factors and associated cross sections exhibit a dramatic decline, resulting in negligible population of those states. The predictions differ from that suggested by the Bethe high-energy asymptotic-limit which favors dipole transitions, and assume significance in situations where excited states are important as in laser modeling, astrophysical and fusion plasmas, and in laboratory studies of excited Rydberg states. For heavy-particle ($n\ell \rightarrow n'\ell'$) collisional-transitions the additional undulations which appear in the cross sections over a wide energy-range are predicted and explained.

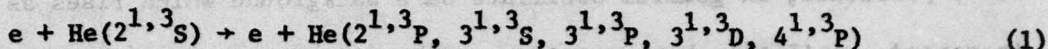
IONIZATION: The ionization by electron impact of rare gas atoms (He^* , Ne^* , Ar^* , Kr^* , Xe^*) initially in their metastable states is treated by the Born and by the binary encounter approximations, the only basic methods at present used for ionization cross sections. This work is fully documented in Sections 5.2 and 6 of this report.

The cross sections for excitation and ionization of He^* , Ne^* , Ar^* , Kr^* and Xe^* calculated in this report as a function of electron-impact energy E are quite basic and important to the kinetic modeling of both rare gas-rare gas excimer lasers and of rare gas-halide lasers.

SECTION II

SUMMARY OF WORK PERFORMED

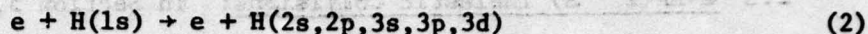
2.1 e-He($2^{1,3}S$) Collisions: In Section 3, the collision processes



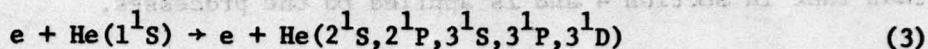
are examined as a function of impact energy E by application of both the Born and the various Vainshtein, Presnyakov and Sobel'man approximations where we find that excitation to the $3^{1,3}D$ and $3^{1,3}S$ states dominate the $3^{1,3}P$ and $4^{1,3}P$ excitations except at very high E . These results indicated that a much more elaborate theoretical treatment was required, a treatment which included couplings between excited states and which allowed in particular for the influence of the ($2^{1,3}S - 2^{1,3}P$) dipoles in the collision process.

2.2 e-H($1s$), e-He(1^1S) Collisions: In Section 4, the much more elaborate treatment called, "The multichannel eikonal treatment of atomic collisions," is proposed. Among its many advantages discussed fully, this description includes couplings in a very efficient way and convergence of cross sections in the impact-parameter representation is quickly achieved. These advantages are to be contrasted with the customary quantal close-coupling approximation which (a) becomes prohibitively difficult to apply with increase of impact-energy E and of number of atomic states being plagued with slow convergence and (b) has serious inherent problems associated with its application to electron-excited atom collisions.

In Section 4 the present method is fully tested by comparing the cross sections for the following processes involving ground-state atoms initially,



and



with available theoretical and experiment results. Not only do the integral cross sections σ demonstrate very good agreement but also we find that other more basic parameters to the collision physics such as the differential cross section $d\sigma/d\Omega$, and the λ and χ parameters as a function of scattering angle θ and impact energy E are well reproduced. These parameters are of more basic significance to the collision physics than is a knowledge of σ above. For example, for the 2^1P excitation in (3),

$$\lambda = \frac{|f_0|^2}{|f_0|^2 + |f_1|^2} \quad (4)$$

and

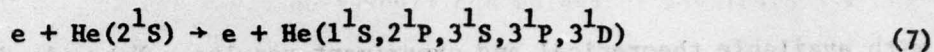
$$\chi = \alpha_1 - \alpha_2 \quad (5)$$

where

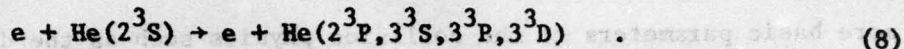
$$f_M = |f_M| \exp(i\alpha_M) \quad ; \quad M = 0, 1 \quad (6)$$

are the inelastic scattering amplitudes for excitation of the 2^1P_0 and $2^1P_{\pm 1}$ magnetic substates $M=0$ and ± 1 respectively. Thus (4) yields the relative population of the $M=0$ substate and (5) yields the difference in phases of the respective scattering amplitudes, both parameters λ and χ as functions of scattering angle θ and impact-energy E . These parameters therefore yield valuable insight to the polarization of the emitted radiation from the collisionally excited state.

2.3 e-He($2^{1,3}S$) Inelastic Collisions: In Section 5, the multichannel eikonal treatment is further discussed from a slightly different perspective than that in Section 4 and is applied to the processes,



and

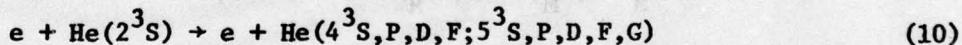


Excitation cross sections -- differential and integral -- and the λ and χ parameters are obtained. Here we also demonstrate that the method satisfies the principle of detailed balance, i.e., the rates for the forward $1^1S \rightarrow 2^1S$ and reverse $2^1S \rightarrow 1^1S$ transitions in e-He collisions satisfy

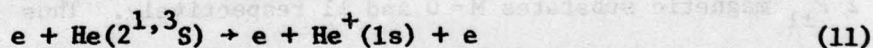
$$k_i^2 \sigma_{if}(k_i) = k_f^2 \sigma_{fi}(k_f) \quad (9)$$

where σ_{if} and σ_{fi} are the cross sections for the forward and reverse transitions, and where k_i and k_f are the wavenumbers of relative motion of the incident and scattered electron respectively.

Also in Section 5, the excitation and the ionization processes,



and



respectively are examined. Important conclusions are reached.

Tables and figures of the cross sections versus impact energy E for the above processes (7) - (11) are displayed in pages 157-159 of this report.

2.4 e-Ne*, Ar*, Kr*, Xe* Ionization: Cross sections for ionization of metastable rare-gas atoms (Ne*, Ar*, Kr*, Xe*) and of metastable N₂* and CO* by electron impact are obtained as a function of impact energy E and are displayed in tables and figures on pages 160-165 of this report.

2.5 General Trends: Section 7 contains a full discussion of, for example, the reasons that the cross section for $2^{1,3}S - 3^{1,3}D$ transitions dominate the $2^{1,3}S - 3^{1,3}P$ dipole transitions in e-He($2^{1,3}S$) collisions at low and intermediate impact-energies E. It is found that this behavior is but a particular case of a more general trend. Certain theoretical predictions are presented here for the preferential population of final states with angular momentum l' in collisions involving an atom initially excited. Not only does this section represent a very fitting conclusion to the work performed in the previous sections but also it points the way to a whole new arena of problems in atomic and molecular collisions of direct reference to feasibility studies of gas lasers and of laser fusion.

2.6 Other Related Work: Finally in Appendix A, another new theoretical description of transitions in electron-atom and heavy-particle collisions at intermediate energies is developed. In Appendix B, new semiclassical treatments of rotational and vibrational transitions in heavy particle collisions is proposed and applied to the rotational excitation of H₂(X¹Σ_g⁺, J) by H(1s) and by He(1¹S). In Appendix C, the multichannel eikonal treatment published in the book, "Electron and Photon Interactions with Atoms," edited by H. Kleinpoppen and M. R. C. McDowell is given.

2.7 Ph.D. Theses: As a result of the research reported here, two former graduate students, K. J. McCann and W. R. Morrison obtained their Ph.D. degrees awarded by Georgia Institute of Technology in 1975 and in 1978. Copies of their theses which served as partial fulfillment for the Ph.D. degrees have been presented separately as reports AFAPL-TR- and AFAPL-TR-78-57.

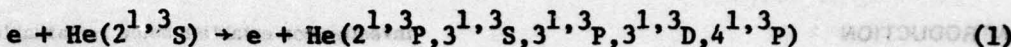
3.3 General Trends: Section 7 contains a full example, the reason that the cross section for $2^1S - 3^1D$ transitions dominates the $2^1S - 3^1P$ dipole transitions in e-He(2,3) collisions at low and intermediate impact energies. It is found that this behavior is but a particular case of a more general trend. Certain theoretical predictions are presented here for the preferential population of final states with angular momentum l in collisions involving an atom initially excited. Not only does this section represent a very fitting conclusion to the work performed in the previous sections but also it points the way to a whole new arena of problems in atomic and molecular collisions of direct relevance to feasibility studies of gas lasers and of laser fusion.

3.6 Other Related Work: Finally in Appendix A, another new theoretical description of transitions in electron-atom and heavy-particle collisions at intermediate energies is developed. In Appendix B, new semiclassical treatments of rotational and vibrational transitions in heavy particle collisions is proposed and applied to the rotational excitation of $H_2(X^1\Sigma_g^+, J)$ by $H(ein)$ and by $He(I, 2^1S)$. In Appendix C, the multichannel algebraic treatment published in the book, "Electron and Photon Interactions with Atoms," edited by H. Kleinpoppen and M. E. G. McDowell

is given.

EXCITATION IN ELECTRON-METASTABLE HELIUM COLLISIONS

In this section the Born and the Vainshtein, Presnyakov and Sobel'man approximations are applied to the theoretical investigation of the cross sections for the excitation processes



as a function of impact energy E. This work is published in Journal of

Applied Physics 46 (1975) 1186-1190 and a detailed account now follows.

3.1 Excitation in Electron-Metastable Helium Collisions:

Excitation in electron-metastable helium collisions*

M. R. Flannery, W. F. Morrison, and B. L. Richmond

School of Physics, Georgia Institute of Technology, Atlanta, Georgia 30332

(Received 14 October 1974)

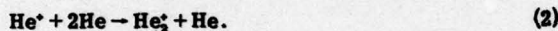
The 2^1P , 3^1S , 3^1P , 3^1D and 4^1P excitations arising from e -He(2^1S) collisions are examined by application of the Born and of the Vainshtein, Presnyakov, and Sobel'man approximations. Total excitation cross sections are calculated for the above transitions for electron impact energy E up to 500 eV. Contrary to expectation, excitation to the 3^1D and 3^1S states dominate the 3^1P and 4^1P excitations except at incident energies above 100 eV.

I. INTRODUCTION

While theoretical and experimental knowledge of collisions between electrons and ground-state atomic species has increased significantly during the past decade, relatively little¹ is known with any great certainty about collisions involving metastables. In a high-density gas discharge, metastable states are populated predominantly by dissociative recombination



between slow electrons and molecular ions formed initially by the rapid three-body association process



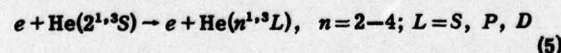
In (1), the excited levels with principal quantum number $n \geq 3$ (except, perhaps, the 3^1S states) are depleted by associative ionization (or the Hornbeck-Molnar process)



thereby ensuring that the 2^1S metastable states, which are also formed by direct electron-impact excitation from the ground state, are the dominant excited atomic species. The rates of the subsequent collision processes involving the metastables are very important to the analysis of gaseous discharges and gaseous nebulae² and are at present unknown. In vacuum uv-lasers, for example, excited molecular states He_2^* are formed mainly by



which radiate photons of wavelength $\sim 610 \text{ \AA}$ to the dissociative ground state, thereby ensuring automatic population inversion. The metastable He^* formed via (1) is primarily depleted by the excitation processes,



the cross sections for which would critically affect the over-all formation rate of He_2^* by (4). Any information on the above processes (5) is very scarce.

In an effort to systematically explore the various processes involving metastables, we will consider in this paper the excitation cross sections for (5) by using initially the simpler theoretical approaches—the Born¹ and the Vainshtein, Presnyakov, and Sobel'man (VPS) approximations.³ Various effects such as the repulsion between the incident and excited electrons, effective-charge, and electron-exchange effects are included to first order in the VPS method. Not only will this present

investigation establish some remarkable properties of the cross sections but also will provide the additional insight to the collision needed as a basis for more refined descriptions.

II. THEORY

According to the Born approximation¹ for electron-atom collisions, the total cross section for excitation of state n from an initial state i of the target atom is given by

$$Q_{in}(k_i) = \frac{8\pi}{k_i^2 a_0^2} \int_{k_i-k_n}^{k_i+k_n} |F_{in}(\mathbf{K})|^2 \frac{dK}{K^2} \quad (6)$$

in atomic units (a_0^2), where

$$F_{in}(\mathbf{K}) = \langle \phi_i(\mathbf{r}_1, \mathbf{r}_2) | \sum_{j=1}^2 \exp(i\mathbf{K} \cdot \mathbf{r}_j) | \phi_n(\mathbf{r}_1, \mathbf{r}_2) \rangle \quad (7)$$

is generalized form factor connecting states i and n of atomic helium, the bound electrons at \mathbf{r}_1 and \mathbf{r}_2 being described by the set of wave functions $\phi_n(\mathbf{r}_1, \mathbf{r}_2)$ with eigenenergies ϵ_n . The vector $\mathbf{K} = \mathbf{k}_i - \mathbf{k}_n$, where \mathbf{k}_i and \mathbf{k}_n are the initial and final wave numbers of relative motion, is the momentum change suffered by the collision. From a knowledge of the form factor (7), the excitation cross sections are easily calculated from (6).

In Born's approximation, however, and in more refined descriptions, e.g., the close-coupling method, the total wave function for the collision system is expanded in terms of unperturbed atomic states, the interaction between the incoming electron and the atom being treated as a perturbation, assumed small. In this instance, the averaged attraction of the incident electron with the screened nucleus is of primary importance, while details of repulsion with the atomic electrons is ignored in the wave function describing the relative motion. However, when an atom is initially in an excited state, the electron is generally quite distant from the core [for H(n), $\langle r_1 \rangle = n^2 a_0$; for He(2^1S), $\langle r_{12} \rangle = 5.3 a_0$] and hence, the incident electron is subjected not to the averaged field of the orbital electron about the core but actually to two strong Coulomb fields—the e - e repulsion and the e -core attraction. These two fields reduce to the averaged field only for distant encounters.

For electron-hydrogen scattering, Vainshtein *et al.*³ have introduced a method whereby a product of Coulombic functions is chosen to represent the zero-order (unperturbed) wave function for the e -H relative motion. The method achieved notable success for e -H ($1s$) excitation and ionization. The extension of their analysis to

e-He(2^1S) collisions is straightforward, and results in the cross section,

$$Q_{in} = \frac{8\pi}{k_1^2 a_0^2} \int_{k_1 - k_n}^{k_1 + k_n} |F_{in}(K)|^2 [f(\nu, x)]^2 \frac{dK}{K^2} \quad (8)$$

in which the integrand of (6) is multiplied by the square of the factor,

$$f(\nu, x) = \left(\frac{\pi\nu}{\sinh \pi\nu} \right) F(-i\nu, i\nu, 1, x), \quad (9)$$

where F is a hypergeometric function with arguments

$$x = \frac{2\epsilon_{n1} + K^2}{2\epsilon_{n1} + 3K^2}, \quad \nu = k_1^{-1} \text{ or } [k_1 + (2\epsilon_1)^{1/2}]^{-1} \quad (10)$$

in which $\epsilon_{n1} = \epsilon_n - \epsilon_1$ is the excitation energy in atomic units (27.2 eV) and where the second value of ν in (10) is designed to account for the fact that the atomic electrons are bound so as to give an effective-charge effect.

The effect of exchange between the incident and atomic electrons is ignored by (6) and (8). Its acknowledgment involves explicit inclusion of spin functions. For singlet-singlet transitions the over-all spin state for the (e-He) system is a doublet and the total wave function for the three electrons denoted by 1, 2, and 3 is, in a two-state treatment, given by,

$$\Psi^s(1, 2, 3) = (N_s/\sqrt{3}) \sum_{1,2,3}^{\text{cyclic}} [\Psi_1^s(1, 2)F_1(3) + \Psi_2^s(1, 2)F_2(3)] \chi^-(1, 2, 3) = \Psi_1 + \Psi_2, \quad (11)$$

where $F_n(3)$ is the wave function describing the projectile-target relative motion, where

$$\chi^-(1, 2, 3) = (1/\sqrt{2})(\alpha_1\beta_2 - \beta_1\alpha_2)\alpha_3, \quad (12)$$

is the normalized doublet spin function, and where $\Psi_1^s(1, 2) = \Psi_2^s(2, 1)$ is the symmetrical spatial wave function for singlet helium. The over-all wave function Ψ^s , normalized by N_s , is antisymmetric with respect to interchange of any two electrons. The Born approximation to the amplitude for scattering by angle θ is therefore

$$F_{in}(\theta) = -\frac{1}{4\pi} \frac{2me^2}{\hbar^2} \sum_{m_1, m_2} \sum_{m_3} \langle \Psi_n | V | \Psi_i \rangle_{\alpha_1, \alpha_2, \alpha_3}, \quad (13)$$

where $V(r_1, r_2, r_3)$ is the e-He electrostatic interaction and $F_i(\xi) = \exp(i\mathbf{k}_i \cdot \mathbf{r})$. On performing the cyclic summations in (11), on summing over the spin substates $m_s = \pm \frac{1}{2}$ in (13) and on using the orthonormal properties of the spin functions α_i and β_i , then, the scattering amplitude reduces, after some analysis, to

$$F_{in}^{ss}(\theta) = N_s^2(f_{in} - g_{in}), \quad (14)$$

where

$$f_{in}(\theta) = -\frac{1}{4\pi} \frac{2me^2}{\hbar^2} \langle \Psi_n^s(1, 2)F_n(3) | V | \Psi_i^s(1, 2)F_i(3) \rangle \quad (15)$$

is the scattering amplitude for direct collisions alone and

$$g_{in}(\theta) = -\frac{1}{4\pi} \frac{2me^2}{\hbar^2} \langle \Psi_n^s(3, 2)F_n(1) | V | \Psi_i^s(1, 2)F_i(3) \rangle \quad (16)$$

represents the scattering amplitude for exchange collisions

in which electrons 1 and 3 have been interchanged. By taking F_{in} to be a plane wave, then (14)–(16) gives rise to the Born-Oppenheimer approximation.¹ By taking F_n to be a plane wave and F_i to be a product of unperturbed Coulombic waves, then

$$g_{in}^{VPS} = (K^2/2k_1^2) f(\nu, \frac{1}{2}) f_{in}^s, \quad (17)$$

$$f_{in}^s = f_{in} \text{ with } F_{in} = \exp(i\mathbf{k}_{in} \cdot \mathbf{r}_3),$$

for the exchange amplitude can eventually be derived from application of the VPS approximation which also assumes $\langle \Psi_i | \Psi_n \rangle = \delta_{in}$ and hence $N_s = 1$ in (14). Then, the total cross section including exchange for singlet-singlet transitions is finally

$$Q_{in}^{1,1}(k_1) = \frac{2\pi k_n}{k_1} \int |F_{in}^{ss}(\theta)|^2 d(\cos \theta) \quad (18)$$

$$= \frac{8\pi}{k_1^2 a_0^2} \int_{k_1 - k_n}^{k_1 + k_n} \frac{|F_{in}(K)|^2}{K^2} \left(f(\nu, x) - \frac{K^2}{2k_1^2} f(\nu, \frac{1}{2}) \right)^2 dK.$$

For the triplet-triplet transitions in (5), the over-all antisymmetric spatial-spin state function can either belong to a doublet or as a quartet spin state. Scattering in the doublet mode occurs in one-third of all collisions while two-thirds of all collisions are in a quartet mode. The total wave function analogous to (11) is therefore

$$\Psi^T(1, 2, 3) = (N_T/\sqrt{3}) \sum_{1,2,3}^{\text{cyclic}} [\Psi_1^T(1, 2)F_1(3) + \Psi_2^T(1, 2)F_2(3)] \chi_{G,D}^+(1, 2, 3) = \Psi_1 + \Psi_2, \quad (19)$$

in which $\Psi_1^T(1, 2)$ is the antisymmetric spatial wave function for triplet helium and where the three-electron normalized spin functions are

$$\begin{aligned} \chi_G^+(1, 2, 3) &= \alpha_1\alpha_2\alpha_3, & M_s &= +\frac{3}{2} \\ \chi_D^+(1, 2, 3) &= (1/\sqrt{3})(\alpha_1\alpha_2\beta_3 + \alpha_1\beta_2\alpha_3 + \beta_1\alpha_2\alpha_3), & M_s &= +\frac{1}{2} \end{aligned} \quad (20a)$$

for the quartet spin state with total magnetic components $M_s = \frac{3}{2}$ and $\frac{1}{2}$, and

$$\chi_D^-(1, 2, 3) = (1/\sqrt{6})[2\alpha_1\alpha_2\beta_3 - \alpha_3(\alpha_1\beta_2 + \alpha_2\beta_1)], \quad M_s = +\frac{1}{2} \quad (20b)$$

represents the doublet state. The functions appropriate to states with negative magnetic quantum numbers are obtained from (12) and (20) by the $\alpha_i \rightarrow \beta_i$ interchange for each of the three electrons in the corresponding function for positive M_s .

By substituting (19) and (20) in (13) and by performing the cyclic summations, then after lengthy, although straightforward, analysis,

$$F_{in}^{TT}(D) = N_T(f_{in} + g_{in}) \quad (21a)$$

and

$$F_{in}^{TT}(Q) = N_T(f_{in} - 2g_{in}) \quad (21b)$$

are obtained for the scattering amplitudes in the doublet (D) and quartet (Q) modes, respectively. Since one-third and two-thirds of all collisions are in the D and Q

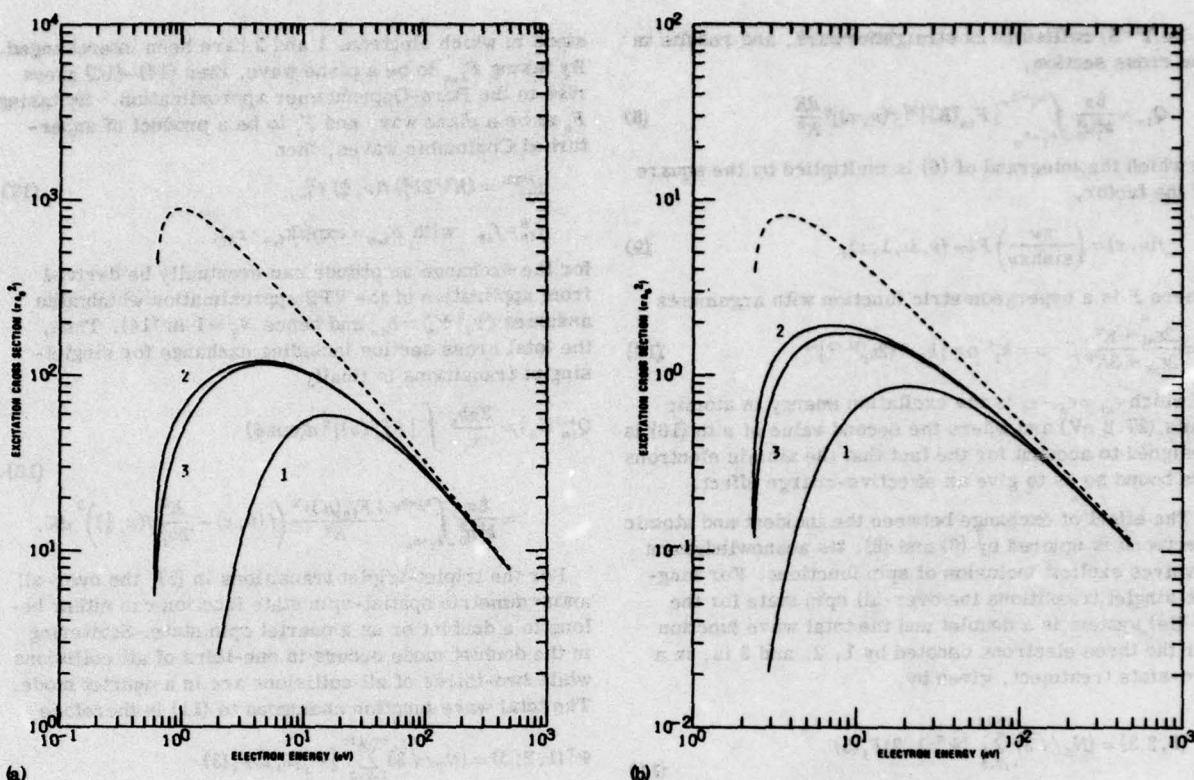


FIG. 1. (a) The 2^1P and (b) the 3^1S cross sections for excitation arising from $e\text{-He}(2^1S)$ collisions as a function of electron impact energy. Broken curve: Born approximation, (6) in text; solid curve: VPS approximation, 1, 2—(8)—(10) in text, with and without effective charge, 3—(18) with effective charge and exchange.

modes, respectively, then

$$|F_{in}^{TT}(\theta)|^2 = \frac{1}{3} |F_{in}^{TT}(D)|^2 + \frac{2}{3} |F_{in}^{TT}(Q)|^2 \quad (22a)$$

$$= |f_{in}|^2 - 2\text{Re}(f_{in}g_{in}^*) + 3|g_{in}|^2. \quad (22b)$$

Hence, the total excitation cross section for triplet-triplet transitions is then

$$Q_{in}^{3,3}(k_i) = 2\pi \frac{k_n}{k_i} \int |F_{in}^{TT}(\theta)|^2 d(\cos\theta) \quad (23a)$$

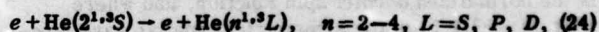
$$= \frac{8\pi}{k_i^2 \omega_0^2} \int \frac{|F_{in}(K)|^2}{K^2} \left([f(\nu, x)]^2 - \frac{K^2}{k_i^2} f(\nu, \frac{1}{2}) f(\nu, x) + \frac{K^4}{k_i^4} [f(\nu, \frac{1}{2})]^2 \right) dK \quad (23b)$$

on application of the VPS approximations (8) and (17) for f_{in} and g_{in} , respectively. Note that at high impact energies, the function $f(\nu, x) \rightarrow 1$ so that the Born and the Ochkur⁴ approximations are recovered for the direct and exchange scattering amplitudes, respectively. The Ochkur method is a simplification to the original Born-Oppenheimer approximation mentioned above and is therefore based on the use of plane waves for the relative motion.

III. RESULTS AND DISCUSSION

The theory outlined above has been applied to the

examination of the excitation processes,



for incident-electron energies E from threshold up to 500 eV. Highly accurate form factors (3) have already been computed by Kim and Inokuti⁵ from the extremely reliable correlated wave functions of Weiss.⁶ The following four sets of cross-section calculations were performed for each transition in (24)—the Born approximation B given by (6), and the three VPS approximations given by (8)—(10), with and without the effective charge, and by (18) and (23) which include the additional effect of electron exchange in singlet-singlet and triplet-triplet transitions, respectively.

In Figs. 1—4 are presented the Born and VPS cross sections (in $\omega_0^2 = 0.88 \times 10^{-16} \text{ cm}^2$) calculated to within 1% accuracy as a function of impact energy E (eV). The present Born values agree with those previously given by Kim and Inokuti⁵ for the $2^1S\text{-}2^1P$ and the triplet-triplet transitions. The optical line strengths S for the $2^1S\text{-}2^1P$ transitions are the largest (25.5 and 57.7 atomic units, respectively⁷) and hence it is only to be expected that the collision cross sections for these excitations dominate. However, Fig. 3 demonstrates a remarkable feature at low E when the collisional excitations are in the following descending order $3^1D > 3^1S > 3^1P > 4^1P$. At high $E > 100$ eV, the natural order $3^1P > 3^1D > 3^1S > 4^1P$ is followed when the cross sections

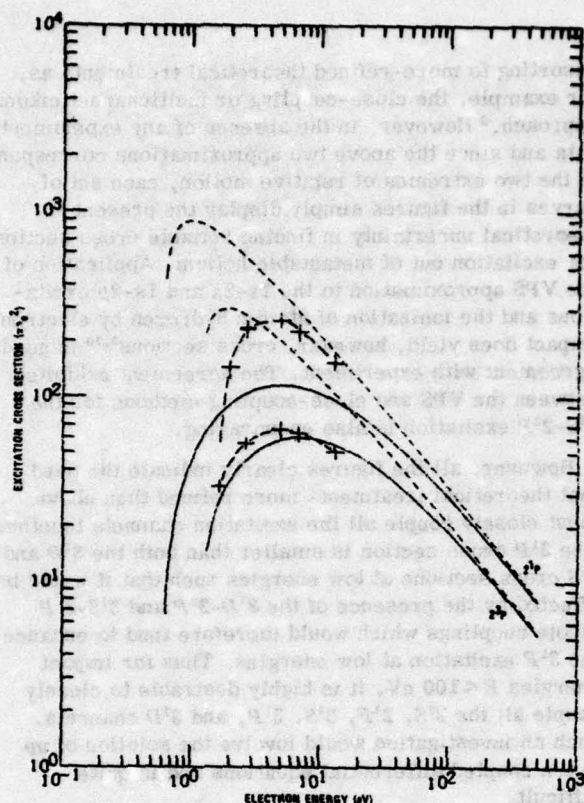


FIG. 2. The $2^{1,3}P$ cross sections for excitation arising from e -He($2^{1,3}S$) collisions. (---): Born approximation; (—): VPS approximation (3) with effective charge and exchange; (x): close-coupling results of Burke *et al.* (Ref. 8).

$\sim E^{-1} \ln E$ for the optically allowed transitions, and $\sim E^{-1}$ for the optically forbidden transitions. For the singlet transitions $\sigma(3^1S) > \sigma(3^1P)$ from threshold up to ~ 12 eV, while $\sigma(3^1D)$ remains greater than $\sigma(3^1P)$ up to 100 eV. Figure 4 demonstrates that similar behavior occurs also for the triplet transitions, the crossover point for the cross sections being shifted however to higher energies, i.e., $\sigma(3^3S) > \sigma(3^3P)$ for $E < 100$ eV and $\sigma(3^3D) > \sigma(3^3P)$ for $E < 1000$ eV.

The basic reason for this unexpected behavior is that the line strength for the $2^{1,3}S$ - $3^{1,3}P$ transitions in helium is abnormally small, i.e., 2.5 atomic units⁷ to be compared with the value⁷ 18.8 for the $2s$ - $3p$ transition in atomic hydrogen. The importance of the quadrupole and higher-order optically forbidden multipole terms relative to the optically allowed dipole term is therefore strong such that the optically forbidden collisional excitations dominate the optically allowed excitation at low and intermediate impact energies.

The effects acknowledged by the various VPS approximations are demonstrated in Fig. 1 for the 2^1P and the 3^1S excitations which were found to be representatives of the optically allowed and forbidden transitions in (24). The use, as in (8) with $\nu = k^{-1}$, of the zero-order Coulombic functions for the relative motion (instead of a plane wave) yields, in general, cross sections which

are lower than the Born values in the low- and intermediate-energy region and which eventually converge onto the correct Born limit at high energies. The optically allowed transitions are affected more by this inclusion than are the optically forbidden excitations. When the effective charge is acknowledged by the use of $\nu = [k_i + (2k_i)^{1/2}]^{-1}$ in (8) and (9), all the cross sections are significantly increased. The additional inclusion of exchange, as by (18) and (23), causes a relatively smaller decrease. The use of more-refined wave functions for the relative motion thus appears to be more important than the inclusion of exchange.

This claim is further supported in Fig. 2 by the close-coupling study of Burke *et al.*⁸ who included distortion and exchange effects in the solution near threshold of the equations¹ closely coupling all the $n=2$ states. The close-coupling results lie in general between Born and VPS treatments except at the lowest E . The agreement exhibited in Fig. 2 between the VPS and close-coupling approximations for the 2^3S - 2^3P is remarkable. The singlet excitation cross sections are, in general, greater than those for the triplet excitations.

In Figs. 3 and 4 are displayed the comparison of the Born cross sections with the VPS approximation (with effective charge and exchange) for the singlet-singlet and triplet-triplet transitions to the $n=3$ and 4 states. Convergence to the Born limit is attained at high energies. The dip in the Born 3^3P and 4^3P cross sections at

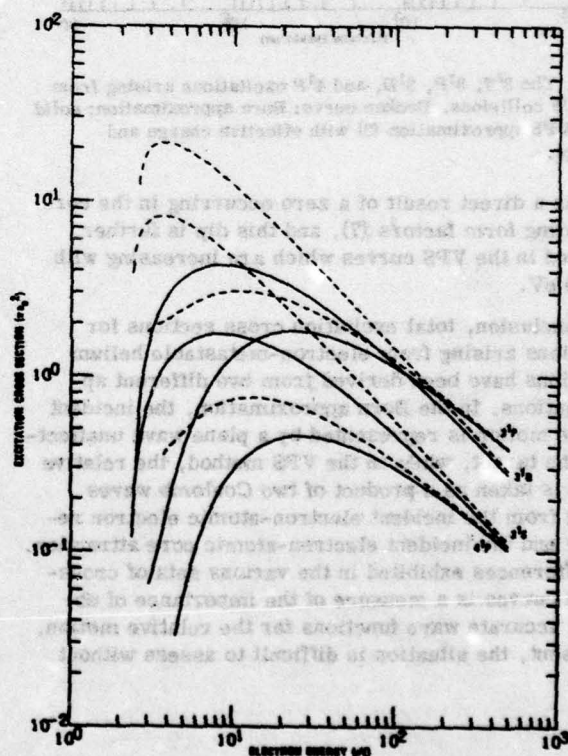


FIG. 3. The 3^1S , 3^1P , 3^1D , and 4^1P excitations arising from e -He(2^1S) collisions. Broken curve: Born approximation; solid curve: VPS approximation (3) with effective charge and exchange.

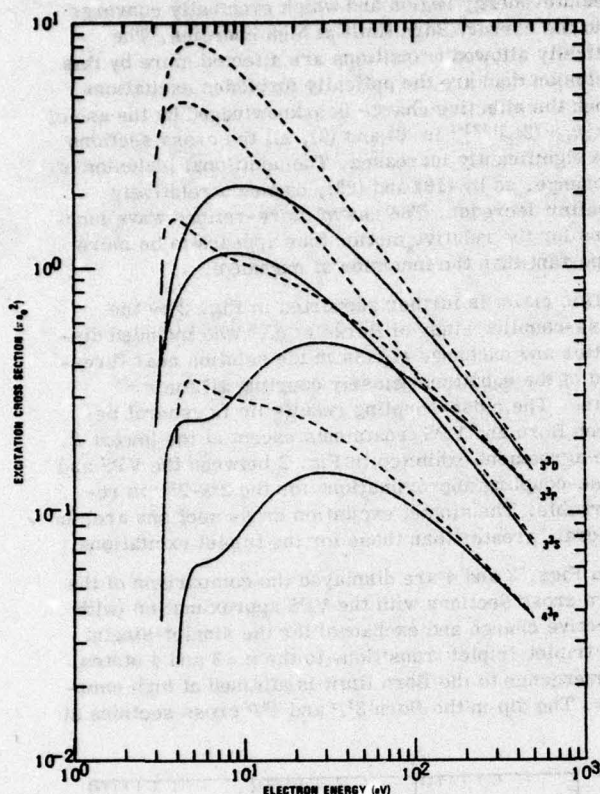


FIG. 4. The 3^3S , 3^3P , 3^3D , and 4^3P excitations arising from e -He(2^3S) collisions. Broken curve: Born approximation; solid curve: VPS approximation (3) with effective charge and exchange.

10 eV is a direct result of a zero occurring in the corresponding form factors (7), and this dip is further reflected in the VPS curves which are increasing with E at 10 eV.

In conclusion, total excitation cross sections for transitions arising from electron-metastable helium transitions have been derived from two different approximations. In the Born approximation, the incident relative motion is represented by a plane wave unaffected by the target, while in the VPS method, the relative motion is taken as a product of two Coulomb waves arising from the incident electron-atomic electron repulsion and the incident electron-atomic core attraction. The differences exhibited in the various sets of cross-section curves is a measure of the importance of obtaining accurate wave functions for the relative motion. At present, the situation is difficult to assess without

resorting to more-refined theoretical treatments as, for example, the close-coupling or multichannel eikonal approach.⁹ However, in the absence of any experimental data and since the above two approximations correspond to the two extremes of relative motion, each set of curves in the figures simply display the present theoretical uncertainty in finding reliable cross sections for excitation out of metastable helium. Application of the VPS approximation to the $1s$ - $2s$ and $1s$ - $2p$ excitations and the ionization of atomic hydrogen by electron impact does yield, however, cross sections^{3,10} in good agreement with experiment. The agreement exhibited between the VPS and close-coupling methods for the 2^3S - 2^3P excitation is also encouraging.

However, all the figures clearly indicate the need that theoretical treatments more refined than above must closely couple all the excitation channels together. The 3^1P cross section is smaller than both the 3^1D and 3^1S cross sections at low energies such that it would be affected by the presence of the 3^1D - 3^1P and 3^1S - 3^1P dipole couplings which would therefore tend to enhance the 3^1P excitation at low energies. Thus for impact energies $E < 100$ eV, it is highly desirable to closely couple all the 2^1S , 2^1P , 3^1S , 3^1P , and 3^1D channels. Such an investigation would involve the solution of up to ten coupled differential equations and is quite difficult.

*Research sponsored by the Air Force Aerospace Research Laboratories, Air Force Systems Command, United States Air Force, Contract F 33615-74-C-4003.

¹B. L. Molsetwitsch and S. J. Smith, *Rev. Mod. Phys.* **40**, 238 (1968).

²D. E. Osterbrock, *Ann. Rev. Astron. Astrophys.* **2**, 95 (1964).

³L. Vainshtein, L. Presnyakov, and I. Sobel'man, *Sov. Phys. Phys.-JETP* **18**, 1383 (1964).

⁴V. I. Ochkur, *Sov. Phys.-JETP* **18**, 503 (1964).

⁵Y.-K. Kim and M. Inokuti, *Phys. Rev.* **181**, 205 (1969). The authors wish to thank Dr. Y.-K. Kim for sending us detailed tables of the form factors which were only partially given in this reference.

⁶A. W. Weiss, *J. Res. Natl. Bur. Stand. (U.S.) A* **71**, 163 (1967).

⁷W. L. Wiese, M. W. Smith, and B. M. Glennon, *Atomic Transition Probabilities*, Natl. Bur. Stand. Publication No. NSRDS-NBS4 (U.S. GPO, Washington, D.C., 1966), Vol. 1.

⁸P. G. Burke, J. W. Cooper, and S. Ormonde, *Phys. Rev.* **183**, 245 (1969).

⁹M. R. Flannery and K. J. McCann, *Phys. Rev.* **10**, 2264 (1974).

¹⁰L. P. Presnyakov, *Sov. Phys.-JETP* **20**, 760 (1965).

SECTION IV

THE MULTICHANNEL EIKONAL TREATMENT OF ATOMIC AND MOLECULAR COLLISIONS

In the following subsections, 4.1-4.5, a new method entitled, "The multichannel eikonal treatment," is fully developed. This method was developed with electron-excited atom collisions in mind, an instance for which no realistic treatment was available. The method is formulated here and is fully tested via application to electron-ground-state-atom collisions, i.e., e-H(1s) and e-He(1¹S) collisions in particular. Accuracy of the treatment is assessed by comparison with previous experimental and theoretical data of the calculated (a) integral cross sections as a function of impact-energy E, (b) differential cross sections as a function of both scattering angle θ and E and (c) the very basic λ and χ parameters as a function of θ and E.

A complete description of all of the above work, which has also been published in:

- (1) J. Phys. B: Atom. Molec. Phys. 7 (1974) L223-L227
- (2) J. Phys. B: Atom. Molec. Phys. 7 (1974) 2518-2532
- (3) Phys. Rev. A 10 (1974) 2264-2272
- (4) J. Phys. B: Atom. Molec. Phys. 7 (1974) L522-L527
- (5) J. Phys. B: Atom. Molec. Phys. 8 (1975) 1716-1733

now follows.

4.1 The Multistate Eikonal Treatment of Electron-Atom Collisions

LETTER TO THE EDITOR

The multistate eikonal treatment of electron-atom collisions

M R Flannery and K J McCann

School of Physics, Georgia Institute of Technology, Atlanta, Georgia 30332, USA

Received 18 February 1974

Abstract. The basic equation for the scattering amplitude as determined from a multistate eikonal description of electron-atom collisions is presented. The relationship with other semiclassical treatments is examined. Four-state eikonal calculations of the cross sections for elastic and the 2s and 2p excitations of H(1s) by electrons with incident energy E in the range $13.6 \text{ eV} \leq E \leq 200 \text{ eV}$ are carried out, and are compared with other refined theoretical treatments and with experiment.

Recently, a variety of theoretical models have been proposed for elastic and inelastic electron-atom collisions at low and intermediate energies. These descriptions include the close-coupling expansion with its pseudo-state modifications (Burke and Webb 1970), a polarized orbital distorted-wave model of McDowell *et al* (1973), the Glauber approximation (Tai *et al* 1970), the impact-parameter approach (Bransden and Coleman 1972, Bransden *et al* 1972), the eikonal approximation of Byron (1971), and the distorted-wave eikonal theory of Chen *et al* (1972). The purpose of this letter is (a) to present a preliminary account of a new generalization of the eikonal method, (b) to illustrate its explicit relationship with other eikonal treatments and with the impact parameter approximation and (c) to present its comparison with experiment and various theories.

Flannery and McCann (1974, in preparation) have developed a multistate eikonal formulation of the stationary state description of a collision between an incident particle B with an atomic system (A + e). The treatment differs from previous approaches of Byron (1971) and of Bransden *et al* (1972) in that no additional assumptions, other than the eikonal approximation to the relative motion and a multistate expansion for the electronic motions, are made. Different speeds for various channels are acknowledged. The basic equation derived for the amplitude for scattering into $\hat{k}_f(\theta, \phi)$ about the incident Z-direction \hat{k}_i is, in the centre-of-mass frame,

$$f_{if}(\theta, \phi) = -\frac{1}{4\pi} \frac{2\mu}{\hbar^2} \int \exp(i\mathbf{K} \cdot \mathbf{R}) d\mathbf{R} \sum_n B_n(\rho, Z) V_{in}(R) \exp i(k_n - k_i)Z \quad (1)$$

where k_n is the wavenumber of relative motion in each channel n , $\mathbf{K} = \mathbf{k}_i - \mathbf{k}_f$ is the momentum change caused by the collision, and V_{in} is the interaction matrix element $\langle \phi_f(r) | \mathcal{V}(r, R) | \phi_n(r) \rangle$ where $\phi_n(r)$ are the eigenstates describing the isolated systems with reduced mass μ . The electrostatic interaction between the B and (A + e) systems at separation $\mathbf{R} \equiv (R, \Theta, \Phi) \equiv (\rho, \Phi, Z)$, in spherical and cylindrical coordinate frames respectively, is $\mathcal{V}(R, r)$. The coefficients B_n satisfy the set of coupled differential (phase Φ -dependent) equations,

$$\frac{i\hbar^2 k_f}{\mu} \frac{\partial B_f}{\partial Z} = \sum_{n=1}^N B_n(\rho, Z) V_{fn}(R) \exp i(k_n - k_f)Z \quad f = 1, 2, \dots, N \quad (2)$$

where N is the number of channels considered. It can be observed that (1), with $B_n = \delta_{ni}$ (where i is the initial state), reproduces the Born-wave amplitude. Also, after some algebraic manipulation, the distorted-wave Born formula of Chen *et al* (1972) is recovered from (1) and (2). Moreover, the expressions for the eikonal elastic scattering amplitude (cf Bransden 1970) follows by solving (2) with $B_n = B_i \delta_{ni}$ for B_i and by performing the Φ -integration in (1). The chief attributes of equations (1) and (2) above are that they account explicitly for different relative speeds in the various channels, and that they permit full inclusion of as many states (or pseudo-states) as desired. It is hoped that more complete details of the theory and its relationship with other theories will eventually be provided in a later paper.

The different exponents within the summation signs of (1) and (2) are significant. With the aid of (2), the scattering amplitude (1) reduces to

$$f_{if}(\theta, \phi) = -\frac{ik_f}{2\pi} \int \exp i[K \cdot R - (k_i - k_f)Z] \frac{\partial B_f(\rho, Z)}{\partial Z} dR. \quad (3)$$

Since \mathcal{V} is composed of central potentials, $V_{nm}(R) \equiv V_{nm}(R, \Theta) \exp(i\Delta\Phi)$ where $\Delta = M_m - M_n$, the integral change in the azimuthal quantum number M , and hence the substitution $C_n(\rho, Z) = B_n(\rho, Z) \exp(-i\Delta\Phi)$ yields a set of phase-independent equations for C_n similar to (2). The amplitude reduces on Φ -integration, to

$$f_{if}(\theta, \phi) = -ik_f i^\Delta \int_0^\infty J_\Delta(K'\rho) I(\rho, \theta) \rho d\rho \quad (4)$$

where K' is the XY -component $k_f \sin \theta$ of K , where J_Δ are Bessel functions of integral order Δ , and where the function

$$I(\rho, \theta) = \int_{-\infty}^{\infty} \exp(i\alpha Z) \frac{\partial C_f(\rho, Z)}{\partial Z} dZ \quad (5)$$

in which the difference between K_z , the Z -component of the momentum change at angle θ , and the minimum momentum change $(k_i - k_f)$ in the collision is

$$\alpha(\theta) = k_f(1 - \cos \theta). \quad (6)$$

We note, in the heavy-particle high-energy limit, when $\theta \approx 0$, that $\alpha \approx 0$ and hence

$$I(\rho, \theta) \approx I_A(\rho) = (C_f(\rho, \infty) - \delta_{if}). \quad (7)$$

Thus the eikonal approximation of Byron (1971) is reproduced from (3) with (7) together with the further assumptions that the quantities k_f , and $(k_i - k_f)$ appearing explicitly in (3) are taken as k_i , and ϵ_{fi}/v_i respectively. If, in addition $k_f \sin \theta$ is approximated by $k_i \sin \theta \approx 2k_i \sin \frac{1}{2}\theta$ for small θ and large k_f , then the scattering amplitude based on the impact parameter description of Bransden and colleagues is recovered.

As a test of the present full eikonal model, calculations based on (1)–(6) have been performed for the processes



in which the $1s, 2s, 2p_0, 2p_{\pm 1}$ states of atomic hydrogen are closely coupled. The total elastic and inelastic cross sections $Q(nl)$ computed by direct integration of $(k_f/k_i) |f_{if}(\theta, \phi)|^2$ over all solid angles are displayed in the table and compared with other refined theoretical calculations (Burke and Webb 1970, Sullivan *et al* 1972, McDowell *et al* 1973), and with experimental data (Long *et al* 1968, Kauppila *et al* 1970) in figures

Table 1. Elastic and inelastic cross sections $Q(nl)\pi a_0^2$ for the processes $e + H(1s) \rightarrow e + H(nl)$; $nl = 1s, 2s, 2p_{0,\pm 1}$, at electron energy E_i (eV)

E (eV)	$Q(1s)$	$Q(2s)$	$Q(2p_0)$	$Q(2p_{\pm 1})$	$Q(2p)$
13.6	0.988	0.143	0.140	0.077	0.217
20	0.703	0.131	0.319	0.297	0.616
30	0.522	0.113	0.362	0.441	0.803
50	0.332	0.085	0.347	0.514	0.861
100	0.202	0.050	0.191	0.439	0.630
200	0.125	0.028	0.118	0.335	0.453

1 and 2. Note that the 2^2S measurements include the cascade contribution $0.23 Q(3p)$ from the $3p$ level such that direct comparison is not possible until we perform similar multistate calculations for the $3p$ -excitation. Also, the experimental $2p$ -cross sections are normalized to our value of $0.453 \pi a_0^2$ at 200 eV instead of the corresponding Born value of $0.485 \pi a_0^2$, which is 7% higher.

The agreement for the $2p$ -excitation between the present treatment, the pseudo-state method and experiment is very good down to impact energies $E_i \sim 20$ eV, below which the effects of exchange and polarization distortion neglected in the present description, become important. Also shown are cross sections computed from the standard four-state impact parameter prescription. The comparison of these results with those labelled S of Sullivan *et al* (1972) is then a direct measure of the effect arising from their inclusion of second-order potentials.

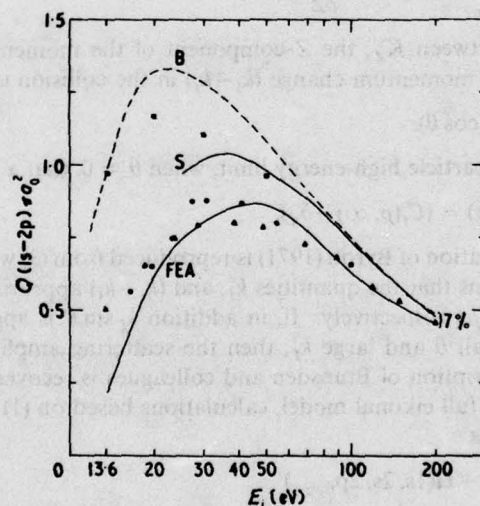


Figure 1. Total cross sections $Q(1s-2p)$ for $e + H(1s) \rightarrow e + H(2p)$ at electron energy E_i (eV). FEA four-state eikonal approximation (present treatment), \blacktriangle experiment (Long *et al* 1968), \bullet pseudo-state (Burke and Webb 1970), \square four-state impact-parameter treatment, S second-order potential method: four-channel approximation (Sullivan *et al* 1972), B Born approximation.

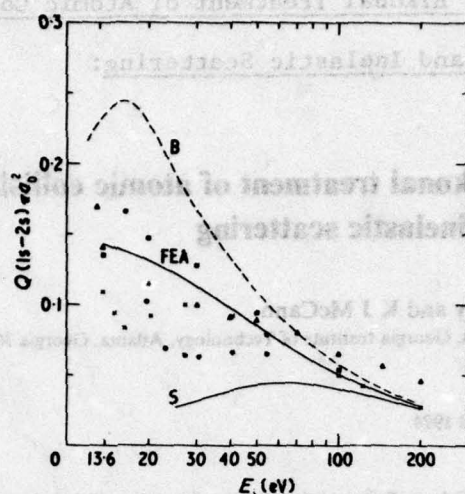


Figure 2. Total cross sections $Q(1s-2s)$ for $e+H(1s) \rightarrow e+H(2s)$ at electron energy E_i (eV). FEA four-state eikonal approximation (present treatment), ● pseudo-state (Burke and Webb 1970), x polarized-orbital distorted wave model (McDowell *et al* 1973), □ four-state impact-parameter treatment, S second-order potential method: four-channel approximation (Sullivan *et al* 1972), B Born approximation, ▲ $Q(1s-2s) + 0.23Q(1s-3p)$: experiment Kauppila *et al* 1970).

For the 2s-excitation, the agreement between the present results and the recent polarized-orbital distorted wave model of McDowell *et al* (1973) is encouraging. All the theoretical results show different variations with impact energy E_i below 40 eV. The experimental situation is somewhat obscured by the difficulty in obtaining direct account of the contributions arising from cascade, mainly from the 3p level. The large difference between the impact parameter cross sections indicates the sensitivity of the 2s-cross section to modification.

Finally, since the main object of this letter is to present the basic outline of the new treatment and to give some preliminary indication as to its success, it is our intention to eventually furnish a more complete theoretical description and a more detailed comparison (including differential cross sections, in particular) with other theoretical models.

Acknowledgment

This research was sponsored by the Air Force Aerospace Research Laboratories, Air Force Systems Command, United States Air Force, Contract F 33615-74-C-4003.

References

- Bransden B H 1970 *Atomic Collisions Theory* (New York: Benjamin) p 82
- Bransden B H and Coleman J P 1972 *J. Phys. B: Atom. molec. Phys.* 5 537-45
- Bransden B H, Coleman J P and Sullivan J 1972 *J. Phys. B: Atom. molec. Phys.* 5 546-58
- Burke P G and Webb T G 1970 *J. Phys. B: Atom. molec. Phys.* 3 L131-4
- Byron F W 1971 *Phys. Rev.* 4 1907-17
- Chen J C Y, Joachain C J and Watson K M 1972 *Phys. Rev.* 5 2460-74
- Kauppila W E, Ott W R and Fite W L 1970 *Phys. Rev.* 141 1099-108
- Long R L, Cox D M and Smith S J 1968 *J. Res. Nat. Bur. Standards* 72 A 521-35
- McDowell M R C, Morgan L A and Myerscough V P 1973 *J. Phys. B: Atom. molec. Phys.* 6 1435-51
- Sullivan J, Coleman J P and Bransden B H 1972 *J. Phys. B: Atom. molec. Phys.* 5 2061-5
- Tai H, Bassel R H, Gerjuoy E and Franco V 1970 *Phys. Rev. A* 1 1819-39

4.2 The Multichannel Eikonal Treatment of Atomic Collisions:

e-H(1s) Elastic and Inelastic Scattering:

The multichannel eikonal treatment of atomic collisions: e-H(1s) elastic and inelastic scattering

M R Flannery and K J McCann

School of Physics, Georgia Institute of Technology, Atlanta, Georgia 30332, USA

Received 22 April 1974

Abstract. A multichannel eikonal description of atomic collisions is presented. The basic formula for the scattering amplitude reduces upon successive approximation to expressions previously derived. In particular, the equations, in the heavy-particle or high-energy limit reduce to the standard impact parameter formulae. A four-state treatment of e-H(1s) elastic and 2s and 2p inelastic scattering is carried out. The calculated cross sections, which illustrate the effects of various approximations, compare very favourably with other refined theoretical methods and with experiment.

1. Introduction

A variety of methods have been proposed for the theoretical description of e-atom collisions at low and intermediate energies. The close coupling expansion with its pseudo-state modifications (Burke and Webb 1970), and the polarized orbital distorted wave model of McDowell *et al* (1973) are among those that follow from the full wave treatment of the collision. Other methods, termed as semiclassical—the eikonal approximations of Byron (1971) and of Chen *et al* (1972), the impact parameter approach (Bransden and Coleman 1972) and the Glauber approximation (cf Tai *et al* 1970)—all essentially separate the relative motion of the incident electron (described by an eikonal-type or Born wavefunction for the electron in a static field) from the internal electronic motions of the atomic system which is described by a multistate expansion.

These semiclassical methods are all amenable to systematic improvement at little extra cost eg additional atomic states, electron-exchange, and polarization effects can be suitably incorporated into the treatment. Moreover, their application to collisions with complex atoms is without the almost insurmountable hurdles associated with the application of the full wave treatment to non-hydrogenic systems. In particular, e-excited atom collisions—important to analysis of gaseous discharges, laser development and astrophysical problems—can be treated with relative ease by these semiclassical methods. It is therefore highly desirable to investigate these methods in greater detail and to propose possible improvements.

In this paper, a new generalization of the eikonal approach to atomic collisions is presented. It accounts explicitly for the changes in speed associated with the various channels and for other effects not acknowledged by the previous semiclassical descriptions. Its relationship with the former treatments is discussed and its overall reliability is assessed by comparing the calculated differential and total cross sections for

e-H(1s) elastic and inelastic collisions with other refined treatments and with experiment. A preliminary account of this generalization has already been presented (Flannery and McCann 1974a).

2. Theory

Consider the collision of a particle B of mass M_B and incident velocity v_i along the Z-axis with a one-electron atomic system (A + e) of mass $(M_A + m)$. The subsequent analysis can be immediately generalized so as to cover multi-electron systems. Let R, R_B, r and r_a denote the A-B, B-(Ae) centre of mass, e-(AB) centre of mass and e-A separations, respectively. In the (ABe) centre-of-mass reference frame, the scattering amplitude for direct transition between an initial state i and a final state f of the collision system, of reduced mass μ , is

$$f_{if}(\theta, \phi) = -\frac{1}{4\pi} \frac{2\mu}{\hbar^2} \langle \Psi_f(k_f; r, R) | V(r, R) | \Psi_i^+(k_i; r, R) \rangle_{r, R} \quad (1)$$

in which $V(r, R)$ is the instantaneous electrostatic interaction between the collision species, and where the scattering is directed along the final relative momentum $\hbar k_f(l, \theta, \phi)$. The final stationary state of the isolated atoms in channel f is Ψ_f , and Ψ_i^+ is the solution of the time independent Schrödinger equation,

$$\left[-\frac{\hbar^2}{2\mu} \nabla_R^2 + H_e(r) + V(r, R) \right] \Psi_i^+(r, R) = E_i \Psi_i^+(r, R) \quad (2)$$

solved subject to the asymptotic boundary condition,

$$\Psi_i^+(r, R) \xrightarrow{\text{large } R} \sum_n \left[e^{ik_n R_B} \delta_{ni} + f_{in}(\theta, \phi) \frac{e^{ik_n R_B}}{R_B} \right] \phi_n(r_a) \quad (3)$$

in which $\phi_n(r_a)$ are eigenfunctions of the Hamiltonian $H_e(r) \approx H_e(r_a)$ for the isolated atomic system (A + e) with internal electronic energy ϵ_n such that the total energy E_i in channel i is $\epsilon_i + \hbar^2 k_i^2 / 2\mu$ which is conserved throughout the collision.

2.1. The multichannel eikonal approximation

The eikonal approximation to (2) sets

$$\Psi_i^+(r, R) = \sum_n A_n(\rho, Z) \exp iS_n(\rho, Z) \chi_n(r, R) \quad (4)$$

where the nuclear separation $R \equiv (R, \Theta, \Phi) \equiv (\rho, \Phi, Z)$ in spherical and cylindrical coordinate frames respectively. The eikonal S_n in (4) is the characteristic-function solution of the classical Hamilton-Jacobi equation (ie the Schrödinger equation in the $\hbar \rightarrow 0$ limit) for the A-B relative motion under the static interaction $V_{nn}(R)$, and is therefore given by

$$S_n(\rho, Z) = k_n Z + \int_{-\infty}^Z [\kappa_n(R) - k_n] dZ \quad (5)$$

in which the local wavenumber of relative motion at R is

$$\kappa_n(R) = \left[k_n^2 - \frac{2\mu}{\hbar^2} V_{nn}(R) \right]^{1/2} \quad (6)$$

and where dZ is an element of path length along the trajectory which, at present, is taken as a straight line. For electron-atom collisions, κ_n in (6) is always real. The use of the actual classical trajectory with its 'built-in' turning point is therefore not as essential as in, for example, positron-atom collisions when κ_n becomes imaginary for sufficiently close rectilinear encounters. The general problems associated with the choice of classical trajectory within a multichannel framework are at present unresolved, although the forced-common turning-point, two-state procedure of Bates and Crothers (1970) is attractive.

The interaction matrix elements

$$V_{nm}(R) = \langle \chi_n(r, R) | V(r, R) | \chi_m(r, R) \rangle \quad (7)$$

connect the various electronic states

$$\chi_n(r, R) = \phi_n(r_a) \exp(ik_n \cdot r) \quad l = \frac{mM_{AB}}{M_A} \quad (8)$$

in which the phase factor which ensures satisfaction of the boundary condition (3) describes the translational motion of the electron relative to the (A-B) centre of mass, and is unimportant to the present development only when rearrangement channels are neglected. Moreover the eikonal (5) ensures that Ψ_i^+ contains, in addition to the incident wave, outgoing scattered waves which differ from the undistorted Born wave, $\exp(ik_n Z)$ by the following amount of phase-distortion,

$$\Phi_n(\rho, Z) \equiv \int_{-\infty}^Z (\kappa_n - k_n) dZ$$

which vanishes outside a cylinder, with axis along the Z direction, with infinite length and with diameter corresponding to the range R_n of the static interaction $V_{nn}(R)$. Thus, at impacts less than the interaction-range, distortion to the incident plane-wave relative motion does occur, thereby causing actual scattering. Applicability of (5) is therefore not confined to small angle scattering alone, although a straight-line element dZ is normally taken in (5). On assuming that the main variation of Ψ_i^+ on ρ is contained in S_n , ie provided $V_{nn}(R)$ varies slowly over many wavelengths $2\pi/\kappa(R)$ of relative motion, and the coefficients $A_n(\rho, Z)$ therefore vary primarily along Z , then substitution of (4) in (2) yields the set of coupled differential equations,

$$\frac{i\hbar^2}{\mu} \kappa_f \frac{\partial A_f(\rho, Z)}{\partial Z} = \sum_{n=1}^N A_n(\rho, Z) V_{fn}(R) \exp i(S_n - S_f) \quad f = 1, 2, \dots, N \quad (9)$$

where N is the number of channels adopted in the expansion (4). The phase substitution

$$B_f(\rho, Z) = A_f(\rho, Z) \exp i \int_{-\infty}^Z (\kappa_f - k_f) dZ \equiv A_f(\rho, Z) \exp i\Phi_f(\rho, Z) \quad (10)$$

with the aid of (6), reduces (9) to

$$\begin{aligned} \frac{i\hbar^2}{\mu} \kappa_f \frac{\partial B_f(\rho, Z)}{\partial Z} + \left[\frac{\hbar^2}{\mu} \kappa_f (\kappa_f - k_f) + V_{ff}(R) \right] B_f(\rho, Z) \\ = \sum_{n=1}^N B_n(\rho, Z) V_{fn}(R) \exp i(k_n - k_f)Z \quad f = 1, 2, \dots, N \end{aligned} \quad (11)$$

a set of N coupled equations to be solved subject to the asymptotic condition

$B_f(\rho, -\infty) = \delta_{fi}$, which ensures that $\Psi_i \sim \phi_i(r_a) \exp(ik_i Z)$ as $Z \rightarrow -\infty$. The scattering amplitude (1) with the undistorted final wave $\Psi_f = \phi_f(r_a) \exp(ik_f \cdot R)$ inserted, is therefore,

$$f_U(\theta, \phi) = -\frac{1}{4\pi} \frac{2\mu}{\hbar^2} \int \exp(i\mathbf{K} \cdot \mathbf{R}) d\mathbf{R} \sum_{n=1}^N B_n(\rho, Z) V_{fn}(\mathbf{R}) \exp i(k_n - k_i)Z \quad (12)$$

where \mathbf{K} is the momentum change $k_i - k_f$ caused by the collision. Since the electrostatic interaction $V(r, \mathbf{R})$ is composed of central potentials, $V_{fn}(\mathbf{R}) = V_{fn}(R, \Theta) \exp i\Delta\Phi$, where $\Delta = M_i - M_f$ is the change in the azimuthal quantum number of the atom. Hence the substitution

$$C_f(\rho, Z) = B_f(\rho, Z) \exp(-i\Delta\Phi) \quad (13)$$

yields the set of phase Φ -independent equations

$$\begin{aligned} \frac{i\hbar^2}{\mu} \kappa_f(\rho, Z) \frac{\partial C_f(\rho, Z)}{\partial Z} + \left[\frac{\hbar^2}{\mu} \kappa_f(\kappa_f - k_f) + V_{ff}(\rho, Z) \right] C_f(\rho, Z) \\ = \sum_{n=1}^N C_n(\rho, Z) V_{fn}(\rho, Z) \exp i(k_n - k_f)Z \end{aligned} \quad (14)$$

solved subject to the boundary condition $C_f(\rho, -\infty) = \delta_{fi}$. On completion of the Φ -integration in (12), the scattering amplitude reduces to

$$f_U(\theta, \phi) = -i^{\Delta+1} \int_0^\infty J_\Delta(K'\rho) [I_1(\rho, \theta) - iI_2(\rho, \theta)] \rho d\rho \quad (15)$$

where K' is the XY -component $k_f \sin \theta$ of \mathbf{K} and where J_Δ are Bessel functions of integral order. Both the functions

$$I_1(\rho, \theta; \alpha) = \int_{-\infty}^\infty \kappa_f(\rho, Z) \left[\frac{\partial C_f(\rho, Z)}{\partial Z} \right] \exp(i\alpha Z) dZ \quad (16)$$

and

$$I_2(\rho, \theta; \alpha) = \int_{-\infty}^\infty \left[\kappa_f(\kappa_f - k_f) + \frac{\mu}{\hbar^2} V_{ff} \right] C_f(\rho, Z) \exp(i\alpha Z) dZ \quad (17)$$

contain a dependence on the scattering angle θ via

$$\alpha = k_f(1 - \cos \theta) = 2k_f \sin^2 \frac{\theta}{2} \quad (18)$$

the difference between the Z -component of the momentum change \mathbf{K} and the minimum momentum change $k_i - k_f$ in the collision. Equations (14)–(18) are the basic formulae given by the present treatment representing the full multistate eikonal description for the scattering amplitude, and can be easily generalized so as to cover collisions involving multielectron systems. It is apparent that a variety of approximations readily follow. Note that in the absence of all couplings except that connecting the initial and final channels ie $C_n = \delta_{ni}$, then either (12) or (15) directly yields,

$$f_U(\theta, \phi) = -\frac{1}{4\pi} \frac{2\mu}{\hbar^2} \int V_{fi}(\mathbf{R}) \exp(i\mathbf{K} \cdot \mathbf{R}) d\mathbf{R} \quad (19)$$

which is the Born-wave scattering amplitude.

2.2. Approximations to the full multistate eikonal equations

(i) The first multistate approximation A to the above treatment follows by expanding κ_f in (17) as

$$\kappa_f(R) \approx k_f - \frac{\mu}{\hbar^2 k_f} V_{ff}(R) \quad (20)$$

valid for kinetic energies $\hbar^2 k_f^2 / 2\mu \gg V_{ff}$. Thus, with (6) for κ_f^2 and (20) for κ_f , both I_2 and the term within square brackets on the LHS of (14) vanish identically so that the scattering amplitude given by approximation A is

$$f_{if}^A(\theta, \Phi) = -\frac{1}{4\pi} \frac{2\mu}{\hbar^2} \int \exp[i(\mathbf{K} \cdot \mathbf{R} + \Delta\Phi)] d\mathbf{R} \sum_{n=1}^N C_n^A(\rho, Z) V_{fn}(R, \Theta) \exp i(k_n - k_i)Z \quad (21a)$$

$$= -i^{A+1} \int_0^\infty J_A(K'\rho) \rho d\rho \int_{-\infty}^\infty \kappa_f \left(\frac{\partial C_f^A}{\partial Z} \right) \exp(i\alpha Z) dZ \quad (21b)$$

where

$$\frac{i\hbar^2}{\mu} \kappa_f \frac{\partial C_f^A}{\partial Z} = \sum_{n=1}^N C_n^A(\rho, Z) V_{fn}(\rho, Z) \exp i(k_n - k_f)Z. \quad (22)$$

(ii) A related multistate approximation B involves setting all the local wavenumbers κ_n in A, ie in (21b) and (22), equal to their asymptotic values k_n . Both approximations A and B yield the Born-wave elastic and inelastic scattering amplitudes when $C_n^A = \delta_{in}$ is substituted in (21a). When the effect of all inelastic channels is neglected, ie when $C_n^B = C_i^B \delta_{in}$ in (22) with $\kappa_f = k_f$, then

$$C_i^B(\rho, Z) = \exp \left[-\frac{i}{\hbar v_i} \int_{-\infty}^Z V_{ii}(\rho, Z') dZ' \right]. \quad (23)$$

On performing the integrations in (21a) with (23), we find that the corresponding elastic scattering amplitude reduces to

$$f_{ii}^B(\theta, \phi) = -ik_i \int_0^\infty J_0 \left(2k_i \rho \sin \frac{\theta}{2} \right) [\exp 2i\chi(\rho) - 1] \rho d\rho \quad (24)$$

where the eikonal

$$\chi(\rho) = -\frac{1}{\hbar v_i} \int_0^\infty V_{ii}[(\rho^2 + Z^2)^{1/2}] dZ. \quad (25)$$

This is just the customary eikonal expression for elastic scattering (cf Glauber 1959, Bransden 1970) by a fixed potential.

In particular when the full wavefunction (4) is projected onto the distorted wave

$$\Psi_f(r, R) = \phi_f(r_s) \exp i \left(k_f \cdot R - \frac{1}{\hbar v_f} \int_{+\infty}^Z V_{ff} dZ \right) \quad (26)$$

for the final state, rather than onto the undistorted wave $\phi_f(r_s) \exp(i\mathbf{k}_f \cdot \mathbf{R})$, as previously used in equation (12), then the preceding analysis follows through with the result,

$$f_{if}^{BW}(\theta, \phi) = -i^{A+1} \int_0^\infty J_A(K'\rho) \rho d\rho \int_{-\infty}^\infty k_f \left(\frac{\partial C_f^B}{\partial Z} \right) \exp i \left(\alpha Z + \frac{1}{\hbar v_f} \int_{-\infty}^Z V_{ff} dZ' \right) dZ \quad (27)$$

where, in approximation B, C_f^B satisfies (22) with $\kappa_f = k_f$. Setting $C_n^B = C_1^B \delta_{in}$ in (22) then, with the aid of (23), the scattering amplitude (27) reduces to

$$f_{if}^{DWB}(\theta, \phi) = -\frac{i^A \mu}{\hbar^2} \int_0^\infty J_\Delta(k_f \rho \sin \theta) \rho \, d\rho \int_{-\infty}^\infty V_f(\rho, Z) \times \exp i[(k_i - k_f) + \alpha]Z + \delta\Phi(Z) \, dZ \quad (28)$$

where

$$\delta\Phi(Z) = -\frac{1}{\hbar v_i} \int_{-\infty}^Z V_{ii} \, dZ - \frac{1}{\hbar v_f} \int_Z^\infty V_{ff} \, dZ. \quad (29)$$

Equation (28) is the distorted-wave Born approximation which is identical to that derived by Chen *et al* (1972) from a different approach.

(iii) In the heavy-particle or high-energy limit, the asymptotic wavenumbers in approximation B tend to

$$k_f = k_i - \frac{\epsilon_{fi}}{\hbar v_i} \left(1 + \frac{\epsilon_{fi}}{2\mu v_i^2} + \dots \right) \quad \epsilon_{fi} = \epsilon_f - \epsilon_i \quad (30)$$

and a third approximation C(α) follows by setting all the individual k_n in approximation B equal to k_i , and any difference $k_n - k_f = \epsilon_{fn}/\hbar v_i$. Hence

$$f_{if}^C(\theta, \phi) = -i^{A+1} k_i \int_0^\infty J_\Delta(K' \rho) \left[\int_{-\infty}^\infty \frac{\partial C_f^C(\rho, Z)}{\partial Z} \exp(i\alpha Z) \, dZ \right] \rho \, d\rho$$

$$\alpha = K_z - \frac{\epsilon_{fi}}{\hbar v_i}. \quad (31a)$$

In addition, for small angle scattering, $\alpha \approx 0$ from (18) and the Z-integration above can therefore be performed so that a further approximation C($\alpha = 0$) is characterized by

$$f_{if}^{C(0)}(\theta, \phi) = -i^{A+1} k_i \int_0^\infty J_\Delta(K' \rho) [C_f^C(\rho, \infty) - \delta_{if}] \rho \, d\rho \quad (31b)$$

where $K'^2 = K^2 - \epsilon_f^2/\hbar^2 v_i^2$ and the amplitudes C_f^C satisfy

$$i\hbar v_i \frac{\partial C_f^C}{\partial Z} = \sum_{n=1}^N C_n^C(\rho, Z) V_{fn}(\rho, Z) \exp\left(\frac{i\epsilon_{fn} Z}{\hbar v_i}\right) \quad (32)$$

in which $v_i = \hbar k_i/\mu$ for $n = 1, 2, \dots, N$, is the incident speed. These equations (31) and (32) are simply the familiar impact-parameter equations which have received widespread application to atom-atom and ion-atom scattering (Flannery and McCann 1973, 1974b-e). Also, (32) with (31b), in which $K' = 2k_i \sin \frac{1}{2}\theta$, have been modified by Bransden and Coleman (1972) so as to acknowledge implicitly the polarization effect on the incident channel due to couplings ignored explicitly by the truncated expansion (4). Byron (1971) has also obtained (31a) although he actually used (31b) and (32) for e-He collisions. The preceding analysis shows, however, that (31-32) are strictly valid only in the heavy-particle or high-energy limit.

In the limit of very high impact-speeds, the phase $\epsilon_{fn} Z/\hbar v_i$ in (32) can be neglected and Byron (1971) solved the infinite set ($N \rightarrow \infty$) of coupled equations exactly to give

$$C_f^C(\rho, Z) = \langle \phi_f(r_s) | \exp -\frac{i}{\hbar v_i} \int_{-\infty}^Z V(r_s, R) \, dZ | \phi_i(r_s) \rangle \quad (33)$$

a solution easily verified and which includes the effects arising from all discrete and continuum atomic states. Substitution in either equation (31a) with $\alpha = K_z$ since $\epsilon_f/v_i = 0$, and with the Φ -integration re-introduced or in equation (31b) with $K' = K$, yields

$$f_{if}^G(\theta, \phi) = -\frac{ik_i}{2\pi} \int e^{ik \cdot \rho} \phi_f^*(r_s) [e^{i\chi(\rho, r_s)} - 1] \phi_i(r_s) dr_s d\rho \quad (34)$$

where the phase shift

$$\chi(\rho, r_s) = -\frac{1}{\hbar v_i} \int_{-\infty}^{\infty} V(r_s, \rho, Z) dZ \quad (35)$$

thereby providing an alternative derivation of the expression of Glauber (1959). Thus, the Glauber approximation is a high-energy approximation which acknowledges all couplings between all discrete and continuum atomic eigenstates. The approximation has been applied by Tai *et al* (1970) to e-H(1s) excitation.

In general, for all the above approximations, the total cross section is given by

$$\sigma_{if}(k_i) = 2\pi \frac{k_f}{k_i} \int_0^\pi |f_{if}(\theta, \phi)|^2 \sin \theta d\theta \quad (36)$$

which, for the special case of approximation C($\alpha = 0$) alone, reduces to the customary impact-parameter expression

$$\sigma_{if}(k_i) = 2\pi \frac{k_f}{k_i} \int_0^\infty |C_f^C(\rho, \infty) - \delta_{if}|^2 \rho d\rho \quad (37)$$

for the total cross section. This expression is valid provided the energy is sufficiently high ($k_i \approx k_f$) and the scattering is into small angles such that the quantity $K'^2 \approx K^2 \approx 2k_i^2 (1 - \cos \theta)$ can be used in the integrand of (31b) and (36) and that the integral

$$\int_{(k_i - k_f) \approx 0}^{(k_i + k_f) \approx \infty} J_\Delta(K\rho) J_\Delta(K\rho') K dK \approx \frac{1}{\rho} \delta(\rho - \rho') \quad (38)$$

can be used to reduce (36) to (37). The JWKB approach of Bates and Holt (1966) involves the use of (37) with C_f^C replaced by the solution A_f of (9). In the next section, the effect of all the various approximate schemes A, B, C(α) and C(0) above to the full multistate eikonal treatments equations (14-15) will be fully examined by direct calculation.

3. Results and discussion

The theory derived in the previous section is now applied to the examination of the elastic and inelastic collisions,



in which the lowest five states 1s, 2s, 2p₀ and 2p _{± 1} of atomic hydrogen are closely coupled. It is worth pointing out that the resulting set of coupled equations are *not* approximations to the five actual coupled differential equations obtained from the full quantal close-coupling method. One advantage of the present procedure is that an infinite number of distorted partial waves of relative motion are automatically acknowledged via the eikonal in (4) and all these waves in turn are further correlated with the target wavefunctions via A_n in (4). This is done at the expense of the full correlation between the incident and atomic electrons included in a quantal close-coupling description of a *given* partial wave.

Differential and total cross sections for (39) are calculated for incident energies E_i in the range $13.6 \text{ eV} \leq E_i \leq 200 \text{ eV}$. In table 1 are displayed the total cross sections obtained from the full eikonal treatment equations (14-18, 36) at three representative impact energies together with comparison values obtained from the approximate schemes A, B, C(α), C(0) and IP previously discussed, and summarized in figure 1.

Table 1. Total cross sections (πa_0^2) at impact energy $E_i(\text{eV})$ for the processes $e + \text{H}(1s) \rightarrow e + \text{H}(nl)$; $nl = 1s, 2s, 2p_{0,\pm 1}$, obtained from various approximate schemes.

$E_i(\text{eV})$	nl	Full eikonal treatment equations (14-18)	Approximate eikonal treatments			Impact parameter treatment	
			A	B	C(α)	C(0)	IP
20	1s	0.841	0.923	0.703	0.651	0.714	1.056
	2s	0.145	0.174	0.131	0.070	0.122	0.147
	2p ₀	0.398	0.524	0.319	0.347	0.373	0.447
	2p _{± 1}	0.322	0.355	0.297	0.307	0.931	0.720
	2p	0.720	0.879	0.616	0.654	1.304	1.167
50	1s	0.365	0.378	0.332	0.373	0.371	0.519
	2s	0.090	0.095	0.085	0.076	0.089	0.083
	2p ₀	0.350	0.360	0.347	0.352	0.303	0.279
	2p _{± 1}	0.515	0.522	0.514	0.515	0.717	0.569
	2p	0.865	0.882	0.861	0.867	1.020	0.848
100	1s	0.224	0.229	0.202	0.202	0.213	0.271
	2s	0.052	0.053	0.050	0.049	0.053	0.054
	2p ₀	0.190	0.192	0.191	0.196	0.176	0.173
	2p _{± 1}	0.439	0.441	0.439	0.443	0.506	0.484
	2p	0.629	0.633	0.630	0.639	0.682	0.657

A: equations (20-22, 36); B: equations (21, 22, 36) with $\kappa_e = k_e$; C(α): equations (31a, 32, 36); C(0): equations (31b, 32, 36); IP: equations (31b, 32, 37).

3.1. Total cross sections

The comparison between the last two columns C(0) and IP in table 1 is a direct measure of the error introduced by the use of (37) rather than (36) for the total cross section. In general, IP exceeds C(0) except for the 2p _{± 1} and 2p excitations. The overestimates for $\Delta = 1(2p_{\pm 1})$ transitions and the underestimate for $\Delta = 0(2p_0)$ transitions are direct consequences of the different behaviour of the Bessel functions J_0 and J_1 in (38) at the non-physical small momentum changes $K < k_i - k_f$ and at the non-physical large momentum changes $K > k_i + k_f$ which are automatically included in equation (37) via assumption (38).

Inclusion of the phase α by approximation C(α), equation (31a), causes a further reduction in the total cross sections at all energies. The difference between the asymptotic speeds v_e is acknowledged via approximation B, equations (21-22) with $\kappa_e = k_e$. This inclusion yields cross sections, column B, in general larger than those given by C(α), particularly at the lower incident speeds, as expected from examination of the LHS of (22). The effect of adopting in (21) the approximate local wavenumber κ_f given by (20), rather than the asymptotic value k_e , as in B, is examined in columns A and B. The cross sections become greater at all energies with the result that the impact parameter cross sections

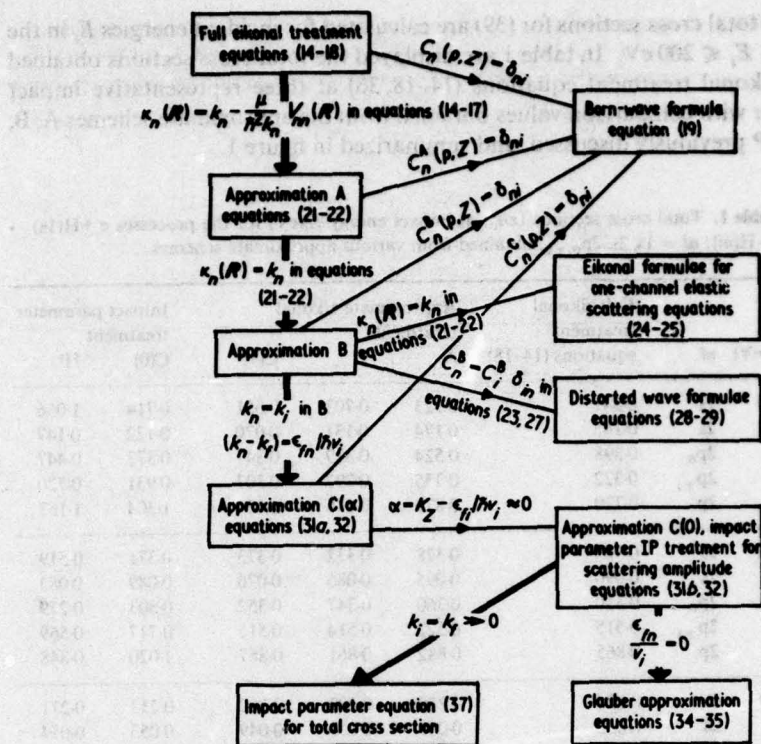


Figure 1. Schematic diagram illustrating approximations to full eikonal multistate treatment.

(column IP) are effectively better than the actual approximation merits; the effect of the various refinements introduced via C(0) and C(α) is largely offset by those acknowledged via B and A.

Finally, the cross sections given by the full multistate description equations (14-18) with the additional integral (17), are somewhat less than those given by A. In conclusion, the changes introduced by the various modifications to the full eikonal treatment are, as exhibited by table 1, significant at the lower incident energies and become vanishingly small at the high impact energies, as they should, since the basic framework of the model is essentially preserved.

3.2. Comparison of various theories and experiment

In table 2 are presented the final elastic and inelastic cross sections $\sigma_{1s-nl}(E_i)$ obtained from the present full multistate eikonal treatment of processes (39) for various impact energies E_i (eV). The present 2s and 2p excitation cross sections are compared in figures 2 and 3, curve FE, with those given by other refined treatments—the pseudo-state method of Burke and Webb (1970), the second-order potential approach of Sullivan *et al* (1972) and the polarized orbital distorted-wave model of McDowell *et al* (1973). Also displayed in figures 2 and 3 are results of approximation B, of the impact parameter IP treatment and of the Born approximation. The 2p experimental data of Long *et al*

Table 2. Elastic and inelastic cross sections (πa_0^2) from the full eikonal approximation to the processes $e + H(1s) \rightarrow e + H(nl)$, $nl = 1s, 2s, 2p_0, 2p_{\pm 1}$ at electron energy E_i (eV).

E_i (eV) \ nl	1s	2s	2p ₀	2p _{±1}	2p
13.6	1.290	0.120	0.345	0.115	0.460
20	0.841	0.145	0.398	0.322	0.720
30	0.615	0.124	0.387	0.449	0.836
50	0.365	0.090	0.350	0.515	0.865
100	0.224	0.052	0.190	0.439	0.629
200	0.129	0.028	0.118	0.335	0.453

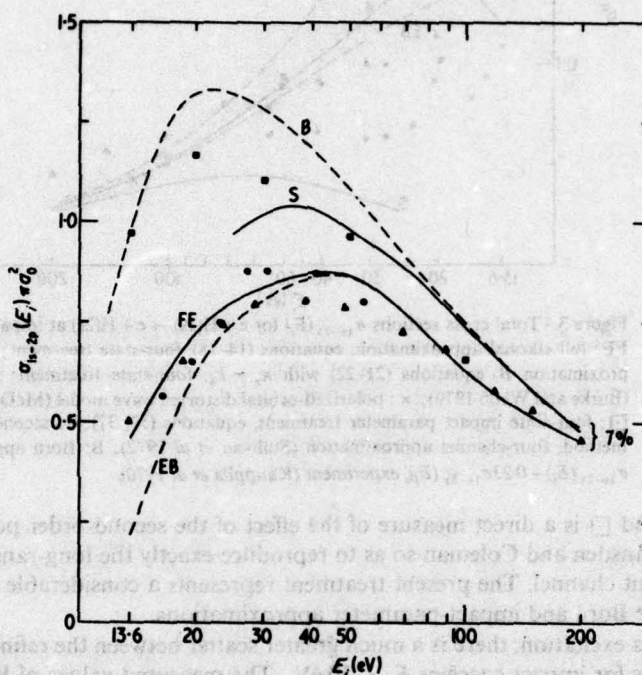


Figure 2. Total cross sections $\sigma_{1s-2p}(E_i)$ for $e + H(1s) \rightarrow e + H(2p)$ at impact energy E_i (eV). FE: full eikonal approximation, equations (14-18), four-state treatment; EB: eikonal approximation B, equations (21-22) with $\kappa_n = k_n$, four-state treatment; Δ : experiment (Long *et al* 1968); \bullet : pseudo-state (Burke and Webb 1970); \square : four-state impact parameter treatment, equations (32, 37); S: second-order potential method, four-channel approximation (Sullivan *et al* 1972); B: Born approximation.

(1968), normalized to the present value of $0.453\pi a_0^2$ at 200 eV (rather than to the corresponding Born results of $0.485\pi a_0^2$ which is 7% higher), and values of $\sigma_{1s-2s} + 0.23\sigma_{1s-3p}$ measured by Kauppila *et al* (1970) are also shown in figures 2 and 3, respectively. Although the Glauber treatment involved a heavy-particle high-energy limit, the Glauber results of Tai *et al* (1970) which are not shown, agree very well with experiment.

The agreement between FE, pseudo-state values and experiment is very good for the 2p excitation. The EB results which were reported earlier (Flannery and McCann 1974a) are indistinguishable from the full treatment FE for $E_i \gtrsim 50$ eV. The difference

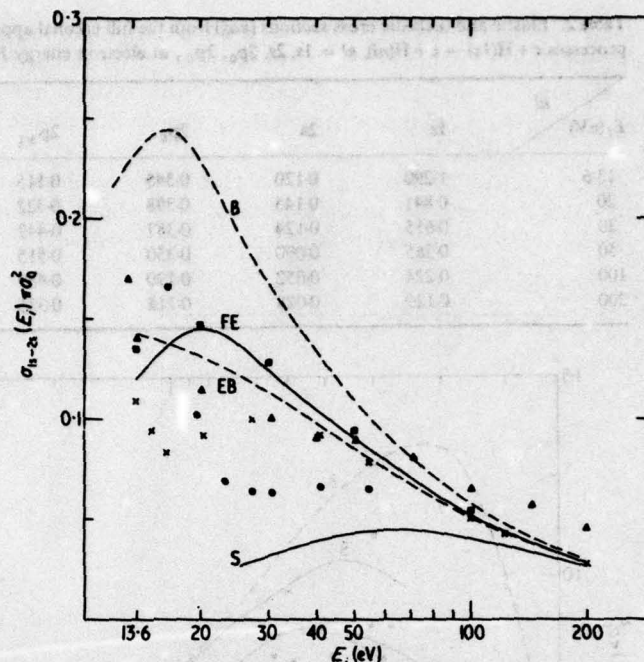


Figure 3. Total cross sections $\sigma_{1s-2s}(E_i)$ for $e + H(1s) \rightarrow e + H(2s)$ at impact energy E_i (eV). FE: full eikonal approximation, equations (14-18), four-state treatment; EB: eikonal approximation B, equations (21-22) with $\kappa_s = k_s$, four-state treatment; \bullet : pseudo-state (Burke and Webb 1970); \times : polarized-orbital distorted wave model (McDowell *et al* 1973); \square : four-state impact parameter treatment, equations (32, 37); S: second-order potential method, four-channel approximation (Sullivan *et al* 1972); B: Born approximation; Δ : $\sigma_{1s-2s}(E_i) + 0.23\sigma_{1s-3p}(E_i)$, experiment (Kauppila *et al* 1970).

between S and \square is a direct measure of the effect of the second-order potential introduced by Bransden and Coleman so as to reproduce exactly the long-range interaction in the incident channel. The present treatment represents a considerable improvement over both the Born and impact-parameter approximations.

For the 2s excitation, there is a much greater scatter between the refined theoretical cross sections for impact energies $E_i < 50$ eV. The measured values of Kauppila *et al* (1970) do not offer any definition since the 3p cascade contribution $0.23\sigma_{1s-3p}$, which, of course, varies with E_i , was included. Direct comparison between FE and experiment will only be possible when the higher $n = 3$ channels are included in the multistate expansion (9). Inclusion of κ_r as in FE rather than the use of k_r as in EB introduces a maximum to the 2s excitation.

The close agreement, for energies $E_i > 40$ eV, of the present treatment with that of McDowell *et al* (1973) who included exchange and polarization effects is either fortuitous or else demonstrates that exchange and polarization effects make little contribution at these energies.

3.3. Differential cross sections

Examination of the differential cross sections,

$$\frac{d\sigma}{d\Omega} = \frac{k_f}{k_i} |f_{if}(\theta, \phi)|^2 \quad (40)$$

permits additional insight into the accuracy and possible limitations of the present treatment. Although the treatment can be suitably modified so as to theoretically acknowledge electron-exchange and that portion of the polarization distortion not included by virtue of the four-state expansion, the present analysis has neglected such effects.

3.3.1. Elastic scattering. Results (MEA) for elastic scattering at 50 eV and 100 eV are shown in figure 4 together with the measured values of Teubner *et al* (1973) and the theoretical predictions of Winters *et al* (1973) and the Glauber results of Franco (1968) and

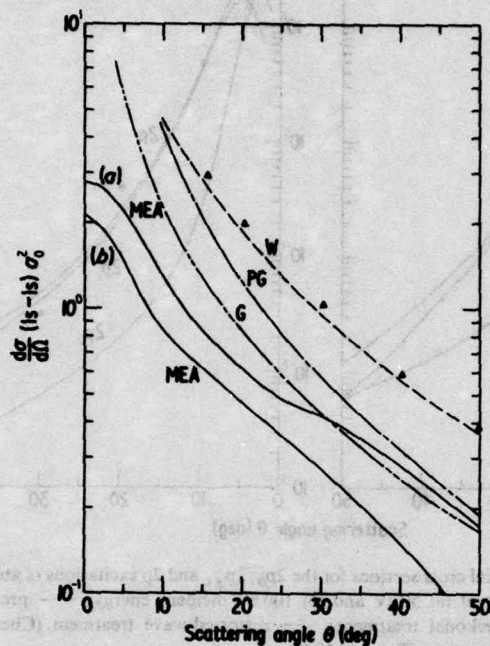


Figure 4. Differential cross sections for elastic scattering at 50 eV. MEA: present four-state (1s, 2s, 2p₀, 2p_{±1}) eikonal treatment at (a) 50 eV, (b) 100 eV; G: Glauber approximation (Franco 1968); PG: polarized Glauber approximation (Mathur 1974); W: second-order potential theory with exchange (Winters *et al* 1973); ▲ Teubner *et al* (1973).

of Mathur (1974). Although the experimental data are subject to $\pm 35\%$ error, comparison between MEA and W clearly demonstrates the necessity of including the full polarization distortion (for distant encounters) electron-exchange and a wave treatment modification (for the closer encounters), all of which were acknowledged by the one-channel approximation of Winters *et al* (1973). The present differential cross sections were rather insensitive to the approximations in § 2.2 (cf table 1).

Further accord with experiment is introduced by inclusion of electron-exchange and a wave treatment of the close collisions (with angular momentum $l \leq 7$) as carried out by Winters *et al* (1973). In conclusion, figure 4 displays the inadequacy of the present treatment to properly describe elastic scattering at all angles; polarization distortion mainly affects small-angle scattering while electron-exchange becomes dominant for larger angle scattering.

3.3.2. *Inelastic scattering.* In figures 5(a), (b) are displayed the $2p_{0,\pm 1}$ and $2p$ differential cross sections at 50 eV and 100 eV, together with the distorted-wave calculations of Chen *et al* (1972). Comparison shows that the effect of coupling with the $2s$ channel is to decrease the $2p$ scattering only at small angles $\lesssim 10^\circ$. The Glauber results of Tai *et al* (1970) are also shown at 100 eV.

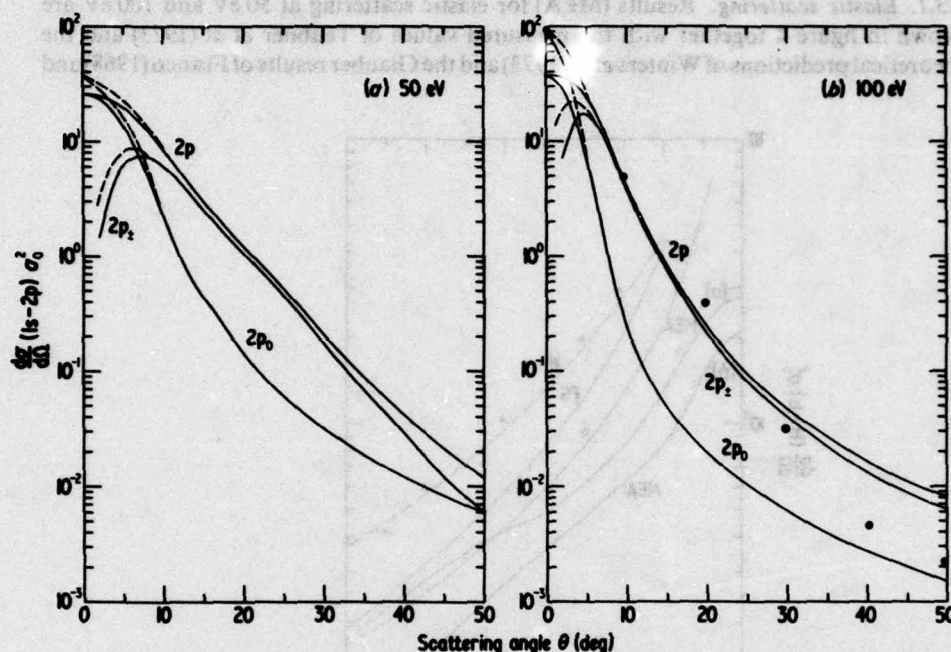


Figure 5. Differential cross sections for the $2p_0$, $2p_{\pm 1}$ and $2p$ excitations of atomic hydrogen by electron impact at (a) 50 eV and (b) 100 eV incident energy; — present four-state ($1s, 2s, 2p_0, 2p_{\pm 1}$) eikonal treatment; --- distorted-wave treatment (Chen *et al* 1972); ● Glauber approximation (Tai *et al* 1970).

Figures 6(a), (b) display the corresponding $2s$ scattering. A two-state treatment has also been carried out and the results agree closely with Chen *et al*, who found that electron-exchange, the importance of which increases with θ , is very small. Figures 6(a) and (b) show that the more important effect arises via coupling with the $2p$ channel, particularly for small momentum transfers. The Glauber approximation is in general agreement with the four-channel calculations except at high-momentum changes.

In summary, a multichannel generalization of the eikonal approach to atomic collisions has been presented. Various approximate schemes have been proposed, and examined in detail for $e\text{-H}(1s)$ collisions. In the heavy-particle or high-energy limit, the basic formulae reduce to the standard impact parameter method. For $e\text{-H}(1s)$ collisions at low and intermediate energies E , the additional refinements introduced are necessary for an adequate description of excitation. Very good agreement with experiment and with other refined treatments is obtained for the $2p$ excitation while the $2s$ excitation (the cross section for which being less definitive for $E < 40$ eV) is in satisfactory accord. However polarization distortion and electron-exchange which are neglected in the present description are very important for elastic scattering at all angles.

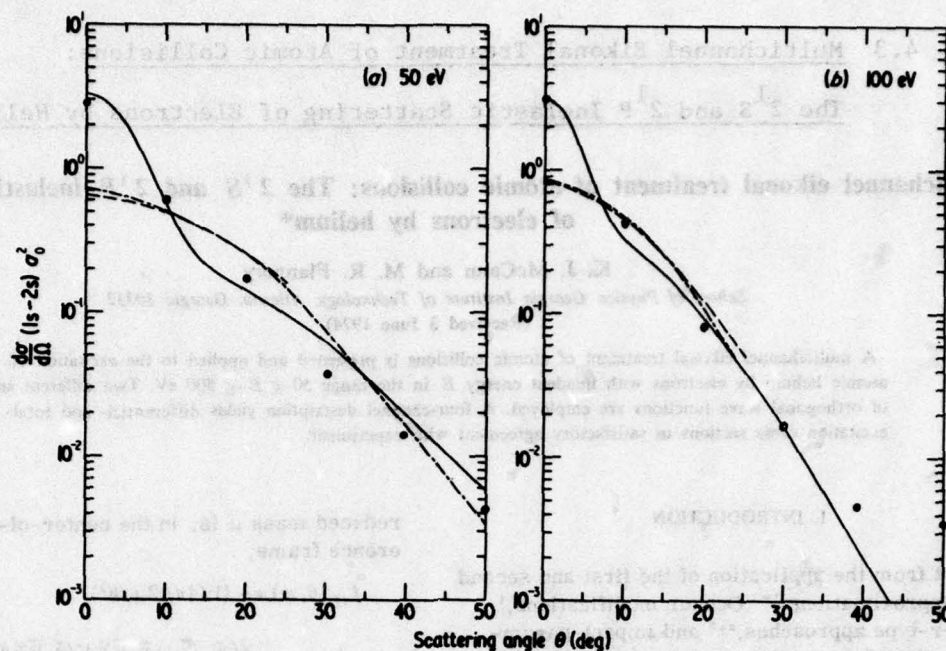


Figure 6. Differential cross sections for the 2s-excitation of atomic hydrogen by electron-impact at (a) 50 eV and (b) 100 eV incident energy: — present four-state (1s, 2s, 2p₀, 2p_{±1}) eikonal treatment; --- present two-state (1s, 2s) eikonal treatment; -.- distorted-wave treatment (Chen *et al* 1972); ● Glauber approximation (Tai *et al* 1970).

Acknowledgment

This research was sponsored by the Air Force Aerospace Research Laboratories, Air Force Systems Command, United States Air Force, Contract F 33615-74-C-4003.

References

- Bates D R and Crothers D S F 1970 *Proc. R. Soc. A* **315** 465-78
- Bates D R and Holt A R 1966 *Proc. R. Soc. A* **292** 168-79
- Bransden B H 1970 *Atomic Collisions Theory* (New York: Benjamin) p 82
- Bransden B H and Coleman J P 1972 *J. Phys. B: Atom. Molec. Phys.* **5** 537-45
- Burke P G and Webb T G 1970 *J. Phys. B: Atom. Molec. Phys.* **3** L131-4
- Byron F W 1971 *Phys. Rev.* **4** 1907-17
- Chen J C Y, Joachain C J and Watson K M 1972 *Phys. Rev.* **5** 2460-74
- Flannery M R and McCann K J 1973 *Phys. Rev. A* **8** 2915-22
- 1974a *J. Phys. B: Atom. Molec. Phys.* **7** L223-7
- 1974b *J. Phys. B: Atom. Molec. Phys.* **7** 840-9
- 1974c *J. Phys. B: Atom. Molec. Phys.* **7** 1347-55
- 1974d *J. Phys. B: Atom. Molec. Phys.* **7** 1558-61
- 1974e *Phys. Rev. A* **9** 1947-53
- Franco V 1968 *Phys. Rev. Lett.* **20** 709-12
- Glauber R J 1959 *Lectures in Theoretical Physics* ed W E Brittin and L G Dunham (New York: Interscience) vol 1 p 369
- Kaupilla W E, Ott W R and Fite W L 1970 *Phys. Rev.* **141** 1099-108
- Long R L, Cox D M and Smith S J 1968 *J. Res. Nat. Bur. Std.* **72A** 521-35
- Mathur K C 1974 *Phys. Rev. A* **9** 1200-4
- McDowell M R C, Morgan Lesley A and Myerscough Valerie P 1973 *J. Phys. B: Atom. Molec. Phys.* **6** 1435-51
- Sullivan J, Coleman J P and Bransden B H 1972 *J. Phys. B: Atom. Molec. Phys.* **5** 2061-5
- Tai H, Bassel R H, Gerjuoy E and Franco V 1970 *Phys. Rev. A* **1** 1819-39
- Teubner P J O, Lloyd C R and Weigold E 1973 *J. Phys. B: Atom. Molec. Phys.* **6** L134-7
- Winters K H, Clark C D, Bransden B H and Coleman J P 1973 *J. Phys. B: Atom. Molec. Phys.* **6** L247-9

4.3 Multichannel Eikonal Treatment of Atomic Collisions:

The 2^1S and 2^1P Inelastic Scattering of Electrons by Helium

Multichannel eikonal treatment of atomic collisions: The 2^1S and 2^1P inelastic scattering of electrons by helium*

K. J. McCann and M. R. Flannery

School of Physics, Georgia Institute of Technology, Atlanta, Georgia 30332

(Received 3 June 1974)

A multichannel eikonal treatment of atomic collisions is presented and applied to the excitation of atomic helium by electrons with incident energy E in the range $50 \leq E \leq 500$ eV. Two different sets of orthogonal wave functions are employed. A four-channel description yields differential- and total-excitation cross sections in satisfactory agreement with experiment.

1. INTRODUCTION

Apart from the application of the first and second Born approximations,¹⁻³ Ochkur modifications,⁴ Glauber-type approaches,^{5,6} and impact-parameter methods^{7,8} to collisional excitation of atomic helium by incident electrons, theoretical knowledge of these collisions for low and intermediate impact energies beyond the inelastic thresholds is very limited. The experimental measurement of the vacuum-uv excitation functions is difficult⁹⁻¹⁹ and requires high resolution, and full account must be taken of cascade and other well-identified problems. In order to provide absolute cross sections, the measurements must then be normalized to some high-energy theoretical cross section, and the energy-point of departure of the actual cross sections from the corresponding Born and Bethe values is extremely uncertain.

In an effort to obtain an accurate description of electron-(excited) atom collisions in the intermediate energy region, a multistate-eikonal treatment of atomic collisions has recently been developed.^{20,21} The method achieved notable success for $e-H(1s)$ excitation and the resulting differential and total cross sections agreed closely with experiment and with other refined treatments. Moreover, the basic formulae which acknowledged different speeds in various channels reduced upon successive approximation to those obtained previously by other authors.^{5,22-24} In an effort to probe the further reliability of the present method, the 2^1S and the 2^1P excitations of atomic helium by electron impact are examined in this paper. The resulting total and differential cross sections are compared with previous treatments and with experiment.

II. THEORY

The scattering amplitude describing a transition between an initial channel i and a final channel f of the electron-helium collision system of

reduced mass μ is, in the center-of-mass reference frame,

$$f_{if}(\theta, \varphi) = -(1/4\pi)(2\mu/\hbar^2) \times \langle \Psi_f(\vec{k}_f; \vec{r}, \vec{R}) | V(\vec{r}, \vec{R}) | \Psi_i^*(\vec{k}_i; \vec{r}, \vec{R}) \rangle_{\vec{r}, \vec{R}} \quad (1)$$

where $V(\vec{r}, \vec{R})$ is the instantaneous electrostatic interaction between the electron at \vec{r} and the helium atom with internal electronic coordinates denoted collectively by \vec{R} , both vectors being relative to the helium nucleus as the origin. The wave numbers for the relative motion in the initial and final channels asymptotically ($\vec{R} \rightarrow \infty$) tend to k_i and k_f , respectively, the final stationary state of the isolated atoms in channel f is Ψ_f , and Ψ_i^* is the solution of the time-independent Schrödinger equation,

$$\left(-\frac{\hbar^2}{2\mu} \nabla_{\vec{r}}^2 + H_e(\vec{r}) + V(\vec{r}, \vec{R}) \right) \Psi_i^*(\vec{r}, \vec{R}) = E_i \Psi_i^*(\vec{r}, \vec{R}), \quad (2)$$

solved subject to the asymptotic boundary condition

$$\Psi_i^*(\vec{r}, \vec{R}) \xrightarrow{\text{large } R} \sum_n \left(e^{i\vec{k}_n \cdot \vec{R}} \delta_n + f_{in}(\theta, \varphi) \frac{e^{i\vec{k}_n \cdot \vec{R}}}{R} \right) \times \varphi_n(\vec{r}_1, \vec{r}_2), \quad (3)$$

in which $\varphi_n(\vec{r}_1, \vec{r}_2)$ are eigenfunctions of the Hamiltonian $H_e(\vec{r})$ for the isolated helium atom with internal electronic energy ϵ_n , such that the total energy E_i in channel i is $\epsilon_i + \hbar^2 k_i^2 / 2\mu$, which is conserved throughout the collision. In the absence of the interaction the wave function for the system in the final channel is therefore $\varphi_f(\vec{r}_1, \vec{r}_2) \exp(i\vec{k}_f \cdot \vec{R})$.

The eikonal approximation to (2) writes the total wave function in the presence of the interaction as

$$\Psi_i^*(\vec{r}, \vec{R}) = \sum_n A_n(\vec{p}, Z) \exp i S_n(\vec{p}, Z) \varphi_n(\vec{r}_1, \vec{r}_2), \quad (4)$$

where the e -ion separation $\vec{R} = (R, \Theta, \Phi) = (\rho, \phi, Z)$ in spherical and cylindrical coordinate frames, respectively. The eikonal S_n in (4) is the characteristic-function solution of the classical Hamilton-Jacobi equation (i.e., the Schrödinger equation in the $\hbar \rightarrow 0$ limit) for the e -He relative motion under the static interaction $V_{nm}(\vec{R})$, and is therefore given by

$$S_n(\vec{p}, Z) = k_n Z + \int_{-\infty}^Z [\kappa_n(\vec{R}) - k_n] dZ, \quad (5)$$

in which the local wave number of relative motion at \vec{R} is

$$\kappa_n(\vec{R}) = [k_n^2 - (2\mu/\hbar^2)V_{nm}(\vec{R})]^{1/2}, \quad (6)$$

and where dZ is assumed to be an element of path length along the trajectory. The interaction matrix elements coupling the various atomic states are

$$V_{nm}(\vec{R}) = \langle \varphi_n(\vec{r}_1, \vec{r}_2) | V(\vec{r}, \vec{R}) | \varphi_m(\vec{r}_1, \vec{r}_2) \rangle. \quad (7)$$

By inserting Eq. (4) into (1), and with the aid of Eqs. (2)-(7), Flannery and McCann²¹ have shown that the scattering amplitude then reduces to

$$f_{if}(\theta, \varphi) = -i^{\Delta+1} \int_0^\infty J_\Delta(K'\rho) \times [I_1(\rho, \theta) - iI_2(\rho, \theta)] \rho d\rho, \quad (8)$$

where K' is the XY component $k_f \sin \theta$ of \vec{K} and where J_Δ are Bessel functions of integral order. Both the functions

$$I_1(\rho, \theta; \alpha) = \int_{-\infty}^\infty \kappa_f(\rho, Z) \left(\frac{\partial C_f(\rho, Z)}{\partial Z} \right) e^{i\alpha Z} dZ \quad (9)$$

and

$$I_2(\rho, \theta; \alpha) = \int_{-\infty}^\infty \left(\kappa_f(\kappa_f - k_f) + \frac{\mu}{\hbar^2} V_{ff} \right) C_f(\rho, Z) \times e^{i\alpha Z} dZ \quad (10)$$

depend on the scattering angle θ , via the parameter

$$\alpha = k_f(1 - \cos \theta) = 2k_f \sin^2(\theta/2), \quad (11)$$

the difference between the Z component of the momentum change \vec{K} and the minimum momentum change $k_i - k_f$ in the collision. The transition amplitudes $C_f(\rho, Z)$ which are related to the original phase Φ -dependent coefficients $A_f(\vec{p}, Z)$ by

$$C_f(\rho, Z) = A_f(\vec{p}, Z) \times \exp \left(i \int_{-\infty}^Z (\kappa_f - k_f) dZ \right) \exp(-i\Delta\Phi), \quad (12)$$

where Δ is the change $M_i - M_f$ in the azimuthal quantum number of the atom, can be shown to satisfy the following set of N -coupled differential equations

$$\begin{aligned} \frac{i\hbar^2}{\mu} \kappa_f(\rho, Z) \frac{\partial C_f(\rho, Z)}{\partial Z} + \left(\frac{\hbar^2}{\mu} \kappa_f(\kappa_f - k_f) + V_{ff}(\rho, Z) \right) C_f(\rho, Z) \\ = \sum_{n=1}^N C_n(\rho, Z) V_{fn}(\rho, Z) e^{i(k_n - k_f)Z}, \\ f=1, 2, \dots, N \end{aligned} \quad (13)$$

to be solved subject to the boundary condition $C_f(\rho, -\infty) = \delta_{if}$. Equations (8)-(13) are basic to the present multichannel eikonal treatment and a variety of approximations readily follow. For example, in the absence of all couplings except that connecting the initial and final channels, i.e., $C_n = \delta_{ni}$ in (13), then (8) reduces to

$$f_{if}(\theta, \varphi) = -\frac{1}{4\pi} \frac{2\mu}{\hbar^2} \int V_{fi}(\vec{R}) \exp(i\vec{K} \cdot \vec{R}) d\vec{R}, \quad (14)$$

which is the Born-wave formula for the scattering amplitude.

When $\kappa_f(\vec{R})$ is approximated by $k_f - (\mu/\hbar^2 k_f) V_{ff}(\vec{R})$ then, with the aid of (6) for κ_f^2 , both I_2 and the term within large parentheses of the left-hand side of (13) vanish identically to give

$$\begin{aligned} f_{if}^A(\theta, \varphi) = -i^{\Delta+1} \int_0^\infty J_\Delta(K'\rho) \rho d\rho \\ \times \int_{-\infty}^\infty \kappa_f \left(\frac{\partial C_f^A}{\partial Z} \right) \exp(i\alpha Z) dZ, \end{aligned} \quad (15)$$

an approximation A to the scattering amplitude, for which the N -coupled equations reduce to

$$\begin{aligned} \frac{i\hbar^2}{\mu} \kappa_f \frac{\partial C_f^A}{\partial Z} = \sum_{n=1}^N C_n^A(\rho, Z) V_{fn}(\rho, Z) e^{i(k_n - k_f)Z}, \\ f=1, 2, \dots, N. \end{aligned} \quad (16)$$

If the local wave number κ_f in (15) and (16) is now replaced by its asymptotic value k_f , then a further approximation B is obtained. For a one-channel approximation B , $C_n^B = C_i^B \delta_{in}$ in (16) with

$\kappa_i = k_i$. After some analysis, the customary eikonal expression²² for elastic scattering by a fixed potential $V_{ii}(\vec{R})$ is then recovered. Moreover, if the distorted wave for the final state

$$\Psi_f(\vec{r}, \vec{R}) = \varphi_f(\vec{r}_1, \vec{r}_2) \exp i \left(\vec{k}_f \cdot \vec{R} - \frac{1}{\hbar v_f} \int_{-\infty}^z V_{ff} dZ \right) \quad (17)$$

is used in (1), then the theory follows through as before, to give, in approximation B

$$f_{if}^{DW}(\theta, \varphi) = -i^{\Delta+1} \int_0^\infty J_\Delta(K' \rho) \rho d\rho \int_{-\infty}^\infty k_f \left(\frac{\partial C_f^B}{\partial Z} \right) \times \exp i \left(\alpha Z + \frac{1}{\hbar v_f} \int_{-\infty}^Z V_{ff} dZ' \right) dZ \quad (18)$$

where, C_f^B satisfies (16), with $\kappa_f = k_f$. Equation (18) represents the multichannel distorted-wave treatment. By setting $C_n^B = C_i^B \delta_{in}$ in a two-state treatment of (16), then, after some analysis, (18) reduces to

$$f_{if}^{DWB}(\theta, \varphi) = -\frac{i^{\Delta+1}}{\hbar^2} \int_0^\infty J_\Delta(k_f \rho \sin \theta) \rho d\rho \int_{-\infty}^\infty V_{fi}(\rho, Z) \times \exp i \{ [(k_i - k_f) + \alpha] Z + \delta \Phi(Z) \} dZ, \quad (19)$$

where

$$\delta \Phi(Z) = -\frac{1}{\hbar v_i} \int_{-\infty}^Z V_{ii} dZ - \left(\frac{1}{\hbar v_f} \right) \int_Z^\infty V_{ff} dZ, \quad (20)$$

formulas which are identical to the distorted Born-wave expressions of Chen *et al.*²³ for e -H collisions. Equations (19) and (20) have been used by Shields and Peacher²⁵ to evaluate differential cross sections for atom-atom collisions.

In the heavy-particle or high-energy limit, the asymptotic wave numbers k_f in approximation B can be replaced by

$$k_f = k_i - (\epsilon_{fi}/\hbar v_i) [1 + (\epsilon_{fi}/2\mu v_i^2) + \dots], \quad \epsilon_{fi} = \epsilon_f - \epsilon_i, \quad (21)$$

and a third approximation $C(\alpha)$ follows by setting all the individual k_n in approximation B equal to k_i , and any difference $k_n - k_f = \epsilon_{fn}/v_i$. Hence

$$f_{if}^C(\theta, \varphi) = -i^{\Delta+1} k_i \int_0^\infty J_\Delta(K' \rho) \times \left(\int_{-\infty}^\infty \frac{\partial C_f^C(\rho, Z)}{\partial Z} \exp(i\alpha Z) dZ \right) \rho d\rho, \quad \alpha = K_z - \epsilon_{fi}/\hbar v_i. \quad (22)$$

In addition, for small-angle scattering at high energies $\alpha \approx 0$ from (11) and the Z -integration above can therefore be performed so that a further approximation $C(\alpha=0)$ is characterized by

$$f_{if}^{C(0)}(\theta, \varphi) = -i^{\Delta+1} k_i \times \int_0^\infty J_\Delta(K' \rho) (C_f^C(\rho, \infty) - \delta_{if}) \rho d\rho \quad (23)$$

where $K'^2 = K^2 - \epsilon_{fi}^2/\hbar^2 v_i^2$, and the amplitudes C_f^C satisfy

$$i\hbar v_i \frac{\partial C_f^C}{\partial Z} = \sum_{n=1}^N C_n^C(\rho, Z) V_{fn}(\rho, Z) \exp \left(\frac{i\epsilon_{fn} Z}{\hbar v_i} \right), \quad (24)$$

in which $v_i = \hbar k_i/\mu$, for $n=1, 2, \dots, N$, is the incident speed. Equations (22)–(24) are simply those derived previously²⁶ for the differential cross sections in the multistate impact parameter description of heavy particle collisions. They have recently been applied to various atom-atom and ion-atom collisions.²⁷ Equation (22) has previously been obtained by Byron⁵ who subsequently applied (23) and (24) to e -H(1s) collisions. In order to acknowledge polarization of the initial state due to the incident electron, Bransden and Coleman²⁴ modified (24) and used (23) with $K' = 2k_i \sin \frac{1}{2} \theta$. The above derivation, however, demonstrates that the validity of the impact parameter equations (22)–(24) is confined only to the heavy-particle or high-energy limit of atomic collisions when $k_i \approx k_f$ and the scattering is mainly in the forward direction.

The Glauber approximation which follows by neglecting the exponential term in (24), and by inserting the exact solution C_f of the resulting equations in (23), is also a heavy-particle-high-energy approximation and one in which no account is taken of the different relative momenta in the various channels. In spite of this, however, it is apparently remarkably successful.

III. RESULTS AND DISCUSSION

The full multichannel eikonal theory, as represented by Eq. (8)–(13), is now applied to the examination of differential and total cross sections for the excitation processes

$$e + \text{He}(1^1\text{S}) \rightarrow e + \text{He}(2^1\text{S}, 2^1\text{P}) \quad (25)$$

in which the four-channels $e - (1^1\text{S}, 2^1\text{S}, 2^1\text{P}_{0,1,1})$ of the e -He system are closely coupled. For this investigation two relevant orthogonal sets of wave functions were adopted. The first set includes the normalized Hartree-Fock ground-state function of

Byron and Joachain,²⁸

$$\varphi_{1s,1s}(\tilde{r}_1, \tilde{r}_2) = (1.6966/\pi)(e^{-1.4r_1} + 0.799e^{-2.41r_1}) \times (e^{-1.4r_2} + 0.799e^{-2.41r_2}), \quad (26)$$

the 2¹P function of Goldberg and Clogston,²⁹

$$\begin{aligned} \varphi_{1s,2p}(\tilde{r}_1, \tilde{r}_2) &= (0.37831/\pi^{1/2}) [r_1 e^{-(0.489r_1+2r_2)} Y_{1m}(\tilde{r}_1) \\ &\quad + r_2 e^{-(0.489r_2+2r_1)} Y_{1m}(\tilde{r}_2)], \quad (27) \end{aligned}$$

and the 2¹S function of Flannery⁷

$$\begin{aligned} \varphi_{1s,2s}(\tilde{r}_1, \tilde{r}_2) &= \frac{0.70640}{\pi(1+\Delta^2)^{1/2}} [e^{-2r_2}(e^{-\lambda r_1} - cr_1 e^{-\mu r_1}) \\ &\quad + e^{-2r_1}(e^{-\lambda r_2} - cr_2 e^{-\mu r_2})], \quad (28) \end{aligned}$$

in which the parameters $\lambda=1.1946$, $\mu=0.4733$, $c=0.26832$, and $\Delta=0.007322$, which ensured orthogonality with (26), were chosen so as to provide a simple curve fit to the multi-parameter function of Cohen and McEachran.³⁰ With the aid of standard integral techniques, the interaction potentials (7), deduced from the above set of wave functions (26)–(28), can be expressed as analytic functions of \tilde{R} .

The second choice of wave functions are the actual analytical multi-parameter Hartree-Fock frozen-core set of McEachran and Cohen³¹ and of Crothers and McEachran,³² which yield very accurate eigenenergies. The set is written

$$\Psi_{1s,nlm}(\tilde{r}_1, \tilde{r}_2) = N_{nl} [\varphi_0(\tilde{r}_1) \varphi_{nlm}(\tilde{r}_2) + \varphi_0(\tilde{r}_2) \varphi_{nlm}(\tilde{r}_1)], \quad (29a)$$

where the normalized function representing the frozen 1s orbital is

$$\varphi_0(\tilde{r}) = 2^{5/2} e^{-2r} Y_{00}(\tilde{r}), \quad (29b)$$

and where the unnormalized orbital for the second electron in state (nlm) is, in atomic units,

$$\begin{aligned} \varphi_{nlm}(\tilde{r}) &= \sum_{j=0}^{l-1} a_j^{nl} (2r)^j e^{-\beta r} L_j^{2l+1}(2\beta r) Y_{lm}(\tilde{r}), \\ \beta &= \frac{2}{n}, \quad (29c) \end{aligned}$$

where the coefficients a_j^{nl} of the associated Laguerre polynomials

$$L_j^\lambda(x) = \sum_{k=0}^{j-\lambda} \frac{(-1)^{k+\lambda} (j!)^\lambda x^k}{k! (j-k-\lambda)! (k+\lambda)!} \quad (29d)$$

have been tabulated^{30–32} for various states of helium. In order to evaluate the interaction matrix elements (7) as analytic functions of \tilde{R} ,

it is convenient to express (29c), with the aid of (29d), as

$$\varphi_{nlm}(\tilde{r}) = \sum_{N=1+l}^{l-1} B_N^{nl} e^{-\beta r} r^{N-1} Y_{lm}(\tilde{r}), \quad (30a)$$

with coefficients given by

$$B_N^{nl} = \sum_{j=N+1}^l \frac{(-1)^{j-1} a_j^{nl} 2^j (j!)^\lambda (2\beta)^{N-1-1}}{(n-l-1)! (j-N-1)! (N+1)!}, \quad (30b)$$

which are tabulated in Table I for the 1¹S, 2¹S and 2¹P states of interest. The overall normalization factor in (29a) is $N_{nl} = [2(H_{nl} + G_{nl}^2)]^{-1/2}$, where

$$H_{nl} = \sum_{N=1+l}^{l-1} \sum_{N'=1+l}^{l-1} B_N^{nl} B_{N'}^{nl} \frac{(N+N')!}{(2\beta)^{N+N'+1}} \quad (30c)$$

and

$$G_{nl} = 2^{5/2} \delta_{10} \sum_{N=1}^l B_N^{nl} \frac{(N+1)!}{(\beta+2)^{N+3}}, \quad (30d)$$

and is also given in Table I. With the aid of (30a) and (30b), and standard integrals, the interaction matrix elements can be expressed in the form

$$\begin{aligned} V_{nlm, n'l'm'}(\tilde{R}) &= \sum_{L=|l-l'|}^{l+l'} \sum_{l_1, l_2}^{l+l'} \left(-\frac{a_{Ll}}{R^L} \right. \\ &\quad \left. + \sum_{i=1}^2 e^{-\alpha_i R} \sum_{s=0}^{18} a_s R^s \right) Y_{L, l+l'}(\tilde{R}). \quad (31) \end{aligned}$$

The tabulation of the coefficients a_m for the various $\alpha_i=4$, $(1/n+1/n')$, and L values is extensive and

TABLE I. Coefficients B_N^{nl} , parameters β , normalization factors N_{nl} , and eigenenergies ϵ_n (a.u.) given by the Hartree-Fock frozen-core set of wave functions (29a)–(30a) for helium.

$N \setminus nl$	1s	2s	2p
1	-1.8385(0) ^a	-5.5677(-1)	0.0000
2	2.9332(-2)	5.2732(-1)	-1.2768(-1)
3	-1.2332(0)	-4.1053(-1)	-5.8948(-2)
4	-4.7143(-3)	3.1444(-1)	-1.5165(-2)
5	1.0769(-1)	-9.0158(-2)	-1.3793(-2)
6	-7.9926(-2)	1.7266(-2)	4.9854(-3)
7	2.0400(-2)	-1.5858(-3)	-1.2073(-3)
8	-2.6249(-3)	7.3009(-5)	1.1661(-4)
9	1.2433(-4)	-3.0679(-7)	-5.2312(-6)
β	2.0	1.0	1.0
N_{nl}	2.2745	9.1927(-2)	3.6218(-2)
ϵ_n (calc)	-0.8725	-0.1434	-0.1224
ϵ_n (expt)	-0.9036	-0.1460	-0.1238

^a Numbers in parentheses indicate the power of 10 by which the entry is to be multiplied.

is available upon request. With a knowledge of the interaction matrices (31), the appropriate set of coupled differential equations (13) can be solved for the real and imaginary parts of C_i by standard numerical procedures.

In Figs. 1 and 2, the resulting differential cross sections,

$$\frac{d\sigma}{d\Omega} = \frac{k_f}{k_i} |f_{if}(\theta, \varphi)|^2 \quad (32)$$

computed from (8)–(13) as a function of scattering angle θ are displayed as solid and double-dashed curves [labeled FE1 and FE2 associated with the first and second choices (26)–(28) and (29a)–(29d) for the wave functions, respectively] at two representative electron-impact energies E_i of 50 eV and 100 eV. Use of the more refined set of wave functions (29a)–(29d) causes the scattering to be increased only in the forward direction ($\theta \leq 20^\circ$) in the case of 2^1P excitation, and into all angles for the 2^1S collision. This amount of enhancement decreases with energy increase. Also shown are recent results labeled S, single-dashed curves, obtained by Berrington *et al.*³³ who used the first set of orthogonal wave functions (26)–(28) in the second-order potential theory of Bransden and Coleman,²⁴ i.e. Eq. (23) with $K' = 2k_i \sin \frac{1}{2} \theta$ and Eq. (24), suitably modified so as to acknowledge polarization of the initial state. While the long-range polarization is expected to be more effective for small-angle scattering (i.e., distant encounters), Berrington *et al.*³³ have shown that the resulting reduction in $d\sigma/d\Omega$ is nonetheless relatively small at small θ and vanishes for larger θ and/or E_i . Figure 1(a) and 1(b) show that the present treatment causes a further reduction both at small and large scattering angles for the 2^1P excitation. In Figs. 2(a) and 2(b) the effect is reversed for the 2^1S excitation. These effects can be attributed to the presence in (9) and (10) of α which tends to reduce all the cross sections particularly at the larger scattering angles and to the more important inclusion in the various channels of the different local momenta $\kappa_n(\vec{R})$ which tend to enhance²¹ the 2^1S excitation at the expense of the 2^1P excitation at energies ≥ 50 eV.

The 2^1S Glauber cross sections of Yates and Tenney³⁴ and of Chan and Chen,³⁵ shown as crosses in Fig. 2, agree closely with the Glauber results of Franco³⁷ who used the same 2^1S wave functions as in FE1. The corresponding 2^1P cross sections³⁸ are in harmony with the present calculations in the angular range 5° – 10° , but are larger for scattering in the forward direction.

The 2^1P and 2^1S differential cross sections measured by various groups^{4, 15–19} are also displayed in Figs. 1 and 2 for comparison purposes.

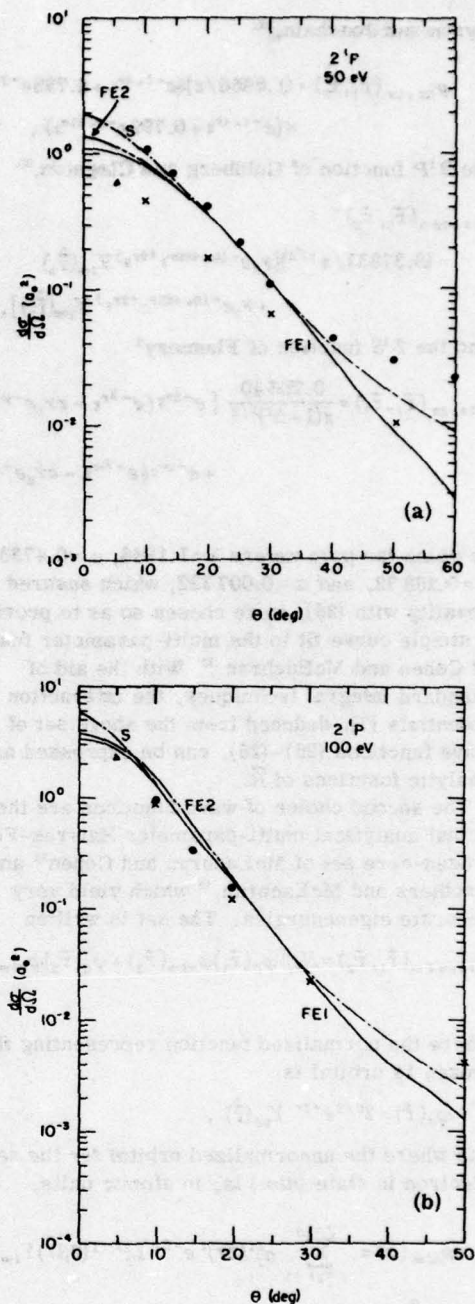


FIG. 1. Differential cross sections for the process $e + \text{He}(1^1S) \rightarrow e + \text{He}(2^1P)$ at incident electron energy (a) 50 eV and (b) 100 eV. Theory: FE1, Four-channel eikonal treatment with first set of atomic wave functions (26)–(28); FE2, four-channel eikonal treatment with second set of atomic wave functions (29); S, second-order potential method with first set of atomic wave functions [Berrington *et al.* (Ref. 33)]. Experiment: Δ , Chamberlain *et al.* (Ref. 17), \times , Crooks and Rudd (Ref. 18), \bullet , Truhlar *et al.* (Ref. 19) at 55.5 eV and Vriens *et al.* (Ref. 15) at 100 eV.

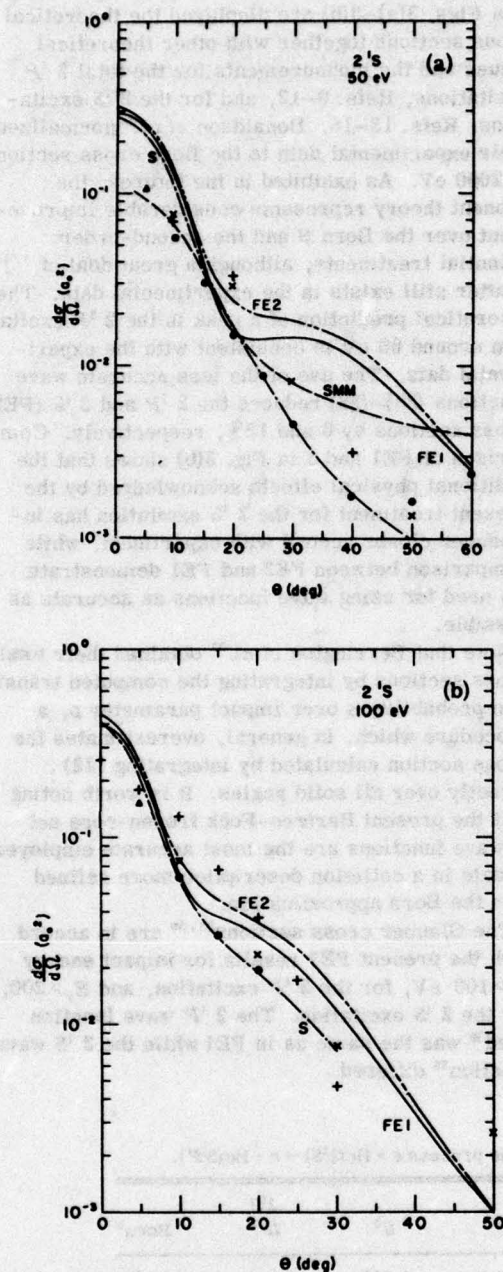


FIG. 2. Differential cross sections for the process $e + \text{He}(1^1\text{S}) \rightarrow e + \text{He}(2^1\text{S})$ at incident electron energy. (a) 50 eV and (b) 100 eV. Theory: FE1, Four-channel eikonal treatment with first set of atomic wave functions (26)–(28); FE2, four-channel eikonal treatment with second set of atomic wave functions (29); S, second-order potential method with first set of atomic wave functions [Berrington *et al.* (Ref. 33)]; +: Glauber approximation (Refs. 34 and 35). Experiment: SMM, Simpson *et al.* (Ref. 16); Δ , Chamberlain *et al.* (Ref. 17); \times , Crooks and Rudd (Ref. 18); \bullet , Rice *et al.* (Ref. 4) at 55.5 eV and Vriens *et al.* (Ref. 15) at 100 eV.

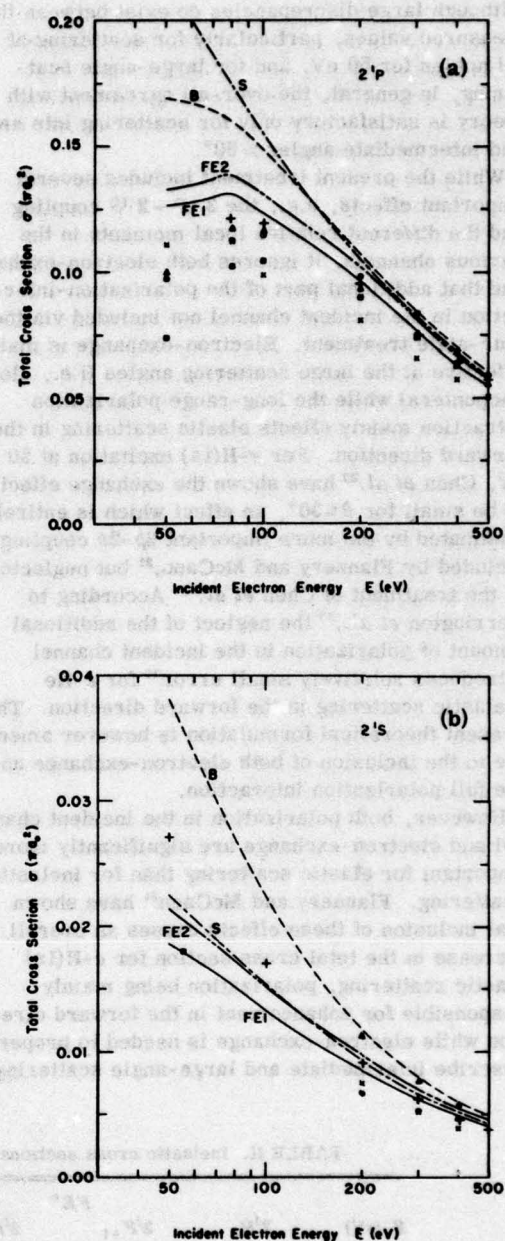


FIG. 3. Total cross sections for (a) the 2^1P and (b) the 2^1S excitations of $\text{He}(1^1\text{S})$ by electron impact. Theory: FE1, Four-channel eikonal treatment with first set of atomic wave functions (26)–(28); FE2, four-channel eikonal treatment with second set of atomic wave functions (29); S, second-order potential method with first set of atomic wave functions [Berrington *et al.* (Ref. 33)]; B, Born-approximation (Ref. 2); +: Glauber approximation (Refs. 35 and 36). Experiment: (2^1P), Δ , Donaldson *et al.* (Ref. 9); \blacksquare , Jobe and St. John (Ref. 10); \times , Moustafa-Moussa (Ref. 11); \bullet , van Eck and de Jongh (Ref. 12); (2^1S), Δ , Lassette *et al.* (Ref. 13); \times , Miller *et al.* (Ref. 14); \circ , Vriens *et al.* (Ref. 15).

Although large discrepancies do exist between the measured values, particularly for scattering at all angles for 50 eV, and for large-angle scattering, in general, the over-all agreement with theory is satisfactory only for scattering into small and intermediate angles $\leq 50^\circ$.

While the present treatment includes several important effects, e.g., the $2^1P - 2^1S$ coupling and the different relative local momenta in the various channels, it ignores both electron-exchange and that additional part of the polarization-interaction in the incident channel not included via the four-state treatment. Electron-exchange is mainly effective at the large scattering angles (i.e., close encounters) while the long-range polarization attraction mainly effects elastic scattering in the forward direction. For $e\text{-H}(1s)$ excitation at 50 eV, Chen *et al.*²³ have shown the exchange effect to be small for $\theta \leq 30^\circ$, an effect which is entirely dominated by the more important $2p\text{-}2s$ coupling included by Flannery and McCann,²¹ but neglected in the treatment of Chen *et al.*²³ According to Berrington *et al.*,³³ the neglect of the additional amount of polarization in the incident channel introduces relatively small error³³ for $e\text{-He}$ inelastic scattering in the forward direction. The present theoretical formulation is however amenable to the inclusion of both electron-exchange and the full polarization interaction.

However, both polarization in the incident channel and electron-exchange are significantly more important for elastic scattering than for inelastic scattering. Flannery and McCann²¹ have shown that inclusion of these effects causes an overall increase in the total cross section for $e\text{-H}(1s)$ elastic scattering, polarization being mainly responsible for enhancement in the forward direction while electron-exchange is needed to properly describe intermediate and large-angle scattering.

In Figs. 3(a)–3(b) are displayed the theoretical cross sections together with other theoretical values and the measurements for the total 2^1P excitations, Refs. 9–12, and for the 2^1S excitations, Refs. 13–15. Donaldson *et al.*⁹ normalized their experimental data to the Born cross sections at 2000 eV. As exhibited in the figures, the present theory represents considerable improvement over the Born B and the second-order potential treatments, although a great deal of scatter still exists in the experimental data. The theoretical prediction of a peak in the 2^1P excitation around 80 eV is consistent with the experimental data. The use of the less accurate wave functions (26)–(28) reduces the 2^1P and 2^1S (FE2) cross sections by 6 and 12%, respectively. Comparison of FE1 and S in Fig. 3(b) shows that the additional physical effects acknowledged by the present treatment for the 2^1S excitation has introduced closer accord with experiment, while comparison between FE2 and FE1 demonstrate the need for using wave functions as accurate as possible.

Note that Berrington *et al.*³³ obtained their total cross sections by integrating the computed transition probabilities over impact parameter ρ , a procedure which, in general, overestimates the cross section calculated by integrating (32) directly over all solid angles. It is worth noting that the present Hartree-Fock frozen-core set of wave functions are the most accurate employed to date in a collision description more refined than the Born approximation.

The Glauber cross sections^{35, 36} are in accord with the present FE1 results for impact energy $E_i > 100$ eV, for the 2^1P excitation, and $E_i > 200$, for the 2^1S excitation. The 2^1P wave function used³⁶ was the same as in FE1 while the 2^1S wave function³⁵ differed.

TABLE II. Inelastic cross sections (πa_0^2) for the process $e + \text{He}(1^1S) \rightarrow e + \text{He}(2^1P)$.

E_i (eV)	FE ^a			P^b	S^c	2^1P IP ^d	Born ^e
	2^1P_0	$2^1P_{\pm 1}$	2^1P				
50	0.0732	0.0600	0.1332	41.9	0.215	0.232	0.1694
80	0.0637	0.0750	0.1387	25.9	0.1596
100	0.0547	0.0759	0.1306	18.1	0.155	0.161	0.1485
200	0.0347	0.0671	0.1018	1.7	0.105	0.107	0.1069
300	0.0237	0.0577	0.0814	-9.8	0.0822	0.083	0.0841
400	0.0173	0.0500	0.0673	-18.2	0.0681	0.069	0.0700
500	0.0120	0.0466	0.0586	-32.0	0.0581	0.058	0.0602

^a Present four-channel eikonal treatment (refined set of wave functions, Eqs. (29a)–(29d).

^b Percentage polarization of emitted radiation.

^c Second-order potential method [Berrington *et al.* (Ref. 33)].

^d Impact-parameter method [Berrington *et al.* (Ref. 33)].

^e Born approximation [Bell *et al.* (Ref. 2)].

TABLE III. Inelastic cross sections (πa_0^2) for the process $e + \text{He}(1^1\text{S}) \rightarrow e + \text{He}(2^1\text{S})$.

E_i (eV)	FE ^a	S ^b	IP ^c	Born ^d
50	0.0215	0.0225	0.031	0.0390
80	0.0175	0.0270
100	0.0153	0.0154	0.0182	0.0222
200	0.0096	0.0093	0.0102	0.0118
300	0.0070	0.0066	0.0071	0.0080
400	0.0054	0.0052	0.0054	0.0060
500	0.0045	0.0042	0.0044	0.0048

^a Present four-channel treatment [refined set of wave functions, Eqs. (29a)–(29d)].

^b Second-order potential method [Berrington *et al.* (Ref. 33)].

^c Impact-parameter method [Berrington *et al.* (Ref. 33)].

^d Born approximation [Bell *et al.* (Ref. 2)].

In Tables II and III are displayed the actual numerical $2^1P_{0,1}$ and 2^1S excitation cross sections FE2, together with those given by Born's approximation B , the four-state impact treatment IP and the second-order potential method S . For the 2^1P excitation at impact energies $E_i \leq 200$ eV, IP and S are higher than B which at 50 eV is, in turn, higher than the present four-state eikonal results FE2 by 34%. For the 2^1S excitation all the cross sections are lower than Born's approximation and the use of the more accurate second set of wave functions (29a) has resulted in (fortuitous) closer accord with IP and S which were determined from wave functions (26)–(28). At 500 eV, the Born cross sections are 3 and 6% higher than the FE2 results for the 2^1P and 2^1S excitations, respectively.

Also tabulated in Table II is the percentage polarization P of the radiation emitted from the 2^1P level obtained from the formula^{3a}

$$P = 100(\sigma_0 - \sigma_1)/(\sigma_0 + \sigma_1), \quad (33)$$

where σ_m is the cross section for excitation of a particular substate m . Direct measurement of P for a vacuum uv emission is extremely difficult.

In conclusion, the theoretical acknowledgment of the different local wave numbers $\kappa_m(\vec{R})$ [Eq. (6)] of relative motion in various channels, the important $2^1P - 2^1S$ dipole coupling, the momentum parameter α [Eq. (11)], and various distortion effects within a multichannel eikonal treatment of atomic collisions has introduced closer accord with experiment for e -He collisions and, in particular, has produced a theoretical peak given also by Glauber's approximation but absent in previous theoretical treatments of the 2^1P cross section. The effect of including these physical effects can, however, be rendered null for the 2^1S excitation by an inappropriate choice of wave functions, i.e., the inclusion of refinements to the collision theory should be preferably accompanied, whenever possible, by a choice of accurate He wave functions. The present agreement for e -He($1s^2$) collisions taken together with the previous²¹ agreement for e -H($1s$) collisions is encouraging and represents the status of the present multichannel eikonal approximation. In particular, this theoretical model finds ready application over a large impact energy range to e -excited atom and e -complex atom collisions, instances for which application of the full wave treatment is prohibitively difficult.

*Research sponsored by the Air Force Aerospace Research Laboratories, Air Force Systems Command, U.S. Air Force Contract No. F33615-74-C-4003.

¹Y. K. Kim and M. Inokuti, Phys. Rev. **175**, 176 (1968).

²K. L. Bell, D. J. Kennedy, and A. E. Kingston, J. Phys. B **2**, 26 (1969).

³A. R. Holt, J. Hunt, and B. L. Moiseiwitsch, J. Phys. B **4**, 1318 (1971).

⁴J. R. Rice, D. G. Truhlar, D. C. Cartwright, and S. Trajmar, Phys. Rev. A **5**, 1 (1972).

⁵F. W. Byron, Phys. Rev. A **4**, 1907 (1971).

⁶V. Franco, Phys. Rev. A **8**, 2927 (1973).

⁷M. R. Flannery, J. Phys. B **3**, 306 (1970).

⁸K. A. Berrington, B. H. Bransden, and J. P. Coleman, J. Phys. B **6**, 436 (1973).

⁹F. G. Donaldson, M. A. Hender, and J. W. McConkey, J. Phys. B **5**, 1192 (1972).

¹⁰J. E. Jobe and R. M. St. John, Phys. Rev. **164**, 117 (1967).

¹¹H. R. Moustafa-Moussa, F. J. de Heer, and J. Schulten,

Physica (Utr.) **40**, 517 (1969).

¹²J. van Eck and J. P. de Jongh, Physica (Utr.) **47**, 141 (1970).

¹³E. N. Lassette, A. Skerbele, and M. A. Dillon, J. Chem. Phys. **52**, 2797 (1970).

¹⁴K. J. Miller, S. R. Mielczarek, and M. Krauss, J. Chem. Phys. **51**, 945 (1968).

¹⁵L. Vriens, C. E. Kuyatt, and S. R. Mielczarek, Phys. Rev. **165**, 7 (1968).

¹⁶J. A. Simpson, M. G. Menendez, and S. R. Mielczarek, Phys. Rev. **150**, 76 (1966).

¹⁷G. E. Chamberlain, S. R. Mielczarek, and C. E. Kuyatt, Phys. Rev. A **2**, 1905 (1970).

¹⁸G. B. Crooks and M. E. Rudd, Ph.D. thesis (University of Nebraska, 1972) (unpublished).

¹⁹D. G. Truhlar, J. K. Rice, A. Kuppermann, S. Trajmar, and D. C. Cartwright, Phys. Rev. A **5**, 762 (1972).

²⁰M. R. Flannery and K. J. McCann, J. Phys. B **7**, L223 (1974).

²¹M. R. Flannery and K. J. McCann, J. Phys. B (to be

- published).
- ²²R. J. Glauber, in *Lectures in Theoretical Physics*, edited by W. E. Brittin *et al.* (Interscience, New York, 1959), Vol. 1, p. 369.
 - ²³J. C. Y. Chen, C. J. Joachain, and K. M. Watson, *Phys. Rev. A* **5**, 2460 (1972).
 - ²⁴B. H. Bransden and J. P. Coleman, *J. Phys. B* **5**, 537 (1972).
 - ²⁵R. H. Shields and J. L. Peacher, *Phys. Rev. A* **9**, 743 (1974).
 - ²⁶M. R. Flannery and K. J. McCann, *Phys. Rev. A* **8**, 2915 (1973).
 - ²⁷M. R. Flannery and K. J. McCann, *Phys. Rev. A* **10**, 1947 (1974); M. R. Flannery and K. J. McCann, *J. Phys. B* **7**, 840, 1349, 1558 (1974).
 - ²⁸F. W. Byron and C. J. Joachain, *Phys. Rev.* **146**, 1 (1966).
 - ²⁹L. Goldberg and A. M. Clogston, *Phys. Rev.* **56**, 696 (1939).
 - ³⁰M. Cohen and R. P. McEachran, *Proc. Phys. Soc. Lond.* **92**, 37 (1967). Note that hydrogenic orbitals contain $L_{n+1}^{2l+1}(2/nr)$.
 - ³¹R. P. McEachran and M. Cohen, *J. Phys. B* **2**, 1271 (1969).
 - ³²D. S. F. Crothers and R. P. McEachran, *J. Phys. B* **3**, 976 (1970).
 - ³³K. A. Berrington, B. H. Bransden, and J. P. Coleman, *J. Phys. B* **6**, 436 (1973).
 - ³⁴A. C. Yates and A. Tenney, *Phys. Rev. A* **6**, 1451 (1972).
 - ³⁵F. T. Chan and S. T. Chen, *Phys. Rev. A* **8**, 2191 (1973).
 - ³⁶F. T. Chan and S. T. Chen, *Phys. Rev. A* **9**, 2393 (1974).
 - ³⁷V. Franco, *Phys. Rev. A* **8**, 2927 (1974).
 - ³⁸I. C. Percival and M. J. Seaton, *Philos. Trans. R. Soc. Lond. A* **251**, 113 (1958).

4.4 A Pseudostate Multichannel Eikonal Study of e-H(1s)

Inelastic Collisions:

LETTER TO THE EDITOR

A pseudostate multichannel eikonal study of e-H(1s) inelastic collisions

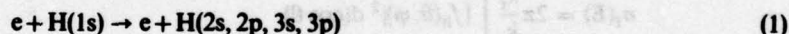
M R Flannery and K J McCann

School of Physics, Georgia Institute of Technology, Atlanta, 30332, USA

Received 7 October 1974

Abstract. The effect of including the $3\bar{s}$ and $3\bar{p}$ pseudostates is examined for the 2s and 2p excitation of atomic hydrogen by incident electrons with energy E (eV) in the range $16.5 \leq E \leq 200$. The 2s excitation is most strongly affected and displays a behaviour consistent with measurement and refined theories which include polarization. The 2p excitation agrees particularly well with the full quantal pseudostate treatment and with experiment. A seven-channel (1s, 2s, 2p, 3s, 3p) treatment is also performed, and the resulting 2s and 2p cross sections lie closer to those of the pseudostate description than to the four-channel (1s, 2s, 2p) results, as expected.

In this letter, the multichannel eikonal approach (Flannery and McCann 1975) is examined for the excitations,



in which the $3\bar{s}$ and $3\bar{p}$ pseudostates of Burke and Webb (1970) are explicitly acknowledged. In this treatment, the amplitude for scattering with final relative momentum k_f in direction (θ, ϕ) with respect to polar axis along the direction of incident relative momentum k_i is, in the CM frame,

$$f_{if}(\theta, \phi) = -i^{A+1} \int_0^\infty J_A(K'\rho) [I_1(\rho, \theta) - iI_2(\rho, \theta)] \rho d\rho \quad (2)$$

where J_A are Bessel functions of integral order, and where K' is the XY component $k_f \sin \theta$ of the momentum change $\mathbf{K} = \mathbf{k}_i - \mathbf{k}_f$. The collision functions

$$I_1(\rho, \theta; \alpha) = \int_{-\infty}^\infty \kappa_f(\rho, Z) \left(\frac{\partial C_f(\rho, Z)}{\partial Z} \right) \exp(i\alpha Z) dZ \quad (3)$$

and

$$I_2(\rho, \theta; \alpha) = \int_{-\infty}^\infty \left(\kappa_f(\kappa_f - k_f) + \frac{\mu}{\hbar^2} V_{ff} \right) C_f(\rho, Z) \exp(i\alpha Z) dZ \quad (4)$$

contain a dependence on the scattering angle θ via

$$\alpha = k_f(1 - \cos \theta) = 2k_f \sin^2(\frac{1}{2}\theta) \quad (5)$$

the difference between the Z component of the momentum change \mathbf{K} and the minimum change $k_i - k_f$ in the collision. The coupling amplitudes C_f are solutions of the following

set of N coupled differential equations

$$\begin{aligned} \frac{i\hbar^2}{\mu} \kappa_f(\rho, Z) \frac{\partial C_f(\rho, Z)}{\partial Z} + \left(-\frac{\hbar^2}{\mu} \kappa_f(\kappa_f - k_f) + V_{ff}(\rho, Z) \right) C_f(\rho, Z) \\ = \sum_{n=1}^N C_n(\rho, Z) V_{fn}(\rho, Z) \exp i(k_n - k_f)Z, \quad f = 1, 2, \dots, N \end{aligned} \quad (6)$$

solved subject to the boundary condition $C_f(\rho, -\infty) = \delta_{if}$. The local wavenumber of relative motion at separation $R \equiv (R, \Theta, \Phi) \equiv (\rho, \Phi, Z)$ is

$$\kappa_n(R) = \left(k_n^2 - \frac{2\mu}{\hbar^2} V_{nn}(R) \right)^{1/2}$$

where the interaction matrix elements

$$V_{mn}(R) = \langle \phi_n(r) | V(r, R) | \phi_m(r) \rangle$$

connect the various electronic states $\phi_n(r)$ describing the isolated systems and where $V(r, R)$ is the instantaneous electrostatic interaction.

The present description has automatically included an infinite number of partial waves of relative motion which are distorted by the static interactions associated with the various channels included in the basis set expansion and which in turn are coupled to the internal electronic motions via the amplitudes C_f in (6). Moreover in contrast to previous semiclassical descriptions† explicit account is taken of the variation during the collision of the different local momenta of relative motion in each channel.

Close-coupling calculations have been performed by using (2)–(6) in which the $1s$, $2s$, $2p_{0,\pm 1}$ states of atomic hydrogen are included together (a) with the $3s$ and $3p$ pseudostates of Burke and Webb (1970) introduced to acknowledge couplings to all higher open channels and (b) with the actual $3s$ and $3p$ atomic states. In tables 1 and 2 are displayed total excitation cross sections

$$\sigma_f(E) = 2\pi \frac{k_f}{k_i} \int |f_{if}(\theta, \phi)|^2 d(\cos \theta) \quad (7)$$

for processes (1) at incident electron energy E (eV). Previous four-channel results F for the $2s$ and $2p$ excitations (Flannery and McCann 1975) converge from above and below

Table 1. Total cross sections (πa_0^2) given by a four-channel treatment F , and two seven-channel treatments (P and R , with and without pseudostates, respectively) of $e + H(1s) \rightarrow e + H(2s \text{ or } 2p)$ at electron energy E (eV).

E	nl	$2s$			$2p_0$	$2p_{\pm 1}$	$2p$		
		F	P	R	P	P	F	P	R
16.5	—	0.151	0.112	0.405	0.125	—	0.530	0.600	
20	0.145	0.127	0.124	0.481	0.224	0.720	0.705	0.730	
30	0.124	0.095	0.115	0.485	0.379	0.836	0.864	0.863	
50	0.090	0.074	0.088	0.421	0.466	0.865	0.887	0.881	
100	0.052	0.048	0.052	0.227	0.421	0.629	0.648	0.645	
200	0.028	0.027	0.028	0.120	0.338	0.453	0.458	0.454	

† Compare Flannery and McCann (1974) when $I_2 = 0$, $\kappa_f = k_f$ in (3) and (6) and the coefficient of C_f in the left-hand side of (6) is neglected, and also Bransden (1970).

Table 2. Total cross sections ($0.01 \pi a_0^2$) given by seven-channel treatment of $e + H(1s) \rightarrow e + H(nl)$; $nl = 3s, 3p_0, 3p_{\pm 1}$, at electron energy E (eV).

E	$3s$	$3p_0$	$3p_{\pm 1}$	$3p$
16.5	1.41	5.04	2.19	7.23
20	1.78	6.67	4.23	10.9
30	1.87	7.25	7.52	14.8
50	1.46	5.65	8.96	14.6
100	0.90	3.13	8.00	11.1
200	0.50	1.61	5.81	7.42

respectively onto the pure seven-channel treatment R . Addition of the pseudostates in P considerably distorts the shape and changes the magnitude of the $2s$ excitation while σ_{2p} remains relatively unaffected. Replacing the pseudostates by the real $3s$ and $3p$ states in general yields cross sections which lie between F and P although closer to P , as expected.

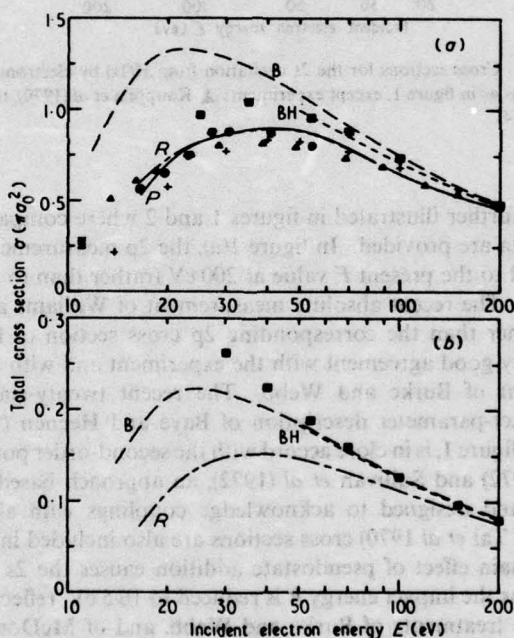


Figure 1. Cross sections (πa_0^2) for (a) the $2p$ and (b) the $3p$ excitations from $H(1s)$ by electrons with energy E (eV). P and R are the present seven-channel results with pseudo and real $3s$ and $3p$ states respectively. Experiment: Δ (Long *et al* 1968), \circ (Williams and Willis 1974); theory: \bullet pseudostate (Burke and Webb 1970), second-order potential method: \blacksquare (a) four-channel approximation (Sullivan *et al* 1972), (b) one-channel approximation (Bransden *et al* 1972), $+$ Glauber approximation (Tai *et al* 1970), BH Baye and Heenen (1974), B Born approximation.

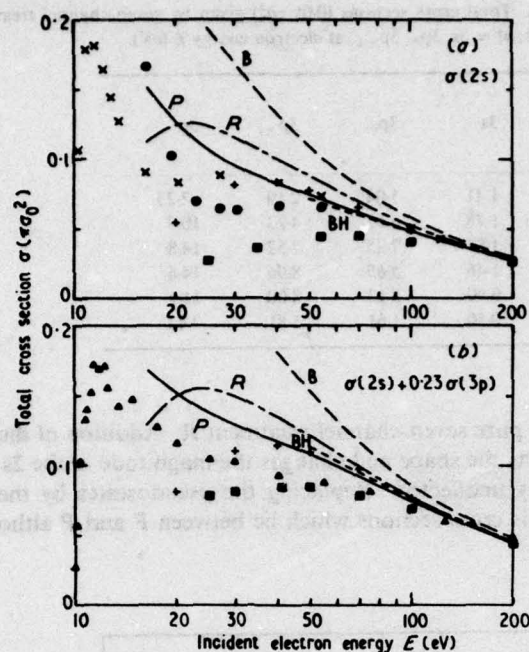


Figure 2. Cross sections for the 2s excitation from H(1s) by electrons with energy E (eV). Notations as in figure 1, except experiment: Δ Kauppila *et al* (1970), theory: \times McDowell *et al* (1974).

These effects are further illustrated in figures 1 and 2 where comparison theoretical and experimental data are provided. In figure 1(a), the 2p measurements of Long *et al* (1968) are normalized to the present F value at 200 eV (rather than to the Born section which is 7% higher). The recent absolute measurement of Williams and Willis (1974) at 11 eV is 13% higher than the corresponding 2p cross section of Long *et al*. The present σ_{2p} are in very good agreement with the experiment and with the fully quantal pseudostate treatment of Burke and Webb. The recent twenty-state second-order diagonalization impact-parameter description of Baye and Heenen (1974) for the 2p and 3p excitations, in figure 1, is in close accord with the second-order potential treatment of Bransden *et al* (1972) and Sullivan *et al* (1972), an approach based on the impact-parameter method, and designed to acknowledge couplings with all excited states. Born and Glauber (cf Tai *et al* 1970) cross sections are also included in the figures.

In figure 2, the main effect of pseudostate addition causes the 2s cross section to continue its increase as the impact energy E is reduced to 16.5 eV, reflecting a behaviour also exhibited by the treatments of Burke and Webb, and of McDowell *et al* (1973). This behaviour is real and is consistent with the measurements shown in figure 2(b) of Kauppila *et al* (1970) who estimate a cascade contribution of $0.23 \sigma_{3p}$ to the observed 2s excitation. The present 3s cross sections are shown in figure 3 together with other theoretical values, for comparison.

Rather than presenting all the differential cross sections, from which σ_i in (7) were obtained, it suffices to report that the 2p scattering did not depart appreciably from the earlier study (Flannery and McCann 1975). In figure 4, the pseudostates reduce the

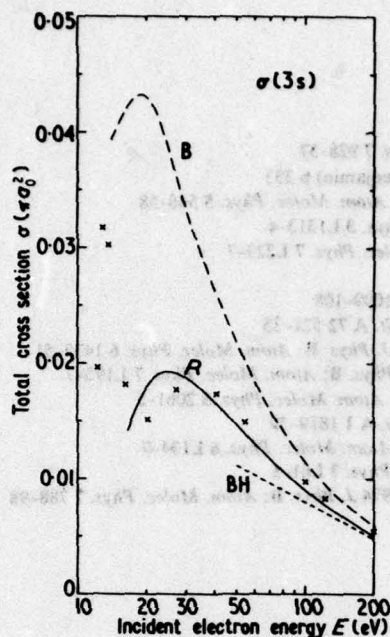


Figure 3. Cross sections (πa_0^2) for the 3s excitation from H(1s) by electrons with energy E (eV). Notation as in figure 2 with \times , McDowell *et al* (1973).

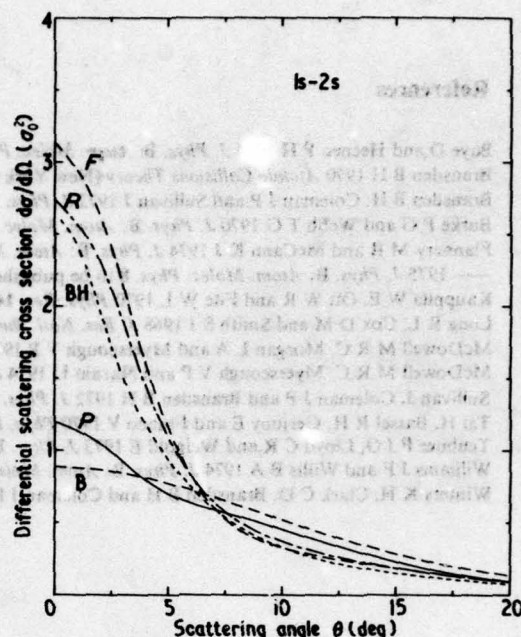


Figure 4. Differential cross sections for 2s excitation from H(1s) at 100 eV impact energy. Notation as in figure 1 with F : four-channel treatment (Flannery and McCann 1975).

2s scattering at 100 eV in the forward direction and enhance the scattering through larger angles, the net result being a slight increase in the total cross section at 100 eV. This behaviour becomes increasingly amplified as the impact energy E is reduced and figures similar to 4 are available upon request.

In contrast, pseudostates increase the four-channel elastic scattering in the forward direction as expected since the potential appropriate to the distant elastic encounters becomes more long range. Hence, agreement with the experiment of Teubner *et al* (1973) became somewhat improved for small-angle scattering. However, because of the neglect of electron exchange needed for a proper description of closer encounters, the present treatment still failed (Flannery and McCann 1975) to provide a good description (cf Winters *et al* 1974) of elastic scattering through the larger scattering angles.

In conclusion, addition of pseudostates does improve the agreement for inelastic collisions of the present multichannel eikonal approach with experiment and with other refined theories which include polarization effects. In particular, the continuing rise of σ_{2s} as E is reduced to below about 20 eV is consistent with experiment (cf figure 2b), although, at these low energies, electron exchange is important and could cause the required reduction needed to improve accord between the present approach and experiment (cf figure 2b).

This research was sponsored by the Air Force Aerospace Research Laboratories, Air Force Systems Command, United States Air Force, Contract F 33615-74-C-4003.

References

- Baye D and Heenen P H 1974 *J. Phys. B: Atom. Molec. Phys.* **7** 928-37
 Bransden B H 1970 *Atomic Collisions Theory* (New York: Benjamin) p 333
 Bransden B H, Coleman J P and Sullivan J 1972 *J. Phys. B: Atom. Molec. Phys.* **5** 546-58
 Burke P G and Webb T G 1970 *J. Phys. B: Atom. Molec. Phys.* **3** L1313-4
 Flannery M R and McCann K J 1974 *J. Phys. B: Atom. Molec. Phys.* **7** L223-7
 — 1975 *J. Phys. B: Atom. Molec. Phys.* **8** to be published
 Kauppi W E, Ott W R and Fite W L 1970 *Phys. Rev.* **141** 1099-108
 Long R L, Cox D M and Smith S J 1968 *J. Res. Natl. Bur. St. A* **72** 521-35
 McDowell M R C, Morgan L A and Myerscough V P 1973 *J. Phys. B: Atom. Molec. Phys.* **6** 1435-51
 McDowell M R C, Myerscough V P and Narain U 1974 *J. Phys. B: Atom. Molec. Phys.* **7** L195-7
 Sullivan J, Coleman J P and Bransden B H 1972 *J. Phys. B: Atom. Molec. Phys.* **5** 2061-5
 Tai H, Bassel R H, Gerjuoy E and Franco V 1970 *Phys. Rev. A* **1** 1819-39
 Teubner P J O, Lloyd C R and Weigold E 1973 *J. Phys. B: Atom. Molec. Phys.* **6** L134-7
 Williams J F and Willis B A 1974 *J. Phys. B: Atom. Molec. Phys.* **7** L61-5
 Winters K H, Clark C D, Bransden B H and Coleman J P 1974 *J. Phys. B: Atom. Molec. Phys.* **7** 788-98

4.5 A Ten-Channel Eikonal Treatment of Differential and Integral Cross Sections and of the (λ, χ) Parameters for the $n = 2$ and 3 Excitations of Helium by Electron Impact

A ten-channel eikonal treatment of differential and integral cross sections and of the (λ, χ) parameters for the $n = 2$ and 3 excitations of helium by electron impact

M R Flannery and K J McCann

School of Physics, Georgia Institute of Technology, Atlanta, Georgia 30332, USA

Received 30 January 1975

Abstract. A ten-channel eikonal treatment of the $n = 2$ and 3 collisional excitations of helium by incident electrons with energy E (eV) in the range $40 \leq E \leq 500$ is performed. Differential and integral inelastic cross sections are obtained, together with theoretical predictions of the (λ, χ) parameters which provide, as functions of scattering angle θ and E , the orientation and alignment vectors and the circular polarization fraction of the radiation emitted from the n^1P levels. The results are in satisfactory agreement with recent measurements.

1. Introduction

The study of angular correlations between the emitted photon and scattered electron in inelastic electron-atom collisions has permitted the measurement of complex transition amplitudes and atomic orientation and alignment vectors (Macek and Jaecks 1971, Fano and Macek 1973) from parameters written as λ and χ by Eminyan *et al* (1974). These collision parameters λ and χ are more basic than the total cross section σ , differential cross section $d\sigma/d\Omega$, or even percentage polarization P of the emitted radiation. They have generally been 'hidden' in most refined theoretical calculations of the collision and 'lost' in experiments designed to measure σ and P alone. By the use of delayed coincidence techniques, Eminyan *et al* (1974) have conducted striking experiments from which this basic information on λ and χ can be extracted without the need for normalization.

This work, together with the measured $d\sigma/d\Omega$ of eg Trajmar (1973) and σ of eg Donaldson *et al* (1972), all provide excellent tests of the various theoretical models recently developed for electron-atom collisions at intermediate impact energies E (see the review of McDowell 1975). For instance, in spite of its apparent success for σ and $d\sigma/d\Omega$, the Glauber approximation exhibits serious deficiencies in its predictions of λ and χ . These shortcomings are directly attributable to gross simplifications such as the assumption of a heavy particle and high-energy limit in the collision dynamics.

In this paper, the multichannel eikonal approach of Flannery and McCann (1974), which pays particular attention to the collision dynamics, is further tested by examining the variation of λ , χ , and $d\sigma/d\Omega$ with θ and E and of σ and P with E for the inelastic collisions,

$$e + \text{He}(1^1\text{S}) \rightarrow e + \text{He}(n^1L), \quad n = 2, 3; L = \text{S, P, D.} \quad (1)$$

All ten channels of (1) will be closely-coupled and the accurate frozen-core Hartree-Fock wavefunctions of Cohen and McEachran (1974) will be used throughout.

2. Theory

2.1. Basic formulae

The key quantity sought by theoretical descriptions of atomic collisions is $f_{if}(\theta)$, the complex scattering amplitude as a function of scattering angle θ (in the CM frame) and of impact energy E for various $i \rightarrow f$ transitions occurring in the collision species with initial and final relative momenta k_i and k_f respectively. For a non-degenerate initial state i , experiment yields (i) the differential cross section

$$\frac{d\sigma}{d\Omega} = \frac{k_f}{k_i} \sum_{M=-L}^L |f_{if}^{(M)}(\theta)|^2 \quad (2)$$

summed over all degenerate magnetic substates M of the final state f of the target with angular momentum L , (ii) the associated total cross section σ and (iii) the polarization fraction P which determines the relative contribution arising from each M to the total σ . In a recent experiment on the 1^1S-2^1P collisional excitation of He by e, Emynyan *et al* (1974) measured, as functions of θ and E , the additional parameters

$$\lambda = \frac{|f_{if}^{(0)}|^2}{|f_{if}^{(0)}|^2 + 2|f_{if}^{(1)}|^2} \quad (3)$$

and

$$|\chi| = |\alpha_1 - \alpha_0| \quad (4)$$

where α_M is the phase of the scattering amplitude

$$f_{if}^{(M)} = |f_{if}^{(M)}| \exp(i\alpha_M) \quad (5)$$

and where the axis of quantization is taken along the incident Z direction defined by \hat{k}_i .

The quantity λ is the relative contribution arising from the $M = 0$ substate to $(d\sigma/d\Omega)$ in (2), while χ is a measure of the coherence between the excitations of the $M = 0$ and 1 substates. A related quantity is the circular polarization fraction of radiation emitted perpendicular to the (assumed) XZ plane of the scattering,

$$\Pi = -2[\lambda(1-\lambda)]^{1/2} \sin \chi \equiv \overline{\Delta L}_Y \equiv L(L+1)O_1^{\text{col}} \quad (6)$$

where $\overline{\Delta L}_Y$ is the expectation value of the angular momentum transferred in the Y direction during the collision and where O_1^{col} is the orientation vector (cf Fano and Macek 1973, Emynyan *et al* 1974).

The overall accuracy of a particular theoretical collision model can therefore be assessed by the closeness between theoretical calculations and experimental measurements of the three independent quantities $d\sigma/d\Omega$, λ and χ as functions of θ and E . For example, the Born approximation predicts that $\lambda_B = \cos^2(\hat{K} \cdot \hat{k}_i)$ for S-P transitions, since $f_{if}^{(M)} \propto |Y_{1M}(\hat{K})|^2$ is a function only of the momentum change

$$\mathbf{K} \equiv (\mathbf{K}, \Theta, \Phi) = \mathbf{k}_i - \mathbf{k}_f,$$

and that $\chi_B = 0$, since $f_{if}^{(M)}$ is always real. The Π polarization is therefore zero. The prescription of Glauber (1959) involved setting $\mathbf{K} \cdot \mathbf{k}_i = 0$ so as to ease subsequent calculation with the result that $f_{if}^{(0)}$ and hence λ_G vanish. Also $\alpha_{\pm 1} = \pm i\Phi$ and so $\chi_G = 0$. By adopting a change of Z axis, however, along $\frac{1}{2}(\mathbf{k}_i + \mathbf{k}_f)$ such that \mathbf{K}_Z in this direction

is identically zero and by following the analysis of Gerjuoy *et al* (1972), then it can be shown that, for S-P transitions, $\lambda_G = \cos^2(\hat{K} \cdot \hat{k}_i)$ in harmony with the first Born approximation. Therefore in spite of its relatively better performance in evaluating both σ and $d\sigma/d\Omega$, the Glauber approximation is at least worse or at best equal to the Born predictions of λ and χ . Moreover, with no simplifying assumptions made to the original six-dimensional eikonal integral, Gau and Macek (1974) have recently shown that non-zero orientation and alignment parameters can be predicted within the Glauber framework.

In the present investigation, the multichannel eikonal description (Flannery and McCann 1974) is applied to the examination of σ , $d\sigma/d\Omega$, P , λ and χ for the $n = 2$ and 3 excitations of helium by electron impact. In this treatment, the complex amplitude for scattering with final relative momentum k_f in direction (θ, ϕ) with respect to the polar axis along the direction of incident relative momentum k_i is, in the CM frame,

$$f_{if}(\theta, \phi) = -i^{\Delta+1} \int_0^\infty J_\Delta(K'\rho) [I_1(\rho, \theta) - iI_2(\rho, \theta)] \rho d\rho \quad (7)$$

where J_Δ are Bessel functions of integral order $(M_i - M_f)$ and where K' is the XY component $k_i \sin \theta$ of the momentum change $K = k_i - k_f$. The collision functions

$$I_1(\rho, \theta; \alpha) = \int_{-\infty}^\infty \kappa_f(\rho, Z) \left(\frac{\partial C_f(\rho, Z)}{\partial Z} \right) \exp(i\alpha Z) dZ \quad (8)$$

and

$$I_2(\rho, \theta; \alpha) = \int_{-\infty}^\infty \left(\kappa_f(\kappa_f - k_f) + \frac{\mu}{\hbar^2} V_{ff} \right) C_f(\rho, Z) \exp(i\alpha Z) dZ \quad (9)$$

contain a dependence on the scattering angle θ via

$$\alpha = k_f(1 - \cos \theta) = 2k_f \sin^2 \frac{1}{2}\theta \quad (10)$$

the difference between the Z component of the momentum change K and the minimum change $k_i - k_f$ in the collision. The coupling amplitudes C_f are solutions of the following set of N coupled differential equations

$$\begin{aligned} & i\hbar^2 \kappa_f(\rho, Z) \frac{\partial C_f(\rho, Z)}{\partial Z} + \left(-\frac{\hbar^2}{\mu} \kappa_f(\kappa_f - k_f) + V_{ff}(\rho, Z) \right) C_f(\rho, Z) \\ &= \sum_{n=1}^N C_n(\rho, Z) V_{fn}(\rho, Z) \exp i(k_n - k_f)Z, \quad f = 1, 2, \dots, N \end{aligned} \quad (11)$$

solved subject to the asymptotic boundary condition $C_f(\rho, -\infty) = \delta_{ff}$. The local wave-number of relative motion at separation $R \equiv (R, \Theta, \Phi) \equiv (\rho, \Phi, Z)$ is

$$\kappa_n(R) = \left(k_n^2 - \frac{2\mu}{\hbar^2} V_{nn}(R) \right)^{1/2}$$

where the interaction matrix elements

$$V_{nm}(R) = \langle \psi_n(r_1, r_2) | V(r_1, r_2, R) | \psi_m(r_1, r_2) \rangle$$

connect the various electronic states $\psi_n(r_1, r_2)$ of atomic helium and where V is the instantaneous e-He electrostatic interaction. In the uncoupled limit, the elastic scattering in each channel is described by the eikonal approximation to scattering by the

corresponding static (diagonal) interaction $V_{nn}(R)$ rather than by the instantaneous interaction $V(R, r_1, r_2)$, (as is the case in Glauber's treatment of elastic scattering). It can be shown directly that, at high energies, the basic equations satisfy the optical theorem,

$$\sum_i \sigma_{it} = \frac{4\pi}{k_i} \text{Im } f_{ii}(0) \equiv 4\pi \int_0^\infty (\text{Re } C_i - 1) \rho \, d\rho = 2\pi \sum_i \int_0^\infty |C_i - \delta_{ii}|^2 \rho \, d\rho. \quad (12)$$

Verification, however, for all impact energies is not as straightforward and would require explicit numerical evaluation of all the cross sections.

2.2. Wavefunctions and interactions

All ten channels of (1) will be closely coupled. We adopt the frozen-core Hartree-Fock $n = 1-3$ helium wavefunctions of Cohen and McEachran (1974) in the form

$$\psi_{1s,nlm}(r_1, r_2) = N_{nl} [\phi_0(r_1)\phi_{nlm}(r_2) + \phi_0(r_2)\phi_{nlm}(r_1)] \quad (13)$$

in which the frozen, inner 1s orbital is (in au)

$$\phi_0(r) = 2^{5/2} e^{-2r} Y_{00}(\theta) \quad (14)$$

and the orbital for the second electron in state (nlm) is rewritten (in au) as

$$\phi_{nlm}(r) = \sum_{N=1}^{J-1} B_N^{nl} e^{-\beta r} r^{N-1} Y_{lm}(\theta), \quad \beta = \frac{2}{n} \quad (15)$$

where J is the maximum number of linear coefficients B_N^{nl} given in terms of Cohen and McEachran's original parameters a_j^{nl} by

$$B_N^{nl} = \sum_{j=N+1}^J \frac{(-1)^{N-l} 2^l (j!)^2 (2\beta)^{N-l-1}}{(N-l-1)!(j-N-l)!(N+l)!} a_j^{nl}, \quad N = 1, 2, \dots, J. \quad (16)$$

The above transformation (16) facilitates subsequent evaluation of the e-He interaction matrix elements

$$V_{ij}(R) = \langle \phi_i(r_1, r_2) | -\frac{2}{R} + \frac{1}{|R-r_1|} + \frac{1}{|R-r_2|} | \phi_j(r_1, r_2) \rangle \quad (17)$$

as analytical functions of R such that the exponential and linear parameters α_i and a_i in the resulting expression,

$$V_{nlm,n'l'm'}(R) = \sum_{L=|l-l'|}^{(l+l')} \left[-\frac{a_{-l}}{R^l} + \sum_{i=1}^2 e^{-\alpha_i R} \sum_{s=-l}^{16} a_s R^s \right] Y_{LM}(R) \quad (18)$$

can be determined exactly and automatically.

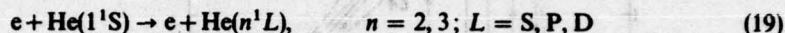
2.3. Test of wavefunctions

Theoretical refinement to the collision model must be accompanied whenever possible by accurate atomic wavefunctions since the goodness thereby introduced by the former may be completely swamped by an inappropriate choice of wavefunctions (cf McCann and Flannery 1974). The overall reliability of the present set of wavefunctions has already been gauged by examination of associated eigenenergies and cusp conditions (Cohen and McEachran 1967, McEachran and Cohen 1969). In this investigation, the present set of wavefunctions did reproduce the accurate Born results of Bell *et al* (1969)

for the $n = 2$ and 3 excitations of He. However, it is worth noting that similar reproductions were achieved for the $n = 4-6$ He excitations only when one adopted additional linear parameters a_j^l , which were not contained in the above cited references (so as to economize in table presentation), but which were obtained from Cohen and McEachran (1974) privately. Therefore, in all the present calculations we have employed the twenty-parameter functions provided by Cohen and McEachran (1974). The non-orthogonality integrals $\langle \Psi_i | \Psi_j \rangle$ were found to be negligible for all channels.

3. Results and discussion

A ten-channel eikonal description (7)–(11) was carried out for the inelastic collisions



and the parameters $d\sigma/d\Omega$, λ and χ determined from (2)–(5) as functions of scattering angle θ for various impact energies $E(\text{eV})$ in the range $40 \leq E \leq 500$. A four-channel ($1^1\text{S}, 3^1\text{S}, 3^1\text{P}_0, \pm 1$) treatment was also performed.

3.1. Total cross sections and polarization fractions

Total excitation cross sections

$$\sigma(E) = 2\pi \frac{k_f}{k_i} \int_0^\pi |f_{if}(\theta)|^2 d(\cos \theta) \quad (20)$$

are displayed in figures 1–4 for each transition in (19), together with comparison experimental and theoretical data. These figures include results from the following recent theories:

- (i) The second-order potential treatments (S) of Berrington *et al* (1973) for the $n = 2$ excitations and of Bransden and Issa (1975) for the $n = 3$ excitations,
- (ii) The second-order diagonalization procedure of Baye and Heenen (1974),
- (iii) The first-order many-body approach (M) of Thomas *et al* (1974) for the $n = 2$ excitations,
- (iv) A four-channel eikonal (E4) study (McCann and Flannery 1974) of the $n = 2$ excitations,
- (v) The Glauber treatment of Chan and Chen (1973, 1974a, b) for the $n = 2$ and 3^1P excitations,
- (vi) The Born results (B) of Bell *et al* (1969).

The experimental data are taken from Brongersma *et al* (1972), Trajmar (1973), Rice *et al* (1972), Vriens *et al* (1968), Miller *et al* (1968), Donaldson *et al* (1972), de Jongh and van Eck (1971) and Moustafa Moussa *et al* (1969). Since figures 1–4 provide a rather detailed comparison, only a few comments are needed. In general, the present ten-channel results (E10) are in good accord with experiment down to 50 eV, below which the scatter in the various measurements preclude any definition. Couplings with the $n = 3$ channels are very important for the 2^1S excitation at all energies, and couplings with the $n = 2$ channels influence the 3^1S excitation appreciably, although the corresponding 2^1P and the 3^1P cross sections are essentially left unaffected. The 2^1P distorted Born wave results (not shown) of Madison and Shelton (1973) are indistinguishable from the present E10 curve. Cross sections in excess of the Born values are obtained

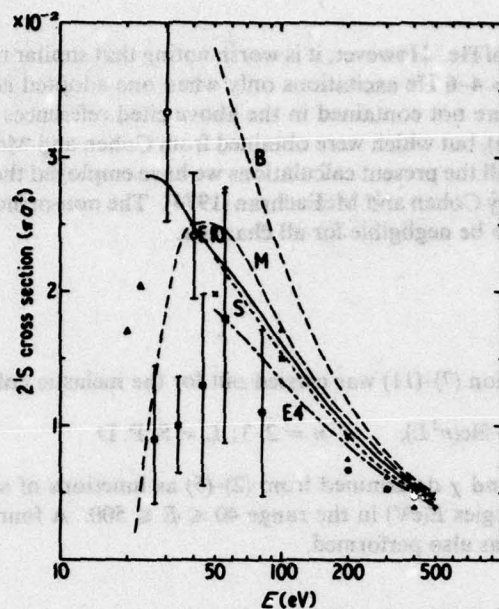


Figure 1. Total cross section for the $1'S-2'S$ transition in He by collision with electrons of energy E (eV). Theory: E10, E4, present ten- and four-channel eikonal treatments, respectively; S, second-order potential method with simple set of wavefunctions (Berrington *et al* 1973); M, first-order many-body approach (Thomas *et al* 1974); B, Born approximation (Bell *et al* 1969); \times , second-order diagonalization method (Baye and Heenen 1974); + Glauber approximation (Chan and Chen 1973, 1974a). Experiment: \blacksquare , Rice *et al* (1972); \blacktriangle , Miller *et al* (1969); \bullet , Vriens *et al* (1968); \circ , Trajmar (1973); \triangle , Brongersma *et al* (1972).

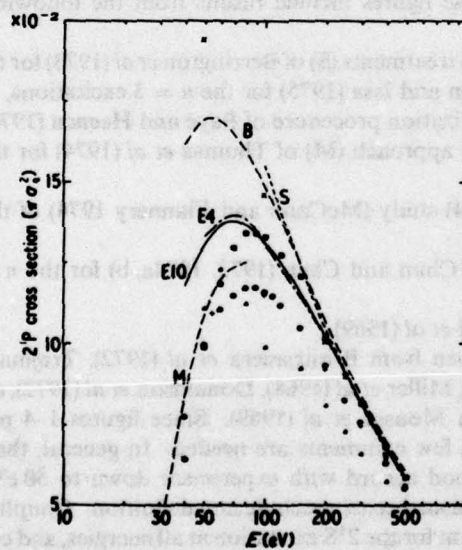


Figure 2. Total cross section for the $1'S-2'P$ transition in He by collision with electrons of energy E (eV). Theory: exactly as in figure 1. Experiment: \bullet , Donaldson *et al* (1972); \blacksquare , de Jongh and van Eck (1971); \triangle , Moustafa Mousse *et al* (1969).

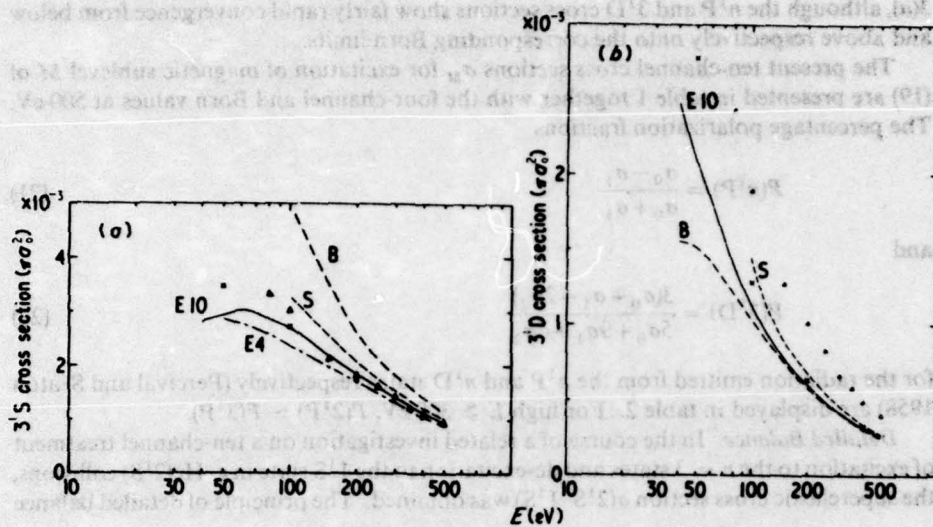


Figure 3. Total cross section for excitation of the (a) 3^1S , (b) 3^1D states of He by collision with electrons of energy E (eV). Theory: as in figure 1 except S, second-order potential method (Bransden and Issa 1975). Experiment: Δ , Moustafa Moussa *et al* (1969).

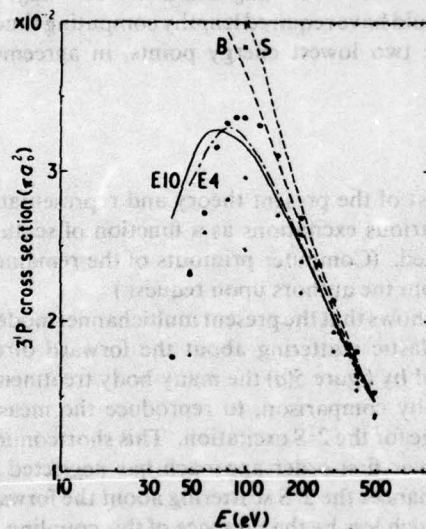


Figure 4. Total cross section for the 1^1S-3^1P transition in He by collision with electrons of energy E (eV). The symbols are as in figure 3.

only for the 3^1D excitation in figure 3(b), when the 3^1P-3^1D dipole coupling becomes extremely important and causes the large enhancement at the lower energies. Note that the Born limit remains unattained even at 500 eV for the n^1S excitations in figures 1 and

3(a), although the n^1P and 3^1D cross sections show fairly rapid convergence from below and above respectively onto the corresponding Born limits.

The present ten-channel cross sections σ_M for excitation of magnetic sublevel M of (19) are presented in table 1 together with the four-channel and Born values at 500 eV. The percentage polarization fractions

$$P(n^1P) = \frac{\sigma_0 - \sigma_1}{\sigma_0 + \sigma_1} \quad (21)$$

and

$$P(3^1D) = \frac{3(\sigma_0 + \sigma_1 - 2\sigma_2)}{5\sigma_0 + 9\sigma_1 + 6\sigma_2} \quad (22)$$

for the radiation emitted from the n^1P and n^1D states respectively (Percival and Seaton 1958) are displayed in table 2. For high $E \geq 300$ eV, $P(2^1P) \simeq P(3^1P)$.

Detailed Balance. In the course of a related investigation on a ten-channel treatment of excitation to the $n = 3$ states and de-excitation to the 1^1S state in e-He(2^1S) collisions, the superelastic cross section $\sigma(2^1S-1^1S)$ was obtained. The principle of detailed balance

$$E_i \sigma_{if}(2^1S-1^1S; E_i) = E_f \sigma_{if}(1^1S-2^1S; E_i)$$

between the excitation and de-excitation cross sections evaluated at the energies E_i and E_f respectively, corresponding to the appropriate channel, was found to be closely satisfied numerically. Moreover, this procedure provided the following additional two cross sections for the 1^1S-2^1S excitation: $2.87 \times 10^{-2} \pi a_0^2$ and $2.82 \times 10^{-2} \pi a_0^2$, $E_i = 25.6$ eV and 30.6 eV, respectively, which would have required lengthy computing time if calculated directly. Figure 1 includes these two lowest energy points, in agreement with the measurements of Trajmar (1973).

3.2. Differential cross sections

These provide a more sensitive test of the present theory and representative cases are displayed in figures 5-7 for the various excitations as a function of scattering angle θ at two incident energies as indicated. (Computer printouts of the remainder at all the energies in table 1 are available from the authors upon request.)

Examination of figures 5 and 6 shows that the present multichannel model is generally quite successful in describing inelastic scattering about the forward direction up to $\theta \simeq 40^\circ$. In particular, as indicated by figure 5(a) the many-body treatment of Thomas *et al* (1974) fails quite markedly, by comparison, to reproduce the measurements of Trajmar (1973) in this angular range for the 2^1S excitation. This shortcoming is presumably attributed to the fact that their first-order approach has neglected the 2^1S-2^1P dipole coupling which strongly enhances the 2^1S scattering about the forward direction. The 2^1P cross section is affected much less by the presence of this coupling, as shown by figure 6. With increasing E , the scattering becomes more concentrated in the forward direction and is therefore well described by the present model.

Although the present version of the multichannel eikonal approximation is clearly invalid for backward scattering, calculations were nevertheless performed for the full angular range $0 \leq \theta \leq 180^\circ$ so as to illustrate certain inadequacies of the treatment. Its failure to properly describe large angle scattering in figures 5 and 6 is a direct result of the *explicit* neglect of electron exchange—some of which, however, is *implicitly*

Table 1. Total excitation cross sections (in units of $10^{-2} \pi a_0^2$) given by a ten-channel treatment of the processes $e + \text{He}(1^1S) \rightarrow e + \text{He}(n^1L)$ at incident electron energies $E(\text{eV})$.

nL $E(\text{eV})$	2^1S	2^1P_0	$2^1P_{\pm 1}$	2^1P	3^1S	3^1P_0	$3^1P_{\pm 1}$	3^1P	3^1D_0	$3^1D_{\pm 1}$	$3^1D_{\pm 2}$	3^1D
40	2.45	6.92	4.86	11.78	2.89 ^{-1†}	1.83	0.85	2.68	1.11 ⁻¹	1.12 ⁻¹	2.46 ⁻²	2.48 ⁻¹
50	2.27	6.95	6.09	13.04	2.93 ⁻¹	1.89	1.15	3.04	8.38 ⁻²	9.55 ⁻²	2.95 ⁻²	2.09 ⁻¹
60	2.12	6.77	6.89	13.66	3.02 ⁻¹	1.86	1.38	3.24	6.92 ⁻²	8.04 ⁻²	3.24 ⁻²	1.82 ⁻¹
80	1.84	6.18	7.50	13.68	2.86 ⁻¹	1.65	1.60	3.25	4.70 ⁻²	5.75 ⁻²	3.39 ⁻²	1.38 ⁻¹
100	1.61	5.52	7.60	13.12	2.69 ⁻¹	1.48	1.69	3.17	3.56 ⁻²	4.31 ⁻²	3.36 ⁻²	1.12 ⁻¹
150	1.22	4.34	7.22	11.56	2.18 ⁻¹	1.12	1.69	2.81	2.10 ⁻²	2.63 ⁻²	3.01 ⁻²	7.74 ⁻²
200	9.86 ⁻¹	3.54	6.67	10.21	1.84 ⁻¹	8.96 ⁻¹	1.60	2.50	1.50 ⁻²	1.85 ⁻²	2.66 ⁻²	6.01 ⁻²
300	7.07 ⁻¹	2.50	5.69	8.19	1.40 ⁻¹	6.22 ⁻¹	1.40	2.02	9.40 ⁻³	1.08 ⁻²	2.13 ⁻²	4.15 ⁻²
400	5.49 ⁻¹	1.81	5.02	6.83	1.12 ⁻¹	4.49 ⁻¹	1.25	1.5	5.5 ⁻³	7.35 ⁻³	1.77 ⁻²	3.19 ⁻²
500	4.49 ⁻¹	1.31	4.54	5.85	9.24 ⁻²	3.30 ⁻¹	1.13	1.1	5.52 ⁻³	5.39 ⁻³	1.52 ⁻²	2.61 ⁻²
500†	4.46 ⁻¹	1.20	4.66	5.86	8.71 ⁻²	3.12 ⁻¹	1.15	1.46	—	—	—	—
500§	4.84 ⁻¹	—	—	6.02	1.09 ⁻¹	—	—	1.49	—	—	—	2.51 ⁻²

† Superscript denotes the power of 10 by which the entry must be multiplied.

‡ Four-channel treatment ($1^1S n^1S n^1P_{0,\pm 1}$).

§ Born (Bell *et al* 1969).

Table 2. Polarization fractions of the radiation emitted from $\text{He}(n^1L)$.

$E(\text{eV}) \backslash n^1L$	2^1P	3^1P	3^1D
40	0.480	0.624	0.377
50	0.391	0.533	0.327
60	0.326	0.459	0.287
80	0.245	0.347	0.211
100	0.185	0.273	0.149
150	0.092	0.140	0.039
200	0.030	0.057	-0.030
300	-0.065	-0.059	-0.122
400	-0.162	-0.164	-0.179
500	-0.268	-0.263	-0.215

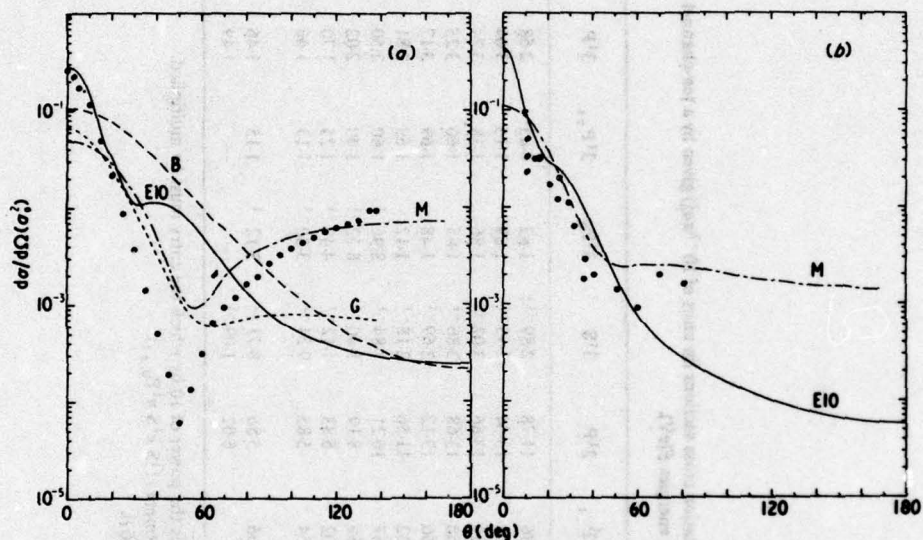


Figure 5. Differential cross sections for the 2^1S excitation of He by electrons with energy (a) 40 eV, (b) 80 eV. Theory: E10, present ten-channel eikonal treatment; M, first-order many-body approach (Thomas *et al* 1974); G, B, Glauber and Born approximations (see Trajmar 1972). Experiment: ●, (a) Trajmar (1973), (b) Rice *et al* (1972).

included by virtue of the multistate expansion—and by the adoption of a straight line trajectory so as to ease computation of both the eikonal (or phase distortion to the relative motion) in each channel and of the transition amplitudes C_n coupling the various channels. The Glauber and Born approaches also suffer from these defects. These effects, however, can be incorporated directly within the basic eikonal model, although a combination of a full quantal partial-wave analysis of the close encounters responsible for these effects and a multichannel eikonal method for the more distant encounters is perhaps a better alternative. There is, however, recent evidence (Bransden and Winters 1975, McDowell *et al* 1975, Winters 1974) that inclusion of exchange may be

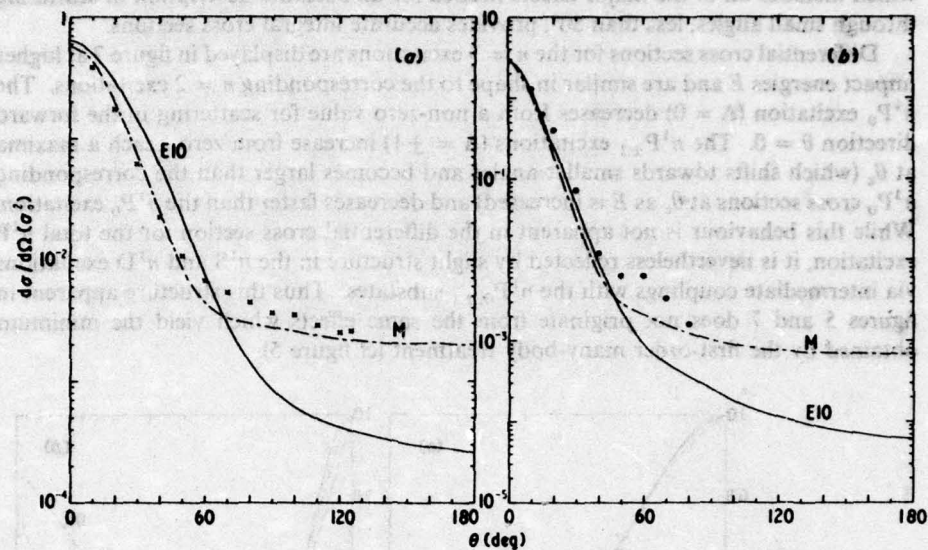


Figure 6. Differential cross sections for the 2^1P excitation of He by electrons with energy (a) 40 eV, (b) 80 eV. Theory: as in figure 5. Experiment: \times , Hall *et al* (1973); \bullet , Truhlar *et al* (1970).

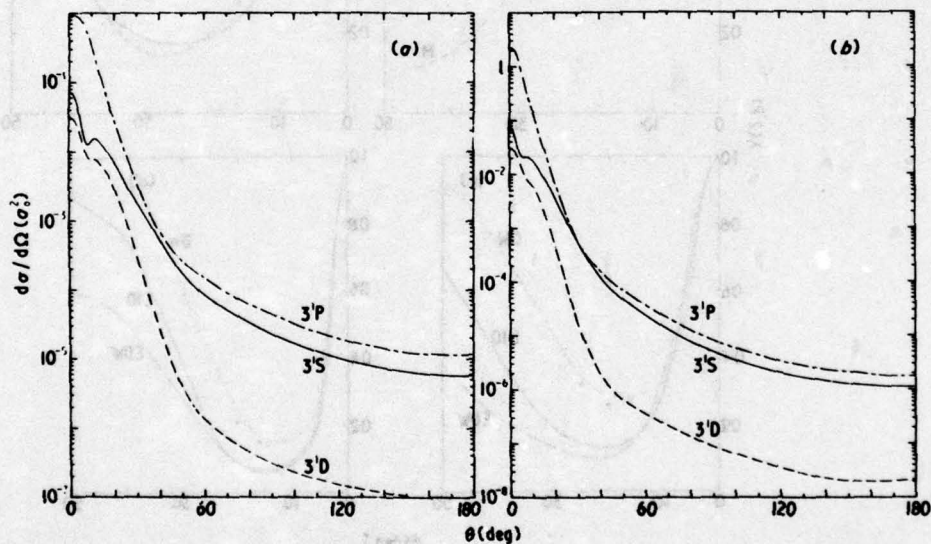


Figure 7. Ten-channel differential cross section for the 3^1S , 3^1P and 3^1D excitations of He by electrons with energy (a) 100 eV, (b) 200 eV.

insufficient to reproduce large-angle inelastic scattering; a proper account of distortion in the final channel together with a consistent treatment of exchange polarization may also be necessary. The contribution arising from these larger scattering angles to the

total excitation cross section is, however, extremely small, such that the present treatment which includes all of the major effects needed for an accurate description of scattering through small angles, less than 50° , provides accurate integral cross sections.

Differential cross sections for the $n = 3$ excitations are displayed in figure 7 at higher impact energies E and are similar in shape to the corresponding $n = 2$ excitations. The n^1P_0 excitation ($\Delta = 0$) decreases from a non-zero value for scattering in the forward direction $\theta = 0$. The $n^1P_{\pm 1}$ excitations ($\Delta = \pm 1$) increase from zero, reach a maxima at θ_c (which shifts towards smaller angles and becomes larger than the corresponding n^1P_0 cross sections at θ_c as E is increased) and decreases faster than the n^1P_0 excitation. While this behaviour is not apparent in the differential cross section for the total n^1P excitation, it is nevertheless reflected by slight structure in the n^1S and n^1D excitations via intermediate couplings with the $n^1P_{0,\pm 1}$ substates. Thus this structure apparent in figures 5 and 7 does not originate from the same effects which yield the minimum obtained by the first-order many-body treatment (cf figure 5).

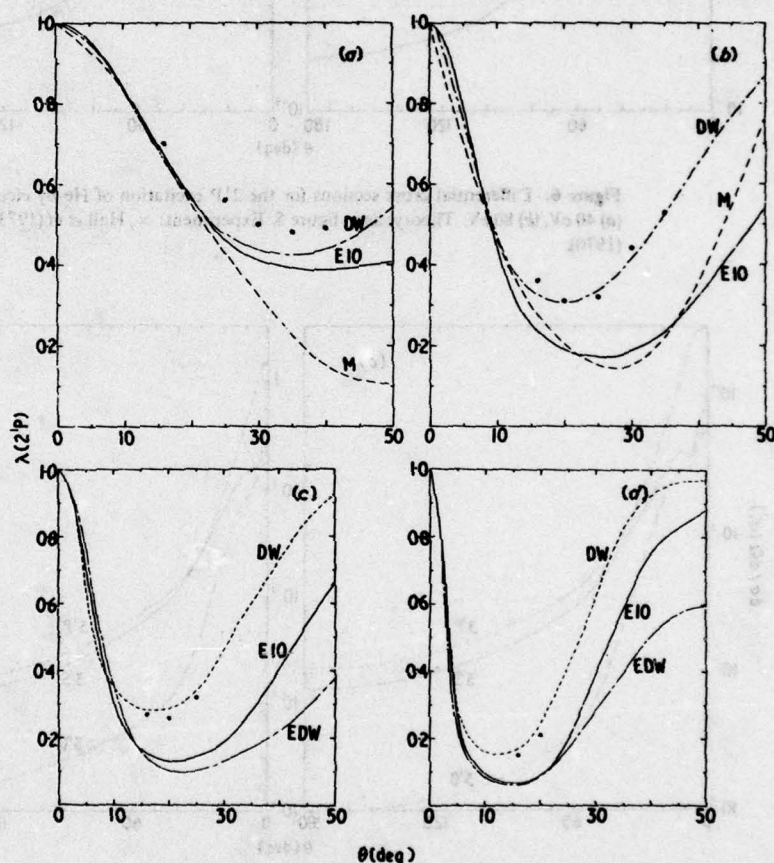


Figure 8. Variation of $\lambda(2^1P)$ with scattering angle θ at impact energies (a) 40 eV, (b) 80 eV, (c) 100 eV and (d) 200 eV. E10, present ten-channel treatment; DW, distorted-wave Born approximation (Madison and Shelton 1973); EDW, eikonal DW (Joachain and Vanderpoorten 1974); M, first-order many-body approach (Thomas *et al* 1974); ●, Emynyan *et al* (1974).

3.3. λ , χ and circular polarization

In figures 8 and 9 the present predictions of $\lambda(2^1P)$ and $\lambda(3^1P)$ obtained from equation (3) are compared with the measurements of Eminyan *et al* (1974, 1975) and with the available distorted wave and many-body calculations. Agreement with experiment is good, particularly at the smaller scattering angles. Measurements, however, are not available for scattering by $\theta \leq 15^\circ$, an angular region for which the present multichannel eikonal treatment is particularly successful (cf figures 5 and 6). It is also worth noting that the goodness of the many-body treatment of the 2^1P total and differential excitation (cf figures 2 and 6) is not maintained for $\lambda(2^1P)$ at the larger scattering angles. Figure 9 demonstrates that the relative agreement between the present approach and measurements becomes improved for the 3^1P excitation, especially at the smaller scattering angles. The apparent structure in $\lambda(3^1P)$ is somewhat reproduced, although shifted to larger scattering angles. There are no other theoretical values available for comparison. After the present λ curves reach their minima at angles θ which decrease with increasing E , they tend monotonically toward unity as $\theta \rightarrow 180^\circ$.

The present variation of λ with E and θ is presented in figure 10. Since λ denotes the relative contribution arising from the $M = 0$ sublevel to the 2^1P differential cross section,

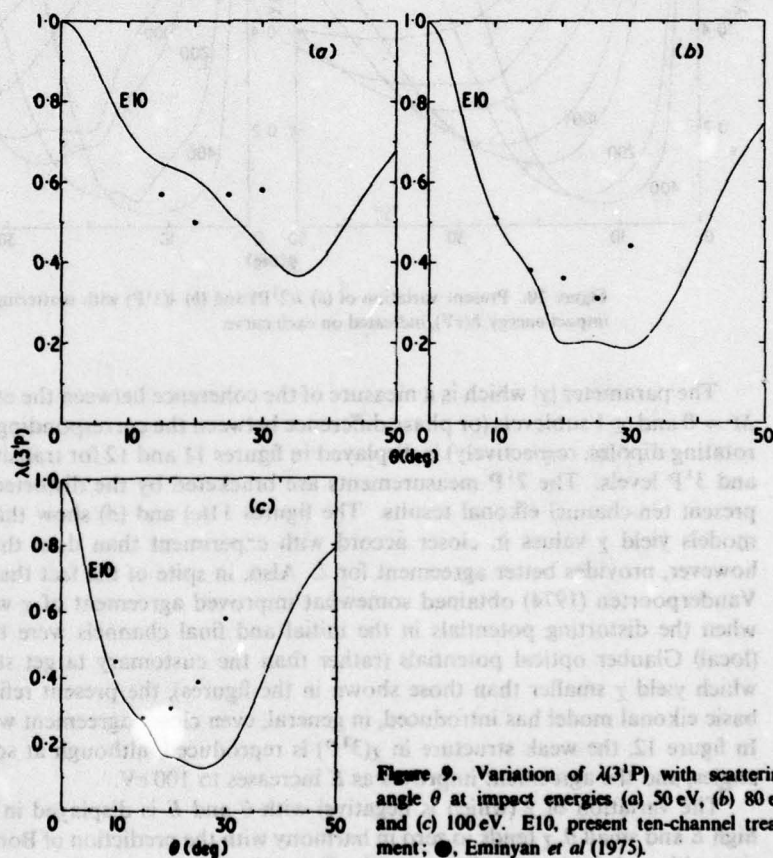


Figure 9. Variation of $\lambda(3^1P)$ with scattering angle θ at impact energies (a) 50 eV, (b) 80 eV and (c) 100 eV. E10, present ten-channel treatment; \circ , Eminyan *et al* (1975).

figure 10 shows quite clearly that for scattering through $\theta \leq 20^\circ$, excitation of the $M = \pm 1$ substates dominates with increasing E , except in the near vicinity of the forward direction $\theta = 0$ when only $\Delta M = 0$ transitions occur. The small-angle region $\theta \leq 20^\circ$ contributes most to the total cross section which is therefore primarily controlled by $M = \pm 1$ excitations at high impact energies (cf table 1). For scattering through larger angles (past the λ minima), the trend is reversed with excitation of the $M = 0$ sublevel dominating at high E , although here its relative contribution to the total cross section is negligible.

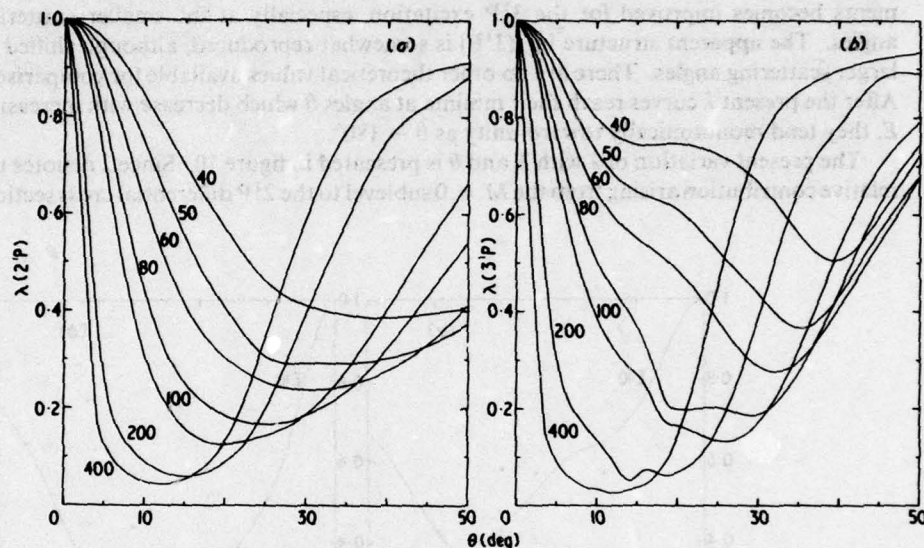


Figure 10. Present variation of (a) $\lambda(2^1P)$ and (b) $\lambda(3^1P)$ with scattering angle θ , and with impact energy E (eV), indicated on each curve.

The parameter $|\chi|$ which is a measure of the coherence between the excitations of the $M = 0$ and ± 1 sublevels (or phase difference between the corresponding oscillating and rotating dipoles, respectively) is displayed in figures 11 and 12 for transitions to the 2^1P and 3^1P levels. The 2^1P measurements are bracketed by the distorted wave and the present ten-channel eikonal results. The figures 11(c) and (d) show that both eikonal models yield χ values in closer accord with experiment than does the DWBA which, however, provides better agreement for λ . Also, in spite of the fact that Joachain and Vanderpoorten (1974) obtained somewhat improved agreement of χ with experiment when the distorting potentials in the initial and final channels were taken to be the (local) Glauber optical potentials (rather than the customary target static potentials, which yield χ smaller than those shown in the figures), the present refinements to the basic eikonal model has introduced, in general, even closer agreement with experiment. In figure 12, the weak structure in $\chi(3^1P)$ is reproduced, although at somewhat larger angles, and the agreement improves as E increases to 100 eV.

The variation of χ (which is negative) with θ and E is displayed in figure 13. For high E and small θ , χ tends to zero in harmony with the prediction of Born's approximation, although for intermediate energies $E \leq 100$ eV, a non-zero limit is attained. When

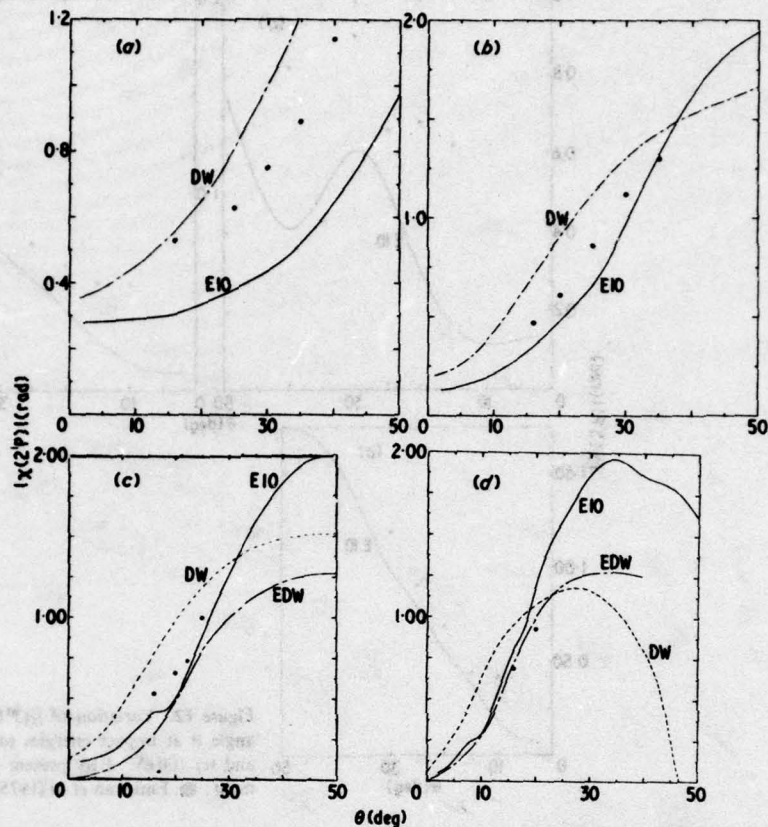


Figure 11. Variation of $|\chi(2^1P)|$ with scattering angle θ at impact energies (a) 40 eV, (b) 80 eV, (c) 100 eV and (d) 200 eV. E10, present ten-channel treatment; DW, distorted-wave Born approximation (Madison and Shelton 1973); EDW, eikonal DW (Joachain and Vanderpoorten 1974); ●, Eminyan *et al* (1974).

χ passes through $\frac{1}{2}\pi$ ie when the phases of the oscillating and rotating dipoles differ by $\frac{1}{2}\pi$, and, provided that the magnitudes of the corresponding amplitudes are about equal (ie $\lambda \approx 0.5$), then at this particular scattering angle θ_c , fully circularly polarized light would be observed in a direction at right angles to the plane of scattering.

The departure from equal population of the $M = 0$ and ± 1 states at θ_c is obtained from figure 10 and hence circularly polarized light will be observed for scattering angles whose shift from θ_c depends on the function $\lambda(\theta)$. The fraction Π of circularly polarized radiation emitted perpendicular to the XZ plane of scattering is the following combination

$$\Pi(\theta, E) = -2[\lambda(1 - \lambda)]^{1/2} \sin \chi \quad (23)$$

of λ and χ . Figure 14 displays the present variation of Π with θ and E . Fully circularly polarized light (ie $\Pi = 1$) is in evidence only for low-energy, large-angle collisions. For scattering in the forward direction, Π is small and almost independent of E . The recognition that Π is also ΔL_Y , the angular momentum transferred in a direction Y perpendicular to the assumed XY plane of scattering, provides some further insight to figure 14.

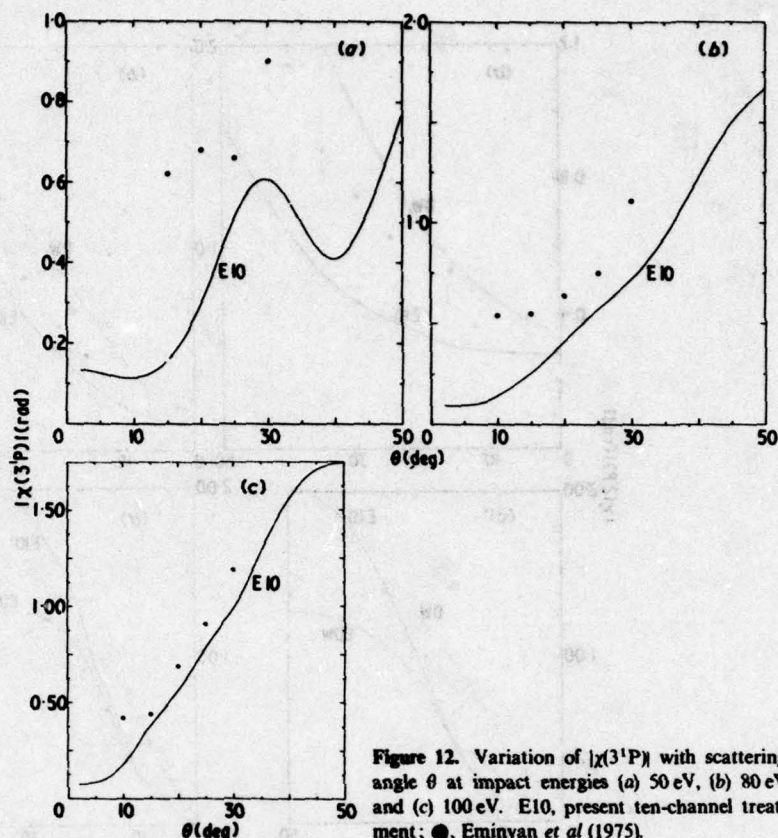


Figure 12. Variation of $|\chi(3^1P)|$ with scattering angle θ at impact energies (a) 50 eV, (b) 80 eV and (c) 100 eV. E10, present ten-channel treatment; ●, Eminyan *et al* (1975).

In the impulsive high-energy limit, the torque N about an origin O due to a force F acting on an electron at position vector $r(x, y, z)$ for time Δt is, from classical mechanics,

$$N = r \times F = \frac{\Delta L}{\Delta t} \quad (24)$$

and hence the Y component of the angular momentum change ΔL is

$$\Delta L_Y = [\langle r \rangle \times \Delta P]_Y = 2k_i \sin \frac{1}{2} \theta \langle z \rangle \quad (25)$$

where ΔP is the linear momentum $2k_i \sin \frac{1}{2} \theta$ transferred and $\langle r \rangle$ is some time average of r during the impulsive encounter. Small-angle collisions with an atom result from distant encounters, and the target atom and hence $\langle z \rangle$ remains essentially unaffected. Thus ΔL_Y increases as $E^{1/2}$ and θ , until sufficiently large E and θ when large-angle, close-encounter collisions dominate, such that the expectation value $\langle z \rangle$ must decrease more rapidly than $E^{1/2} \sin \frac{1}{2} \theta$ so as to cause the decreasing ΔL_Y observed in figure 13.

In conclusion, the present version of the multichannel eikonal treatment provides a successful description of inelastic collisions at intermediate and high impact energies. Its success for total excitation cross sections can be attributed to the fact that here the small-angle scattering ($\theta \leq 50^\circ$) which dominates the total cross section even at low energies ($E \approx 40$ eV) is well described. The main effects, such as intermediate (long-range) couplings between each channel, some polarization of each target state, and

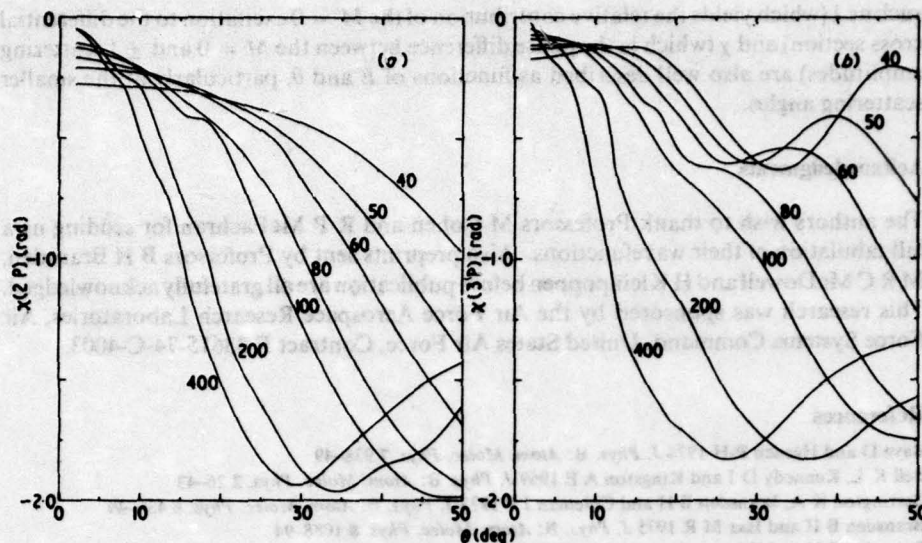


Figure 13. Present variation of (a) $\chi(2^1P)$ and (b) $\chi(3^1P)$ radians with scattering angle θ and with impact energy $E(\text{eV})$ indicated on each curve.

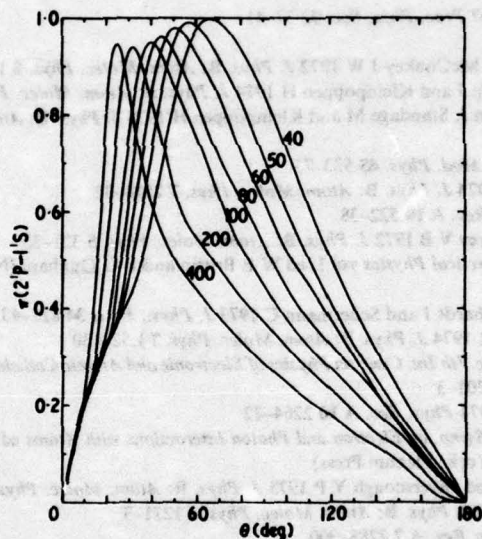


Figure 14 The variation of the fraction π of circularly polarized radiation, emitted from $\text{He}(2^1P)$ and observed at right angles to the scattering plane, with scattering angle θ and with impact energy $E(\text{eV})$ indicated on each curve.

static distortion in each channel needed for a correct description of small-angle scattering are included. Also the multichannel eikonal expansion ensures (i) that convergence in partial-wave contributions is always attained especially in the high-energy limit, (ii) that the long-range couplings can affect distant encounters (or large total angular momentum), and also (iii) that some account of electron exchange is provided. More basic parameters

such as λ (which yields the relative contribution of the $M = 0$ excitation to the differential cross section) and χ (which is the phase difference between the $M = 0$ and ± 1 scattering amplitudes) are also well described as functions of E and θ , particularly at the smaller scattering angles.

Acknowledgments

The authors wish to thank Professors M Cohen and R P McEachran for sending us a full tabulation of their wavefunctions. Also preprints sent by Professors B H Bransden, M R C McDowell and H Kleinpoppen before publication are all gratefully acknowledged. This research was sponsored by the Air Force Aerospace Research Laboratories, Air Force Systems Command, United States Air Force, Contract F 33615-74-C-4003.

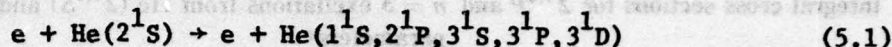
References

- Baye D and Heenen P-H 1974 *J. Phys. B: Atom. Molec. Phys.* **7** 938-49
 Bell K L, Kennedy D J and Kingston A E 1969 *J. Phys. B: Atom. Molec. Phys.* **2** 26-43
 Berrington K A, Bransden B H and Coleman J P 1973 *J. Phys. B: Atom. Molec. Phys.* **6** 436-49
 Bransden B H and Issa M R 1975 *J. Phys. B: Atom. Molec. Phys.* **8** 1088-94
 Bransden B H and Winters K H 1975 *J. Phys. B: Atom. Molec. Phys.* **8** 1236-44
 Brongersma H H, Knoop F W E and Backx C 1972 *Chem. Phys. Lett.* **13** 16-9
 Chan, F T and Chen S T 1973 *Phys. Rev. A* **8** 2191-4
 — 1974a *Phys. Rev. A* **9** 2393-7
 — 1974b *Phys. Rev. A* **10** 1151-6
 Cohen M and McEachran R P 1967 *Proc. Phys. Soc.* **92** 37-41
 — 1974 private communication
 Donaldson F G, Hender M A and McConkey J W 1972 *J. Phys. B: Atom. Molec. Phys.* **5** 1192-210
 Eminyan M, MacAdam K B, Slevin J and Kleinpoppen H 1974 *J. Phys. B: Atom. Molec. Phys.* **7** 1519-42
 Eminyan M, MacAdam K B, Slevin J, Standage M and Kleinpoppen H 1975 *J. Phys. B: Atom. Molec. Phys.* **8** in press
 Fano U and Macek J H 1973 *Rev. Mod. Phys.* **45** 533-73
 Flannery M R and McCann K J 1974 *J. Phys. B: Atom. Molec. Phys.* **7** 2518-32
 Gau J N and Macek J 1974 *Phys. Rev. A* **10** 522-38
 Gerjuoy E, Thomas B K and Sheorey V B 1972 *J. Phys. B: Atom. Molec. Phys.* **5** 321-33
 Glauber R J 1959 *Lectures in Theoretical Physics* vol 1, ed W E Brittin and L G Dunham (New York: Interscience) p 369
 Hall R I, Joyez G, Mazeau J, Reinhardt J and Schermann C 1973 *J. Phys., Paris* **34** 827-43
 Joachain C J and Vanderpoorten R 1974 *J. Phys. B: Atom. Molec. Phys.* **7** L528-30
 de Jongh J P and van Eck J 1971 *Proc. 7th Int. Conf. on Physics of Electronic and Atomic Collisions* (Amsterdam: North-Holland) Abstracts pp 701-3
 McCann K J and Flannery M R 1974 *Phys. Rev. A* **10** 2264-72
 McDowell M R C 1975 *Proc. Int. Symp. on Electron and Photon Interactions with Atoms* ed H Kleinpoppen and M R C McDowell (New York: Plenum Press)
 McDowell M R C, Morgan L A and Myerscough V P 1975 *J. Phys. B: Atom. Molec. Phys.* **8** 1053-72
 McEachran R P and Cohen M 1969 *J. Phys. B: Atom. Molec. Phys.* **2** 1271-3
 Macek J and Jaecks D H 1971 *Phys. Rev. A* **7** 2288-300
 Madison D H and Shelton W N 1973 *Phys. Rev. A* **7** 499-513
 Miller K J, Mielczarek S R and Krauss M 1968 *J. Chem. Phys.* **51** 945-57
 Moustafa Moussa H R, de Heer F J and Schulten J 1969 *Physica* **40** 517-49
 Percival I C and Seaton M J 1958 *Phil. Trans. R Soc. A* **251** 113-38
 Rice J K, Truhlar D G, Cartwright D C and Trajmar S 1972 *Phys. Rev. A* **5** 762-82
 Thomas L D, Caanack G, Taylor H S and Yarlagadda B S 1974 *J. Phys. B: Atom. Molec. Phys.* **7** 1719-33
 Trajmar S 1973 *Phys. Rev. A* **8** 191-203
 Truhlar D G, Rice J K, Kupperman A, Trajmar S and Cartwright D C 1970 *Phys. Rev. A* **1** 778-802
 Vriens L, Simpson J A and Mielczarek S R 1968 *Phys. Rev.* **165** 7-15
 Winters K H 1974 *PhD Thesis* University of Durham

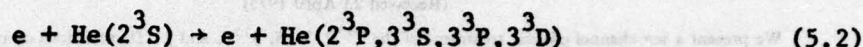
SECTION V

THE EXCITATION AND IONIZATION OF $\text{He}(2^{1,3}\text{S})$ BY ELECTRON IMPACT

Here, integral and differential cross sections for the collisional processes

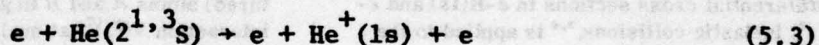


and



are obtained as a function of impact-energy E , by application of the multichannel eikonal treatment. Also, the angular-correlation parameters λ and χ , which respectively provide the relative population and relative phase of the collisionally excited P magnetic substates, and the circular polarization fraction Π of radiation emitted from these P states are determined as functions of scattering angle θ and E .

Also in this section cross sections for the $2^3\text{S} + n^3\text{L}$ ($n=4,5$; $L=\text{S-F}$) excitations and for the single ionization process,



are calculated by the Born approximation.

A full description of all of the above work, which has been published in:

- (1) Phys. Rev. A 12 (1975) 846-855
- (2) J. Phys. B: Atom. Molec. Phys. 10 (1977) 621-635

now follows.

5.1 Ten-Channel Eikonal Treatment of Electron-Metastable-Helium

Collisions: Differential and Integral Cross Sections for $2^{1,3}P$

and $n = 3$ Excitations from $He(2^{1,3}S)$ and the (λ, χ, Π) Parameters

Ten-channel eikonal treatment of electron-metastable-helium collisions: Differential and integral cross sections for $2^{1,3}P$ and $n = 3$ excitations from $He(2^{1,3}S)$ and the (λ, χ, Π) parameters*

M. R. Flannery and K. J. McCann

School of Physics, Georgia Institute of Technology, Atlanta, Georgia 30332

(Received 23 April 1975)

We present a ten-channel eikonal treatment of the $2^{1,3}P$, $3^{1,3}S$, $3^{1,3}P$, and $3^{1,3}D$ excitations of atomic helium, initially in the $2^{1,3}S$ metastable states, by incident electrons with energy E (eV) in the range $5 \leq E \leq 100$. Integral and differential inelastic cross sections are obtained. Also, the angular-correlation parameters λ and χ , which respectively provide the relative population and relative phase of the collisionally excited P magnetic substates, and the circular polarization fraction Π of radiation emitted from these P states, are determined as functions of scattering angle θ and E . No measurements exist to date. The principle of detailed balance is explicitly demonstrated for the 2^1S-1^1S superelastic collision.

I. INTRODUCTION

In contrast to collisions involving ground-state atoms, relatively little is known with any great certainty about excitation processes involving atoms initially in a prepared excited state. Such knowledge is very important to the detailed analysis of gaseous discharges, astrophysical plasmas, and formation of excimers¹ (excited metastable molecules, often rare gases).

In this paper, the multichannel eikonal model², which provided a satisfactory account of integral and differential cross sections in $e-H(1s)$ and $e-He(1s^*)$ inelastic collisions,^{3,4} is applied to the excitation processes

$$e + He(2^{1,3}S) \rightarrow e + He(2^{1,3}P, 3^{1,3}S, 3^{1,3}P, 3^{1,3}D).$$

(1)

Frozen-core Hartree-Fock wave functions⁵ for helium are used throughout, and the $n=1, 2$, and 3 channels of each singlet and triplet series will be closely coupled. In addition to the evaluation of integral and differential cross sections for (1), the angular-correlation parameters λ and χ , which are more basic to the collision process, and which provide valuable information on the circular polarization of the emitted radiation from the $n^{1,3}P$ states, will also be studied as a function of impact energy E and scattering angle θ (in the c.m. frame).

Contrary to that experienced for transitions from ground atomic states, both the Born and the Vainshtein, Presnyakov, and Sobel'man (VPS) approximations predict¹ that collisional excitations from the $2^{1,3}S$ metastable-helium state to the $3^{1,3}D$ and $3^{1,3}S$ (optically forbidden) levels are more probable than excitations to the (optically allowed) $3^{1,3}P$ and $4^{1,3}P$ levels except at incident energies

above 100 eV. Hence, couplings between all the states in the $n=2$ and 3 channels are extremely important and require inclusion for a proper treatment of Eq. (1).

II. THEORY

A. Basic approximation

In an effort to clarify more fully the basis of the present approach, an alternative derivation of the multichannel eikonal treatment is instructive. The wave function for the scattering of two (structured) atoms A and B in general, by their mutual interaction $V(\vec{r}, \vec{R})$ at nuclear separation $\vec{R}(X, Y, Z)$, is

$$\begin{aligned} \Psi_i^+(\vec{r}, \vec{R}) &= \psi_i(\vec{r}) e^{i\vec{k}_i \cdot \vec{R}} \\ &+ \int \int d\vec{r}' d\vec{R}' G_0^+(\vec{r}, \vec{R}; \vec{r}', \vec{R}') \\ &\times V(\vec{r}', \vec{R}') \Psi_i^+(\vec{r}', \vec{R}'), \end{aligned} \quad (2)$$

where the two-particle Green's function G_0^+ , appropriate to \mathcal{H}_0 , the Hamiltonian of the unperturbed system of energy E_i at infinite \vec{R} , satisfies

$$(E_i - \mathcal{H}_0 + i\epsilon) G_0^+(\vec{r}, \vec{R}; \vec{r}', \vec{R}') = \delta(\vec{r} - \vec{r}') \delta(\vec{R} - \vec{R}'), \quad (3)$$

in which the composite internal coordinates are denoted by \vec{r} relative to each parent nucleus. The free-particle Green's function, which propagates the effect of the interaction V at (\vec{r}', \vec{R}') to (\vec{r}, \vec{R}) , can be expanded, in terms of the complete set of eigenfunctions of \mathcal{H}_0 , as

$$\begin{aligned} G_0^+(\vec{r}, \vec{R}; \vec{r}', \vec{R}') &= \lim_{\epsilon \rightarrow 0^+} \frac{1}{(2\pi)^3} \frac{2\mu}{\hbar^2} \sum_n \psi_n(\vec{r}) \psi_n^*(\vec{r}') \int \frac{e^{i\vec{k} \cdot (\vec{R} - \vec{R}')} d\vec{k}}{k_n^2 - k^2 + i\epsilon}, \end{aligned} \quad (4a)$$

with $\psi_n(\vec{r})$ describing the internal structure at infinite nuclear separation \vec{R} , where the relative motion is planar with propagation vector $\vec{k}(k_x, k_y, k_z)$. For heavy-particle collisions, and for electron-atom inelastic collisions at intermediate and high impact energy, scattering about the forward

direction contributes most to the total cross section,²⁻⁴ and it is therefore a good approximation to assume that the major contributions to the propagator (4a) arise only from those waves at $Z' < Z$ with $k^2 \approx k_z^2$ such that

$$G_0^*(\vec{r}, \vec{R}; \vec{r}', \vec{R}') = \lim_{\epsilon \rightarrow 0^+} \frac{1}{(2\pi)^3} \frac{2\mu}{\hbar^2} \int_{-\infty}^{\infty} e^{ik_z(x-x')} dk_z \int_{-\infty}^{\infty} e^{ik_y(y-y')} dk_y \sum_n \psi_n(\vec{r}) \psi_n^*(\vec{r}') \left(\int_{-\infty}^{\infty} \frac{e^{ik_z(z-z')}}{k^2 - k_z^2 + i\epsilon} dk_z \right) H(Z - Z'), \quad (4b)$$

where $H(Z - Z')$ is the Heaviside step function (unity for $Z' < Z$ and zero otherwise). Hence, by contour integration, and with introduction of the impact parameter $\rho(X, Y)$,

$$G_0^*(\vec{r}, \vec{R}; \vec{r}', \vec{R}') = \frac{i\mu}{\hbar^2} \sum_n \frac{e^{ik_z(z-z')}}{k_z} \delta(\vec{\rho} - \vec{\rho}') \times H(Z - Z') \psi_n(\vec{r}) \psi_n^*(\vec{r}'). \quad (4c)$$

The reduction of (4a) to (4c) can also be obtained by the method of stationary phase (cf. Schiff⁶ and Gerjuoy and Thomas⁷). The multichannel eikonal approximation follows by setting

$$\Psi_i^* = \psi_i(\vec{r}) e^{is_i(\vec{R})} - \frac{i\mu}{\hbar^2} \sum_n \int_{\vec{R}'} \frac{e^{ik_n(z-z')}}{k_n} \psi_n(\vec{r}) \delta(\vec{\rho} - \vec{\rho}') H(Z - Z') \sum_{n'} A_n(\vec{\rho}', Z') V_{nn'}(\vec{R}') e^{is_{n'}(\vec{R}')} d\vec{\rho}' dZ'. \quad (8)$$

The projection of (8) onto the orthonormal set $\psi_n(\vec{r})$ is

$$(A_n e^{is_n} - \delta_{nn}) e^{is_i(\vec{R})} = -\frac{i\mu}{\hbar^2} \int_{-\infty}^Z \frac{e^{-ik_n z'}}{k_n(\vec{\rho}, Z')} \sum_{n'} A_{n'}(\vec{\rho}, Z') V_{nn'}(\vec{\rho}, Z') e^{is_{n'}(\vec{\rho}, z')} dZ', \quad (9)$$

which on differentiation yields

$$\frac{\partial}{\partial Z} (A_n e^{is_n - \kappa_n Z}) = -\frac{i\mu}{\kappa_n \hbar^2} \sum_{n'} A_{n'}(\vec{\rho}, Z) V_{nn'}(\vec{R}) e^{is_{n'}(\vec{R}) - \kappa_{n'} Z}. \quad (10)$$

Ignoring the second term on the left-hand side of (7) and assuming a straight-line trajectory along the Z axis, i.e., $|\nabla S_n| \approx \partial S_n / \partial Z \approx \kappa_n$, and $\partial \kappa_n / \partial Z \approx 0$ [equivalent to the neglect of $\nabla^2 S_n$ in (7)], Eq. (10) becomes

$$\frac{i\hbar^2}{\mu} \kappa_n \frac{\partial A_n}{\partial Z} = \sum_{n'} A_{n'}(\vec{\rho}, Z) V_{nn'}(\vec{R}) e^{is_{n'}(\vec{R}) - \kappa_{n'} Z}, \quad (11)$$

a set of first-order coupled differential equations to be solved for A_n . Thus, for a finite number of states $n=1, 2, \dots, N$, the direct transition matrix element T_{fi} or its associated scattering amplitude f_{fi} can be evaluated from

$$\Psi_i^*(\vec{r}, \vec{R}) = \sum_n A_n(\vec{\rho}, Z) \psi_n(\vec{r}) e^{is_n(\vec{R})}, \quad (5)$$

where the eikonal S_n for the relative motion in excitation channel n under the static interaction

$$V_{nn}(\vec{R}) = \langle \psi_n(\vec{r}) | V(\vec{r}, \vec{R}) | \psi_n(\vec{r}) \rangle \quad (6)$$

with $n=m$, satisfies

$$(\nabla S_m)^2 - i\hbar(\nabla^2 S_m) = k_m^2 - (2\mu/\hbar^2) V_{mm} \approx \kappa_m^2(\vec{R}) \quad (7)$$

exactly. The Green's function corresponding to (5) is (4c), with k_z replaced by the local wave number κ_n , and hence, (2) with (5) reduces to

$$\begin{aligned} T_{fi} &= \langle \psi_f(\vec{r}) e^{is_f(\vec{R})} | V(\vec{r}, \vec{R}) | \sum_n A_n \psi_n(\vec{r}) e^{is_n(\vec{R})} \rangle_{\vec{r}, \vec{R}} \\ &= -4\pi \frac{\hbar^2}{2\mu} f_{fi}(\vec{k}_i, \vec{k}_f) \\ &= \sum_n \langle e^{is_f(\vec{R})} | V_{fn}(\vec{R}) | A_n(\vec{\rho}, Z) e^{is_n(\vec{R})} \rangle_{\vec{\rho}, Z}, \end{aligned} \quad (12a)$$

(12b)

the basis of the multichannel eikonal treatment.² The transition matrix for rearrangement collisions between the projectile at \vec{R} and a target electron at \vec{r}_i is obtained from (12a) by the $\vec{R} \rightarrow \vec{r}_i$ interchange in the wave function for the final state f .

The above derivation therefore shows that the multichannel eikonal treatment is based on the following three assumptions: (a) the Green's function (4c), (b) $|\nabla S_n| = \kappa_n$, and (c) a straight-line trajectory used to find the eikonal S_n , all included within a restricted basis set of N target states.

B. Basic formulas

For a nondegenerate initial state i , the experimental differential cross section for $i \rightarrow f$ excitation is, as a function of scattering angle θ ,

$$\frac{d\sigma}{d\Omega} = \frac{k_f}{k_i} \sum_{M=-L}^L |f_{if}^{(M)}(\theta)|^2, \quad (13)$$

summed over all degenerate magnetic sublevels M of the final level f of the target with angular momentum L , thereby suppressing all knowledge of the populations and phases of each substate. However, two quantities capable of measurement⁸ and calculation as functions of θ and impact energy E , can be defined for excitation of the $n^{1,3}P$ levels, by

$$\lambda = |f_{if}^{(0)}|^2 / (|f_{if}^{(0)}|^2 + 2|f_{if}^{(1)}|^2) \quad (14)$$

and

$$\chi = \alpha_1 - \alpha_0, \quad (15)$$

where α_M is the phase of the scattering amplitude

$$f_{if}^{(M)} = |f_{if}^{(M)}| e^{i\alpha_M} \quad (16)$$

and where the axis of quantization of the target is taken along the incident Z direction defined by \hat{k}_i . The parameter λ is the relative contribution arising from the $M=0$ sublevel to (13), while χ is a measure of the coherence between the excitations of the $M=0$ and 1 sublevels, i.e., the phase difference between the corresponding oscillating and rotating dipoles, respectively. A related quantity is therefore the circular-polarization fraction of the radiation emitted from the $n^{1,3}P$ levels in a direction perpendicular to the (assumed) XZ plane of the scattering.

$$\frac{i\hbar^2}{\mu} \kappa_f(\rho, Z) \frac{\partial C_f(\rho, Z)}{\partial Z} + \left(\frac{\hbar^2}{\mu} \kappa_f(\kappa_f - k_f) + V_{ff}(\rho, Z) \right) C_f(\rho, Z) = \sum_{n=1}^N C_n(\rho, Z) V_{fn}(\rho, Z) \exp i(k_n - k_f)Z, \quad f=1, 2, \dots, N, \quad (22)$$

solved subject to the asymptotic boundary condition $C_f(\rho, -\infty) = \delta_{if}$.

III. RESULTS AND DISCUSSION

In order to express the interaction matrix elements (6) as analytical functions of \vec{R} , it proves convenient to transform the frozen-core Hartree-Fock wave functions of Cohen and McEachran.⁵ Thus, the spatial wave functions for the $n=1-3$ states of helium are

$$\psi_{1s, nlm}(\vec{r}_1, \vec{r}_2) = N_{nl} [\phi_0(\vec{r}_1) \phi_{nlm}(\vec{r}_2) \pm \phi_0(\vec{r}_2) \phi_{nlm}(\vec{r}_1)], \quad (23)$$

in which the \pm signs refer to the symmetric (sin-

$$\Pi = -2[\lambda(1-\lambda)]^{1/2} \sin \chi = \langle \Delta L_y \rangle, \quad (17)$$

where $\langle \Delta L_y \rangle$ is the expectation value of the angular momentum transferred in the Y direction during the collision.⁹

The basic formula (12) for the scattering amplitude can be further reduced for two-particle interactions for which $V_{fi}(\vec{R}) = V_{fi}(\rho, Z) e^{i\Delta\Phi}$, to yield²

$$f_{if}(\theta, \phi) = -i^{\Delta+1} \int_0^\infty J_{\Delta}(K' \rho) \times [I_1(\rho, \theta) - i I_2(\rho, \theta)] \rho d\rho, \quad (18)$$

where J_{Δ} are Bessel functions of integral order, $(M_i - M_f)$ the change in magnetic quantum number, and where K' is the XY component $k_f \sin \theta$ of the momentum change $\vec{K} = \vec{k}_i - \vec{k}_f$. The collision functions

$$I_1(\rho, \theta; \alpha) = \int_{-\infty}^{\infty} \kappa_f(\rho, Z) \left(\frac{\partial C_f(\rho, Z)}{\partial Z} \right) e^{i\alpha Z} dZ \quad (19)$$

and

$$I_2(\rho, \theta; \alpha) = \int_{-\infty}^{\infty} [\kappa_f(\kappa_f - k_f) + (\mu/\hbar^2) V_{ff}] \times C_f(\rho, Z) e^{i\alpha Z} dZ \quad (20)$$

contain a dependence on the scattering angle θ via

$$\alpha = k_f(1 - \cos \theta) = 2k_f \sin^2(\theta/2), \quad (21)$$

the difference between the Z component of the momentum change K and the minimum change $k_i - k_f$ in the collision. The coupling (phase Φ -independent) amplitudes C_f are solutions of the following set of N coupled differential equations

glet) and antisymmetric (triplet) cases, respectively. The frozen, inner $1s$ orbital is (in a.u.)

$$\phi_0(\vec{r}) = 2^{5/2} e^{-2r} Y_{00}(\hat{r}), \quad (24)$$

and the orbital for the second electron in state (nlm) is rewritten (in a.u.) as

$$\phi_{nlm}(\vec{r}) = \sum_{N=1}^{J-1} B_N^{nl} e^{-\beta r} r^{N-1} Y_{lm}(\hat{r}), \quad \beta = 2/n, \quad (25)$$

where J is the maximum number of linear coefficients B_N^{nl} given in terms of Cohen and McEachran's original parameters a_j^{nl} by³

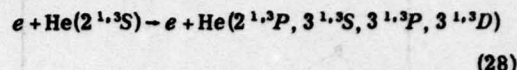
$$B_N^i = \sum_{j=N+1}^J \frac{(-1)^{N-i} 2^i (j+1)^2 (2\beta)^{N-i-1}}{(N-i-1)!(j-N-i)!(N+i)!} a_j^i, \\ N=1, 2, \dots, J. \quad (26)$$

The above transformation (26) facilitates subsequent evaluation of the e -He interaction matrix elements

$$V_{ij}(\vec{R}) = \langle \phi_i(\vec{r}_1, \vec{r}_2) | -\frac{2}{R} + \frac{1}{|\vec{R} - \vec{r}_1|} + \frac{1}{|\vec{R} - \vec{r}_2|} | \phi_j(\vec{r}_1, \vec{r}_2) \rangle \quad (27)$$

as analytical functions of \vec{R} , for all combinations of i and j appropriate to a ten-state treatment. In addition to the $n=2$ and $n=3$ channels, the superelastic 1^1S channel was included for singlet-singlet transitions. The above frozen-core approximation for He implies that correlation effects between the inner and outer atomic electrons have been explicitly neglected [although some implicit account is assumed by virtue of (25)], and is therefore effectively exact for highly excited Rydberg states. Metastable helium is unique in that its excitation energy, 19.8 eV above the ground state, is the largest of all the singly excited atoms, its outer electron is relatively weakly bound (~ 4.8 eV), and the mean interelectronic separation in the 2^1S state is $\sim 5.3a_0$. Therefore, the main response of target helium to the projectile electron is expected to arise from the outer electron such that the use of a frozen-core orbital for the inner electron within a close-coupling scattering wave function (5) is expected to be quite accurate. This is further supported by the fact that the dominant contributions to the integral inelastic cross sections for singly excited transitions arise from small scattering angles $\theta \leq 20^\circ$ (cf. Fig. 5) which result from distant encounters. At the lowest impact energy (5 eV), however, the angular distribution tends to become more isotropic such that close encounters are gaining in relative importance. This situation is difficult to assess without resort not only to correlated atomic wave functions, but also to a more elaborate scattering formalism involving some mechanism which permits response of the inner electron to the projectile. If correlation effects with the inner electron are to be included in the atomic function, then similar refinements involving its interaction with the projectile must also be included in a more elaborate scattering formalism, not based on an atomic close-coupling expansion valid only for weak perturbations, but on some perturbed three-body expansion. It is worth noting that the atomic wave functions adopted in this paper are the most accurate ones used to date in any scattering description more refined than Born's approximation.

In Figs. 1-3 are displayed the integral cross sections for the processes



at incident-electron energies E (eV) in the range $5 \leq E \leq 100$, together with comparison Born values determined from the highly accurate form factors of Kim and Inokuti.¹⁰ It is worth noting that the coupled-state calculations were much more time consuming (~ 5 h U1108) than a corresponding treatment of excitation from the ground state^{3,4} which involved ~ 1 h U1108. This additional time resulted from the closeness of the initial 2^1S with neighboring 2^1P channels which, because of their long-range static and coupled interactions, necessitated the inclusion of large impact parameters $\rho \sim 100$ a.u. in order to achieve convergence for both the solutions of the coupled equations (22) and for the integration (18) involving the Bessel functions which oscillated rapidly at these large ρ .

In general, transitions between singlet states of given configurations are much more probable than the corresponding triplet-triplet transitions. Figs. 1-3 show that the multichannel treatment preserves the Born predictions of the relative importance of transitions to the 2^1P , 3^1D , 3^1S , and 3^1P states, written in order of decreasing probability, except at $E \gtrsim 25$ eV and $\gtrsim 70$ eV when excitations of the 3^1P and 3^3P states, respectively,

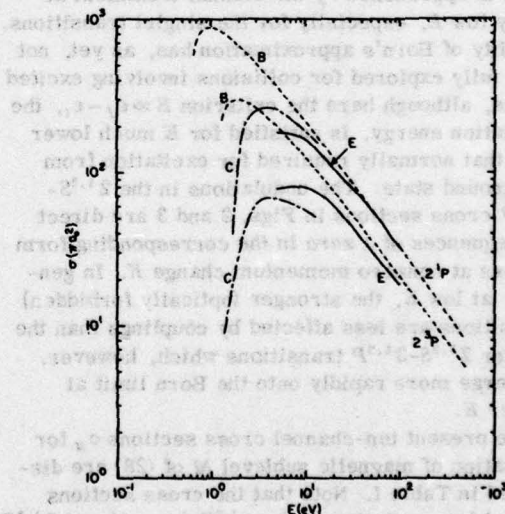


FIG. 1. Cross sections (πa_0^2) for the 2^1S - 2^1P transitions induced in helium by electron impact at energy E (eV). E: Present multichannel eikonal treatment. B: Born approximation (Refs. 1, 10). C: Burke *et al.* (Ref. 11).

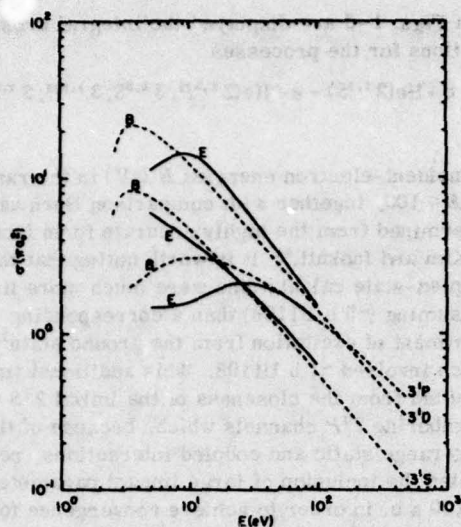


FIG. 2. Cross sections (πa_B^2) for the 2^1S-3^1S , 3^1P , 3^1D transitions induced in helium by electron impact at energy E (eV). E: Present treatment. B: Born approximation (Refs. 1, 10).

become greater than the 3^1S excitations. The results of Burke *et al.*,¹¹ who used simple analytic wave functions, closely coupled the $n=1$ and $n=2$ states for total (system) angular momentum $L=0$ and $L=1$, and used a Born approximation for higher L , are also displayed in Fig. 1 for comparison. A remarkable feature is that the Born limit is approached by the eikonal treatment at fairly low E , especially for the singlet transitions. Validity of Born's approximation has, as yet, not been fully explored for collisions involving excited atoms, although here the criterion $E \gg \epsilon_f - \epsilon_i$, the excitation energy, is satisfied for E much lower than that normally required for excitation from the ground state. The undulations in the 2^1S-3^1P cross sections in Figs. 2 and 3 are direct consequences of a zero in the corresponding form factors at nonzero momentum change K . In general, at low E , the stronger (optically forbidden) transitions are less affected by couplings than the weaker 2^1S-3^1P transitions which, however, converge more rapidly onto the Born limit at higher E .

The present ten-channel cross sections σ_M for excitation of magnetic sublevel M of (28) are displayed in Table I. Note that the cross sections $\sigma(nlm)$ for excitation of the n^1P ($m=\pm 1$) and 3^1D ($m=\pm 2$) substates dominate the cross sections $\sigma(nl)$ for excitation of the respective levels (nl) at high impact energies. This behavior is consistent with the high-energy limit to Born's approxi-

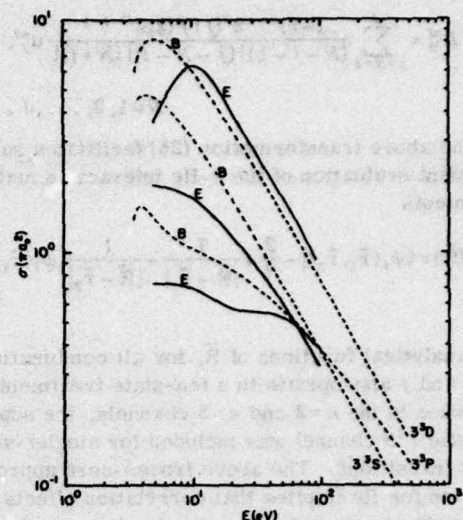


FIG. 3. Cross sections (πa_B^2) for the 2^3S-3^3S , 3^3P , 3^3D transitions induced in helium by electron impact at energy E (eV). E: Present treatment. B: Born approximation (Refs. 1, 10).

mation, which predicts that the ratio $\sigma(nlm)/\sigma(nl)$ is $2|P_l^m(0)|^2/(2l+1)$, where the associated Legendre functions $P_l^m(0)$ are zero for odd $(l-m)$, and are largest when $|m|=l$. Alternatively, when impulsive conditions prevail, the change ΔL_z in the angular momentum perpendicular to the XZ scattering plane is directly proportional to the linear momentum change $K \approx 2k \sin \frac{1}{2}\theta$, which is perpendicular to the incident direction and which vanishes for high-energy scattering in the forward direction, thereby permitting angular momentum changes only in the Z direction to occur. Cross sections for the 2^1S-1^1S superelastic collision are also provided such that the detailed balance relation

$$k_i^2 \sigma_{i,j}(k_i) = k_f^2 \sigma_{j,i}(k_f), \quad (29)$$

$$k_i^2 = k_f^2 + (2\mu/\hbar^2)(\epsilon_f - \epsilon_i)$$

between the forward and reverse rates for the process can be tested, thereby permitting assessment of the overall accuracy of the calculations. Thus, the crosses in Fig. 4 refer to the present 2^1S-1^1S results for the left-hand side of (29), with $E \geq 5$ eV, while the dots, representing the right-hand side of (29), are taken from a previous ten-channel treatment⁴ of the 2^1S excitation from the ground state for $E \geq 40$ eV. The maximum deviation corresponds to an error of 2.5% in σ .

The plane-polarization fractions¹²

TABLE I. Integral cross sections (πa_0^2) for the 2^1S-n^1L and 2^3S-n^3L transitions (S and T, respectively) in helium by collision with incident electrons of energy E (eV).

nL (m)	E (eV)	S	T	S	T	S	T	S	T	S	T
		5	10	20	50	100					
$2P(0)$		5.71 ¹	3.07 ¹	4.01 ¹	2.38 ¹	1.02 ¹	1.29 ¹	9.94 ⁻¹	2.26	2.58 ⁻¹	1.64
$2P(\pm 1)$		1.23 ²	4.63 ¹	1.22 ²	5.53 ¹	9.51 ¹	4.70 ¹	5.63 ¹	2.81 ¹	3.16 ¹	1.67 ¹
$2P(\Sigma)$		1.80 ²	7.70 ¹	1.62 ²	7.91 ¹	1.05 ²	5.99 ¹	5.73 ¹	3.04 ¹	3.19 ¹	1.83 ¹
$3S$		5.92	1.95	3.99	1.72	2.52	1.20	1.19	6.18 ⁻¹	6.29 ⁻¹	3.21 ⁻¹
$3P(0)$		1.08	6.42 ⁻¹	8.40 ⁻¹	3.78 ⁻¹	9.29 ⁻¹	2.38 ⁻¹	4.57 ⁻¹	2.60 ⁻¹	1.80 ⁻¹	2.00 ⁻¹
$3P(\pm 1)$		3.72 ⁻¹	9.48 ⁻²	7.36 ⁻¹	3.24 ⁻¹	1.10	3.40 ⁻¹	1.36	2.68 ⁻¹	1.02	1.80 ⁻¹
$3P(\Sigma)$		1.45	7.37 ⁻¹	1.58	7.02 ⁻¹	2.03	5.78 ⁻¹	1.82	5.28 ⁻¹	1.20	3.80 ⁻¹
$3D(0)$		2.73	1.34	3.03	1.72	1.49	8.34 ⁻¹	4.69 ⁻¹	2.81 ⁻¹	2.34 ⁻¹	2.17 ⁻¹
$3D(\pm 1)$		6.56	1.89	7.16	3.20	3.58	1.81	8.96 ⁻¹	6.35 ⁻¹	2.29 ⁻¹	2.51 ⁻¹
$3D(\pm 2)$		1.78	3.87 ⁻¹	3.89	1.40	3.52	1.45	1.92	8.55	1.02	5.41 ⁻¹
$3D(\Sigma)$		1.11 ¹	3.62	1.41 ¹	6.32	8.59	4.09	3.28	1.77	1.48	1.01
1^1S		1.47 ⁻¹	...	8.63 ⁻²	...	5.06 ⁻²	...	2.91 ⁻²	...	1.72 ⁻¹	...

^a Exponents indicate the power of 10 by which the entry is to be multiplied.

$$P(n^1P-n^1S) = \frac{\sigma_0 - \sigma_1}{\sigma_0 + \sigma_1}, \quad (30a)$$

$$P(n^3P-2^3S) = \frac{15(\sigma_0 - \sigma_1)}{41\sigma_0 + 67\sigma_1}$$

and

$$P(3^1D-2^1P) = \frac{3(\sigma_0 + \sigma_1 - 2\sigma_2)}{5\sigma_0 + 9\sigma_1 + 6\sigma_2}, \quad (30b)$$

$$P(3^3D-n^3P) = \frac{213(\sigma_0 + \sigma_1 - 2\sigma_2)}{671\sigma_0 + 1271\sigma_1 + 1058\sigma_2}$$

for the dipole radiation emitted from the excited states are presented in Table II. The effect of the couplings on the magnetic substates is strongly evident, particularly for the P - S transitions, when little correspondence is exhibited between columns 2 and 4 and between 3 and 5.

A. Differential cross sections

In Fig. 5 are displayed the differential cross sections for the singlet-singlet transitions, as a function of scattering angle θ and impact energy E (eV). The structure present in the 3^1P excitation but absent in the 2^1P excitation is a direct consequence of the very important, strong $3^1D(m=0, \pm 1, \pm 2)$ - 3^1P close couplings which affect the magnetic substates of 3^1P more than do the 1^1P - 1^1S couplings. The relative importance of close encounters (large-angle scattering) for optically forbidden vs optically allowed transitions is exhibited by the slower decrease with θ in Figs. 5(b) and 5(d) relative to that in Figs. 5(a) and 5(c).

No measurements or other theoretical calculations are available. However, since excitation from the 1^1S state was very well described (when compared with experiment) by the multichannel eikonal approach for $0 \leq \theta \leq 40^\circ$, a range contributing effectively all of the integral cross section, the data in Fig. 5 are presumed quite accurate for small-angle scattering. Electron-exchange effects, important for large-angle scattering,⁴ have been

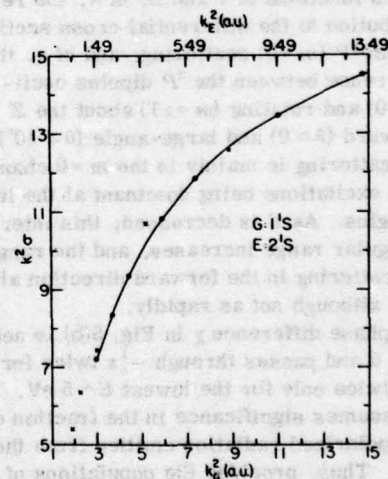


FIG. 4. Test of detailed balance between the forward and reverse rates of the 1^1S - 2^1S collisional excitation in helium by electrons with wave number k_0 and k_b in the 1^1S and 2^1S channels, respectively. \bullet : Previous $\sigma(1^1S-2^1S)$ data (Ref. 4). \times : Present $\sigma(2^1S-1^1S)$ data.

TABLE II. Polarization fractions of radiation of wavelength λ (Å) emitted from the collisionally excited states n' to state n .

$n'-n$ λ (Å)	2^1P-n^1S 20581(2) ^a 584(1)	2^3P-2^3S 10830	3^1P-n^1S 5016(2) 537(1)	3^3P-2^3S 3889	3^1D-2^1P 6678	3^3D-2^3P 5876
E (eV)						
5	-0.037	0.040	0.706	0.302	0.262	0.175
10	-0.207	-0.020	0.391	0.123	0.138	0.104
20	-0.647	-0.076	0.256	0.048	-0.021	0.025
50	-0.932	-0.171	-0.196	0.096	-0.248	-0.052
100	-0.968	-0.161	-0.478	0.116	-0.383	-0.072

^a Value of lower-level n in parenthesis.

explicitly neglected, although some (small) allowance does result by virtue of a multistate target expansion. Also differential cross sections for excitation of the m substates are available from the authors. No measurements exist as yet, although when various theoretical and experimental data for the $1^1S-2^1P_0$ differential magnetic sublevel cross sections were compared for electron-helium scattering at 60 and 80 eV, Chutjian and Srivastava¹³ concluded that the corresponding multichannel eikonal treatment provided the best agreement with their recent measurements.

Cross sections obtained for the corresponding triplet-triplet transitions are smaller than and demonstrate behavior similar to that in Fig. 5. They are available from the authors upon request.

B. Angular correlation parameters and circular polarization fractions

In Figs. 6(a) and 6(b) are presented graphical displays, as functions of θ and E , of λ , the relative contribution to the differential cross section arising from 1P ($m=0$) scattering, and of χ , the phase difference between the 1P dipoles oscillating ($m=0$) and rotating ($m=\pm 1$) about the Z axis. Forward ($\theta \approx 0$) and large-angle ($\theta \approx 40^\circ$) inelastic scattering is mainly in the $m=0$ channel, with $m=\pm 1$ excitations being dominant at the intermediate angles. As E is decreased, this intermediate angular range increases, and the range for $m=0$ scattering in the forward direction also increases, although not as rapidly.

The 2^1P phase difference χ in Fig. 5(b) is negative for all θ and passes through $-\frac{1}{2}\pi$ twice for all E , and $-\pi$ twice only for the lowest $E \sim 5$ eV. This behavior assumes significance in the fraction of circularly polarized radiation emitted from the 2^1P states. Thus, provided the populations of the $m=0$ and ± 1 sublevels are equal (i.e., $\lambda \approx 0.5$), then $\Pi = -\sin\chi$; fully circularly polarized light is observed when $\chi \approx -\frac{1}{2}\pi$, and is absent when $\chi \approx -\pi$ at two scattering angles θ . Figure 5(a), however

shows that the $m=0$ and $m=\pm 1$ substates are not equally populated, in general, except at specific θ , and the combined effect of phase difference and departure from equal populations is exhibited in Fig. 6 which displays Π given by (17) as a function of θ and E . This figure shows that circularly polarized light is observed when the electrons are scattered through fairly large angles which decrease as E increases. Moreover, Π passes through zero twice, only for $E=5$ eV, as expected from Fig. 5(b). Figure 7 also provides the angular momentum (17) transferred at right angles to the scattering plane, and hence the maxima, almost reaching unity, correspond to the transfer of ~ 1 unit of angular momentum (\hbar) to the atom which is therefore left in the $m=0$ state.

Similar graphical displays of λ , χ , and Π have been obtained for the remaining transitions (and are available from the authors). No experimental data exist. However, a corresponding ten-channel treatment⁴ of the 1^1S-2^1P , 3^1P transitions in helium by electron impact resulted in satisfactory agreement with the recent λ , χ measurements of Eminyan *et al.*⁸

Finally, the effect of the neglect of electron exchange and of couplings with channels $n \geq 4$ is difficult to assess without resort to more detailed and elaborate calculations. For transitions from the 1^1S state, electron exchange is effective only for the close encounters resulting in large-angle scattering. These large angles, however, provide negligible contribution to the inelastic integral cross sections,^{4,14} which are determined solely by scattering mainly in the forward direction ($\theta \lesssim 20^\circ$) at intermediate impact energies. Also, explicit inclusion¹ of exchange within the the VPS approximation for $e\text{-He}(2^{1,3}S)$ collisions causes little change for $E \gtrsim 10$ eV. A better representation of the direct scattering function is apparently more important and is obtained by the present inclusion of close couplings.

We note that a fully quantal close-coupling cal-

culation would in practice be prohibitively difficult in that an extremely large number of angular momentum states L of relative motion are distorted by the strong dipole interactions evident in the present study. Thus, the normal procedure of

performing fully quantal computations for $L=0 \sim L_{\max} \sim 10$ and a Born approximation for $L > 10$ simply will not suffice, since the present investigation has shown that impact parameters $\rho \sim 100$ a.u. ($\equiv L/k_i$) are influenced appreciably by the

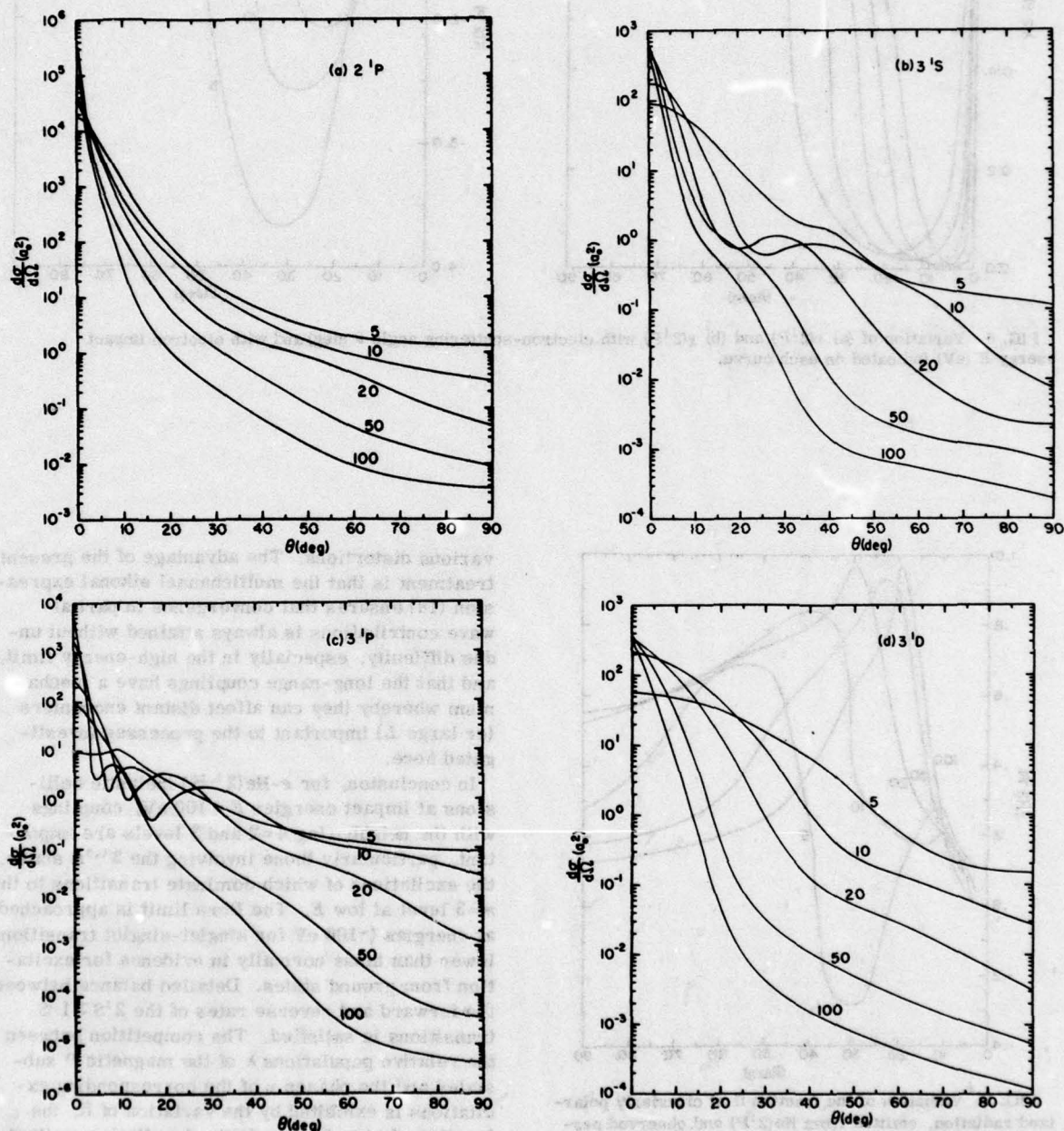


FIG. 5. Differential cross sections (a^2/sr) as a function of scattering angle θ (deg) and impact energy E (eV) indicated on each curve for (a) 2^1P , (b) 3^1S , (c) 3^1P , and (d) 3^1D excitations, summed over final magnetic substates m .

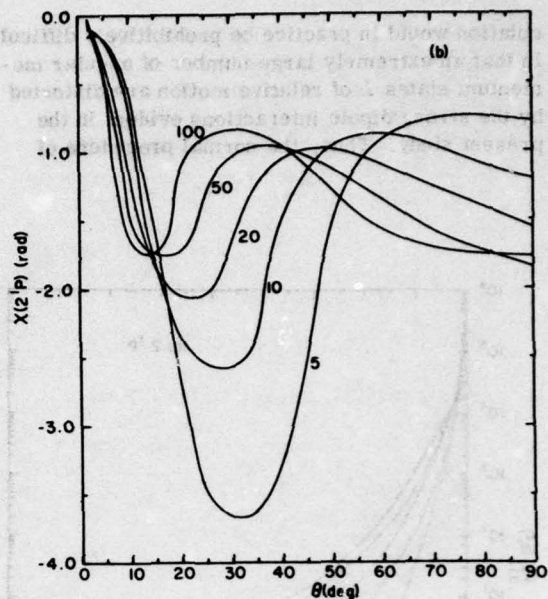
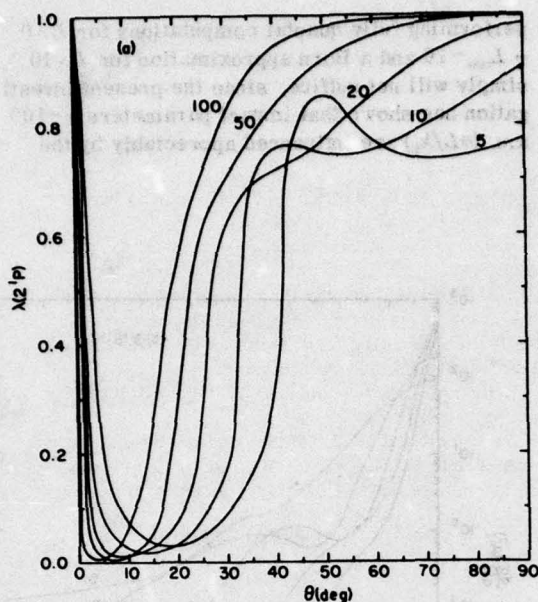


FIG. 6. Variation of (a) $\lambda(2^1P)$ and (b) $\chi(2^1P)$ with electron-scattering angle θ (deg) and with electron impact energy E (eV) indicated on each curve.

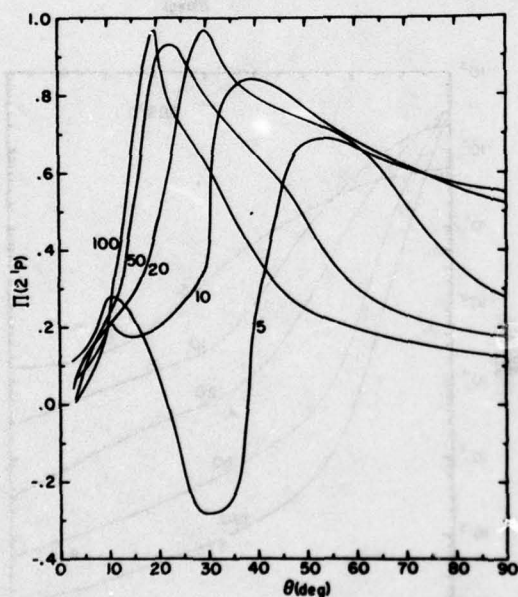


FIG. 7. Variation of the fraction Π of circularly polarized radiation, emitted from $\text{He}(2^1P)$ and observed perpendicular to the scattering plane, with electron-scattering angle θ and impact energy E (eV) indicated on each curve.

various distortions. The advantage of the present treatment is that the multichannel eikonal expression (18) ensures that convergence in partial-wave contributions is always attained without undue difficulty, especially in the high-energy limit, and that the long-range couplings have a mechanism whereby they can affect distant encounters (or large L) important to the processes investigated here.

In conclusion, for $e\text{-He}(2^1S)$ inelastic collisions at impact energies $E \leq 100$ eV, couplings with the neighboring $n=2$ and 3 levels are important, particularly those involving the $3^1,^3D$ states, the excitations of which dominate transitions to the $n=3$ level at low E . The Born limit is approached at energies (~ 100 eV for singlet-singlet transitions) lower than those normally in evidence for excitation from ground states. Detailed balance between the forward and reverse rates of the $2^1S \rightleftharpoons 1^1S$ transitions is satisfied. The competition between the relative populations λ of the magnetic P substates and the phases χ of the corresponding excitations is exhibited by the variation of Π , the fraction of circularly polarized radiation emitted from these P states, with impact energy E and scattering angle θ .

- *Research sponsored by the Air Force Aerospace Research Laboratories, Air Force Systems Command, U.S. Air Force Contract No. F33651-74-C-4003.
- ¹M. R. Flannery, W. F. Morrison, and B. L. Richmond, J. Appl. Phys. **46**, 1186 (1975).
- ²M. R. Flannery and K. J. McCann, J. Phys. B **7**, 2518 (1974); **7**, L522 (1974).
- ³K. J. McCann and M. R. Flannery, Phys. Rev. A **10**, 2264 (1974).
- ⁴M. R. Flannery and K. J. McCann, J. Phys. B (to be published).
- ⁵M. Cohen and R. P. McEachran, Proc. Phys. Soc. **92**, 37 (1967); J. Phys. B **2**, 1271 (1969); additional coefficients not tabulated in these references were obtained by private communication (1974).
- ⁶L. I. Schiff, Phys. Rev. **103**, 443 (1956).
- ⁷E. Gerjuoy and B. K. Thomas, Rep. Prog. Phys. **37**, 1345 (1974).
- ⁸M. Eminyan, K. B. MacAdam, J. Slevin, and H. Kleinpoppen, J. Phys. B **7**, 1519 (1974).
- ⁹U. Fano and J. H. Macek, Rev. Mod. Phys. **45**, 533 (1973).
- ¹⁰Y.-K. Kim and M. Inokuti, Phys. Rev. **181**, 205 (1969). The authors wish to thank Dr. Y.-K. Kim for sending us detailed tables of the form factors which were only partially given in this reference.
- ¹¹P. G. Burke, J. W. Cooper, and S. Ormonde, Phys. Rev. **183**, 245 (1969).
- ¹²I. C. Percival and M. J. Seaton, Philos. Trans. R. Soc. Lond. A **251**, 113 (1958).
- ¹³A. Chutjian and S. K. Srivastava, J. Phys. B (to be published).
- ¹⁴D. H. Madison and W. N. Shelton, Phys. Rev. A **7**, 499 (1973).

5.2 Cross Sections for Excitation and Ionization in e-He($2^{1,3}S$)

Collisions:

Cross sections for excitation and ionization in e-He($2^{1,3}S$) collisions

D Ton-That†, S T Manson‡ and M R Flannery†

†School of Physics, Georgia Institute of Technology, Atlanta, Ga 30332, USA

‡Department of Physics, Georgia State University, Atlanta, Ga 30303, USA

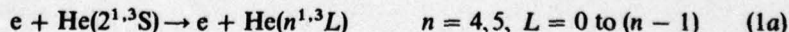
Received 6 July 1976

Abstract. Cross sections for the 2^3S-n^3L ($n = 2-5$, $L = S-F$) excitations and for single ionization in e-He($2^{1,3}S$) collisions are determined by using the Born approximation. For a given n , the 2^3S-n^3D transitions dominate at intermediate energies and this trend is continued for transitions to the near continuum. For larger energies ϵ of the ejected electron, higher angular momentum l waves progressively dominate. While up to nine partial waves are in general required for convergence of the bound-free form factor, as many as 30 are needed when momentum changes are in the vicinity of the Bethe ridge for large ϵ . Binary-encounter results for ionization are also obtained and agree with the Born values at intermediate energies. The present calculations and the recent measurements of Dixon *et al* are in satisfactory accord at intermediate energies. The contributions to ionization arising from multiple processes are also discussed.

1. Introduction

Relatively little is known about collisions between electrons and metastable rare-gas atoms which are of direct importance to gaseous discharges, astrophysical and atmospheric plasmas, the development of excimer and monohalide rare-gas lasers (cf Flannery *et al* 1975) and of ion engines (cf Martin 1974). Nor is much known concerning the validity of the Born approximation for electron collisions with excited atoms containing a loosely bound electron. The recent ten-channel eikonal results of Flannery and McCann (1975) for $2^{1,3}S-n^{1,3}L$ ($n = 2, 3$; $L = S, P, D$) collisional excitations of helium approach the corresponding Born values (Flannery *et al* 1975) at relatively modest impact energies $E \sim 100$ eV, which are, however, very much greater than the transition energy ΔE . Also, contrary to expectation, both the Born and ten-channel eikonal treatments predict that transitions to the optically forbidden $3^{1,3}D$ and $3^{1,3}S$ states are much stronger, by up to an order of magnitude, than the dipole-allowed $2^{1,3}S-3^{1,3}P$ collisional excitations, except of course at high energies where the dipole transitions predominate.

In an effort to determine whether this behaviour is characteristic of transitions to higher discrete and continuum states, and to obtain information on the corresponding cross sections (as functions both of impact energy E and of the angular momentum of the final target state) the following collisional excitation and ionization processes



621

will be studied in the Born approximation. The cross sections for ionization (1b) can be compared with the recent measurements of Dixon *et al* (1976a) and with results to be obtained from the binary-encounter approximation, which can be considered to be applicable since the averaged electronic separation in He is about $5a_0$ (Pekeris 1962). It is worth noting that the Born (Prasad 1966) and classical (Abrines *et al* 1966) predictions for ionization of metastable hydrogen are in close accord with the experimental data (Dixon *et al* 1975) over a wide range of electron impact energies.

2. Theory

The cross section for ionization of a singly excited atom B with mass M_B and ionization potential I by an incident particle A with mass M_A , speed v and relative energy E is, in the (elastic) binary-encounter approximation, given by (cf Vriens 1969, Flannery 1971)

$$\sigma_{nl}^I(E) = \frac{\pi}{M_{Ae} v^2} \int_I^E d\epsilon_T \int_0^\infty f_{nl}(u) \frac{du}{u} \int_{P^-}^{P^+} \frac{4}{P^4} \Gamma(P) dP \quad (2)$$

where the distribution in speed u of the valence electron described by a spatial wavefunction $\phi_{nlm}(r)$ is, with all quantities in atomic units,

$$f_{nl}(u) = \frac{1}{(2l+1)} \sum_{m=-l}^l \int \left| \frac{1}{(2\pi)^{3/2}} \int \phi_{nlm}(r) e^{-im \cdot r} dr \right|^2 u^2 d\hat{u} \quad (3)$$

and M_{Ae} is the reduced mass of the (A-e) binary system.

For a specified energy transfer ϵ_T to the valence electron, the momentum change P can vary between the lower limit,

$$P^- = \max [M|u' - u|, M_{AB}|v' - v|] \quad (4)$$

$$M = m \left(1 + \frac{m}{M_i} \right) \quad M_{AB} = \frac{M_A M_B}{(M_A + M_B)}$$

where m and M_i are the electronic and ionic masses respectively, and the upper limit,

$$P^+ = \min [M(u' + u), M_{AB}(v' + v)] \quad (5)$$

where the post-binary-collision speeds of the projectile and target particles are respectively,

$$v' = (v^2 - 2\epsilon_T/M)^{1/2} \quad (6)$$

and

$$u' = (u^2 + 2\epsilon_T/M)^{1/2}. \quad (7)$$

In the general expression (2), the function $\Gamma(P)$ which represents the departure of the differential cross section for (A-e) elastic scattering from the Rutherford value, is set to unity for direct (e-e) collisions for which $M \simeq M_{AB} \simeq m$.

The Born approximation to the cross section for single ionization of a two-electron atom by an incident electron is written, with all quantities in atomic units, as

$$\sigma_{nl}^I(E) = \int_0^{E(I-I)} d\epsilon \frac{1}{(2l+1)} \sum_{m=-l}^l \int \sigma_{nlm}^I(\epsilon, \hat{k}_e) d\hat{k}_e \quad (8)$$

in terms of

$$\sigma_{nlm}^I(\epsilon, \hat{k}_e) = \frac{8\pi}{k_i^2} \int_{K^-}^{K^+} \left| \left\langle \psi_f(\epsilon, \hat{k}_e; r) \left| \sum_{i=1}^2 e^{i\mathbf{k}_i \cdot \mathbf{r}_i} \left| \psi_i(n^{1,3}L; r) \right\rangle \right. \right|^2 \frac{dK}{K^3} \quad (9)$$

the differential cross section for ejection of the electron with momentum k_e into unit solid angle and unit energy interval. The limits to the momentum change ($k_i - k_e$) of the scattered electron are,

$$K^\mp = (2E)^{1/2} \mp [2(E - I - \epsilon)]^{1/2} \quad (10)$$

where the energy ϵ of ejection is $\frac{1}{2}k_e^2$ au and where the kinetic energy transferred to the ion is neglected. While the parameter α in the ϵ integration limit in (8) is unity for ionization involving distinguishable particles, Rudge and Seaton (1965) have shown that, for ionization of atomic hydrogen by electrons with random spin orientations, $\alpha = 0.5$ when electron-exchange effects are fully neglected. This choice ensures that the faster of the scattered and ejected electrons is always described by a plane wave. For electron impact ionization of helium (when neither choice is rigorously based), the spatial wavefunctions for the initial discrete and final continuum states are

$$\psi_i(n^{1,3}L; r) = \frac{1}{\sqrt{2}} [\phi_{1s}(r_1)\phi_{nlm}(r_2) \pm \phi_{1s}(r_2)\phi_{nlm}(r_1)] \quad (11)$$

and

$$\psi_f(\epsilon, \hat{k}_e^{1,3}L; r) = \frac{1}{\sqrt{2}} [\phi_{1s}(r_1)\phi_e(\hat{k}_e; r_2) \pm \phi_{1s}(r_2)\phi_e(\hat{k}_e; r_1)] \quad (12)$$

in which the $\text{He}^+(1s)$ core is considered frozen. The one-electron orbitals ϕ_{nlm} are chosen to form an orthonormal set such that the form factor in (9) is simply

$$\langle \psi_f | e^{i\mathbf{k}_e \cdot \mathbf{r}_1} + e^{i\mathbf{k}_e \cdot \mathbf{r}_2} | \psi_i \rangle = \langle \phi_e(\hat{k}_e; r) | e^{i\mathbf{k}_e \cdot \mathbf{r}} | \phi_{nlm}(r) \rangle. \quad (13)$$

The continuum orbital for the ejected electron is now expanded as

$$\phi_e(\hat{k}_e; r) = \sum_{l'=0}^{\infty} \sum_{m'=-l'}^{l'} \frac{i^{l'}}{r} e^{-i\eta_{l'}} F_{el'}(r) Y_{l'm'}(\hat{r}) Y_{l'm'}^*(\hat{k}_e) \quad (14)$$

in which the radial part has asymptotic behaviour

$$F_{el'}(r) \underset{r \rightarrow \infty}{\sim} \left(\frac{2}{\pi k_e} \right)^{1/2} \sin \left(k_e r - \frac{1}{k_e} \ln(2k_e r) - \frac{1}{2}l'\pi + \eta_{l'} \right) \\ \eta_{l'} = \arg \Gamma(l' + 1 - i/k_e) + \delta_{l'}(k_e) \quad (15)$$

where the additional phaseshift $\delta_{l'}$ is a measure of the departure of the electron-ion interaction from a pure Coulomb one. The amplitude $2^{1/4}/\pi^{1/2}\epsilon^{1/4}$ of (15) is chosen so as to fulfil the normalization condition

$$\langle \phi_e(\hat{k}_e; r) | \phi_e(\hat{k}_e'; r) \rangle = \delta(\epsilon - \epsilon') \delta(\hat{k}_e - \hat{k}_e') \quad (16)$$

where $\epsilon = \frac{1}{2}k_e^2$ is in atomic units. With $\epsilon = k_e^2$ in Rydberg units, then the amplitude of (15) would be $\pi^{-1/2}\epsilon^{-1/4}$ in order to satisfy (16).

Alternatively, the differential cross section per unit momentum interval ($d\sigma/dk_e$) is given by (9) with the asymptotic amplitude of $F_{el'}$ chosen as $(2^{1/2}/\pi^{1/2}k_e)$ thereby

ensuring that

$$\langle \phi_e(\mathbf{k}_e; r) | \phi_e(\mathbf{k}_e'; r) \rangle = \delta(\mathbf{k}_e - \mathbf{k}_e') \quad (17)$$

rather than (16).

By writing the orbital for the bound (nlm) state as

$$\phi_{nlm}(r) = (1/r) P_{nl}(r) Y_{lm}(\hat{r}) \quad (18)$$

and with the aid of

$$e^{i\mathbf{k} \cdot \mathbf{r}} = 4\pi \sum_{l'=0}^{\infty} \sum_{m'=-l'}^{l'} i^{l'} j_{l'}(Kr) Y_{l'm'}^*(\hat{\mathbf{K}}) Y_{l'm'}(\hat{r}) \quad (19)$$

where $j_{l'}$ denotes the spherical Bessel function, then, in terms of the Wigner 3j-symbols (cf Messiah 1966), the form factor (13) is

$$F_{e\mathbf{k}_e, nlm}(\mathbf{K}) = (4\pi)^{1/2} \sum_{l'} \sum_{m'} i^{l'} M_{el', nl}^{l''}(K) Y_{l'm'}(\hat{\mathbf{k}}_e) Y_{l''m''}^*(\hat{\mathbf{K}}) \times (-1)^{m'} [(2l+1)(2l'+1)(2l''+1)]^{1/2} \begin{pmatrix} l & l' & l'' \\ 0 & 0 & 0 \end{pmatrix} \begin{pmatrix} l & l' & l'' \\ m & -m' & m'' \end{pmatrix} \quad (20)$$

where the radial matrix element

$$M_{el', nl}^{l''} = \int_0^{\infty} i^{-l'} e^{i\eta_{l'}} F_{el'}(r) j_{l'}(Kr) P_{nl} dr. \quad (21)$$

The partial cross section (9) therefore entails, in general, eight summations and a double integration. However, when the modulus of (20) is squared, integrated over \mathbf{k}_e (assumed to be uncorrelated with \mathbf{K}), and summed over m and m' , then it follows that

$$\frac{1}{(2l+1)} \sum_{m=-l}^l \int |F_{e\mathbf{k}_e, nlm}(\mathbf{K})|^2 d\mathbf{k}_e = \sum_{l''} (2l'+1)(2l''+1) \begin{pmatrix} l & l' & l'' \\ 0 & 0 & 0 \end{pmatrix}^2 |M_{el', nl}^{l''}(K)|^2 \quad (22)$$

for a given momentum change K . For initial s states, then, from (8) and (9)

$$\sigma_{ns}^l(\epsilon) = \frac{8\pi}{k_i^2} \int_{K^-}^{K^+} \sum_{l'=0}^{\infty} (2l'+1) |M_{el', ns}^{l''}(K)|^2 \frac{dK}{K^3} \quad (23)$$

is the differential cross section per unit ejected-energy interval. The integral Born cross section for excitation of the discrete level ($n'l'$) is also given by each l' term of (23) but with $F_{el'}$ in (21) replaced by the bound-state function $P_{n'l'}$. For excitation, additional allowance will be made for core relaxation.

3. Method

In the present study, the electronic discrete and continuum wavefunctions $\psi(r_1, r_2)$ for helium are antisymmetrized products of one-electron orbitals $\phi_{nlm}(r)$ forming an orthonormal set obtained from a central-field approximation. The corresponding radial functions P_{nl} and F_{el} are therefore the appropriate solutions of the radial Schrödinger equation

$$\frac{d^2 P_{nl}}{dr^2} + 2 \left(E - V(r) - \frac{l(l+1)}{2r^2} \right) P_{nl} = 0 \quad E = \begin{cases} \epsilon_{nl} < 0 \\ \epsilon > 0 \end{cases} \quad (24)$$

which are normalized to unity for $E < 0$ and per unit energy interval for $E > 0$ as implied by (16). The spherical interaction $V(r)$ which tends to $(-2/r)$ and $(-1/r)$ as $r \rightarrow 0$ and ∞ , respectively, is determined from the Hartree-Slater approximation, i.e. the Hartree method modified by Slater (1951) to take some account of electron exchange. This approximation for V as determined by Herman and Skillman (1963) for ground-state atoms alone has been extensively used with encouraging results (cf Fano and Cooper 1968, Dehmer *et al* 1975, Manson and Purcell 1976 and references therein). In this paper, some variations to the standard treatment are explored by adopting the following choices for V .

Case (A). A self-consistent field (scf) iteration for the ground-state configuration $(1s)^2$ provides V_0 which is used to generate P_{nl} and F_{el} which are automatically orthogonal. This V_0 is the standard selection tabulated by Herman and Skillman (1963).

Case (B). An scf iteration for the initial-state $(1s)(2s)$ configuration yields V_1 which, when inserted in (24), provides orthonormal P_{nl} and F_{el} for $n = 1-5$, $l = 0-(n-1)$, $l' = 0-30$ and for a wide range (0-110 eV) of energies ϵ for the ejected electron.

Case (C). scf iterations for the three configurations $(1s)(2s)$, $(1s)(2p)$ and $(1s)(3d)$ yield three potentials $V_i^{(L)}$ ($L = 0, 1, 2$) which are used to generate $P_{n,l=0,3,4}^{(0)}$, $P_{n,l=1}^{(1)}$ and $P_{n,l=2}^{(2)}$ respectively for the (nl) states of the $n = 1-5$ levels. The form-factor in (9) for bound-bound transitions is, for the $L = 1$ and 2 cases, given by

$$F_{fi}(K) = \left\langle \psi_f(n^{1,3}L) \left| \sum_{i=1}^2 e^{i\mathbf{K} \cdot \mathbf{r}_i} \right| \langle \phi_{1s}^{(L)} | \phi_{1s}^{(0)} \rangle \phi_{2s}^{(0)} \pm \langle \phi_{1s}^{(L)} | \phi_{2s}^{(0)} \rangle \phi_{1s}^{(0)} \right\rangle \quad (25)$$

where the $\phi_{1s}^{(L)}$ which respectively result from $V_i^{(L)}$, $L = 1$ and 2, are in general different from $\phi_{1s}^{(0)}$ and are not orthogonal to both $\phi_{1s}^{(0)}$ and $\phi_{2s}^{(0)}$ because some core relaxation has been provided for those less penetrating orbitals with non-zero angular momentum. The f and g orbitals are generated in $V_i^{(0)}$ for simplicity since it is found that little improvement is gained by further modification.

Case (D). scf iterations for the $(1s)(nl)$ configuration of the final bound state $\psi_f(n^{1,3}L)$ provide $V_i^{(L)}$ which are used to generate P_{nl} for the lower bound states.

Case (E). scf independent iterations for the initial and final configurations, $(1s)(2s)$ and $(1s)(nl)$ respectively, yield independent scf solutions $\psi_i(2^{1,3}S)$ and $\psi_f(n^{1,3}L)$ with orthogonality satisfied by restricting the final bound states to $L \neq S$.

In the above five procedures, explicit dependence on electron spin appears only in the symmetry of the total spatial wavefunctions (11) and (12) and not in the interaction potential (which includes equal allowance for spin in the singlet and triplet cases). Spin effects are also acknowledged by the use of the corresponding experimental values of the excitation and ionization energies in the momentum-change limits (10) for the cross section (9).

All of the above possibilities were fully investigated via appropriate modifications to the standard Herman-Skillman program. By comparison of the resulting excitation energies (in cases (A), (B) and (D)), form factors and Born electron impact cross sections for the $2^{1,3}S-2^{1,3}P$, $3^{1,3}S$, $3^{1,3}P$, $3^{1,3}D$ and $4^{1,3}P$ transitions with those previously determined (Kim and Inokuti 1969, Flannery *et al* 1975) from highly accurate correlated functions (Weiss 1967), we have concluded that for the triplet transitions, method (B) achieves very good agreement (with cross sections to within 2.5% over a wide energy range) which is improved somewhat by modification (C). For singlet transitions, method (A) yields the closest, but yet rather poor, agreement (with cross

sections to only within 40%). The reasons for this dissimilarity in agreement are two-fold and are rather instructive.

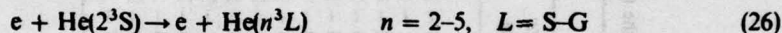
The (B), (C) combination provides an adequate account of core relaxation while ensuring that all of the excited 3S , 3P and 3D states are orthogonal to *all lower states of the same symmetry*. The same degree of orthogonality between the singlet states, especially that between the 2^1S and the 1^1S singlet ground state, is obtained via method (A) which, however, fails to account satisfactorily for core relaxation of the excited states and which fails to satisfy the Sharma-Coulson (1962) requirement that variational calculations of the (1s) and (ns) orbitals of helium should *not* be orthogonal for excited 1S states. Moreover, while the exchange interaction is attractive for the triplet states and repulsive for the *excited* singlet states (as predicted from perturbation theory which gives zero exchange effect for 1^1S), the Slater prescription assigns an exchange correction which is always negative (even for the 1^1S state) and which is therefore very biased towards the triplets.

The above considerations help explain the difference in quality of the present agreement obtained for the singlet and triplet cases. Also, the above (B), (C) combination is an extremely useful (and fast) method for obtaining accurate orthogonal wavefunctions for all the triplet (excited) states of helium.

4. Results and discussion

4.1. Excitation

In table 1 are displayed the excitation energies (from method (B)) and cross sections for the processes



at impact energies E in the range $5 \text{ eV} \leq E \leq 1000 \text{ eV}$. These cross sections agree with the available highly accurate cross sections (Kim and Inokuti 1969, Flannery *et al* 1975) to within 2.5% over the entire energy range, except for the 2^3S-3^3P transition for which the largest departure is 8.5%. The more accurate results, where available, are presented in table 1 for reference. The cross sections for the remaining transitions from the metastable level to the $n = 4$ and 5 levels are presumably even more accurate since the central-field approximation improves as the valence electron becomes more loosely bound and much less correlated with the core electron, as exhibited in table 1 by the closeness between the experimental and derived excitation energies. Table 1 also shows that the optically forbidden transitions to the D states of the (3-5) levels dominate all other transitions, except at the highest energies when the S-P dipole excitations gain in relative importance, in accord with Bethe's approximation. This behaviour is even true for transitions to the ionization threshold and is preserved in more elaborate treatments of excitation (Flannery *et al* 1975, Flannery and McCann 1975). The data in table 1 are useful and directly relevant to current modelling of excimer and monohalide rare-gas lasers.

4.2. Ionization

In figure 1 are displayed present cross sections determined from the binary-encounter formulae (2)-(7) for the ionization process



Table 1. (a) Transition energies ΔE (eV) and (b) Born cross sections (πa_0^2) for the (2^3S - n^3L) collisional excitations of helium by electrons of energy E (eV).

$n^3L =$	2^3P	3^3S	3^3P	3^3D	4^3S	4^3P	4^3D	4^3F	5^3S	5^3P	5^3D	5^3F	5^3G
(a) ΔE (exp) ^a	1.145	2.899	3.187	3.254	3.774	3.888	3.916	3.917	4.152	4.208	4.223	4.223	4.223 ^c
ΔE (derived) ^b	1.184	2.875	3.177	3.230	3.749	3.868	3.891	3.892	4.126	4.186	4.198	4.198	4.198
(b) E (eV)													
5	1.97 + 2 ^d 4.67 ^d		1.42 ^d	8.25 ^d	7.84 - 1	3.37 - 1	1.89	3.19 - 1	2.59 - 1	1.26 - 1	7.10 - 1	1.67 - 1	7.66 - 3
10	1.24 + 2	3.14	1.04	6.05	6.21 - 1	2.78 - 1	1.52	2.51 - 1	2.34 - 1	1.18 - 1	6.22 - 1	1.47 - 1	6.19 - 3
20	7.48 + 1	1.75	8.51 - 1	3.46	3.52 - 1	2.46 - 1	8.60 - 1	1.35 - 1	1.34 - 1	1.11 - 1	3.50 - 1	7.93 - 2	3.22 - 3
30	5.46 + 1	1.20	7.27 - 1	2.39	2.43 - 1	2.15 - 1	5.93 - 1	9.14 - 2	9.24 - 2	9.79 - 2	2.41 - 1	5.35 - 2	2.15 - 3
40	4.35 + 1	9.17 - 1	6.37 - 1	1.83	1.85 - 1	1.90 - 1	4.51 - 1	6.88 - 2	7.05 - 2	8.70 - 2	1.83 - 1	4.03 - 2	1.62 - 3
50	3.64 + 1	7.41 - 1	5.69 - 1	1.48	1.49 - 1	1.71 - 1	3.64 - 1	5.52 - 2	5.69 - 2	7.82 - 2	1.48 - 1	3.23 - 2	1.29 - 3
70	2.77 + 1	5.35 - 1	4.72 - 1	1.07	1.08 - 1	1.42 - 1	2.63 - 1	3.95 - 2	4.11 - 2	6.54 - 2	1.07 - 1	2.31 - 2	9.24 - 4
100	2.06 + 1	3.77 - 1	3.80 - 1	7.56 - 1	7.61 - 2	1.15 - 1	1.85 - 1	2.77 - 2	2.90 - 2	5.30 - 2	7.51 - 2	1.62 - 2	6.47 - 4
200	1.15 + 1	1.90 - 1	2.40 - 1	3.82 - 1	3.84 - 2	7.35 - 2	9.35 - 2	1.38 - 2	1.46 - 2	3.36 - 2	3.78 - 2	8.11 - 3	3.24 - 4
300	8.15	1.27 - 1	1.80 - 1	2.56 - 1	2.57 - 2	5.51 - 2	6.25 - 2	9.22 - 3	9.78 - 3	2.52 - 2	2.53 - 2	5.40 - 3	2.16 - 4
400	6.37	9.56 - 2	1.45 - 1	1.92 - 1	1.93 - 2	4.46 - 2	4.69 - 2	6.92 - 2	7.34 - 3	2.04 - 2	1.90 - 2	4.05 - 3	1.62 - 4
500	5.25	7.65 - 2	1.23 - 1	1.54 - 1	1.54 - 2	3.77 - 2	3.76 - 2	5.53 - 3	5.88 - 3	1.73 - 2	1.52 - 2	3.24 - 3	1.29 - 4
600	4.48	6.38 - 2	1.07 - 1	1.28 - 1	1.29 - 2	3.28 - 2	3.13 - 2	4.61 - 3	4.90 - 3	1.50 - 2	1.27 - 2	2.70 - 3	1.08 - 4
1000	2.87	3.83 - 2	7.16 - 2	7.70 - 2	7.73 - 3	2.20 - 2	1.88 - 2	2.77 - 3	2.94 - 3	1.01 - 2	7.61 - 3	1.62 - 3	6.47 - 5

^a From Moore (1949).

^b From method (B) in text.

^c Extrapolated from 5^3F .

^d From Kim and Inokuti (1969) and Flannery *et al* (1975).

Exponent gives power of ten by which entry is to be multiplied.

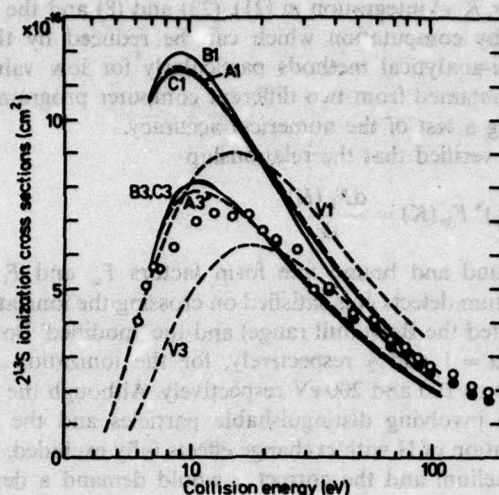


Figure 1. Comparison of present binary-encounter treatments of the cross sections for outer-shell ionization of $\text{He}(2^{1,3}\text{S})$ with different orbital-velocity distributions, as determined from methods (A) and (B) in text (curves A, B), and from Hartree-Fock functions (C) of Cohen and McEachran (1967a, b). Curves V are results of Vriens (1964) using the exponential distribution of Gryzinski (1965). The associated numerals 1 and 3 refer to 2^1S and 2^3S targets respectively. The circles (open and full) are measurements of Dixon *et al* (1976a) for the sum of all electron impact processes leading to single (but not double) ionization of a predominantly $\text{He}(2^3\text{S})$ target.

in which the ion is left in the ground state. The frozen-core $2^{1,3}\text{S}$ Hartree-Fock functions of Cohen and McEachran (1967a, b) and the $2^{1,3}\text{S}$ Hartree-Slater functions obtained from both methods (A) and (B) above are used in (3) to generate the velocity distributions $f_{nl}(u)$ for the valence electron. The cross sections associated with the rather accurate Hartree-Fock functions are in excellent agreement, especially at low energies, with the cross sections derived from method (B) for 2^3S ionization, and in good agreement with those derived from method (A) for 2^1S ionization, respectively. This closeness provides an additional check on the quality of our present 2^3S wavefunction, and indicates that the present 2^1S Hartree-Slater function is quite adequate for bound-free transitions, the form factor (13) for which tends to be controlled by interelectronic distances r_{12} larger than those important for bound-bound transitions. Also shown for completeness are the previous binary-encounter results of Vriens (1964) based on an exponential velocity distribution (Gryzinski 1965) which is, however, completely at variance (cf Burgess and Percival 1968) with any quantal distribution. The recent experimental data of Dixon *et al* (1976a) for ionization of a predominantly 2^3S target are also displayed; the earlier measurements of Fite and Brackman (1963), Long and Geballe (1970) and modifications thereof have already been discussed extensively by Dixon *et al* (1976a).

In order to achieve convergence of the differential and integral cross sections (23) and (8) for ionization over the impact energy range E , it is necessary to compute the Born matrix element $M'_{ei,2s}(K)$ for a wide range of energy ϵ and angular momentum l' of the ejected electron and also of the momentum change K of the scattered electron. This necessitates the calculation of 9-30 partial l' waves for each set of (ϵ, K) values appropriate to impact energies E up to 100 eV. This determination,

together with the triple (r, K, ϵ) integration in (21), (23) and (8) and the l' summation, requires extremely lengthy computation which can be reduced by the use, where possible, of various semi-analytical methods particularly for low values of l' . The resulting cross sections obtained from two different computer programs are in close accord, thereby providing a test of the numerical accuracy.

In addition, we have verified that the relationship

$$\lim_{n \rightarrow \infty} (n - \delta_l)^3 F_{ln}(K) = \frac{dF_{ln}(K)}{d\epsilon} \quad (28)$$

involving the bound-bound and bound-free form factors F_{ln} and F_{le} respectively, and the asymptotic quantum defects δ_l is satisfied on crossing the ionization threshold.

In figure 2 are presented the Born (full range) and the 'modified' Born (half range) cross sections, (8) with $\alpha = 1$ and $\frac{1}{2}$ respectively, for the ionization processes (27) at collision energies E up to 100 and 200 eV respectively. Although the former choice is correct for ionization involving distinguishable particles and the latter is used for electron impact ionization of H with exchange effects fully excluded, neither choice is rigorously based for helium and the correct α would demand a detailed account of exchange effects.

In the present case, the full-range results F are in closer accord than the half-range results H with the experimental data for ionization of the predominantly 2^3S target at low and intermediate impact energies E . Calculations (Ton-That and Flannery 1977a) for bigger targets (Ne^* , Ar^*) show an evolution from this trend, favouring the half-range results rather than the full-range ones. While convergence between F and H is obtained at the higher E , as expected, the measurements are up to 30% higher. This discrepancy which may be due to the theoretical neglect of additional processes will be studied in further detail below by means of a Bethe

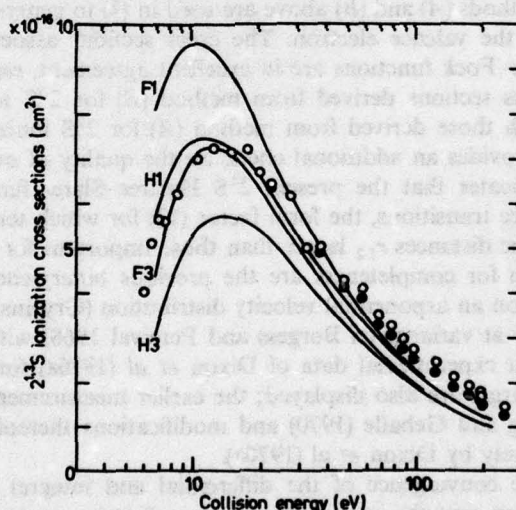


Figure 2. Comparison of present Born cross sections for outer-shell ionization of $He(2^{1,3}S)$ by electron impact; curves F and H are for respective integrations over the full range and the lower-half range of energy of the ejected electron. The associated numerals 1 and 3 refer to 2^1S and 2^3S targets respectively. The circles are measurements as in figure 1.

plot. The half-range cross sections for ionization of the triplet states agree to within a few per cent with the corresponding Born calculations (not shown) of G Peach (1976 private communication) who used a Clementi-type fit for the initial state and, for continuum waves, hydrogenic functions, except the s, p and d partial waves.

Figure 3 provides a comparison of the measured cross sections with the present Born full-range values to 100 eV and with the binary-encounter results to 1000 eV. Also shown is an additional binary-encounter contribution which arises from direct ejection of the inner-shell electron such that the product ion is left as $\text{He}^+(2s)$. This mechanism does not fully account for the discrepancy with the observations at collision energies $E \geq 200$ eV.

This difference is further amplified in figure 4 where Bethe plots, i.e. $\sigma_i(E) \times E$ plotted against $\lg E$, of the various results are displayed. (The inclusion of dipole-allowed transitions yields an $E^{-1} \lg E$ dependence for the ionization cross section $\sigma_i(E)$ at large impact energies E , thereby resulting in a straight-line Bethe plot at high E .) The lower set of experimental data includes a correction made to the higher original set for charge-exchange reactions between metastable He and residual molecular ions in the experimental collision region (see Dixon *et al* 1976a). The remaining difference between the theoretical Born curve corresponding to a ground-state $\text{He}^+(1s)$ product ion and the measurements cannot be attributed to the $2^1S/2^3S$ admixture in the target gas since the difference between the cross sections for singlet and triplet ionization decreases as E increases (see figure 3).

Other processes, neglected theoretically, which enter as E increases are (a) inner-shell ionization, (b) autoionization over certain small discrete regions of E , (c) double ionization (which is also *not* included in the measurements) and (d) ionization of one electron with simultaneous excitation of the other electron. Of all the above processes, (a) is expected to be the largest contributor over a wide energy range

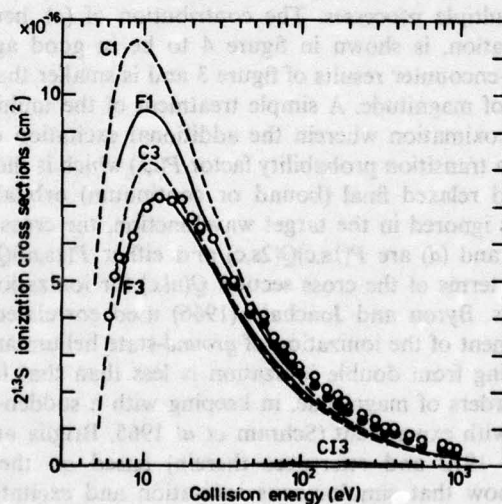


Figure 3. Cross sections for electron impact ionization of $\text{He}(2^{1,3}S)$. Curves F and C are the full-range Born and binary-encounter treatments respectively. Numerals 1 and 3 refer to 2^1S and 2^3S targets respectively. CI3 denotes the present binary-encounter treatment of inner-shell ionization of $\text{He}(2^3S)$ and the C3 full curve includes this contribution. The circles are measurements as in figure 1.

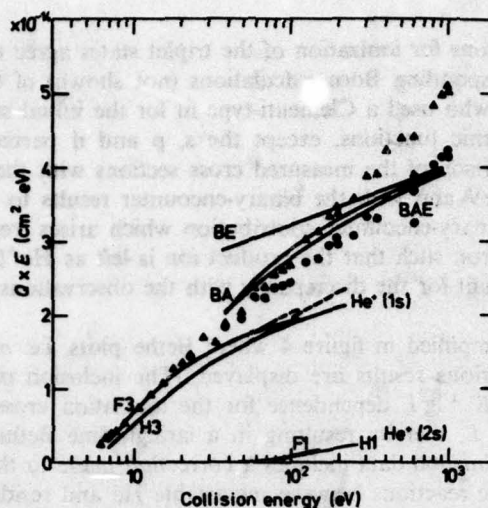


Figure 4. Bethe plot (cross section multiplied by collision energy E plotted against $\lg E$) for electron impact ionization of $\text{He}(2^3\text{S})$. Full curves F3 and H3 are full-range and half-range Born results for outer-shell ionization alone, F1 and H1 are the corresponding results for inner-shell ionization, included by the F3 and H3 broken curves. BE, BA and BAE represent cross sections of Briggs and Kim (1971) determined from closure in the Bethe approximation BE, the Born asymptotic with and without exchange BAE and BA respectively. The triangles and circles denote measurements of Dixon *et al* (1976a) for the sum of all electron impact processes leading to single (but not double) ionization of a predominantly $\text{He}(2^3\text{S})$ target.

since it can be regarded as a single scattering process, while the remaining wide-energy-range processes are multiple processes. The contribution of (a), here determined by the Born approximation, is shown in figure 4 to be in good agreement with the corresponding binary-encounter results of figure 3 and is smaller than outer-shell ionization by one order of magnitude. A simple treatment of the multiple processes adopts the sudden approximation wherein the additional excitation or ionization involved is described by a transition probability factor $P(i,f)$ which is the overlap squared of selected initial and relaxed final (bound or continuum) orbitals. Thus, for example, when exchange is ignored in the target wavefunction, the cross sections for the multiple processes (c) and (d) are $P(1s,c)Q(2s,c)$ and either $P(1s,nl)Q(2s,c)$ or $P(2s,nl)Q(1s,c)$, respectively, in terms of the cross section $Q(nl,c)$ for ionization of the (nl) orbital by a single process. Byron and Joachain (1966) used correlated atomic wavefunctions in a Born treatment of the ionization of *ground-state* helium and found that the contribution (DI) arising from double ionization is less than that for single ionization (SI) by about two orders of magnitude, in keeping with a sudden-collision model (Mittleman 1966) and with experiment (Schram *et al* 1965, Briglia and Rapp 1966). Calculations (Gillespie 1972 and references therein) based on the sudden approximation for $\text{He}(1^1\text{S})$ show that simultaneous ionization and excitation (SICE see below) are lower than SI by about three orders of magnitude (or at best by two orders, cf Dixon *et al* 1976b). Although excited states of helium have lower thresholds for multiple processes than the ground state, the correlation between the core and valence electrons, which is important in multiple processes if the energy

transfer is not too large, is much less (the atomic electrons have separations of about $5a_0$ and binding energies of approximately 46 eV and 5 eV respectively). While some doubt has been cast on the usefulness of the sudden approximation for multiple processes (Kaminsky and Popova 1976, see also Dixon *et al* 1976b), recent measurements (Schmidt *et al* 1976), however, do not suggest that a revision of the experimental results for double ionization of helium in its ground state is necessary.

The above arguments are, however, difficult to reconcile with the findings of Briggs and Kim (1971) who obtained various Born asymptotic limits for single and double ionization of the triplet states by subtracting the sum of the Born asymptotes for the discrete excitations from the asymptotes of the total inelastic cross section obtained from closure sum rules. The resulting Bethe ($A \ln E$) term and the asymptotic Born (half-range) term, $A \ln E + \gamma + \dots$, with and without the Mott correction for exchange, are reproduced in figure 4. The difference between the curves H3 and BA should arise from the effects of inner-shell ionization (ISI) and, to a lesser extent, of double ionization (DI) and single ionization with core excitation (SICE). Results from our present Born treatment of ISI are shown explicitly and, when added to the SI results H3 and F3, yield the broken curves in figure 4. The remaining difference, if all is well, must arise from (unacceptably large) contributions from DI and SICE. The asymptotic procedure has been estimated by Briggs and Kim (1971) to be reliable only for collision energies $E > 400$ eV such that the correct plots for smaller energies may deviate from those shown. We note, however, that the difference between BA and H3 can mainly be resolved by assigning some value to the second parameter γ smaller than that given by Briggs and Kim (1971). This parameter is difficult to evaluate correctly and involves a sum of integrals of the generalized and optical oscillator strengths (Inokuti *et al* 1967).

In summary, figure 4 depicts (a) full Born calculations of both SI and ISI, the SI results agreeing rather closely with similar calculations of G Peach (1976 private communication), (b) Born asymptotes of Briggs and Kim (1971) including all contributions (SI, ISI, DI, SICE) to ionization and (c) measurements of the combined SI, ISI and SICE contributions. Accord between (a) and (c) is introduced at high energies E only if the yield from the (neglected) multiple SICE process is roughly three times that from the single ISI process. Also the apparent agreement between (b) and (c) at large E suggests that DI is negligible in comparison to SICE, an unlikely event. The resolution of the discrepancies between (a), (b) and (c) can only be obtained if the various contributions to ionization are arranged in order of importance as SI, SICE, ISI and DI, an order at variance with that naturally assumed.

The theoretical cross sections obtained from the Born and the binary-encounter approximations for ionization of the $2^{1,3}S$ states are presented in table 2. The full-range and the half-range Born results mutually converge with increasing impact energy E , as expected. In the intermediate energy range $1 < E(\text{au}) < 8$, the binary-encounter values, when compared with the full-range Born results, display fair agreement which originates from the overall agreement in magnitude and shape between the quantum-mechanical and the binary-encounter results for the form factor (20) squared (FFS), or for the associated generalized oscillator strength (GOS) away from the optical $K \rightarrow 0$ limit. The increasing discrepancy in the GOS for small momentum changes $K \simeq \epsilon_T/v$ associated with larger impact energies E yields an E^{-1} asymptotic limit for the binary-encounter cross sections rather than the correct $E^{-1} \ln E$ limit obtained when proper account is taken of the dipole transitions for such low momentum changes.

Table 2. Born (full-range (BF) and half-range (BH)) and binary-encounter (BE) cross sections (10^{-16} cm^2) for the ionization of $\text{He}(2^{1,3}S)$ by electrons with energy $E(\text{au})$.

$E(\text{au})$	2^3S			2^1S		
	BF	BH	BE	BF	BH	BE
0.25	4.35	3.04	5.59	8.07	5.69	10.51
0.50	7.16	5.70	7.81	9.05	7.36	10.38
0.75	6.15	5.33	6.49	7.39	6.47	8.45
1.00	5.25	4.65	5.48	6.22	5.59	7.02
1.5	4.03	3.67	4.16	4.75	4.35	5.16
2.0	3.18	3.00	3.35	3.72	3.54	4.05
2.5	2.66	2.55	—	3.11	2.99	—
3	2.29	2.26	2.39	2.68	2.65	2.81
4	1.80	1.76	1.87	2.10	2.06	2.15
5	—	1.46	1.53	—	1.71	1.74
6	—	1.25	1.29	—	1.46	1.46
7	—	1.11	—	—	1.29	—
8	—	0.98	0.99	—	1.14	1.11

4.3. The rate of convergence of the partial-wave expansion

For most values of ϵ and K , the number of the l partial waves† required for convergence of FRS with respect to l is relatively small, nine or less in the present case. However, for large ϵ , the required number increases sharply near the Bethe ridge defined by

$$K_{BR}^2 = 2\epsilon_T = 2(I + \epsilon) \quad (29)$$

where up to 30 partial waves are required. This is interpreted as follows. The region where the initial bound state orbital $P_l(r)$ is substantial defines for our purposes the maximal region of overlap. The continuum orbital $F_{el}(r)$ and the spherical Bessel function $j_{l'}(Kr)$ (cf equation (21)) initially increase in amplitude from the origin as $(\sqrt{2\epsilon_T})^{l'+1}$ and $(Kr)^{l''}$ respectively. These sharp dependences on l' and l'' can be regarded as centrifugal-barrier effects. $F_{el}(r)$ and $j_{l'}(Kr)$ then evolve into oscillating functions. An increase in l (i.e. l' and l'') results in a shift of the pattern of these functions out of the overlap region together with a stretching of their first lobe.

When ϵ is large enough, the continuum orbital F_{el} oscillates many times within the overlap region. If either $K^2 \ll 2\epsilon_T$ or $K^2 \gg 2\epsilon_T$, then, due to the varying relative phase of $j_{l'}$ and F_{el} , the contribution from their oscillatory regions is small and the effective region of overlap is therefore reduced to the inner lobes of $j_{l'}$ or F_{el} . As l increases, the slower oscillating of the two functions shifts out of this reduced region of overlap more quickly than this region can widen such that fast convergence with l is obtained.

When $K^2 \sim K_{BR}^2 = 2\epsilon_T$, the resonance which can occur between F_{el} and $j_{l'}$ in the oscillatory region implies that this region can contribute substantially to (21) and yields a peak with respect to K and ϵ_T , the so-called Bethe ridge (Inokuti 1971). The effective region of overlap is now the maximal overlap region. Moreover, the greater ϵ is, the larger is the number of initial low- l oscillations of F_{el} in the

† Hereafter l is used to denote either l' or l'' interchangeably.

AD-A062 163

GEORGIA INST OF TECH ATLANTA SCHOOL OF PHYSICS
CALCULATION OF ELECTRON IMPACT CROSS SECTIONS FROM METASTABLE S--ETC(U)
AUG 78 M R FLANNERY

F/G 7/4

F33615-74-C-4003

UNCLASSIFIED

2 OF 3

AD
A062163



ADADI -TD-7A-5A

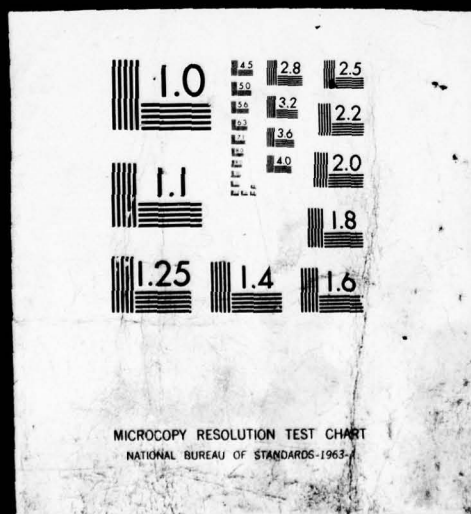
NI



TTTTT

2 OF 3

AD
A062163



overlap region and the larger is the value of l attained before the oscillatory pattern of $j_l F_{el}$ is pulled out of the overlap region. This results in a slow convergence with respect to l in the vicinity of the Bethe ridge—the $(2l+1)$ factor even favours an initial rise with respect to l eventually subdued by the stretching of the first lobe of $j_l F_{el}$ —and therefore a broad peak with respect to l is exhibited.

On the other hand, as $\epsilon \rightarrow 0$, F_{el} oscillates only a few times in the maximal region of overlap. Increasing l quickly pulls F_{el} out of this region thereby ensuring that, even if there is an initial rise with l , fast convergence with respect to l soon sets in, whatever K . This convergence can be accelerated for small or large K by the centrifugal-barrier effect in j_l or by a reduction of the effective region of overlap.

Overall, the rate of convergence with respect to l is relatively slower where the FFS is relatively large (as a function of K). Whatever ϵ , the optical transitions dominate the sum (23) over l in the limit of small momentum transfer ($K \rightarrow 0$).

Just above the threshold of ionization, the s-d transition still dominates as it does for bound-bound excitation, and therefore indicates that for a given l , the number of oscillations within the range of the initial state does not vary much for final orbitals whether bound or near-threshold continuum. These arguments can indeed be extended to bound-bound transitions (Ton-That and Flannery 1977b). Even at or below the threshold of ionization, the dominant transitions (here, s-d) still tend to peak with respect to K near the Bethe ridge $K^2 \sim 2\epsilon_T$ and so does the FFS summed over l . This fact seems to be a peculiarity of initial s states.

In accordance with our previous discussion, the dominant transition shifts from s-d to s-f, and on to s-g, etc as ϵ increases while K remains in the vicinity of the Bethe ridge.

5. Conclusion

In summary, we have calculated electron impact Born excitation and Born and binary-encounter ionization cross sections of $\text{He}(2^{1,3}\text{S})$. The cross sections for excitation from $\text{He}(2^3\text{S})$ given here are presumed to be accurate Born values. The results for ionization of $\text{He}(2^3\text{S})$ are in fair agreement with the measurements (Dixon *et al* 1976b) at low and intermediate impact energy E when the helium ion is left in its ground state. The present results in conjunction with those of Briggs and Kim (1971) raise some questions about the magnitude of multiple processes involving ionization of $\text{He}(2^3\text{S})$. We have also discussed the relation between the orbital angular momentum of the final state and the relative importance of its contribution to a partial-wave expansion of the form factor squared, emphasizing the limitation imposed by the range of the initial-state orbital.

Acknowledgments

This research was sponsored by the Air Force Aero Propulsion Laboratory, Air Force Systems Command, United States Air Force, Contract F33615-76-C-2033, the Army Research Office, Contract DAHCO4 74 G 0217 and the National Science Foundation, Grant THY72-05156 A01. We are grateful to Dr A J Dixon, Dr M F A Harrison and Dr G Peach for discussion and for providing their results prior to publication.

References

- Abrines R, Percival I C and Valentine V A 1966 *Proc. Phys. Soc.* **89** 515-23
 Briggs J S and Kim Y-K 1971 *Phys. Rev. A* **3** 1342-8
 Briglia D D and Rapp D 1966 *Bull. Am. Phys. Soc.* **11** 69
 Burgess A and Percival I C 1968 *Advances in Atomic and Molecular Physics* vol 4 (New York: Academic) p 124
 Byron F W and Joachain C J 1966 *Phys. Rev. Lett.* **25** 1139-42
 Cohen M and McEachran R P 1967a *Proc. Phys. Soc.* **92** 37-41
 —1967b *Proc. Phys. Soc.* **92** 539-42
 Dehmer J L, Inokuti M and Saxon R P 1975 *Phys. Rev. A* **12** 102-21
 Dixon A J, von Engel A and Harrison M F A 1975 *Proc. R. Soc. A* **343** 333-45
 Dixon A J, Harrison M F A and Smith A C H 1976a *J. Phys. B: Atom. Molec. Phys.* **9** 2617-31
 Dixon A J, McCarthy I E and Weigold E 1976b *J. Phys. B: Atom. Molec. Phys.* **9** L195-8
 Fano U and Cooper J W 1968 *Rev. Mod. Phys.* **40** 441-507
 Fite W L and Brackman R T 1963 *Proc. 6th Int. Conf. on Ionization Phenomena in Gases* vol 1, ed P Hubert and E Crémieu-Alcan (Paris: SERMA) pp 21-6
 Flannery M R 1971 *J. Phys. B: Atom. Molec. Phys.* **4** 892-5
 Flannery M R and McCann K J 1975 *Phys. Rev. A* **12** 846-55
 Flannery M R, Morrison W R and Richmond B L 1975 *J. Appl. Phys.* **46** 1186-90
 Gillespie E S 1972 *J. Phys. B: Atom. Molec. Phys.* **5** 1916-21
 Gryzinski M 1965 *Phys. Rev. A* **138** 322-35
 Herman F and Skillman S 1963 *Atomic Structure Calculations* (Englewood Cliffs, NJ: Prentice-Hall)
 Inokuti M 1971 *Rev. Mod. Phys.* **43** 297-347
 Inokuti M, Kim Y-K and Platzman R L 1967 *Phys. Rev.* **164** 55-61
 Kaminsky A K and Popova M I 1976 *J. Phys. B: Atom. Molec. Phys.* **9** L177-80
 Kim Y-K and Inokuti M 1969 *Phys. Rev.* **181** 205-14
 Long D R and Geballe R 1970 *Phys. Rev. A* **1** 260-5
 Manson S T and Purcell J E 1977 *Phys. Rev. A* in press
 Martin A R 1974 *J. Phys. B: Atom. Molec. Phys.* **7** 1161-6
 Messiah A 1966 *Quantum Mechanics* vol 2 (New York: Wiley)
 Mittleman M 1966 *Phys. Rev. Lett.* **16** 498-9
 Moore C E 1949 *Atomic Energy Levels* NBS Circular No 467, vol 1 (Washington, DC: US Govt Printing Office)
 Pekeris C L 1962 *Phys. Rev.* **126** 1470-6
 Prasad S 1966 *Proc. Phys. Soc.* **87** 393-8
 Rudge M R H and Seaton M J 1965 *Proc. R. Soc. A* **283** 262-90
 Schmidt V, Sandner N and Kuntzemüller H 1976 *Phys. Rev. A* **13** 1743-7
 Schram B L, de Heer F J, Van der Wiel M J, Boerboom A J H, Moustafa H R, Schutten J and Kistemaker J 1965 *Proc. 4th Int. Conf. on Physics of Electronic and Atomic Collisions* (New York: Science Bookcrafters) Abstracts pp 434-41
 Sharma C S and Coulson C A 1962 *Proc. Phys. Soc.* **80** 81-96
 Slater J C 1951 *Phys. Rev.* **81** 385-90
 Ton-That D and Flannery M R 1977 *Phys. Rev. A* in press
 —1977b in preparation
 Vriens L 1964 *Phys. Lett* **8** 260-1
 —1969 *Case Studies in Atomic Collision Physics* vol 1, ed E W McDaniel and M R C McDowell (Amsterdam: North Holland) pp 337-98
 Weiss A W 1967 *J. Res. NBS A* **71** 163-8

SECTION VI

CROSS SECTIONS FOR IONIZATION OF METASTABLE RARE-GAS ATOMS

(Ne*, Ar*, Kr*, Xe*) AND OF METASTABLE N₂*, CO* MOLECULES BY ELECTRON IMPACT

Cross sections for the ionization processes

$$\vec{e} + X^*[1s^2, 2s^2, \dots (n-1)p^5 ns; {}^3P_{0,2}] \rightarrow \vec{e} + X^+[1s^2, 2s^2, \dots (n-1)p^5] + e, \quad (6.1)$$

for X \equiv Ne, Ar, Kr and Xe (with n = 3, 4, 5 and 6 respectively)

$$\vec{e} + N_2(A^3\Sigma_u^+) \rightarrow \vec{e} + N_2^+(A^2\Pi_u) + e, \quad (6.2)$$

$$\vec{e} + N_2(a^1\Sigma_u^-) \rightarrow \vec{e} + N_2^+(A^2\Pi_u) + e \quad (6.3)$$

and

$$\vec{e} + CO(a^3\Pi) \rightarrow \vec{e} + CO^+(X^2\Sigma^+) + e \quad (6.4)$$

are here determined as a function of impact-energy E via the Born and binary-encounter approximations. A full description of this work, which has been published in Phys. Rev. A 15 (1977) 517-526, now follows.

6.1 Cross Sections for Ionization of Metastable Rare-Gas Atoms

(Ne*, Ar*, Kr*, Xe*) and of Metastable N₂*, CO* Molecules

by Electron Impact

Cross sections for ionization of metastable rare-gas atoms (Ne*, Ar*, Kr*, Xe*) and of metastable N₂*, CO* molecules by electron impact*

D. Ton-That and M. R. Flannery

School of Physics, Georgia Institute of Technology, Atlanta, Georgia 30332

(Received 30 September 1976)

Cross sections for the collisional ionization of the metastable atoms Ne*, Ar*, Kr*, and Xe* by electrons with impact energy E in the range $6 < E < 250$ eV are determined in the Born and binary-encounter approximations. For low energies ϵ of ejection, the s - d and s - f bound-free transitions dominate the associated form factor, while transitions to continuum states with progressively higher angular momentum gain importance with increasing ϵ . While up to nine partial waves are normally sufficient for convergence of the bound-free form factor at a given energy ϵ and momentum change K of the ejected electron, as many as 30 are required for those K in the vicinity of the Bethe ridge at large ϵ . These properties are the origin of the overall closeness obtained between the Born and binary-encounter cross sections. Also inner-shell ionization, as described by the binary-encounter treatment, becomes increasingly important as the target atom becomes more complex. Cross sections for ionization of metastable N₂* and CO* are also determined. Good agreement with available measurements (for Ne* and Ar*) is obtained.

I. INTRODUCTION

Apart from the Born and binary-encounter treatments for the ionization of metastable helium¹ by electron impact, little is known about the cross sections for ionization of metastable rare-gas atoms X (Ne*, Ar*, Kr*, Xe*) by electron impact. This information is important in the modeling and feasibility studies of certain excimer lasers. In particular, very recent observations²⁻⁵ of high-power laser emission from a new class of molecules—the noble-gas monohalides (ArF*, KrF*, and XeF*, for example)—have demonstrated the potential of a new class of high-power high-efficiency and partially tunable lasers operating around 3000 Å. The lasing transition originates on an excited molecular state XF* formed directly by X*-F₂ rearrangement collisions or indirectly by three-body ion-ion recombination between the positive ions X⁺ produced by electron-impact ionization of X^(*) and the negative ions F⁻ formed by dissociative attachment in (e-F₂) collisions. The ionization of metastable rare-gas atoms therefore plays a key role, as a mechanism for depletion of atomic metastables in the former case and as a source of production of metastable excimers via ionic recombination in the latter case.

In this paper, cross sections for the ionization of metastable Ne*, Ar*, Kr*, and Xe* by electron impact are determined as a function of the collision energy E by means of the Born approximation and the binary-encounter method which is also applied to the ionization of metastable N₂* and CO*. It is worth noting that the corresponding theoretical treatments of electron-impact ionization of

H(2s) and He(2^{1,3}S) yield cross sections¹ in good agreement with recent measurements.^{6,10}

II. BASIC FORMULAS

The cross section for ionization of a singly excited atom B with mass M_B and ionization potential I by an incident particle A with mass M_A , speed v , and relative energy E is, in the (elastic) binary-encounter approximation given by^{11,12}

$$\sigma_{ni}^I(E) = \frac{\pi}{M_{AB}v^2} \int_I^E d\epsilon_T \int_0^\infty f_{ni}(u) \frac{du}{u} \int_{P^-}^{P^+} \frac{4}{P^4} \Gamma(P) dP, \quad (1)$$

where the distribution in speed u of the valence electron described by a spatial wave function $\phi_{ni,m}(\vec{r})$ is, with all quantities in atomic units,

$$f_{ni}(u) = \frac{1}{(2l+1)} \times \sum_{m=-l}^l \int \left| \frac{1}{(2\pi)^{3/2}} \int \phi_{ni,m}(\vec{r}) e^{-i\vec{u}\cdot\vec{r}} d\vec{r} \right|^2 u^2 d\vec{u} \quad (2)$$

and M_{AB} is the reduced mass of the (A-e) binary system.

For a specified energy transfer ϵ_T to the valence electron, the momentum change P can vary between the lower limit,

$$P^- = \max[M|u' - u|, M_{AB}|v' - v|], \quad (3)$$

$$M = m \left(1 + \frac{m}{M_i}\right), \quad M_{AB} = \frac{M_A M_B}{M_A + M_B},$$

where m and M_i are the electronic and ionic masses, respectively, and the upper limit

$$P^* = \min[M(u' + u), M_{AB}(v' + v)], \quad (4)$$

where the post binary-collision speeds of the projectile and target particles are, respectively,

$$v' = (v^2 - 2\epsilon_T/M)^{1/2}, \quad (5)$$

$$u' = (u^2 + 2\epsilon_T/M)^{1/2}. \quad (6)$$

In the general expression (1), the function $\Gamma(P)$, which represents the departure of the differential cross section for $(A-e)$ elastic scattering from the Rutherford value, is set to unity for direct $(e-e)$

$$\sigma_{nl}^I(\epsilon, \hat{k}_e) = \frac{8\pi}{k_i^2} \int_{K^-}^{K^+} \left| \langle \psi_f(\epsilon, \hat{k}_e; \hat{r}) | \sum_{i=1}^N e^{i\hat{k} \cdot \hat{r}_i} | \psi_i(n^3 P_{0,2}; \hat{r}) \rangle \right|^2 \frac{dK}{K^3}, \quad (8)$$

where $\psi_{i,f}(\hat{r})$ are the initial and final electronic wave functions for the rare-gas atom with electronic coordinates denoted collectively by \hat{r} . The limits to the momentum change $(\hat{k}_i - \hat{k}_f)$ of the scattered electron are

$$K^\pm = (2E)^{1/2} \mp [2(E - I - \epsilon)]^{1/2}, \quad (9)$$

where the energy ϵ of ejection is $\frac{1}{2}k_e^2$ a.u. and where the kinetic energy transferred to the ion is neglected. While the parameter α in the ϵ -integration limit in (7) is unity for ionization involving distinguishable particles, Rudge and Seaton¹³ have shown that, for ionization of atomic hydrogen by electrons with random spin orientations, $\alpha = 0.5$ when electron-exchange effects are fully neglected. While this choice however ensures that the faster of the scattered and ejected electrons is always described by a plane wave, neither choice is rigorously based for ionization of atoms more complex than hydrogen. The spatial wave function $\psi_i(\hat{r})$ for the initial bound metastable state of the rare-gas atom is taken as a simple product of the one-electron orbitals with quantum numbers (nlm)

$$\phi_{nlm}(\hat{r}_j) = (1/r_j) P_{nl}(r_j) Y_{lm}(\hat{r}_j), \quad j = 1, 2, \dots, N \quad (10)$$

where the Y_{lm} are spherical harmonic functions. The corresponding wave function $\psi_f(\hat{r})$ for the final ionized state includes the orbital

$$\phi_e(\hat{k}_e; \hat{r}) = \sum_{l'=0}^{\infty} \sum_{m'=-l'}^{l'} \frac{i^{l'}}{r} e^{-i\eta_{l'}} F_{el'}(r) \times Y_{l'm'}(\hat{r}) Y_{l'm'}^*(\hat{k}_e) \quad (11)$$

for the electron ejected in direction \hat{k}_e with energy ϵ . In this study, these orbitals are obtained from a central-field approximation such that the above radial functions P_{nl} and F_{el} are appropriate solu-

collisions for which $M \approx M_{AB} \approx m$.

The Born approximation to the cross section for single ionization of an atom with N electrons by an incident electron can be written, with all quantities in atomic units, as

$$\sigma_{nl}^I(E) = \int_0^{\alpha(E-I)} d\epsilon \frac{1}{(2I+1)} \sum_{m=-l}^l \int \sigma_{nlm}^I(\epsilon, \hat{k}_e) d\hat{k}_e \quad (7)$$

in terms of the differential cross section for ejection of the electron with momentum \hat{k}_e per unit solid angle and unit energy interval,

tions of the radial Schrödinger equation,

$$\frac{d^2 P_{nl}(r)}{dr^2} + 2 \left(E - V(r) - \frac{l(l+1)}{2r^2} \right) P_{nl}(r) = 0, \quad (12)$$

$$E = \begin{cases} \epsilon_{nl} < 0 \\ \epsilon > 0 \end{cases}$$

where the spherically symmetric interaction $V(r)$, which tends to $(-N/r)$ as $r \rightarrow 0$ and to $(-1/r)$ as $r \rightarrow \infty$ and which is frozen for all the orbitals, is determined in a manner described in the following section. All the bound and continuum orbitals therefore form an orthonormal set such that the form factor in (8) reduces to a one-electron form factor involving only the ejected electron.

The bound solutions P_{nl} to (12) are normalized to unity (for $E < 0$) and the radial continuum function behaves asymptotically as

$$F_{el'}(r) \sim \left(\frac{2}{\pi k_e} \right)^{1/2} \sin[k_e r - (1/k_e) \ln(2k_e r) - \frac{1}{2} l' \pi + \eta_{l'}], \quad \text{as } r \rightarrow \infty, \quad (13)$$

$$\eta_{l'} = \arg \Gamma(l' + 1 - i/k_e) + \delta_{l'}(k_e),$$

where the additional phase shift $\delta_{l'}$ is a measure of the departure of the electron-ion interaction from pure Coulomb. The amplitude $2^{1/4}/\pi^{1/2} \epsilon^{1/4}$ is chosen so as to fulfill the normalization condition,

$$\langle \phi_e(\hat{k}_e; \hat{r}) | \phi_{e'}(\hat{k}_e'; \hat{r}) \rangle = \delta(\epsilon - \epsilon') \delta(\hat{k}_e - \hat{k}_e'), \quad (14)$$

where $\epsilon = \frac{1}{2}k_e^2$ is in atomic units such that the ionization cross section (7) is obtained by integrating (8) over \hat{k}_e and ϵ . By first performing the \hat{k}_e integration, it can then be shown that the differential cross section per unit ϵ is, for initial s states,

$$\sigma_{\epsilon}^{l'}(\epsilon) = \frac{8\pi}{k_i^2} \int_{\epsilon-}^{\epsilon+} \sum_{l''=0}^{\infty} (2l''+1) |M_{\epsilon l'', m}^{l'}(\epsilon, K)|^2 \frac{dK}{K^3}, \quad (15)$$

where the radial matrix element to be evaluated is

$$M_{\epsilon l'', m}^{l'}(\epsilon, K) = \int_0^{\infty} i^{-l'} e^{i\eta_{l'}} F_{\epsilon l'}(r) j_{l''}(Kr) P_m(r) dr \quad (16)$$

in which j_l is the spherical Bessel function.

Antisymmetry of the target wave function is omitted although some account of exchange effects in the target is introduced by the use of the Hartree-Slater approximation for the interaction potential $V(r)$.

III. WAVE FUNCTIONS FOR THE RARE-GAS ATOMS

The singly excited states of rare-gas atoms, in general, follow neither the pure LS nor the jj angular momentum coupling schemes. These excited states are obtained by single excitation of one of the np outer-shell electrons of the ground-state configuration to a $n'l'$ state. The binding energy of (or effective charge seen by) this excited valence electron is substantially less than for the np electrons, and the excited electron is, on the average, relatively distant from all the core electrons, including the np -shell electrons. The spin-orbit interaction of the electrons of the atomic core can therefore be greater than the electrostatic interaction of these electrons with the excited electron and this effect manifests itself in the distinctive "core splitting" structure of the spectrum. The intermediate coupling scheme which describes the angular momentum structure is therefore closest to the pure jl (or jK) coupling wherein the orbital angular momentum \tilde{l} of the valence electron is coupled to the total angular momentum \tilde{j} of the atomic core and their resultant \tilde{K} is in turn coupled¹⁴ to the valence electron spin to give the total angular momentum \tilde{J} of the atom.

Whatever the coupling, pure or intermediate, the total angular momentum J of the atom is a good quantum number and remains invariant under the various recoupling transformations. For the lowest excited configuration $np^5(n+1)s$, J can take the values 0, 1 (twice), and 2. Since dipole transitions within the same configuration are parity-forbidden and since the ground state is 1S_0 , the $(np)^5(n+1)s$ states with $J=0$ and $J=2$ are therefore metastable. Expansion of these states from an intermediate coupling to a jK basis projects onto the $^2P_{1/2}[K=\frac{1}{2}]_{J=0}$ state, for $J=0$, and onto the

$^2P_{3/2}[K=\frac{3}{2}]_{J=2}$ state, for $J=2$. Alternatively an expansion to an LS basis projects onto 3P_0 for $J=0$ and 3P_2 for $J=2$. Since no mixing is involved in each case, either set of pure-state notations provides convenient labeling of the metastable states. Of the remaining LS states, 1P_1 and 3P_1 , the possible metastability arising from 3P_1 is lost by its mixing with 1P_1 which is dipole connected with the 1S_0 ground state.

In this study the effective field (potential) $V(r)$ is the same for all target electrons. Moreover the atomic core is regarded as frozen and the continuum electron moves in the same field as the initially bound excited valence electron. This potential is determined in the Hartree-Slater approximation via the following modification to the standard program of Herman and Skillman.¹⁵ A self-consistent field (SCF) iteration for the initial excited-state configuration $[1s^2 2s^2 \dots np^5(n+1)s]$ yields $V_i(r)$ which when inserted in (12) provides orthonormal $P_{(n+1)s}$ and $F_{\epsilon l'}$ for a wide range of angular momentum l' (from 0 to about 30) and of energies ϵ of the ejected electron. This procedure which differs from the standard one, based on an interaction $V_0(r)$ obtained from a SCF iteration of the ground-state configuration, has been found¹ to yield considerable improvement for the helium excited states with symmetry different to that of lower-lying states. This improvement is attributed to the allowance of core relaxation whilst the symmetry condition avoids the necessity of explicit orthogonalization of the wave functions to those of lower-lying states, the ground state, in particular. In the present case the excited and ground-state configurations $np^5(n+1)s$ and np^6 are orthogonal because of the orbital angular momentum of the valence electron. As the number of atomic electrons increases, the Hartree-Slater approximation for exchange is expected to improve. On the other hand, core relaxation in the excited states diminishes whilst relativistic effects such as spin-orbit coupling, which are not included in the present treatment, become important. The same orbitals are used for the 3P_2 and 3P_0 (or $[\frac{3}{2}]_2$ and $[\frac{3}{2}]_0$) states since the major contribution to their splitting comes from spin-orbit coupling in the core,¹⁶ an effect not included in the present treatment.

Knowledge of the bound and continuum orbitals permits evaluation of the Born radial matrix element (16) and of the speed distribution (2) for use in the binary-encounter formula (1).

Whilst preserving or introducing the following approximations of (a) omission of antisymmetry, (b) magnetic quantum-number independence of the radial orbitals $P_m(r)$ and $F_{\epsilon l'}(r)$, (c) explicit $\tilde{K} \cdot \tilde{r}$ dependence of the continuum orbitals [cf. Eq. (11)]

i.e., uncoupling of the orbital angular momentum l' of the ejected continuum electron from all other angular momenta, and (d) lack of selection of the angular momentum configuration of the residual ion, one finds that the introduction of explicit coupling of the individual angular momenta (spin and orbital) of the target electrons in an intermediate, pure jK or other coupling scheme, leaves the expression (15), initially derived without coupling, unchanged.

IV. RESULTS AND DISCUSSION

A. Ionization of Ne^* , Ar^* , Kr^* , Xe^*

The ionization cross sections of metastable Ne, Ar, Kr, and Xe versus the impact energy E are

displayed in Figs. 1(a)–1(d). The same cross section is assigned to the 3P_2 and 3P_0 metastable states which are treated as degenerate. The ionization potentials I used in the expressions (1), (7), and (9) are the weighted average of the potentials of the $^3P_{2,0}$ states for ionization without core transitions. The values so derived from the tables of Moore¹⁶ are given in Table I, together with the p^5 inner-shell ionization potentials.

As the target varies from Ne^* to Xe^* , its physical size increases, its ionization potential decreases and the ionization cross sections exhibit the systematic increase in Figs. 1(a)–1(d). Moreover, the binary encounter curves BE drop in relation to BF, the Born cross sections obtained from integration over the full range of energy ϵ of

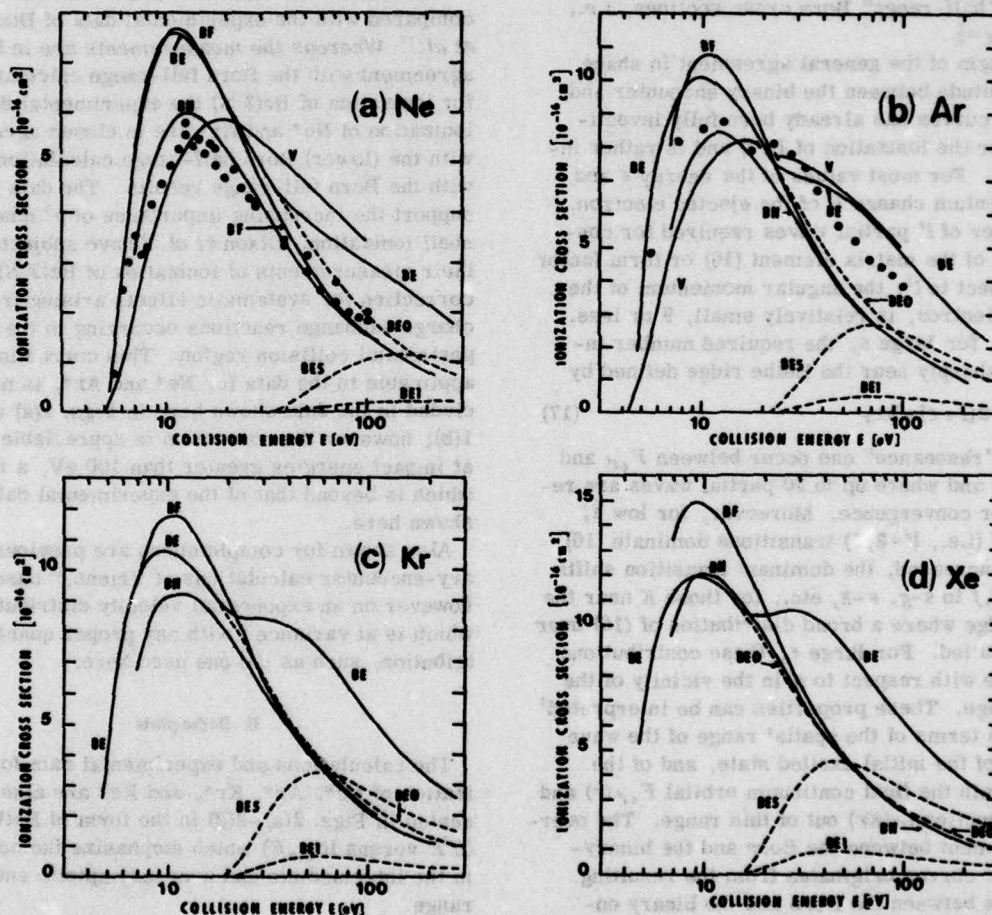


FIG. 1. Cross sections (10^{-16} cm^2) for collisional ionization of metastable (a) Ne^* , (b) Ar^* , (c) Kr^* , and (d) Xe^* by electrons with impact energy E (eV). BF and BH are the present Born results for outer-shell ionization obtained from integrations over the full and lower-half ranges of energy ϵ of the ejected electron, i.e., $\alpha = 1$ and $\frac{1}{2}$ respectively in (7) of text. The binary-encounter (quantal distribution) cross sections are denoted by BE0 for outer-shell ionization, by BE1 for ionization of one of the electrons in the np^5 shell, by BE5 for the total ionization of the np^5 shell and by BE for the sum of BE0 and BE5. Previous binary encounter (exponential distribution) results of Vriens are represented by V. ●: measurements of Dixon, Harrison, and Smith (Ref. 17).

TABLE I. Potentials I_0 and I_1 for ionization of the ns outer-shell and the $(n-1)p^5$ inner-shell of metastable rare-gas atoms. $X^*(ns)$ means $X^*(1s^2, 2s^2, \dots, (n-1)p^5, ns)$.

$X^*(ns)$	I_0 (eV)	I_1 (eV)
Ne*(3s)	4.95	32.13
Ar*(4s)	4.21	20.88
Kr*(5s)	4.09	18.16
Xe*(6s)	3.44	15.41

the ejected electron, i.e., $\alpha=1$ in (7). For example, the separation between BE and BF (which is remarkably small for He*¹ and Ne*) widens with variation of the target from Ne* to Xe* until BE eventually comes into close agreement with BH, the "half-range" Born cross sections, i.e., (7) with $\alpha=\frac{1}{2}$.

The origin of the general agreement in shape and magnitude between the binary encounter and the Born curves has already been fully investigated¹ (for the ionization of He*) and is rather instructive. For most values of the energy ϵ and the momentum change K of the ejected electron, the number of l' partial waves required for convergence of the matrix element (16) or form factor with respect to l' , the angular momentum of the ejected electron, is relatively small, 9 or less. However, for large ϵ , the required number increases sharply near the Bethe ridge defined by

$$K_{\text{Bethe}}^2 = 2(I + \epsilon) = 2\epsilon_T \quad (17)$$

where a "resonance" can occur between $F_{\epsilon, l'}$ and $j_{l'}$ in (16) and where up to 30 partial waves are required for convergence. Moreover, for low ϵ , the s - d, f (i.e., $l'=2, 3$) transitions dominate (16). As ϵ is increased, the dominant transition shifts from s - d, f to s - g , s - h , etc., for those K near the Bethe ridge where a broad distribution of (16) over l' is exhibited. For large ϵ , these contributions maximize with respect to K in the vicinity of the Bethe ridge. These properties can be interpreted mainly in terms of the spatial range of the wave function of the initial excited state, and of the drift of both the final continuum orbital $F_{\epsilon, l'}(r)$ and Bessel function $j_{l'}(Kr)$ out of this range. The overall agreement between the Born and the binary-encounter curves originates from the resulting closeness between the Born and the binary-encounter determinations¹¹ of the form factor squared in (8) away from the optical $K \rightarrow 0$ limit. The impact energies for which the ionization cross section is relatively large involves momentum transfers K for which the form factor requires many partial waves and is substantial. This situation, where many partial waves and therefore

multipoles are required, is generally well described by the binary-encounter method.

Also shown in Fig. 1 is the binary-encounter contribution arising from the p^5 inner-shell, obtained by multiplying the ionization cross section for ejection of a single p electron by the occupation number of the p^5 shell. The outer valence electron remains in its initial excited state. Again, as the target varies from Ne* to Xe*, the inner-shell ionization potentials drops, the inner-shell ionization cross section increases in magnitude, absolute as well as relative to the outer-shell ionization cross section, and its effect on the shape of the excitation (ionization) function becomes more prominent by the display of a secondary maximum.

The results for ionization of Ne* and Ar* are compared with the experimental data of Dixon *et al.*¹⁷ Whereas the measurements are in better agreement with the Born full-range calculations¹ for ionization of He(2³S) the experimental data for ionization of Ne* and Ar* are in closer agreement with the (lower) Born half-range calculations than with the Born full-range results. The data for Ar* support the increasing importance of p^5 inner-shell ionization. Dixon *et al.*¹⁰ have subjected their measurements of ionization of He(2³S) to a correction for systematic effects arising from charge exchange reactions occurring in the experimental collision region. This correction, if applicable to the data for Ne* and Ar*, is not included in the data shown here in Figs. 1(a) and 1(b); however the correction is appreciable only at impact energies greater than 100 eV, a range which is beyond that of the experimental data shown here.

Also shown for completeness are previous binary-encounter calculations of Vriens,¹⁸ based however on an exponential velocity distribution which is at variance¹⁹ with any proper quantal distribution, such as the one used here.

B. Bethe plots

The calculations and experimental data for ionization of Ne*, Ar*, Kr*, and Xe* are also presented in Figs. 2(a)–2(d) in the form of Bethe plots ($\sigma^2 E$ versus $\log_{10} E$) which emphasize the behavior in the intermediate and near-asymptotic energy range.

These plots show that the slopes of the Born curves for outer-shell ionization of metastable Ne, Ar, Kr, and Xe at impact energies beyond 100 eV are quite small in comparison with, say, that¹ for outer-shell ionization of He(2³S) (cf. Fig. 4 of Ref. 1) thereby indicating that the outer-shell photoionization cross sections of metastable Ne,

Ar, Kr, and Xe are substantially smaller than the corresponding cross section of He(2³S) over an appreciable range of ejected electron energy beginning from threshold. Thus, a reversal, between target He(2³S) on one hand, and metastable Ne, Ar, Kr, and Xe targets on the other, occurs in the magnitudes of the cross sections depending on whether the outer-shell ionization is caused by electron impact or by photon impact. However, the effective photoionization cross section also involves the contribution from the contiguous inner shell; for Ne*-Xe* the inner shell (*p*³) has five electrons instead of one for He(2³S) and it begins to contribute at lower impact energies.

For the heavy rare gases the E^{-1} asymptotic dependence (instead of the correct $E^{-1} \log_{10} E$) of

the ionization cross section normally exhibited in the binary encounter approximation does not appear until $E \geq 1$ keV. This late onset, combined with the weakness of the dipole transition oscillator strength discussed earlier, corresponds to the fact that the binary encounter curves for outer-shell ionization remains above the Born curve BF as the impact energy becomes large, instead of crossing below as implied by the asymptotic dependence (cf. Figs. 1 and 2).

While there is reasonable accord between the Bethe plots associated with the theoretical and experimental results at low energies when only ionization of the outer-shell occurs, the Fig. 2, in contrast to Fig. 1, clearly shows that any measure of agreement between the asymptotic slopes is ob-

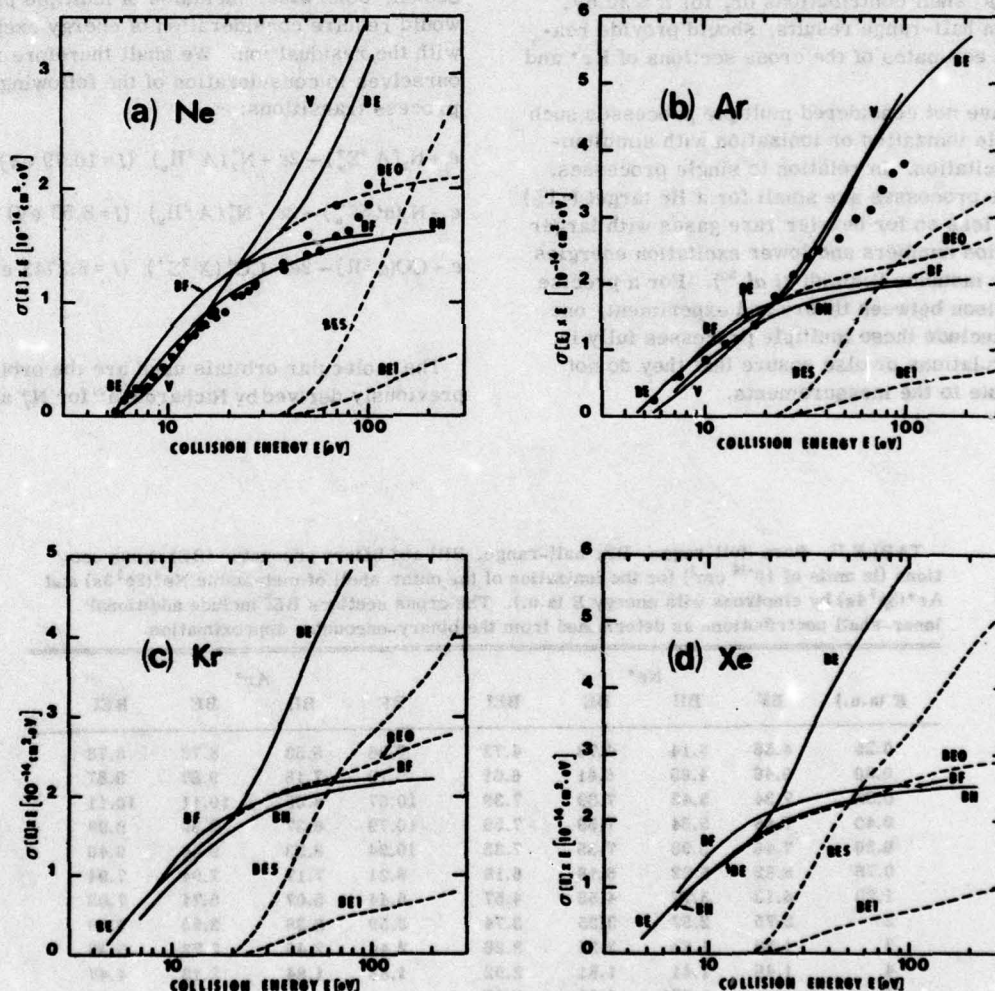


FIG. 2. Bethe plots (cross section times collision energy E versus $\log_{10} E$) for electron-impact ionization of metastable (a) Ne*, (b) Ar*, (c) Kr*, and (d) Xe*. Labeling of curves as in Fig. 1.

tained only by inclusion of the p^5 inner-shell contributions, especially for Ar^* . These inner-shell contributions are adequately described¹ by the binary-encounter method and for Kr^* and Xe^* , become larger and increasingly important at the lower impact energies.

C. Tabulation

The numerical values of the electron-impact ionization cross section of Ne^* , Ar^* , Kr^* , and Xe^* calculated in the full-range and half-range Born approximations (for ionization from the outer shell alone) and in the binary-encounter approximation (with and without the inner-shell contributions) are given in Tables II and III. Measurements for electron-impact ionization of Kr^* and Xe^* are not available; the binary-encounter results inclusive of p^5 shell contributions or, for $E \leq 20$ eV, the Born half-range results, should provide reasonable estimates of the cross sections of Kr^* and Xe^* .

We have not considered multiple processes such as double ionization or ionization with simultaneous excitation. In relation to single processes, multiple processes are small for a He target ($\sim 1\%$) but are less so for heavier rare gases with larger occupation numbers and lower excitation energies (see for instance Schmidt *et al.*²⁰). For a precise comparison between theory and experiment, one should include these multiple processes fully in the calculations or else ensure that they do not contribute to the measurements.

D. Ionization of metastable N_2 and CO

Ionization of diatomic molecules like N_2 and CO in metastable states is also important for gas laser dynamics. We have therefore applied the binary-encounter approximation of Sec. II to the electron-impact ionization of N_2 in the $A^3\Sigma_u^+$ and $a'^1\Sigma_u^-$ metastable states and of CO in the $a^3\Pi$ metastable state.

The electronic configurations of the metastable states of N_2 and CO as well as those of the low-lying states of N_2^+ and CO^+ are shown in Table IV. It shall be assumed that single processes, involving only one target electron, are more important than multiple processes requiring multielectron target transitions. This assumption also makes the ionization problem tractable within the framework of the binary-encounter approximation of Sec. II; otherwise, inclusion of multiple processes would require consideration of energy exchange with the residual ion. We shall therefore restrict ourselves to consideration of the following single-process transitions:

$$e + \text{N}_2(A^3\Sigma_u^+) \rightarrow 2e + \text{N}_2^+(A^2\Pi_u) \quad (I = 10.79 \text{ eV}), \quad (18)$$

$$e + \text{N}_2(a'^1\Sigma_u^-) \rightarrow 2e + \text{N}_2^+(A^2\Pi_u) \quad (I = 8.56 \text{ eV}), \quad (19)$$

$$e + \text{CO}(a^3\Pi) \rightarrow 2e + \text{CO}^+(X^2\Sigma^+) \quad (I = 8.2743 \text{ eV}). \quad (20)$$

The molecular orbitals used are the orbitals previously derived by Richardson²¹ for N_2^+ and Huo²²

TABLE II. Born (full-range, BF; half-range, BH) and binary encounter (BE) cross sections (in units of 10^{-16} cm^2) for the ionization of the outer-shell of metastable $\text{Ne}^*(2p^5 3s)$ and $\text{Ar}^*(3p^5 4s)$ by electrons with energy E (a.u.). The cross sections BEI include additional inner-shell contributions as determined from the binary-encounter approximation.

E (a.u.)	Ne^*				Ar^*			
	BF	BH	BE	BEI	BF	BH	BE	BEI
0.25	4.56	3.14	4.73	4.73	7.98	5.53	8.73	8.73
0.30	6.46	4.65	6.61	6.61	9.79	7.18	9.87	9.87
0.35	7.34	5.45	7.39	7.39	10.67	8.05	10.11	10.11
0.40	7.68	5.84	7.59	7.59	10.79	8.37	9.99	9.99
0.50	7.46	5.98	7.35	7.35	10.34	8.33	9.46	9.46
0.75	8.82	5.22	6.18	6.18	8.21	7.17	7.94	7.94
1.25	4.13	3.77	4.55	4.57	5.44	5.07	5.71	7.05
2	2.75	2.57	3.25	3.74	3.59	3.38	3.90	6.40
3	1.90	1.83	2.34	3.26	2.44	2.40	2.73	5.35
4	1.46	1.41	1.81	2.92	1.88	1.84	2.13	4.47
6	...	0.971	1.24	2.47	...	1.25	1.52	3.31
8	...	0.741	0.949	2.06	...	0.951	1.20	2.64

TABLE III. Born (full-range, BF; half-range, BH) and binary encounter (BE) cross sections (in units of 10^{-16} cm²), for the ionization of the outer-shell of metastable Kr*(4p⁵5s) and Xe*(5p⁵6s) by electrons with energy E (a.u.). The cross sections BEI include additional inner-shell contributions as determined from the binary-encounter approximation.

E (a.u.)	Kr*				Xe*			
	BF	BH	BE	BEI	BF	BH	BE	BEI
0.25	9.54	6.69	5.83	9.48	13.19	9.56	11.09	11.09
0.30	10.99	8.26	10.46	10.48	14.70	11.38	11.85	11.85
0.35	11.67	9.12	10.66	10.66	14.86	12.03	11.95	11.95
0.40	11.74	9.19	10.50	10.50	14.61	12.02	11.77	11.77
0.50	11.11	9.11	9.96	9.96	13.56	11.32	11.09	11.09
0.75	8.82	7.81	8.34	8.60	10.44	9.37	9.08	10.40
1.25	5.85	5.45	5.91	8.35	6.83	6.32	6.25	10.41
2	3.91	3.63	4.01	7.44	4.47	4.23	4.25	8.74
3	2.63	2.58	2.84	5.97	3.02	2.97	3.07	6.81
4	2.01	1.97	2.24	4.89	2.32	2.26	2.43	5.63
6	...	1.31	1.60	3.64	...	1.52	1.71	4.29
8	...	1.02	1.25	2.96	...	1.17	1.31	3.48

for CO*, who used Slater-type-orbital (STO) bases. [Similar orbitals have also been calculated by Rose and McKoy²³ using Gaussian-type-orbital (GTO) bases.] Hence, the appropriate Fourier transforms are obtained and averaged over angles as in (2) to give the initial speed distribution $f(u)$. Although a spherical distribution may be a poor approximation because of the molecular axis, the effects of rotation and random orientation of the molecular target partially offset this inadequacy. The ionization potentials used in (1) for each molecular orbital are the vertical ionization potentials derived from the data of Gilmore²⁴ for N₂ and Krupenie²⁵ for CO, at the equilibrium internuclear

distance of the initial state, even though the molecular orbital may have been derived at the nuclear separation of the ground state. The cross sections for the ionization processes (18)–(20) at impact energies below 200 eV are shown in Fig. 3.

Since Richardson²¹ gives the same $1\pi_g$ orbital for N₂(A³ Σ_u^+) and N₂(a'¹ Σ_u^-), expression (1) adopts the same speed distribution for these two states. The only difference arises from the ionization potentials and the main effect is a reduction in the magnitude of the ionization cross section.

On the other hand, N₂(a'¹ Σ_u^-) and CO(a³ Π) have very similar potentials for single-process ionization. Any slight differences between the curves

TABLE IV. Electronic configurations for N₂⁺, N₂⁺, CO*, CO*.

Configuration ^a	(1 σ_g) ²	(1 σ_g) ²	(2 σ_g) ²	(2 σ_u) ¹ $i=2$	(1 π_u) ¹ $j=4$	(3 σ_g) ¹ $k=2$	(1 π_g) ¹ $l=0$
N ₂ X ¹ Σ_g^+							
A ³ Σ_u^+				2	3	2	1
a' ¹ Σ_u^-				2	3	2	1
N ₂ ⁺ X ² Σ_g^+				2	4	1	0
A ² Π_u				2	3	2	0
B ² Σ_u^+				{ 1 2	{ 4 3	{ 2 1	{ 1
Configuration ^b	(1 σ) ²	(2 σ) ²	(3 σ) ²	(4 σ) ¹ $i=2$	(1 π) ¹ $j=4$	(5 σ) ¹ $k=2$	(2 π) ¹ $l=0$
CO X ¹ Σ^+							
a ³ Π				2	4	1	1
CO* X ² Σ^+				2	4	1	
A ³ Π				2	3	2	
B ³ Σ^+				1	4	2	

^a Cf. Gilmore, Ref. 24.

^b Cf. Krupenie, Ref. 25.

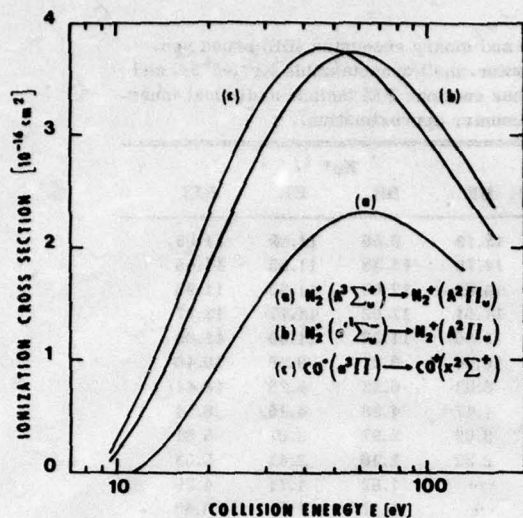


FIG. 3. Binary-encounter cross sections (10^{-16} cm^2), (a), (b), and (c), for the ionization of metastable $\text{N}_2^*(A^3\Sigma_u^+)$, $\text{N}_2^*(A'^1\Sigma_u^-)$, and $\text{CO}^*(a^3\Pi)$, respectively, by electrons with energy E (eV). The final state of the residual ion is indicated.

for ionization of $\text{N}_2(a'^1\Sigma_u^-)$ and $\text{CO}(a^3\Pi)$ are therefore attributed to differences between the $1\pi_g$ orbital of N_2^* and the 2π orbital of CO^* . Any similarity between the properties of N_2 and CO usually originates from the isoelectronic character of these molecules, while any difference arises from the heteronuclear aspect.

While the ground states of N_2 and CO have similar electronic configurations, $\text{N}_2^*(a'^1\Sigma_u^-)$ and $\text{CO}^*(a^3\Pi)$ —and for that matter $\text{N}_2^*(A^3\Pi_u)$ and $\text{CO}^*(X^2\Sigma^+)$ —have slightly different electronic configurations. However, since the binary encounter method of Sec. II relies mainly on the properties of

the valence electron ($1\pi_g$ or 2π), the difference between the configurations of the remaining electrons is reflected only indirectly through its effect on the valence electron ($1\pi_g$ or 2π).

Metastable N_2 and CO have greater ionization potentials than metastable rare gases and have correspondingly smaller electron-impact ionization cross sections as seen by comparing Fig. 1 with Fig. 3.

V. CONCLUSION

Electron-impact ionization cross sections of $[np^5(n+1)s]$ metastable Ne, Ar, Kr, and Xe have been calculated in the Born and the binary-encounter approximations. The further approximations used here make explicit coupling of the target angular momenta—to reflect the peculiarities of the heavy rare-gas spectra—unnecessary.

As the atomic number of the target increases, the cross section for ionization from the outer shell increases. Ionization of the inner p^5 shell also becomes increasingly important with increasing target complexity. Moreover the binary-encounter results drop in relation to the Born results.

The maximum of the experimental data of Dixon *et al.*¹⁷ is in fair agreement with that of the Born half-range calculations. Beyond the maximum the inner-shell contribution becomes evident. The Bethe plots suggest that the outer-shell photoionization cross sections of metastable Ne, Ar, Kr, and Xe are overall smaller than that of $\text{He}(2^3S)$.

The binary-encounter approximation has also been used for the single-process ionization of the π valence electron of metastable N_2 and CO . Their greater ionization potentials lead to cross sections smaller than for He^* , Ne^* , Ar^* , Kr^* , and Xe^* .

*Research sponsored by the Air Force Propulsion Laboratory, Air Force Systems Command, USAF under Contract No. F33615-76-C-2003 and by US-ERDA under contract E-(40-1)-5002/7.

¹D. Ton-That, S. T. Manson, and M. R. Flannery, *J. Phys. B* (to be published).

²J. J. Ewing and C. A. Brau, *Appl. Phys. Lett.* **27**, 350 (1975); **27**, 435 (1975); *Phys. Rev. A* **12**, 129 (1975); *J. Chem. Phys.* **63**, 4640 (1975).

³C. P. Wang, H. Mirels, D. G. Sutton, and S. N. Suchard, *Appl. Phys. Lett.* **28**, 326 (1976).

⁴R. Burnham, N. W. Harris, and N. Djeu, *Appl. Phys. Lett.* **28**, 86 (1976).

⁵E. R. Ault, R. S. Bradford, Jr., and M. L. Bhaumik, *Appl. Phys. Lett.* **27**, 413 (1975).

⁶J. E. Velazco and D. W. Setser, *J. Chem. Phys.* **62**, 1990 (1975).

⁷M. F. Golde, *J. Mol. Spectros.* **58**, 261 (1975).

⁸J. Tellinghuisen, J. M. Hoffman, G. C. Tisone, and A. K. Hays, *J. Chem. Phys.* **64**, 2484 (1976).

⁹A. J. Dixon, A. von Engel, and M. F. A. Harrison, *Proc. R. Soc. London A* **343**, 333 (1975).

¹⁰A. J. Dixon, M. F. A. Harrison, and A. C. H. Smith, *J. Phys. B* **9**, 2617 (1976). See also Ref. 17.

¹¹L. Vriens, *Case Studies in Atomic Collision Physics I*, edited by E. W. McDaniel and M. R. C. McDowell (North-Holland, Amsterdam, 1969), p. 337.

¹²M. R. Flannery, *J. Phys. B* **4**, 892 (1971).

¹³M. R. H. Rudge and M. J. Seaton, *Proc. Roy. Soc. London A* **283**, 262 (1965).

¹⁴I. I. Sobel'man, *Introduction to the Theory of Atomic Spectra* (Pergamon, New York, 1972), Chap. 3, Sec. 10.6, p. 53 and Chap. 5, Sec. 20.5-7, pp. 185-193.

¹⁵F. Herman and S. Skillman, *Atomic Structure Calculations*.

- lations (Prentice-Hall, Englewood Cliffs, N. J., 1963).
- ¹⁶C. E. Moore, *Atomic Energy Levels*, NBS Circ. No. 467 (U.S. GPO, Washington, D.C., 1949), Vol. I.
- ¹⁷A. J. Dixon, M. F. A. Harrison, and A. C. H. Smith, *Abstracts of Papers of Eighth International Conference on the Physics of Electronic and Atomic Collisions*, edited by B. C. Cobic and M. V. Kurepa (Institute of Physics, Belgrade, Yugoslavia, 1973), Vol. 1, p. 405; and private communication.
- ¹⁸L. Vriens, *Phys. Lett.* **8**, 260 (1964).
- ¹⁹A. Burgess and I. C. Percival, *Advances in Atomic and Molecular Physics* (Academic, New York, 1968), p. 124.
- ²⁰V. Schmidt, N. Sandner, and H. Kuntzemüller, *Phys. Rev. A* **13**, 1743 (1976).
- ²¹J. W. Richardson, *J. Chem. Phys.* **35**, 1829 (1961).
- ²²W. M. Huo, *J. Chem. Phys.* **45**, 1554 (1966).
- ²³J. B. Rose and V. McKoy, *J. Chem. Phys.* **55**, 5435 (1971).
- ²⁴F. R. Gilmore, *J. Quant. Spectrosc. Radiat. Transfer* **5**, 369 (1965).
- ²⁵P. H. Krupenie, *The Band Spectrum of Carbon Monoxide* NSRDS-NBS 5 (U.S. GPO, Washington, D.C., 1966).

SECTION VII

SYSTEMATIC TRENDS IN THE INELASTIC CROSS SECTIONS AND FORM FACTORS

FOR $n\ell \rightarrow n'\ell'$ DIRECT COLLISIONAL TRANSITIONS

It is becoming increasingly apparent in collisions involving an atom initially excited that a certain useful guideline developed with ground-state atoms in mind is not of general validity. For example, both the Born¹ and the more elaborate ten-channel eikonal² treatments of e-He($2^{1,3}S$) collisions predict that transitions to the optically forbidden $3^{1,3}D$ and $3^{1,3}S$ states are much stronger, by up to an order of magnitude, than the dipole-allowed $2^{1,3}S-3^{1,3}P$ collisional excitations, except, of course, at high impact-energies E when the cross sections for dipole transitions, with their characteristic $E^{-1} \ln E$ slower-varying asymptotic-dependence, eventually dominate. Also the $2^{1,3}S-3^{1,3}D$ transition is the major contributor from $2^{1,3}S$ to the population of the $n=3$ level of He. These findings were verified by the recent measurements of Lake and Garscadden.³ The obvious analogy with ground-state species and with optical properties of the atom would suggest (erroneously) that the $2^{1,3}S-3^{1,3}P$ transition in e-He($2^{1,3}S$) collisions would dominate the population of the $n=3$ level at all impact-energies. (It is however worth noting that the ($2^{1,3}S-2^{1,3}P$) cross section is much larger² than those for excitation out of the $n=2$ level.)

Also a study⁴ of excitation to the $n=4$ and 5 levels in e-He($2^{1,3}S$) collisions revealed that transitions to the $n^{1,3}D$ states are again predominant for a given n , except at the highest energies when the S-P dipole excitations gain in relative importance in accord with Bethe's approximation. Moreover, this trend continues for higher n , even for the bound-free transitions in He where we have found,⁴ for low energies ϵ of electron-ejection, that the ionization cross section is again dominated by the contribution arising from the ϵd partial-wave describing the

ejected-electron.

In an effort to probe the origin of this behavior and to establish certain general patterns observed in variation of the initial excited state, the $n'l \rightarrow n'l'$ transition in hydrogenic systems will be studied. In so doing, we will attempt to examine, for a fixed value of n' , the variation of that value of l' which yields the largest cross section with change of n and of l , the quantum numbers for the initial state.

As well as being of fundamental significance in themselves, the findings may have rather important and far-reaching implications in situations where excited states are of particular significance, as in, for example, laser modeling, gaseous discharges, recombination and astrophysical plasmas. In H I and H II regions of hot stars, the interpretation⁵ of the observed emission between highly excited Rydberg states $n=110 \rightarrow n'=109$, for example, is based on evaluation of the coefficients describing departure from thermodynamic equilibrium. These coefficients are functions of cross sections for collisional transitions between excited states. In both this case and in similar laser-modeling studies of excimer and rare gas-halide systems, it has been tacitly assumed that the dipole transitions $l' = l \pm 1$ dominate at all energies and, in the absence of any further information, the cross sections are determined by the Bethe limit, or some modification thereof.

Here we shall show that this assumption is rather questionable at intermediate impact-energies, and that the result observed for e-He($2^{1,3}S$) collisions is but a particular case of a more general trend.

7.1 THE INELASTIC FORM FACTOR IN COLLISIONAL TRANSITIONS

The Born approximation to the transition matrix element T_{fi} for inelastic scattering of a structureless particle by a target atom with composite electronic coordinates denoted by \underline{r} and with electronic wave function $\psi_n(\underline{r})$ is⁶

$$T_{fi}^B(k_i, k_f) = \langle \psi_f(\underline{r}) e^{i\mathbf{k}_f \cdot \underline{R}} | V(\underline{r}, \underline{R}) | \psi_i(\underline{r}) e^{i\mathbf{k}_i \cdot \underline{R}} \rangle_{\underline{r}, \underline{R}}, \quad (1)$$

where \mathbf{k}_i and \mathbf{k}_f are the initial and final wave-vectors of relative motion of the collision partners moving under their mutual electrostatic interaction $V(\underline{r}, \underline{R})$ at nuclear separation \underline{R} . This matrix element (1) is usually written as,

$$T_{fi}^B = \int V_{fi}(\underline{R}) e^{i\mathbf{K} \cdot \underline{R}} d\underline{R} \equiv \overline{V_{fi}(\underline{R})}, \quad \mathbf{K} = \mathbf{k}_i - \mathbf{k}_f, \quad (2)$$

the Fourier transform of the interaction

$$V_{fi}(\underline{R}) = \langle \psi_f(\underline{r}) | V(\underline{r}, \underline{R}) | \psi_i(\underline{r}) \rangle \quad (3)$$

coupling the initial and final states of the target. However, on changing the integration-variables in (1) from $(\underline{r}, \underline{R})$ to $(\underline{r}, \underline{r}_{12} \equiv \underline{r} - \underline{R})$, the transition-matrix element simply reduces to,

$$\begin{aligned} T_{fi}^B(\mathbf{K}) &= F_{fi}(\mathbf{K}) \left[\int V(r_{12}) e^{i\mathbf{K} \cdot \underline{r}_{12}} d\underline{r}_{12} \right] \\ &\equiv F_{fi}(\mathbf{K}) T_{el}^B(\mathbf{K}), \end{aligned} \quad (4)$$

a product of the T-matrix element for potential scattering of the projectile by a fixed potential $V(r_{12})$, provided by the interaction of the structureless projectile with the "frozen" target-electrons, and

$$F_{fi}(\mathbf{K}) = \langle \psi_f(\underline{r}) | e^{i\mathbf{K} \cdot \underline{r}} | \psi_i(\underline{r}) \rangle, \quad (5)$$

the inelastic form-factor for the $i \rightarrow f$ transition in the target. Expression (4) yields valuable insight to the collision process in that it separates the (target) property responsible for the actual transition, and characterized by the inelastic form factor, from the background potential scattering. This separation of properties is not readily apparent from the usual expression (2).

Moreover, the form of (4) suggests that an improvement^{6,7} to Born's approximation is given by,

$$T_{fi}(K) = F_{fi}(K) T_{el}^B(K) \quad (6)$$

where T_{el} is now the actual (or most accurate available) T-matrix (off-the-energy-shell!) for potential scattering of the projectile by the static electrons of the target. This feature has been exploited by Flannery⁸ in various treatments of collisions involving highly-excited states. The relative control of the former property over the latter in the collision process is determined by the sensitivity of T_{el}^B to those momentum-changes K important to the collision. For a Coulombic interaction e^2/r_{12} (as in e-atom collisions), the potential scattering term T_{el}^B in (4) is simply $4\pi e^2/K^2$, a quantity which exerts a dramatic influence on (4) only in the limit of vanishing momentum changes K . Therefore, for most intermediate K , any unusual variation of the transition matrix T_{fi}^B with excited state ($n'l'$) will originate mainly from the form-factor F_{fi} . This inelastic form factor not only is the driver-mechanism for collisional transitions in Born's approximation, but is also a very basic factor in more elaborate collisional treatments, such as the quantal close-coupling and multichannel eikonal methods. In fact, Flannery⁹ has already shown how the whole array of interaction matrix elements $V_{ij}(R)$ which appear in close-coupling formulations may be

derived from detailed knowledge of F_{1j} such that any systematic variation in F_{1j} will be reflected in V_{1j} and hence in the cross sections² obtained from collisional treatments even more elaborate than Born's approximation.

Also, a detailed study^{4,10} of the convergence rate of the l' partial-wave expansion for the ejected electron in the associated bound-free form-factor for electron-impact ionization revealed certain regularities (given in ref. 4) which were fully preserved in the corresponding partial l' -ionization cross sections. For example, the peaks of the form-factor as a function of momentum-change K exhibited interesting regularities with l' , regularities which were reflected directly in the corresponding cross sections. This suggests that the bound-bound form factor might also exhibit similar displays, and if so, may well have important implication for $n'l \rightarrow n'l'$ collisional transitions, in general.

7.2 SYSTEMATIC TRENDS AND ANALYSIS OF THE INELASTIC FORM FACTOR

In an effort to further explore the findings¹⁻⁴ outlined in the introduction for $e\text{-He}(2^{1,3}\text{S})$ collisions and to predict certain peculiarities not previously observed for transitions between excited states, we shall examine in detail the form factor for $n\ell \rightarrow n'\ell'$ transitions in hydrogen. By a computer analysis, the largest peak F_{\max} , with respect to the momentum-transfer K , of the form factor (modulus squared, summed over m' and averaged over m where m and m' are the azimuthal quantum numbers) is located. The variation of this peak F_{\max} with n , ℓ , n' and ℓ' should yield useful information on the corresponding collisional cross section which generally involves a K -integration about this maximum, except at the lowest impact energies.

Figure 1, for $1s \rightarrow n'\ell'$ transitions ($n' = 2, 4, 10$ and 20), simply shows that $|F_{\max}|^2$ peaks at $\ell' = 1$, as expected. Also this behavior is reflected directly in the maxima of the corresponding Born cross sections for $e\text{-H}(1s)$ inelastic collisions.

However, Fig. 2, for $2s, 2p \rightarrow n'\ell'$ transitions, clearly indicates that the form factor is dominated by an ℓ' -value of 2, irrespective of n' or the initial angular-momentum quantum number ℓ . This behavior is identical to that already observed⁴ in the form factors for $e\text{-He}(2^{1,3}\text{S})$ excitation and ionization, a behavior also preserved past the ionization threshold in partial ℓ' -wave contributions to the ionization cross section. Also, from the transitions originating from the $n = 3$ level, those terminating in the $\ell' \approx 4$ state provide the largest peak in the form factor, except for the highest value $\ell = 2$ of the initial angular momentum when $\ell'_{\max} = 3$.

The overall trend emerging in Fig. 2 becomes more clarified in Fig. 3 which shows that transitions of the $n = 4$ level are dominated by those with $\ell'_{\max} \approx 5$ or 6 if available, or by $(\ell'_{\max} - 1)$ for those with $\ell = 3$,

the largest possible initial angular momentum. As Fig. 3 indicates, the maximum value of the form factor in general oscillates as l' is increased but, on the average, it slowly rises to a relatively large peak value at $l' \approx l'_{\max}$ before exhibiting a final precipitous decrease. By including large values of n' which can therefore accommodate large l' , this decrease is quite marked. As l is increased, there is a slight tendency for l'_{\max} to shift to lower values.

By averaging over l before varying K and l' , the oscillations can be suppressed and the key issue becomes more transparent. For example, Fig. 4 illustrates the results for $n(=2,3,4) \rightarrow n'l'$ transitions, and the rise and rapid fall about $l'_{\max} \approx 2, 4$ and 5 respectively becomes most evident. In situations where that value of l'_{\max} is excluded, the form factor steadily increases with variation of l' from 0 to $(n'-1)$.

The important deduction from all of these figures is that the inelastic form factor is much more sensitive to variation of the initial principal quantum number n (which determines the physical size of the atom) than it is to variation of the initial angular-momentum quantum number l . The dominant transition between any two levels is not primarily controlled by any dipole property, except when transitions originate in a state with angular momentum $(l'_{\max} \pm 1)$ which, of course, is now primarily n -dependent.

Figure 5 further crystallizes the situation for $n=10 \rightarrow n'=20$ transitions by exhibiting the oscillatory behavior of the maximum form-factor superimposed on an increasing background until, irrespective of l , a value $l'_{\max} \sim 15$ is attained after which the extremely rapid decrease with l' is well marked.

The origin of the behavior, displayed in Figs. 1-5, lies of course

in the variation of the overlap between the initial ($n\ell$) and final ($n'\ell'$) wave functions, modulated by the phase $\exp(i\mathbf{K}\cdot\mathbf{r})$, as ℓ' is increased. The general results we have observed here were obtained from a computer analysis of the form-factor. Similar findings have also been obtained¹¹ for other (n, n') combinations by using an exact analytic expression¹² for the form factor which was practical only for levels $n' \lesssim 10$. While a rigorous mathematical analysis of the properties of the form factor for transitions between excited-states in general is extremely complex, some physical insight as to the existence of a unique value ℓ'_{\max} is possible.

The region where the initial bound state orbital is substantial defines, for our purposes, the maximal region of overlap. The radial orbital for the final state ($n'\ell'$) evolves in the limit of high n' to the Bessel function $J_{2\ell'+1}(\sqrt{8}r)$ ¹³ which, in general, oscillates many times within the overlap region. The Bessel function increases from the origin as $(\sqrt{8}r)^{\ell'}$. As ℓ' increases, the oscillating pattern tends to shift out of the overlap region together with a stretching of the first lobe. When this lobe embraces the maximal region of overlap, the overlap exhibits a maximum for this particular value of $\ell' = \ell'_{\max}$. As ℓ' increases, the first lobe shifts out of the overlap region and the overlap decreases thereafter. For $\ell' < \ell'_{\max}$, the oscillations of the Bessel function with ℓ' therefore yields the oscillations observed in Fig. 5. The $(2\ell'+1)$ -statistical weight factor of the final state ($n'\ell'$) favors an initial rise of the form factor with respect to ℓ' eventually subdued by the stretching of the first lobe. One of the effects of the modulating factor $\exp(i\mathbf{K}\cdot\mathbf{r})$, which can be expanded in terms of spherical Bessel functions $j_{\ell''}(Kr)$ is to effectively reduce the region of overlap (because of the varying relative phase of the Bessel functions) and therefore the magnitude of the form factor. The important

effect, however, is to introduce the possibility of a resonance between the Bessel functions at a specific value of K . The effective region of overlap is now the maximal region and a peak in the form factor results. As l' increases, the first lobe of the resonance pattern approaches the maximal region of overlap, embraces it and then shifts out, thereby yielding a value l'_{\max} at which the form-factor peaks.

Figure 6, for example, illustrates the variation of the overlap of the 4d-orbital with the $(n'=10, l'=4-7)$ orbitals of hydrogen as l' is increased. It is very clear that with increase of l' , the final orbital (a) shifts out of the overlap region, (b) becomes flatter on increasing from the origin and (c) involves less oscillation within the overlap region. Also there is a value $l'_{\max} \approx 6$ that results in maximum overlap which mainly arises from the first lobe of the final orbital. For $l' < l'_{\max}$ the overlap yields an oscillatory pattern superimposed on an overall rise, while $l' > l'_{\max}$ involves an ever-decreasing overlap.

A more difficult problem lies in the theoretical prediction of the variation of l'_{\max} with the initial quantum number n . Some progress is however, possible for the case when $n' \gg n \gg 1$, in which instance it proves convenient to write the spatial function for the (nl) -state

$$\psi_{nl}(\mathbf{r}) = \frac{1}{(2\pi)^{3/2}} \int \phi_{nl}(\mathbf{p}) \exp(-i\mathbf{r} \cdot \mathbf{p}) d\mathbf{p} \quad (7)$$

in terms of its associated momentum-space wave function

$\phi_{nl}(\mathbf{p}) \equiv G_{nl}(\mathbf{p}) Y_{lm}(\hat{\mathbf{p}})$, so that the form factor (5) reduces to

$$F_{f1}(\mathbf{K}) = \int \phi_{nl}(\mathbf{p}-\mathbf{K}) \phi_{n'l'}^*(\mathbf{p}) d\mathbf{p} \quad (8)$$

The unit-normalized radial momentum function for $H(nl)$ is¹³

$$G_{nl}(p) = \left[\frac{2}{\pi} \frac{(n-l-1)!}{(n+l)!} \right]^{1/2} n^{l+1} 2^{2(l+1)} l! \frac{n^l p^l}{(n^2 p^2 + 1)^{l+2}} C_{n-(l+1)}^{l+1} \left(\frac{n^2 p^2 - 1}{n^2 p^2 + 1} \right) \quad (9)$$

where the Gegenbauer polynomials $C_N^q(x)$ cause any oscillatory behavior in G_{nl} .

Since l'_{\max} is relatively insensitive to l , we can adopt, in (9) the value $l = (n-1)$ to give

$$G_{n,n-1} = \left[\frac{2}{\pi(2n-1)!} \right]^{1/2} 2^{2n} (n-1)! n^{(n+1)} \frac{p^{n-1}}{(n^2 p^2 + 1)^{n+1}} \quad (10)$$

which contains only one lobe and which increases from the origin extremely slowly as p^{n-1} , reaches a maximum at

$$p_{\max} = \frac{1}{n} \left(\frac{n-1}{n+3} \right)^{1/2} \text{ a.u.} \quad (11)$$

and then decreases as $p^{-(n+3)}$. The extent of this lobe defines a maximal overlap region R . The momentum wave-function $G_n(p)$ for the final $n'l'$ -state oscillates in general many $(n'-l'-1)$ times before exhibiting an outermost lobe, with the number of oscillations decreasing and with the general pattern shifting inwards as l' is increased. As Fig. 7 shows, the significant contribution to the overlap integral in momentum-space arises from the overlap of this final lobe, which, for $n' > n$, is smaller than the initial-state lobe with maximum at p_{\max} . The overall systematic behavior of Figs. 1-5 can therefore be understood from Fig. 7 as follows. For low l' , $G_{n'l'}$ oscillates many times within the maximal overlap region R and its outermost lobe is small and diffuse. As l' is increased, the lobe becomes more compact and shifts inwards, while its peak continually

increases and becomes comparable with the initial lobe. The overall pattern becomes less oscillatory and, when combined with the inward motion, yields an overlap which oscillates with l' on an increasing background. Maximal overlap is now obtained at $l' = l'_{\max} \approx 5,6$ when the outer lobe of $G_{n'l'}$, shifts inward to the vicinity of p_{\max} of G_{nl} . The inner oscillations of $G_{n'l'}$, which have now been pushed into the innermost region of R where the initial function G_{nl} is increasing, by comparison, only very slowly as p^{n-1} , yield little contribution to the overlap. For $l' > l'_{\max}$, the outer-lobe of $G_{n'l'}$, moves steadily inwards through the region R resulting in ever diminishing overlap, while the innermost oscillations are ineffective. This behavior yields a precipitous decrease in the form factor for $l' > l'_{\max}$, reflected in Figs. 1-5, in general, and in Fig. 4 in particular.

The zero of the outermost lobe of $G_{n'l'}$, arises from the last zero in the Gegenbauer function $G_{n-(l'+1)}^{l'+1}(x)$ which occurs at¹⁴

$$x_0 = 1 - \frac{j_{l'+1/2,1}^2}{2[n'-(l'+1)]^2} \left\{ 1 - \frac{2(l'+1)}{[n'-(l'+1)]} + O\left(\frac{1}{n'^2}\right) \right\} \quad (12)$$

where $j_{\alpha,1}$ is the first zero of the Bessel function $J_{\alpha}(x)$. For $l' \ll n'$, the third and higher terms of (12) can be neglected. Under this assumption, the zero of the outermost lobe occurs with the aid of (12) in (9), at p_0 where

$$p_0^2 = \frac{4}{j_{l'+1/2,1}^2} \sim \frac{4}{(l'+1/2) \left\{ 1 + \frac{1.9}{(l'+\frac{1}{2})^{2/3}} + \dots \right\}} \quad (13)$$

The initial function contains $(p-K)$ rather than p . For $n' \gg n$, the momentum change K is of the order of the initial momentum value $(p_1^2)^{1/2} = 1/n$ a.u. such that the maximum of $\phi_{n,n-1}(p-K)$ becomes displaced from (11) to a value

$$\overline{p}_{\max} \approx (p_{\max}^2 + k^2)^{1/2} = \left[\frac{2}{n} \left(\frac{n+1}{n+3} \right) \right]^{1/2} \quad (14)$$

Maximal overlap is obtained when the final zero of $G_{n'l'}$, located at p_0 is in the vicinity of \overline{p}_{\max} , i.e. when

$$l' = l'_{\max} \approx \left(n \left[\frac{2(n+3)}{(n+1)} \right] \right)^{1/2} - \frac{1}{2} \xrightarrow{\text{high } n} (n\sqrt{2} - \frac{1}{2}) \quad (15)$$

which gives the variation of l'_{\max} with the initial principal quantum number n . For example, this expression predicts that transitions out of the $n = 10$ and 4 levels will be dominated by those terminating on states with final angular momentum $l'_{\max} \approx 15$ and 6, respectively, in accord with Figs. 5 and 4. Even for lower $n = 2$ and 3, (15) yields (to the nearest integer) values just one unit higher.

Somewhat less information can also be obtained¹¹ from a consideration of the overlap between the corresponding spatial radial wave functions, the final orbital being replaced¹³ in the high n' -limit by $(2r)^{-1/2}$ times the Bessel function $J_{2l'+1}(\sqrt{8r})$, valid for $l' \ll n'$. The first zero of this final orbital occurs at¹⁴

$$x_0 \equiv \sqrt{8r_0} = j_{2l'+1,1} \approx (2l'+1), \quad \text{for large } l', \quad (16)$$

while the effective range of the initial nl -orbital is $r_n \approx n^2$.

Maximum overlap is obtained for l'_{\max} when $r_0 \approx r_n$ with the result that

$$l'_{\max} \approx n\sqrt{2} - \frac{1}{2} \quad (17)$$

which is the limit of (15) for very high n .

Thus, the systematic trends (oscillations, l'_{\max} , and rapid fall-off) in Figs. 1-5 can be fully understood. Note, however, that the sharp drop itself will not be observed unless the final n' is sufficiently

large so as to accommodate l'_{\max} , i.e. unless $n' > n^* \approx n\sqrt{2} - \frac{1}{2}$ for high n . For $n' < n^*$ only the overall initial rise is evident. Therefore, the range $(0-l'_{\max})$ in final-state angular momentum over which the maxima of the associated inelastic form factors are exhibiting an overall rise is fully specified for assigning

$$l'_{\max} = \min \left\{ (n'-1), \sim \left(n \left[\frac{2(n+3)}{(n+1)} \right]^{1/2} - \frac{1}{2} \right) \right\}. \quad (18)$$

7.3 TRENDS IN EXCITATION CROSS SECTIONS

The prediction here that the peaks in the inelastic form factors for $n\ell-n'\ell'$ transitions occur at $\ell' = \ell'_{\text{max}}$, a value which depends rather strongly on the initial principal quantum number n and which is rather insensitive to the initial angular-momentum quantum number ℓ , acquires further significance if it is reflected in the corresponding collisional cross sections. The pattern has already been exhibited¹⁻⁴ in $e\text{-He}(2^{1,3}\text{S})$ collisions involving both excitation to the $n=3, 4$ and 5 levels of He and ionization. Not only does this pattern emerge in Born's approximation but it has already been established in the more elaborate multichannel eikonal treatment,² and has also emerged in recent experiments.³

A. e-excited atom collisions

Since these investigations originated with an effort to explore the origin of results¹⁻⁴ for $e\text{-He}(2^{1,3}\text{S})$ collisions and eventually culminated in prediction for collisional transitions in general, we subsequently searched the literature to seek further substantiation for our findings. Indeed, Tables I-III in the review article of Moiseiwitsch and Smith¹⁵ provide partial evidence, although not actually isolated. These tables (after Vainshtein¹⁶) show, for $e\text{-H}(n\ell)$ collisions, that the $2s+n'd$ ($n'=3-9$) transitions dominate population of a given level n' at low and intermediate impact-energies, analogous to our findings for $e\text{-He}(2^{1,3}\text{S})$ collisions. The tables also show that the cross sections for the $3s+n'\ell'$ ($\ell'=0,1,2$) transitions increase as ℓ' is raised. However, the $3s + n'f, +n'g$ transitions, the strongest according to our predictions, are not given.

In the ($n=3+n'=4$) work of McCoyd et al.¹⁷ this prediction is indeed substantiated. Their Figs. 1-4 exhibit quite clearly the dominance of the $3\ell+4f$ transition in populating the $n' = 4$ level from $n = 3$.

However, these trends were not apparently noticed, as evidenced by an accompanying paper¹⁸ which was confined only to optically-allowed transitions between the $n=4$ and $n'=5$ levels. We have predicted from Fig. 6 that the full $4l \rightarrow n'g$ ($l' = 5$) array of transitions control the population of levels n' . Dipole transitions ($l = l' \pm 1$) are also covered by this prediction and the figures of Fisher *et al.*¹⁸ show that $4f-5g$ is indeed dominant. But, unfortunately, Fisher *et al.*¹⁸ have not included the $4s \rightarrow n'g$, $4p \rightarrow n'g$, and the $4d \rightarrow n'g$ transitions which, according to our predictions, also yield substantial contributions to excitations out of the $n = 4$ level.

In an effort therefore to provide more exhaustive evidence for our predictions, we have carried out full Born calculations for extensive arrays of $(nlm \rightarrow n'l'm')$ transitions in $H(nlm)$ induced by collision with electrons and with hydrogen-atoms for a wide range of impact-energies. Rather than presenting here all of the copious supply of cross-section data (which did involve lengthy computing time particularly for transitions between high- n states and which may be obtained, if required, from the authors) we have attempted to isolate the key features by reporting here only the maximum value Q and \bar{Q} (with respect to impact-energy) of the respective cross sections $Q_{nl,n'l'}$ and of the average value

$$Q_{n,n'l'} = \frac{1}{n} \sum_{l=0}^{(n-1)} Q_{nl,n'l'} = \frac{1}{n} \sum_{l=0}^{(n-1)} \frac{1}{(2l+1)} \sum_{m,m'} Q_{nlm,n'l'm'} \quad (19)$$

where the individual cross sections are obtained from (4) to give

$$Q_{nlm,n'l'm'} = \frac{1}{(8\pi)} \left(\frac{2m}{\hbar^2 k_f^2} \right)^2 \int_{(k_1 - k_f)}^{(k_1 + k_f)} |F_{nlm,n'l'm'}(\tilde{\mathbf{K}})|^2 |T_{el}(\mathbf{K})|^2 K dK \quad (20)$$

For electron-atom collisions, $T_{el} = 4\pi e^2/K^2$, and the cross sections for $nl \rightarrow n'l'$ transitions generally peak about the same impact-energy for different (l, l') .

Accordingly in Figs. 8-11 are displayed some representative plots of our results. Since Moisewitsch and Smith¹⁵ have already tabulated $Q_{2s,n'l'}$, Fig. 8 shows only the variation with l' of the averaged \bar{Q} from the 2s and 2p states. Transitions to $n'd$ states dominate, as expected from consideration of the form-factor (cf. Fig. 2). The remaining Figs. 9-11 illustrate the behavior for collisional transitions out of the states associated with levels $n=3, 4$ and 10. In general, both Q and \bar{Q} tend to peak about that value of l'_{\max} as predicted by (18) although, for the higher initial l -values, Q peaks at $(l'_{\max}-1)$, as expected from the form-factors in Figs. 3 and 5. The inclusion of high- n' final states emphasizes the oscillatory rise following by the rather precipitous decline as higher l' 's are added. Transitions out of the $n=4$ level are dominated, for example, in Fig. 10 by those terminating on level with $l'_{\max} \approx 5$ or 6, if available; otherwise the cross sections reflect an oscillatory rise with l' [as in Figs. 9 and 10 for the (3-4) and (4-5) cases]. From among those strong transitions which terminate on l'_{\max} (or $l'_{\max}-1$, for the higher l -values) those with dipole character, i.e. $n(l'_{\max}-1) \rightarrow n'l'_{\max}$ are generally larger (e.g. $2p \rightarrow 3d$, $3d \rightarrow nf$, $4f \rightarrow ng$). However, the main feature is not the character of the transition, but is the value of l'_{\max} which is primarily n -dependent. Whether or not this value of l'_{\max} precludes a dipole transition is a secondary feature. For example, for the $n=10 \rightarrow n'=20$ transition in Fig. 11, $l'_{\max} \approx 15$ such that any of the strong ($nl \rightarrow n'l'_{\max}$) transitions which terminate on the $n'=20$ level cannot be dipole in character.

In summary, the systematic variation of the form factor with n and l' is reflected in the cross sections for e -atom collisions by exhibiting an oscillatory increase with l' , by reaching a peak at a value of l' given by (18) and then by following a rapid decline with l' . Thus, even in spite of their large statistical weight $(2l'+1)$, the final

states with $l' \gg l'_{\max}$, are not populated in e-atom collision as compared with those with $l' \approx l'_{\max}$. However, couplings introduced between the various angular momenta of levels n and n' , as in a close-coupling treatment, would tend to enhance the weaker transitions at expense of the stronger ones which would be only weakly diminished.²

B. Atom-excited atom collisions

Another attractive feature in writing the Born T-matrix as (4), or as the presumably more-accurate T-matrix (6), arises in heavy-particle collisions. We note that the essential factor which causes the cross sections to approach dipole-character at high impact-energies is T_{el}^B , which, for e-atom collisions is $4\pi e^2/K^2$ and is singular as $K \rightarrow 0$, the optical limit. In the case of single excitation in atom-atom collisions, however, T_{el}^B for scattering of the projectile by the "frozen" electrons of the target does not contain such a singularity (e.g. for the screened Coulombic interaction $e^2 r^{-1} e^{-\lambda r}$ between the projectile and target electrons, T_{el}^B is $4\pi e^2/[K^2 + \lambda^2]$). The absence of this singularity at $K = 0$ is to allow the form factor in (4) or (6) to exert even more control in the collision process, than in the e-atom case. Therefore, the above predictions will be tested by calculating the Born cross sections for the collision processes.

$$H(1s) + H(nl) \rightarrow H(1s) + H(n'l') \quad (21)$$

for which

$$T_{el}(K) = \frac{4\pi e^2}{K^2} \left[1 - F_{11}^2(K) \right] = \frac{4\pi e^2(8+K^2)}{(4+K^2)^2} \quad (22)$$

is not singular as $K \rightarrow 0$. Cross sections were obtained for all of the $(nl \rightarrow n'l')$ combinations covered for electron-impact, resulting in similar but more pronounced trends for Q and \bar{Q} . As illustrated by Figs. 12 and 13

for specified $nl \rightarrow n'l'$ transitions in $H(1s) - H(n, l=0)$ collisions, a sharper peak about l'_{\max} is observed (provided sufficient l' are accessible) in keeping with the prediction that single excitations in heavy-particle collisions correlate more closely with the behavior of the corresponding inelastic form factor, due to the absence of a singularity for zero momentum-changes. The general features of Figs. 12 and 13 remain preserved for higher initial values of $l = 0-(n-1)$. On averaging over these l -values, the key peak about an unique l'_{\max} is more transparent as in Figs. 14 and 15. There are, however, several interesting differences.

The plots of $Q_{nl, n'l'}$ versus impact energy E reveal a series of maxima, rather than one pronounced peak as for e-atom collisions. These undulations are displayed in Fig. 16, represent a real effect, and are attributed again to direct reflection of the form-factor. For example, Fig. 17 shows the variation of the integrand of (20) with K for the $4s-8s$ transition together with the lower limit $K_{\min} = (k_i - k_f)$ of integration for various impact energies E (in units of the transition energy $\Delta\epsilon$). As E is increased, K_{\min} moves inwards and samples the various oscillations of the integrand. For example, as E increases from $\sim 60 \Delta\epsilon$ to $\sim 1000 \Delta\epsilon$, two oscillations in Fig. 17 are traversed and are directly reflected in the variation with E of the cross section $Q_{4s, 8s}$ in Fig. 16. However, as l' is increased beyond l'_{\max} a well-defined peak tends to emerge with the remaining undulations becoming, by comparison, increasingly suppressed. This unusual oscillatory behavior of the cross sections, particularly for those transitions between states with low values of angular momentum, could be experimentally detected with modern equipment.¹⁹⁻²⁵

Moreover, in the limit of collisions of very slow atoms with highly excited atoms, the scattering, as described by $T_{el}(K)$ in (6), of the

"frozen" electrons of the target by the slow projectile is isotropic with the result that details of the collisional transition as given by (6) is governed entirely by the form factor.

Finally, some experimental evidence for the preferential population of high angular momentum states in ion-excited atom collisions has recently been reported¹⁹ and indicates the emergence of the general patterns as described here.

There are, however, several interesting differences between the present results and those of Ref. 19. The plot of $\sigma_{\text{max}}/\sigma_{\text{tot}}$ versus impact energy E reveals a series of maxima, rather than one pronounced peak as for a-atom collisions. These oscillations are displayed in Fig. 10, representing a real effect, and are attributed again to direct reflection of the form-factor. For example, Fig. 17 shows the variation of the integrand of (10) with K for the $4s \rightarrow 3s$ transition together with the lower limit $K_{\text{min}} = (E - E_{\text{exc}})^{1/2}$ of integration for various impact energies E (in units of the transition energy E_{exc}). As E is increased, K_{min} moves towards and samples the various oscillations of the integrand. For example, as E increases from ~ 0.5 to ~ 1000 , two oscillations in Fig. 17 are traversed and are directly reflected in the variation with E of the cross section σ_{max} in Fig. 18. However, as E is increased beyond E_{max} , a well-defined peak tends to emerge with the remaining undulations becoming, by comparison, increasingly suppressed. This unusual oscillatory behavior of the cross section, particularly for those transitions between states with low values of angular momentum, could be experimentally detected with modern

equipment.¹⁹⁻²⁵

Moreover, in the limit of collisions of very slow atoms with highly excited atoms, the scattering, as described by $T_{\text{el}}^{(0)}(K)$ in (6), of the

7.4 SUMMARY AND CONCLUSIONS

Here we have predicted new and interesting "peculiarities" involved in collisional excitation between excited states. The study originated with an effort to explain previous results¹⁻⁴ for excitation in $e\text{-He}(2^{1,3}S)$ collisions, which were found, as the investigation progressed, to be particular instances of a more general and basic trend. Our conclusions take the form of certain predictions which, as we have shown here, are fully substantiated by systematic trends in the cross sections for $n\ell \rightarrow n'\ell'$ transitions in hydrogen induced by both electron and by heavy-particle impact.

Even though the systematic trends which originated with the form factor have only been, in general, observed with the Born cross sections for collisional transitions between excited states they are expected, as discussed in Sec. II, to be maintained also in more elaborate descriptions as in the ten-channel eikonal treatment² of $e\text{-He}(2^{1,3}S)$ excitational collisions, as yet the only application of a closely-coupled method to transitions between excited states.

The trends for electron-atom collisions become more pronounced for heavy-particle collisions which, in addition, exhibit interesting oscillations with impact-energy for transitions between excited states, particularly those with low ℓ -values.

The population of the level n' ($>n$) arising in $n\ell \rightarrow n'\ell'$ collisional transitions is found to be primary controlled at low and intermediate impact speeds by the $n(\ell = 0 - n-1) \rightarrow n'\ell'_{\max}$ array of transitions for which

$$\ell'_{\max} = \min \left\{ (n'-1), \sim n \left[\frac{2(n+3)}{(n+1)} \right]^{1/2} - \frac{1}{2} \right\} \quad (23)$$

While the probabilities of these transitions are fairly insensitive to the

initial l -value, these transitions with dipole character ($l=l'_{\max} \pm 1$) are somewhat more probable. In general, the inelastic form factor and the excitation cross sections for ($n l \rightarrow n' l'$) transitions exhibit, on variation of l' alone, an oscillatory behavior superimposed on an overall rise until a pronounced maximum at l'_{\max} in (23) is attained. With further increase of l' both the form factor and associated cross sections exhibit a dramatic decrease with the result that population of states with $l' \gg l'_{\max}$ is negligible by comparison.

A related purpose is therefore to express a note of caution in following the arbitrary assumption in $n l \rightarrow n' l'$ collisional excitation that the $l' = l \pm 1$ transitions are the strongest and are the ones that only need calculation. This assumption, which is without foundation except at high impact-speeds, has tacitly been accepted in modeling studies of the role of excited states in laboratory (laser) and astrophysical plasmas. The dipole transitions $n (l'_{\max} \pm 1) \rightarrow n' l'_{\max}$ are of course covered by our prediction and are therefore strong, as are also the $n l \rightarrow n' l'_{\max}$ array of transitions, in general. Finally, these predictions are very relevant to current experimental investigations¹⁹⁻²⁵ of collisional processes involving highly excited Rydberg states of atoms.

References

*Visiting Fellow, 1977-78 on leave from Georgia Institute of Technology.

1. Y.-K. Kim and M. Inokuti, Phys. Rev. 181, 205 (1969); M. R. Flannery, W. F. Morrison and B. L. Richmond, J. Appl. Phys. 46, 1186 (1975).
2. M. R. Flannery and K. J. McCann, Phys. Rev. A 12, 846 (1975).
3. M. L. Lake and A. Garscadden, preprint and Bull. Am. Phys. Soc. 22, 196 (1977).
4. D. Ton-That, S. T. Manson and M. R. Flannery, J. Phys. B 10, 621 (1977).
5. A. K. Dupree and L. Goldberg, Ann. Rev. Astron. Astrophys. 8, 231 (1970).
6. N. F. Mott and H. S. W. Massey, The Theory of Atomic Collisions, (Clarendon Press, Oxford, 1965), 3rd ed., pp. 335, 475-459.
7. M. R. Flannery, J. Phys. B 8, 2470 (1975), especially page 2481.
8. M. R. Flannery, Ann. Phys. N.Y. 61, 465 (1970); 79, 480 (1973).
9. M. R. Flannery, J. Phys. B 2, 913 (1969).
10. D. Ton-That and M. R. Flannery, Phys. Rev. A 15, 517 (1977).
11. D. Ton-That and M. R. Flannery, Bull. Am. Phys. Soc. 21, 1247 (1976).
12. M. R. Flannery, Phys. Rev. 183, 231 (1969), Appendix.
13. H. A. Bethe and E. E. Salpeter, Quantum Mechanics of One- and Two-Electron Atoms (Springer-Verlag, Berlin, 1957), p. 18, p. 39.
14. Urs W. Hochstrasser, in Handbook of Mathematical Functions, edited by M. Abramowitz and I. A. Stegun (National Bureau of Standards Applied Mathematics Series 55, Washington, D. C. 1967), Chapter 12.
15. B. L. Moiseiwitsch and S. J. Smith, Rev. Mod. Phys. 40, 238 (1968).
16. L. A. Vainshtein, Opt. Spectrosc. USSR 18, 538 (1965).
17. G. C. McCoyd, S. N. Milford and J. J. Wahl, Phys. Rev. 119, 149 (1960).
18. L. Fisher, S. N. Milford and F. R. Pomilla, Phys. Rev. 119, 153 (1960).

19. B. Andresen and E. Veje, Phys. Rev. A 16, 1980 (1977).
20. T. F. Gallagher, R. M. Hill and S. A. Edelstein, Phys. Rev. A 13, 1448 (1976); 14, 744 (1976).
21. T. F. Gallagher, L. M. Humphrey, R. M. Hill, W. E. Cooke and S. A. Edelstein, Phys. Rev. A 15, 1937 (1977).
22. W. E. Cooke, T. F. Gallagher, R. M. Hill and S. A. Edelstein, Phys. Rev. A 16, 2473 (1977) and references therein.
23. R. F. Stebbings, F. G. Kellert, G. P. Hildebrandt, G. W. Foltz, K. A. Smith and F. B. Dunning, Abstracts of X International Conference on the Physics of Electronic and Atomic Collisions, Paris, 1977, p. 170.
24. R. F. Stebbings, C. J. Latimer, W. P. West, F. B. Dunning and T. B. Cook, Phys. Rev. A 12, 1453 (1975).
25. W. P. West, G. W. Foltz, F. B. Dunning, C. J. Latimer and R. F. Stebbings, Phys. Rev. Lett. 36, 854 (1976).

Figure Captions

- Fig. 1. Variation of the peak of the $(1s-n'l')$ inelastic form factor squared and of the maximum cross section for given $e-H(1s)$ inelastic collisions with changes in final angular momentum l' .
- Figs. 2,3 Variation of the peak of the inelastic form factor for given $n \rightarrow n'$ transitions with changes in initial and final angular momenta l and l' respectively.
- Fig. 4. Variation with final angular momentum l' of the peak of the inelastic form factor averaged over l for given $n \rightarrow n'$ transitions.
- Fig. 5. Variation with final angular momentum l' of the peak of the form factor for $(10s,p,d \rightarrow 20l')$ transitions and of the peak of the form factor averaged over all values $(0,1,\dots,9)$ of the initial angular momentum l .
- Fig. 6. The $4d$ and $10(l'=4-7)$ hydrogen radial-orbitals, R_{nl} , times r in configuration-space. Note the outward shift in the $10l'$ -orbital and the consequent variation in overlap with increase of l' . Here maximum overlap is obtained for $l' = l'_{\max} = 6$.
- Fig. 7. The $4d$ and $10(l'=4-7)$ radial wave functions $F_{nl}(p)$ times p in momentum-space. Note the inward shift in the $10l'$ -function and the consequent variation in overlap with increase of l' .
- Fig. 8. Variation with l' of the maximum l -averaged cross section for given $2l \rightarrow n'l'$ transitions in $e-H(2)$ collisions.
- Figs. 9-11. Variation with l' of the maximum cross section (with and without l -average) for given $nl-n'l'$ transitions in $e-H(nl)$ collisions.

Fig. 12. Variation with l' of the maximum cross section for specified $nl \rightarrow n'l'$ transitions in $H(1s) - H(nl)$ collisions.

Fig. 13. Variation with l' of the maximum cross section for specified $nl \rightarrow n'l'$ transitions in $H(1s) - H(nl)$ collisions.

Fig. 14. Variation with l' of the maximum l -averaged cross section for specified $n \rightarrow n'l'$ transitions in $H(1s) - H(nl)$ collisions.

Fig. 15. Variation with l' of the maximum l -averaged cross section for specified $n \rightarrow n'l'$ transitions in $H(1s) - H(nl)$ collisions.

Fig. 16. Cross section for $4s \rightarrow n'l'$ transitions in $H(1s) - H(4s)$ collisions at energy E (in units of transition-energy $\Delta\epsilon$) for various l' -values indicated on each curve.

Fig. 17. Variation of the integrand Eq. (20) of text with momentum change K . Vertical lines indicate the lower K -limit of integration at various impact-energies E (in units of transition-energy $\Delta\epsilon = 0.64$ eV).

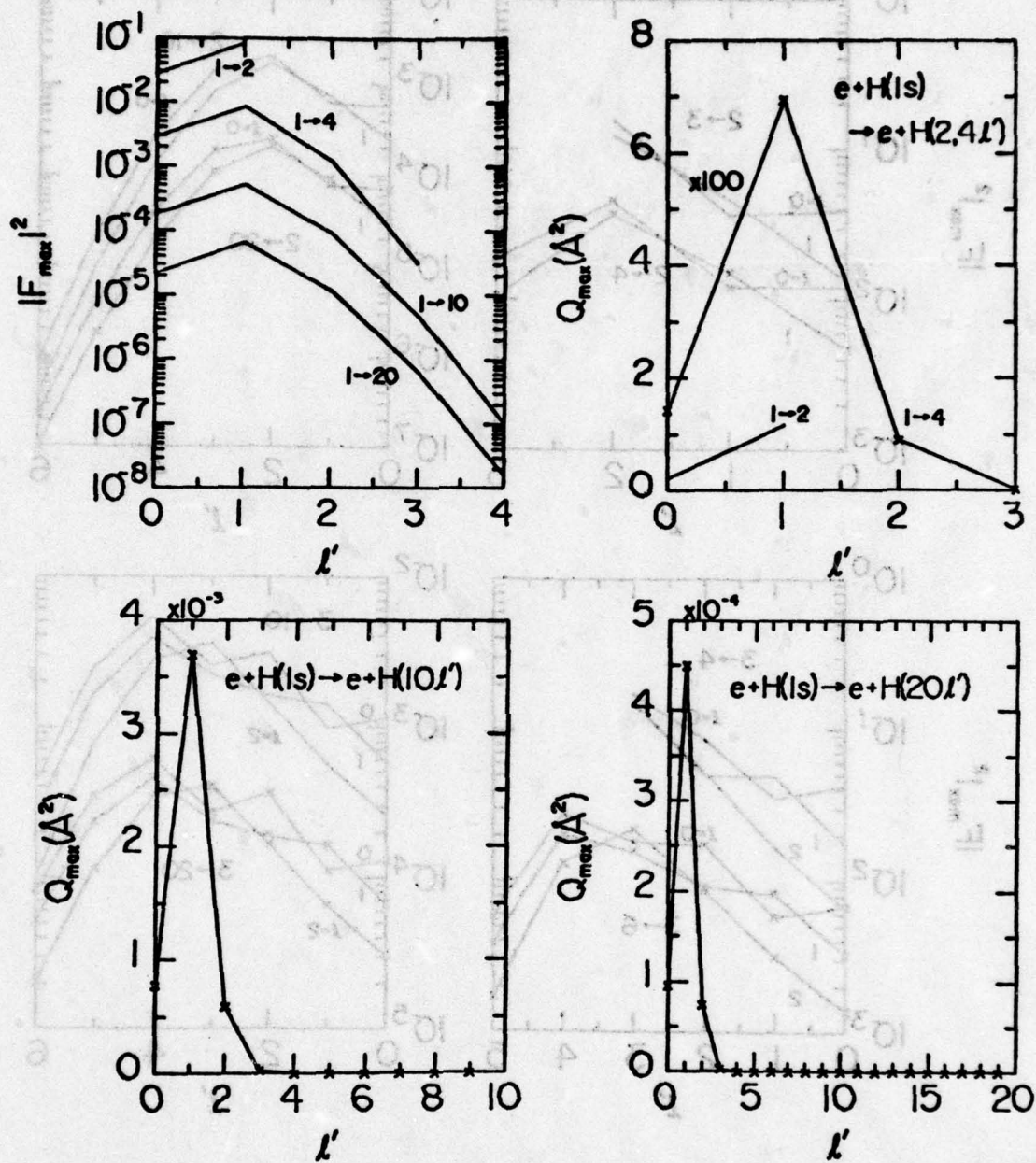


Figure 1

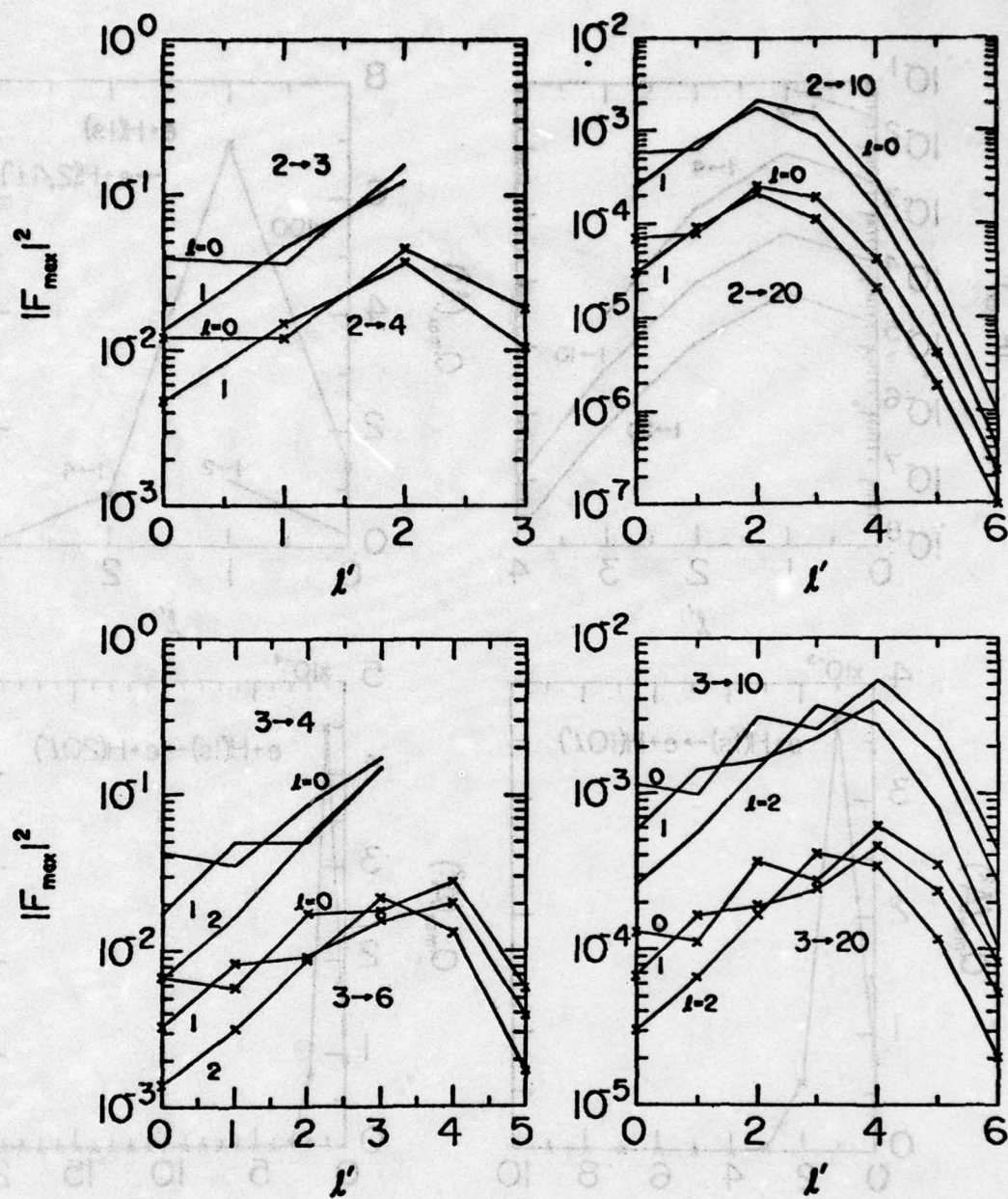


Figure 2

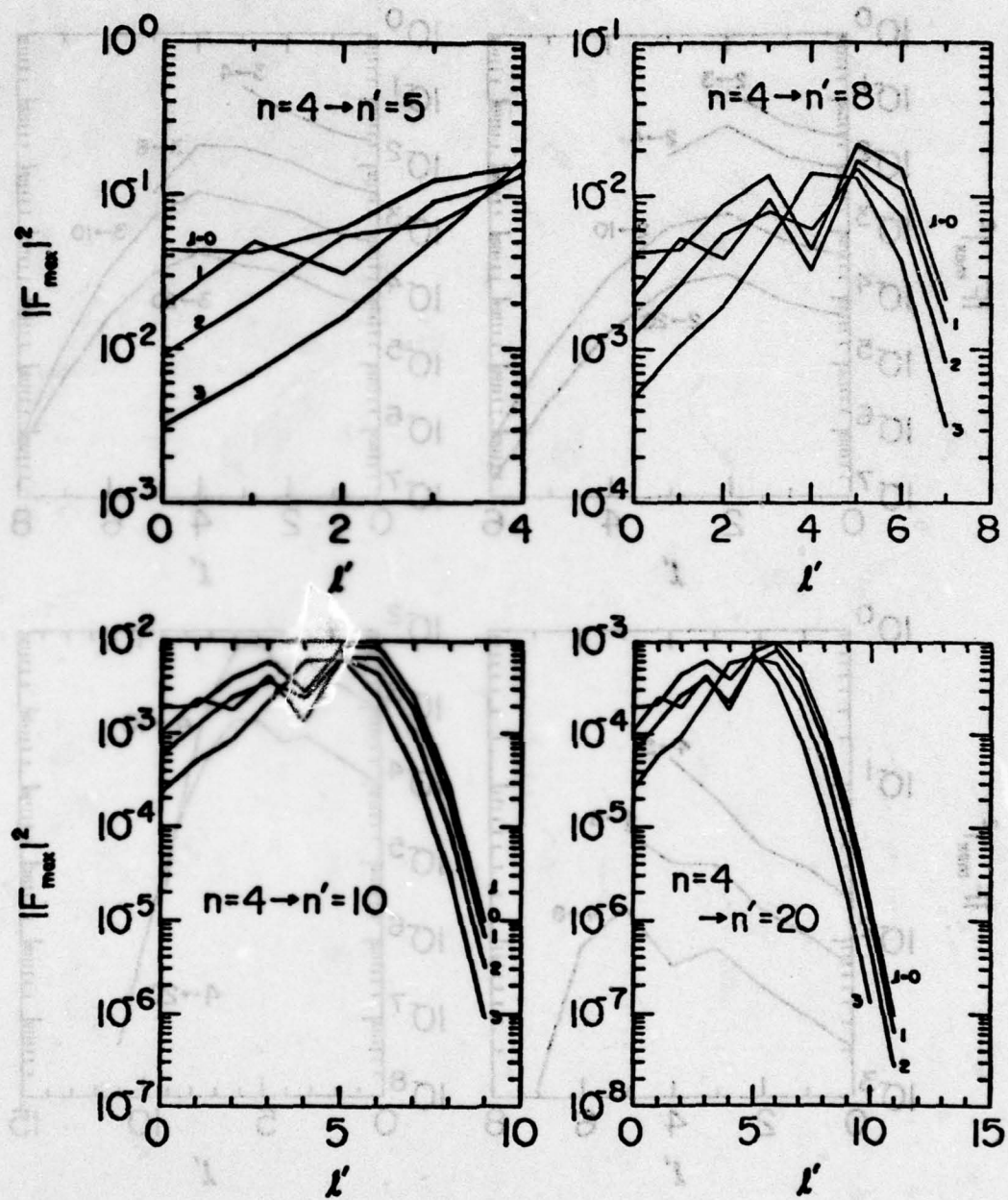


Figure 3

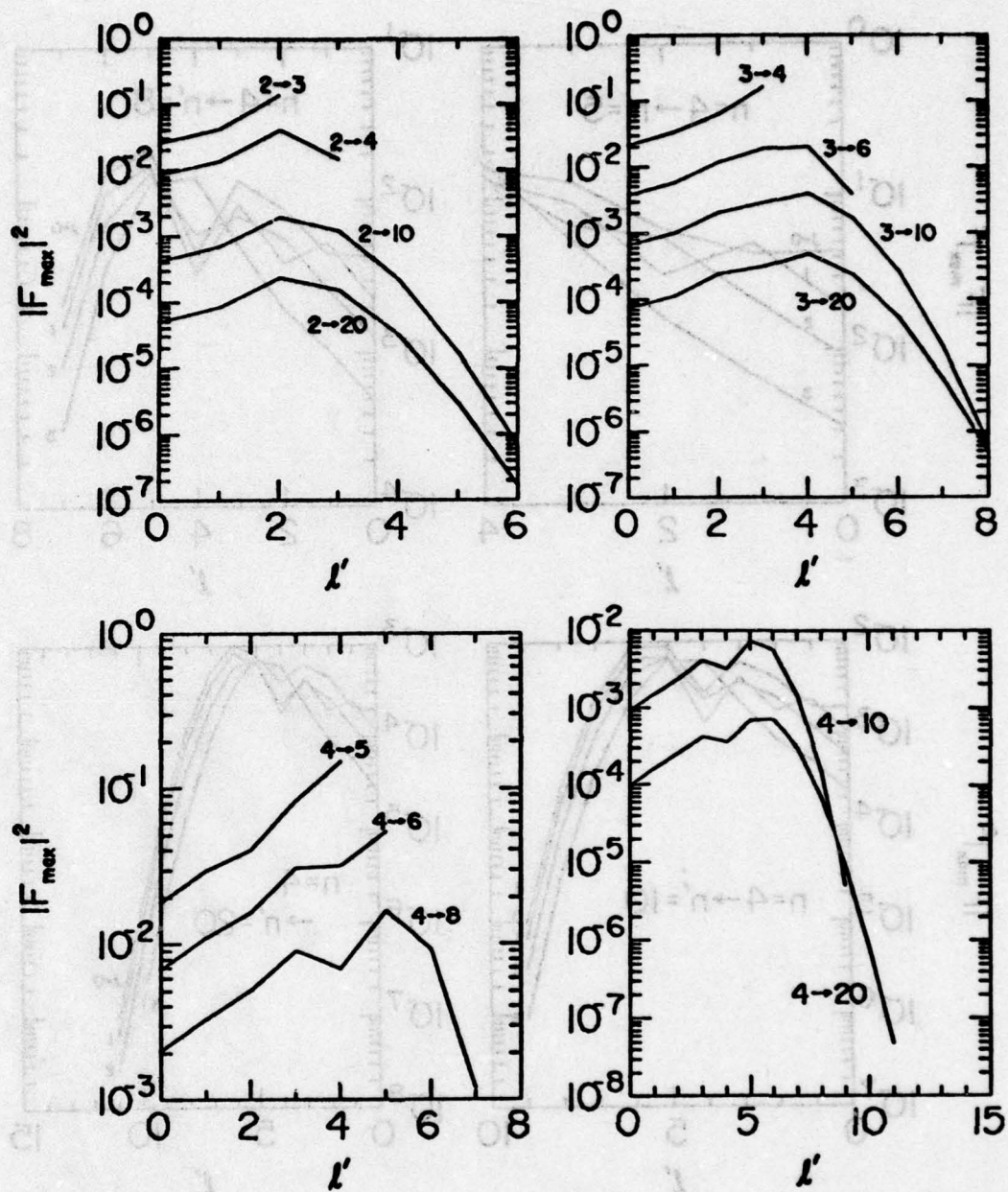


Figure 4

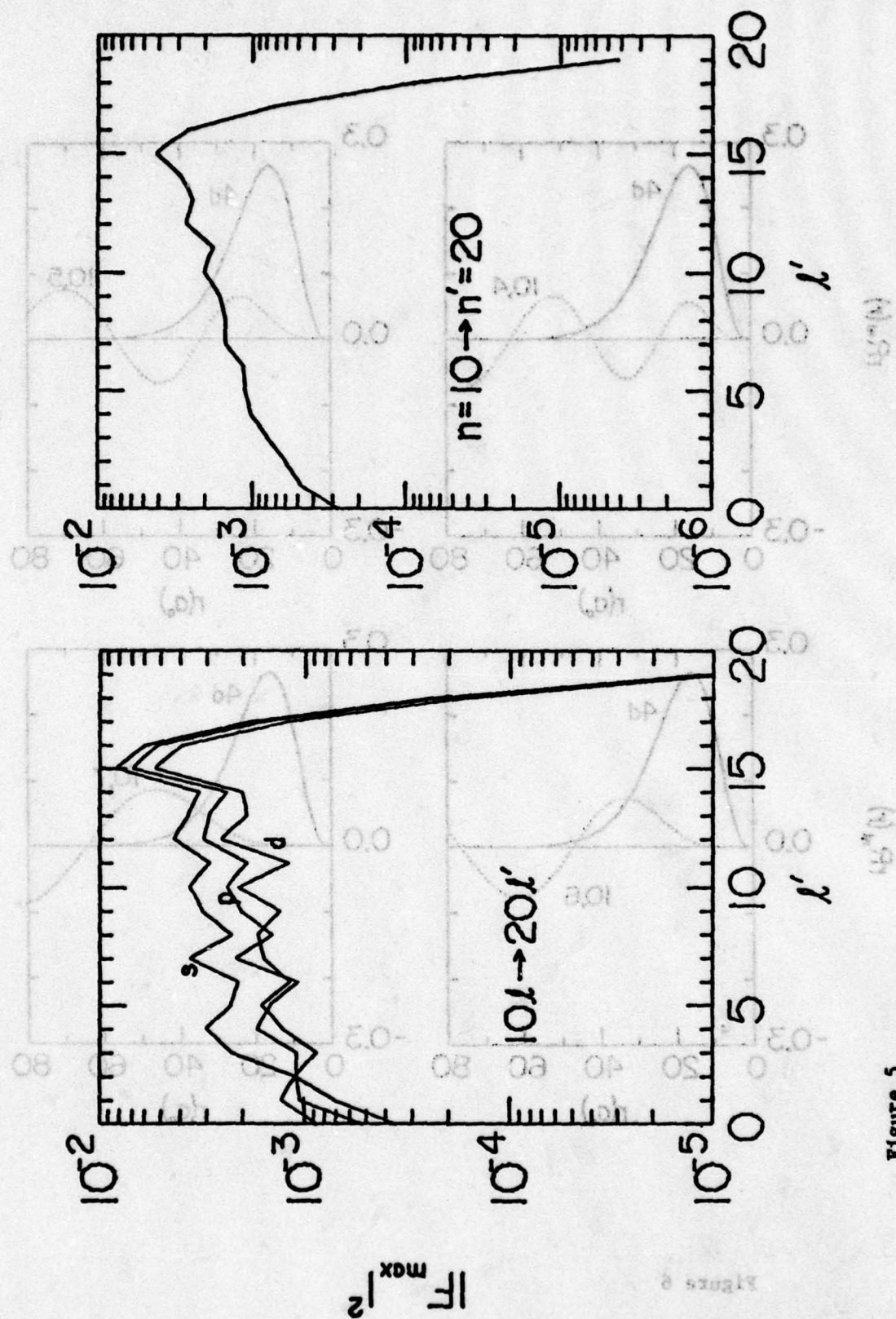


Figure 5

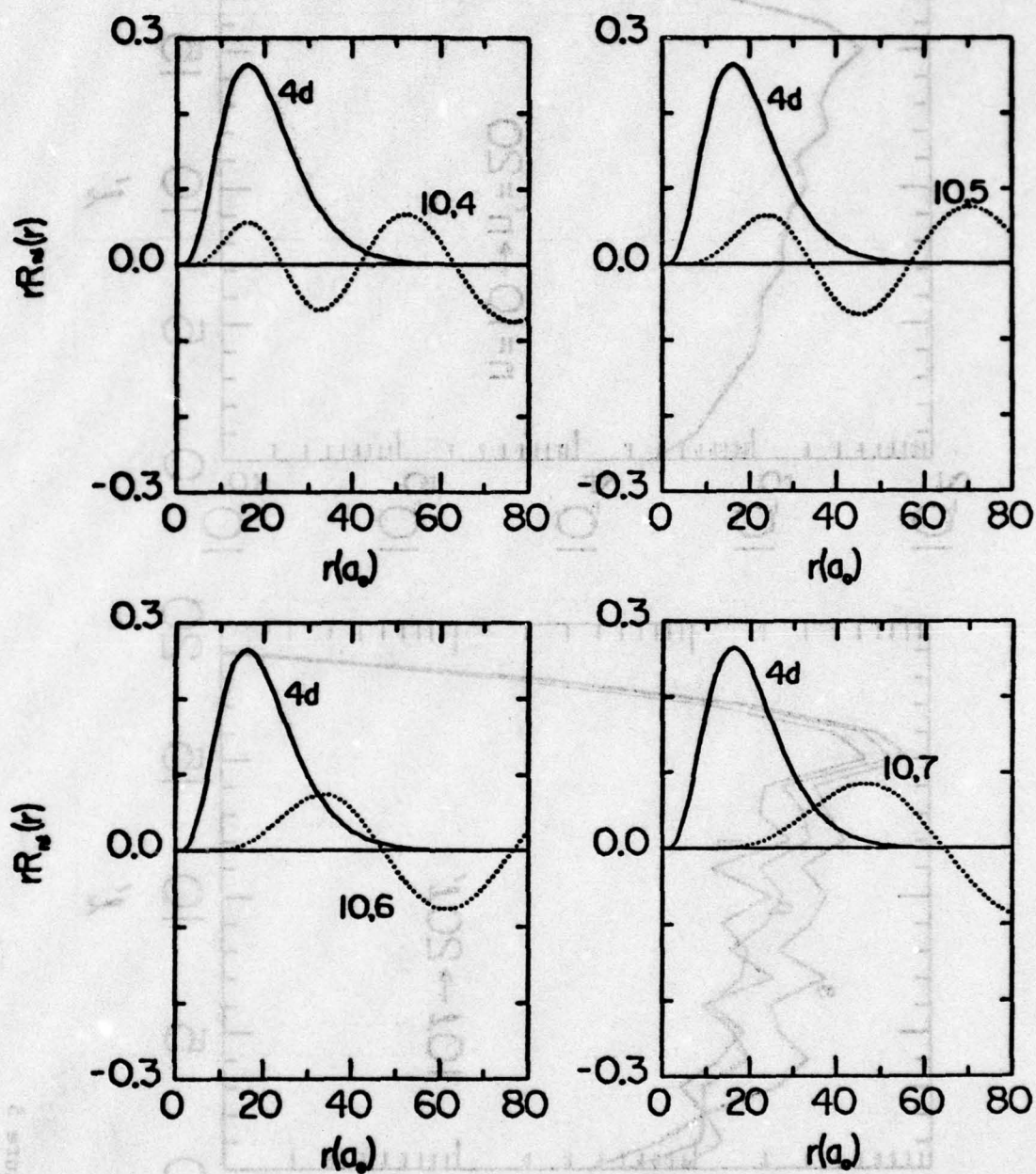


Figure 6

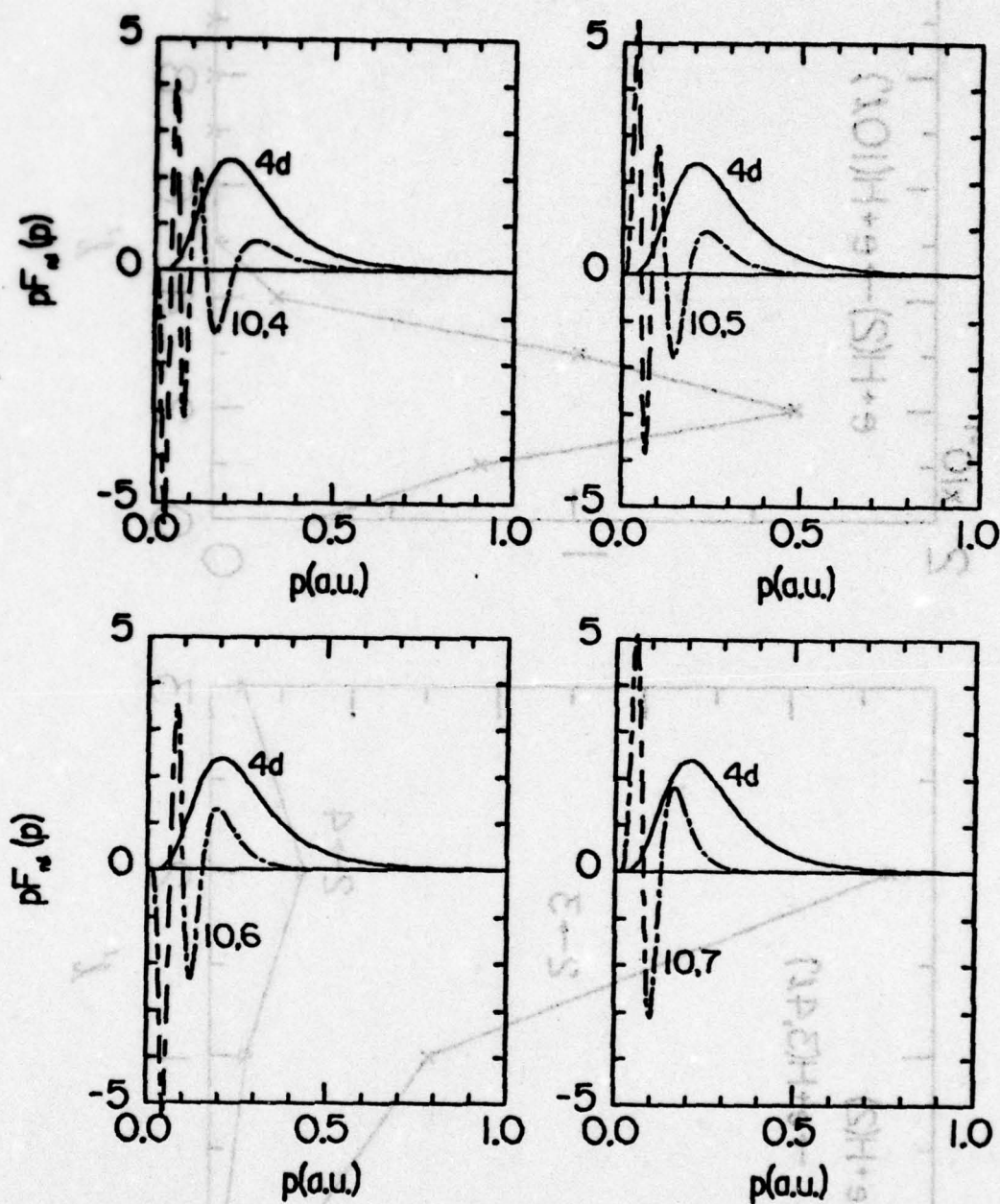


Figure 7

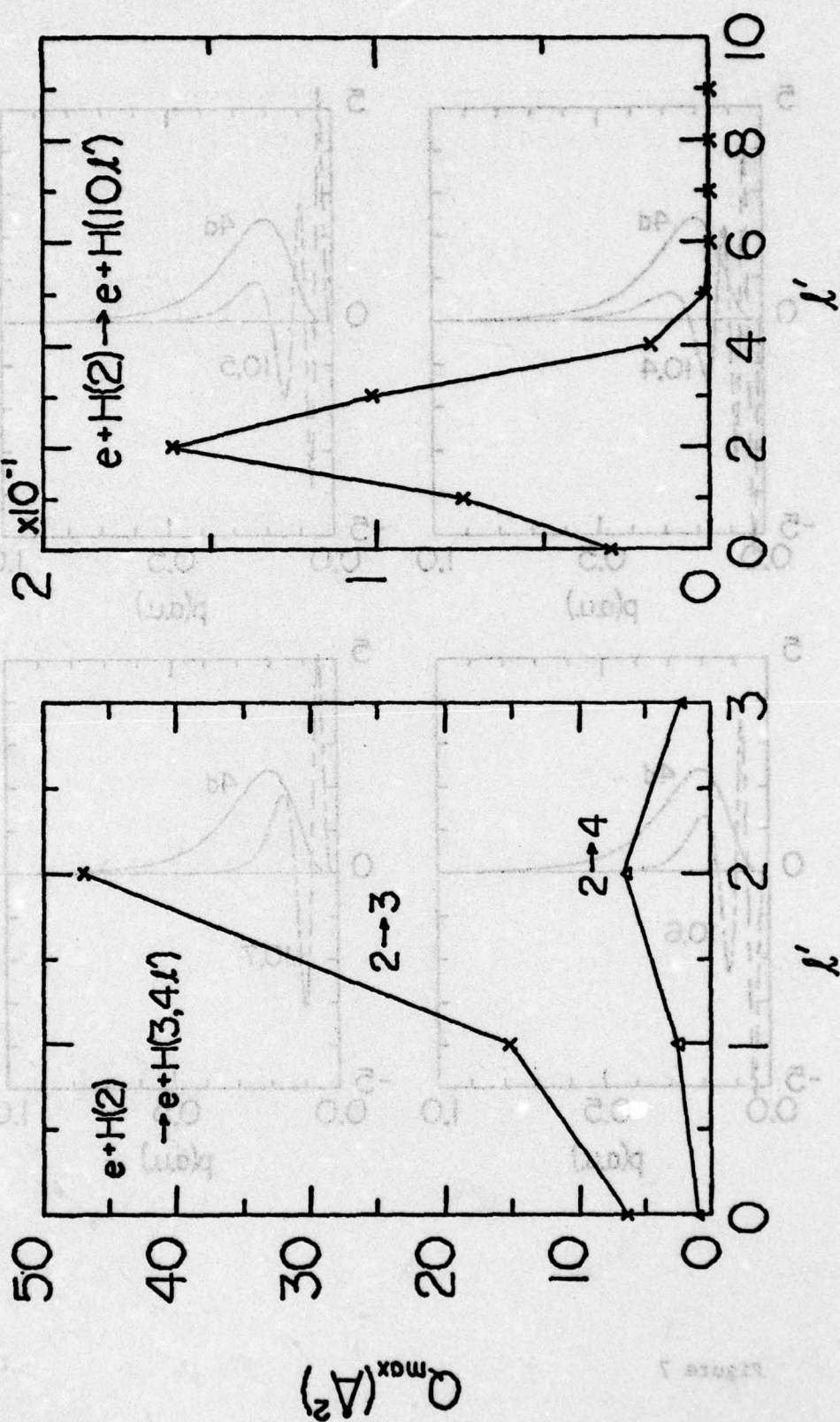


Figure 8

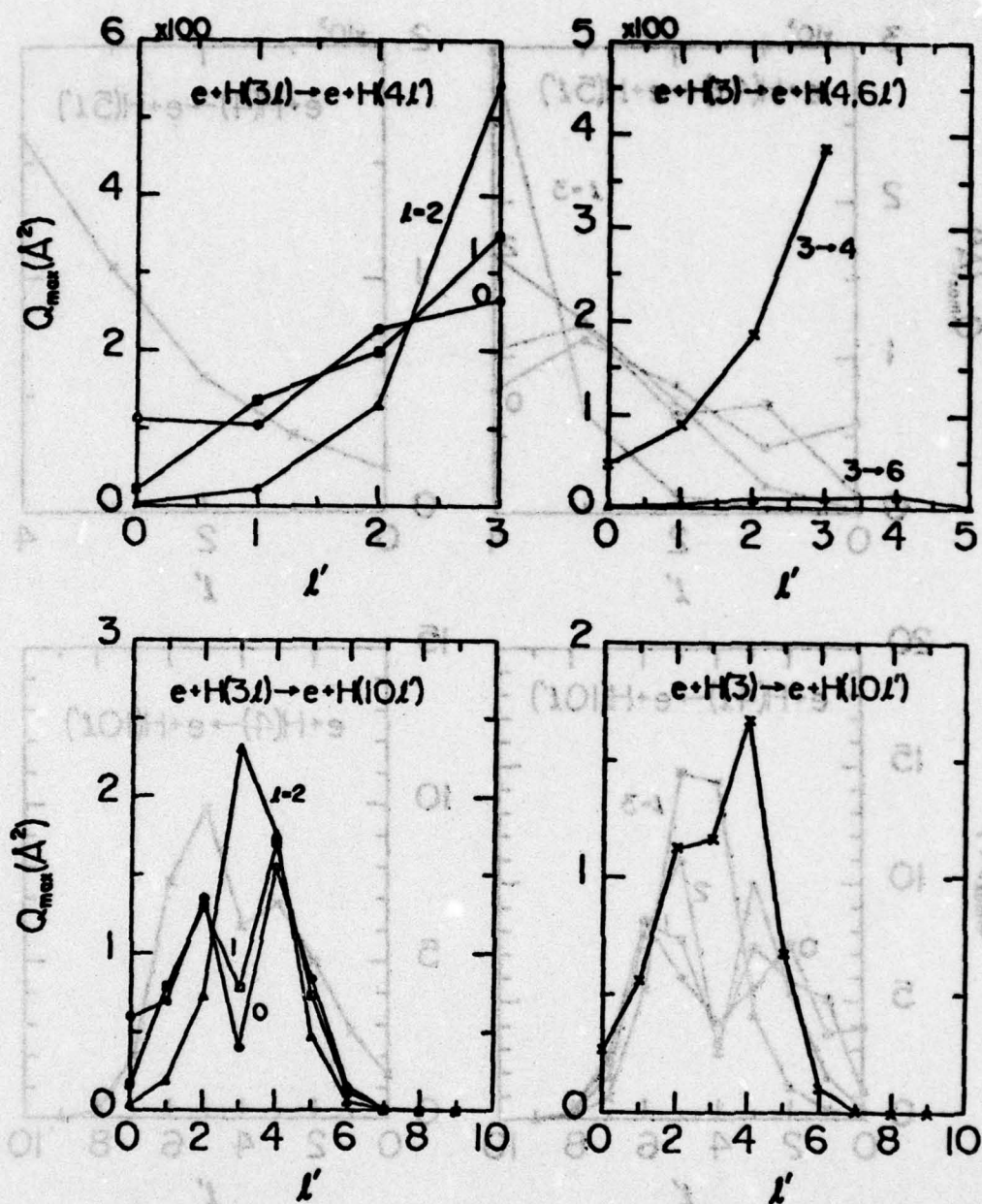


Figure 9

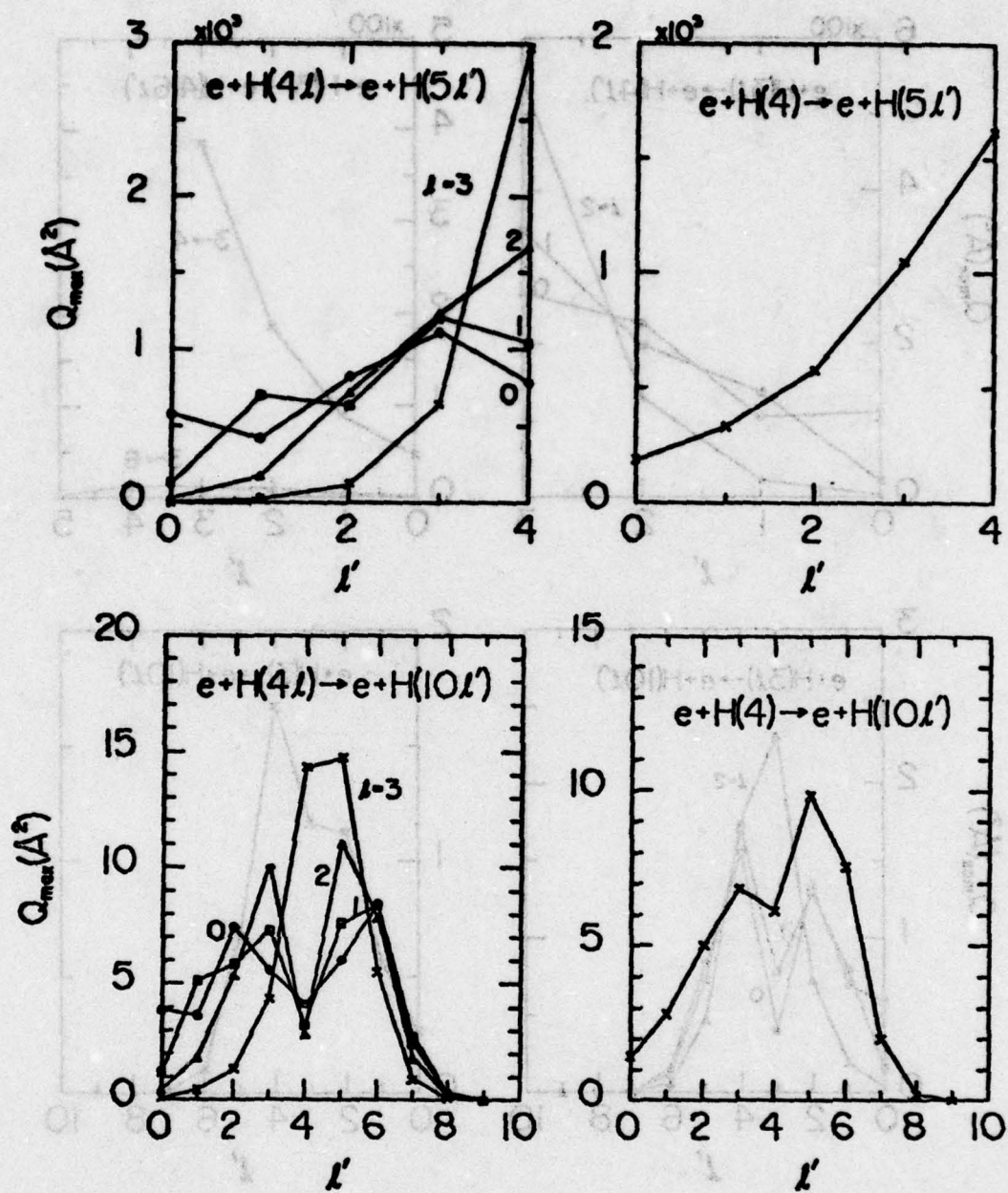


Figure 10

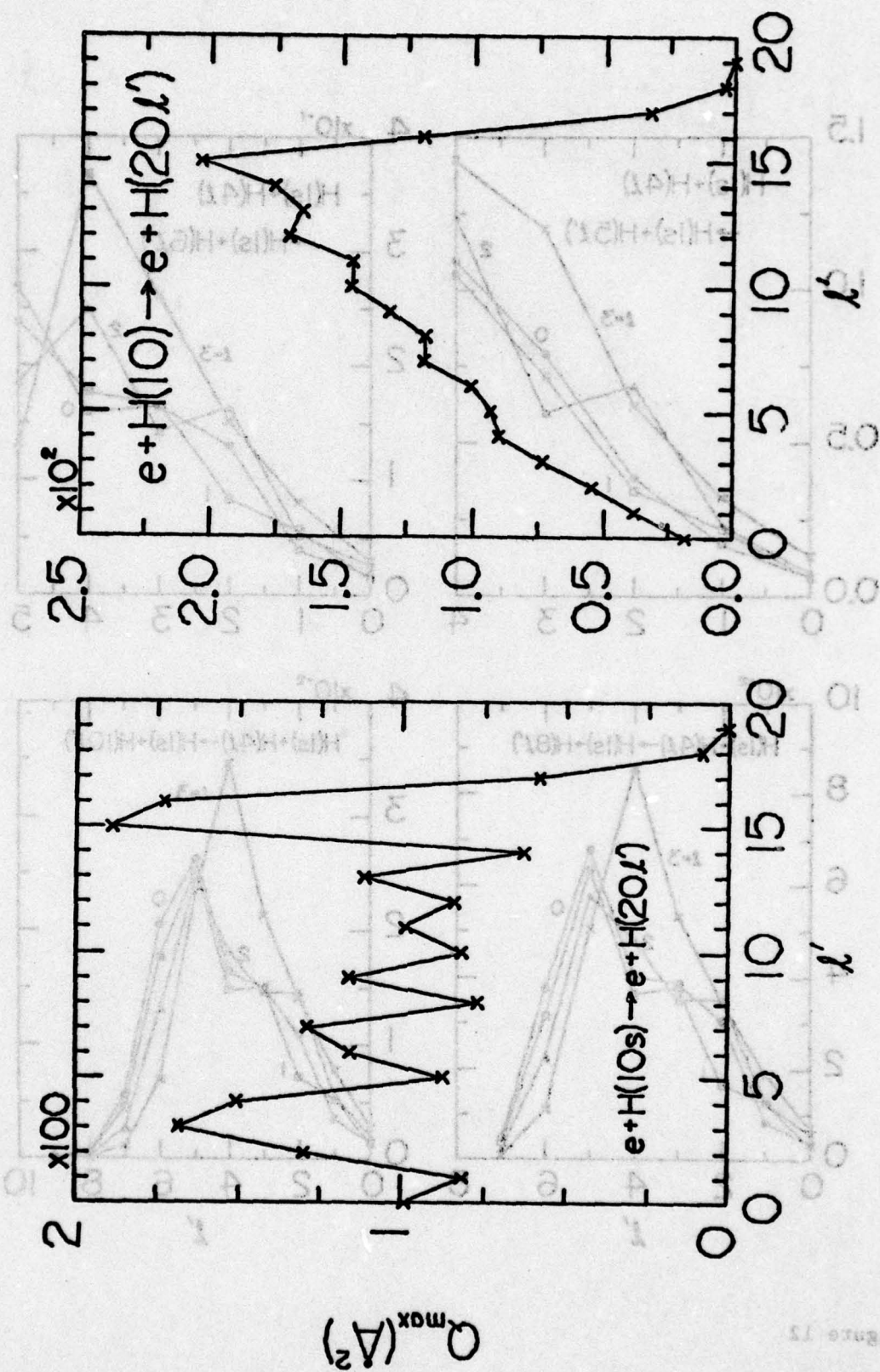


Figure 11

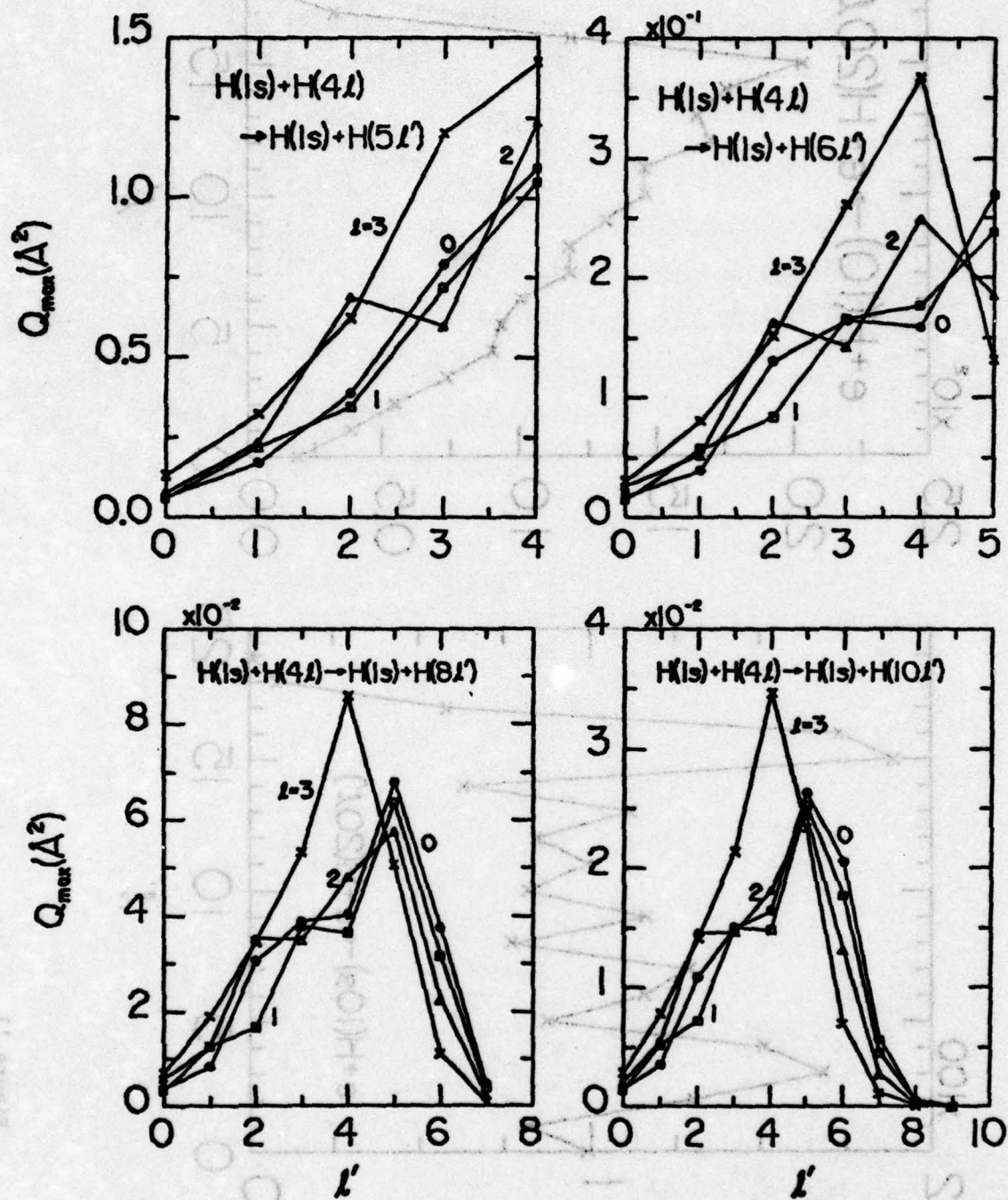


Figure 12

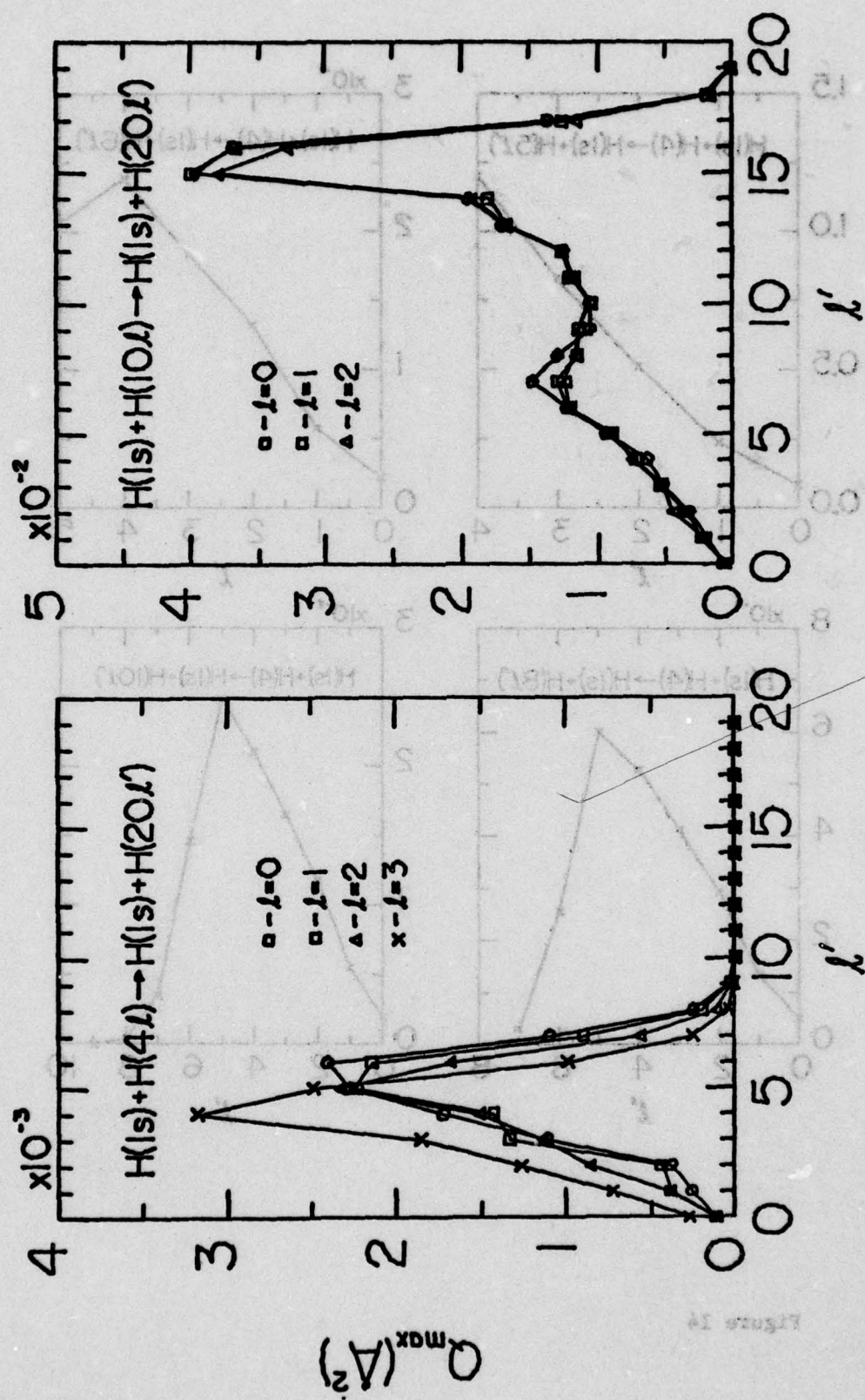


Figure 13

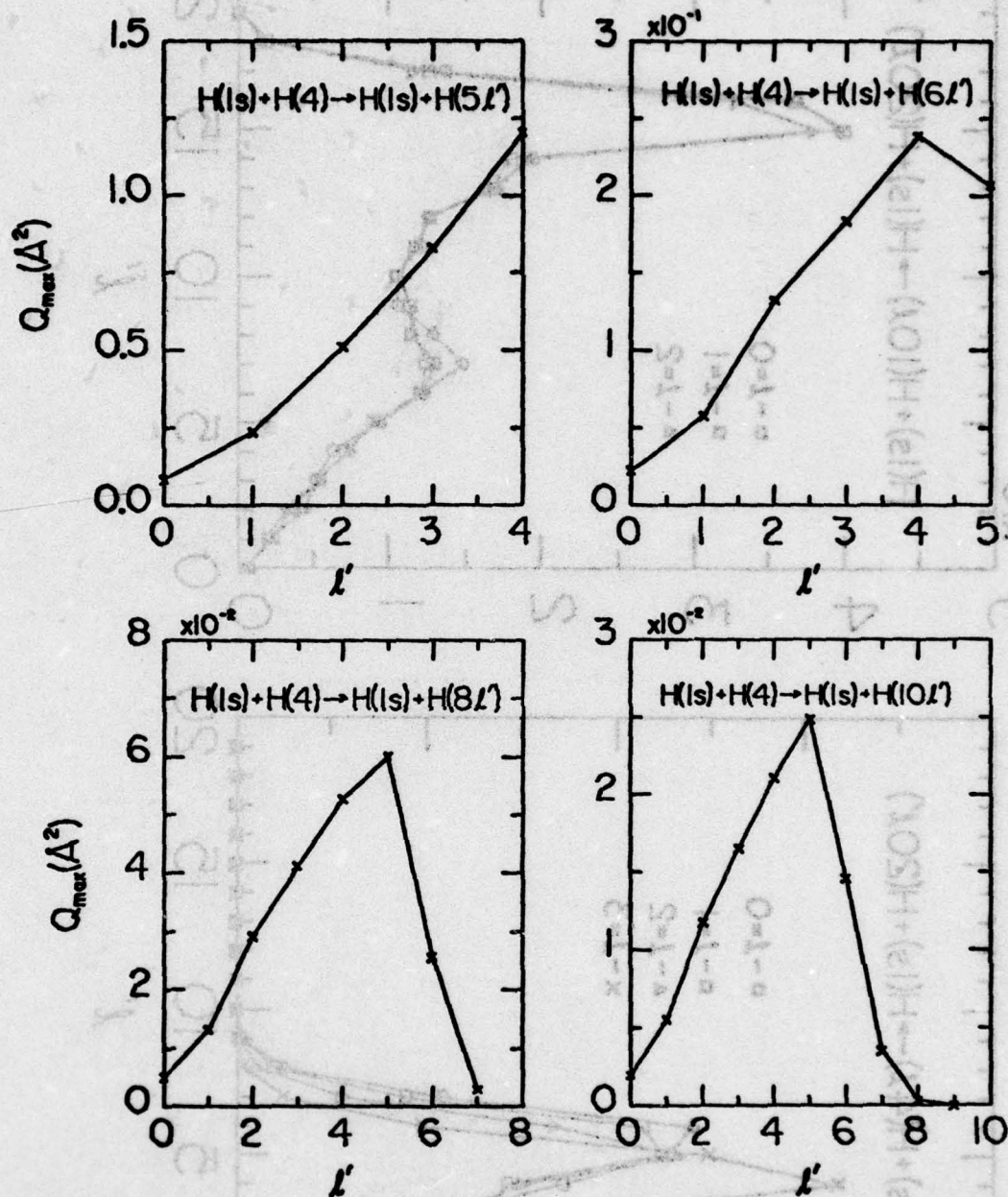


Figure 14

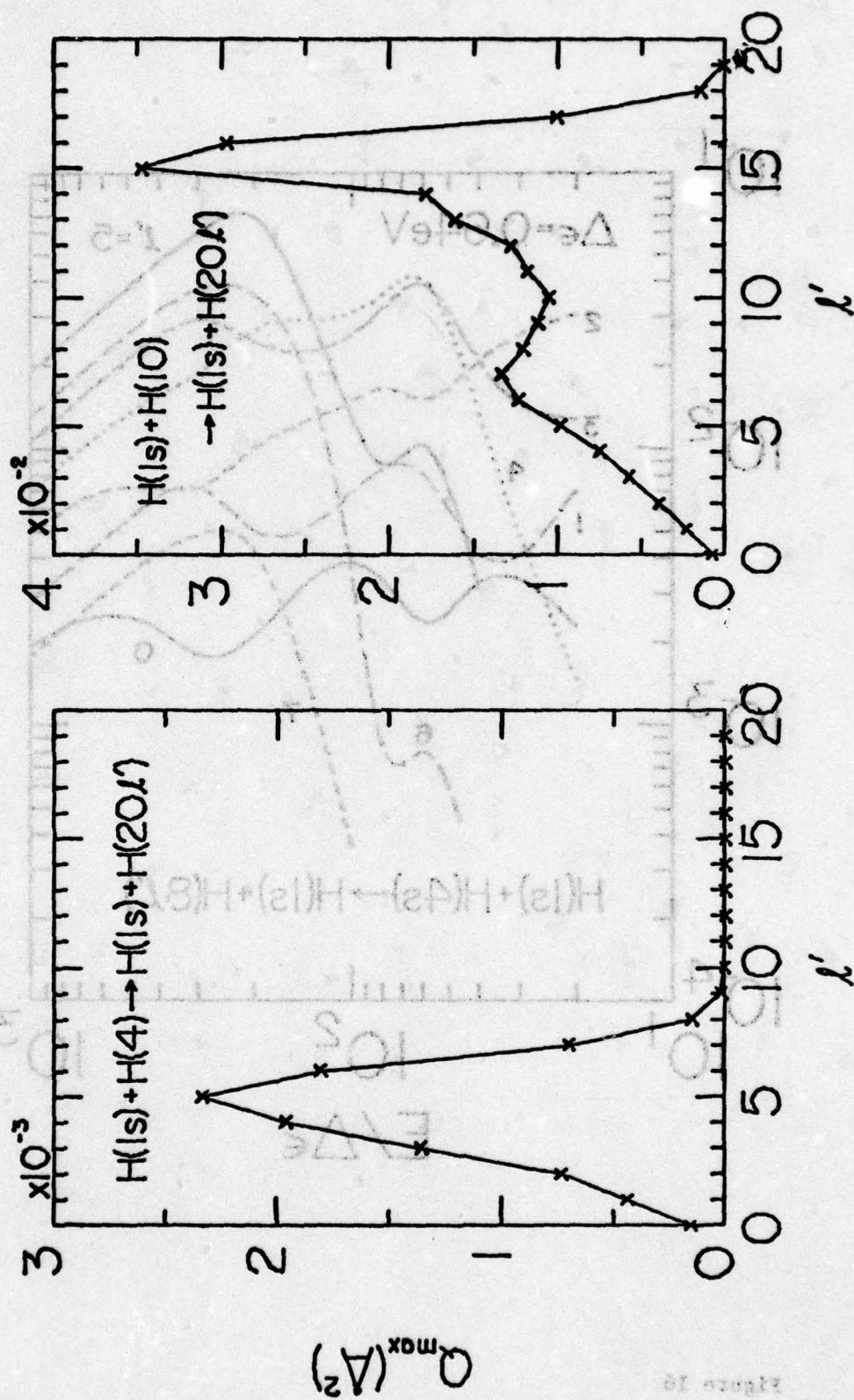


Figure 15

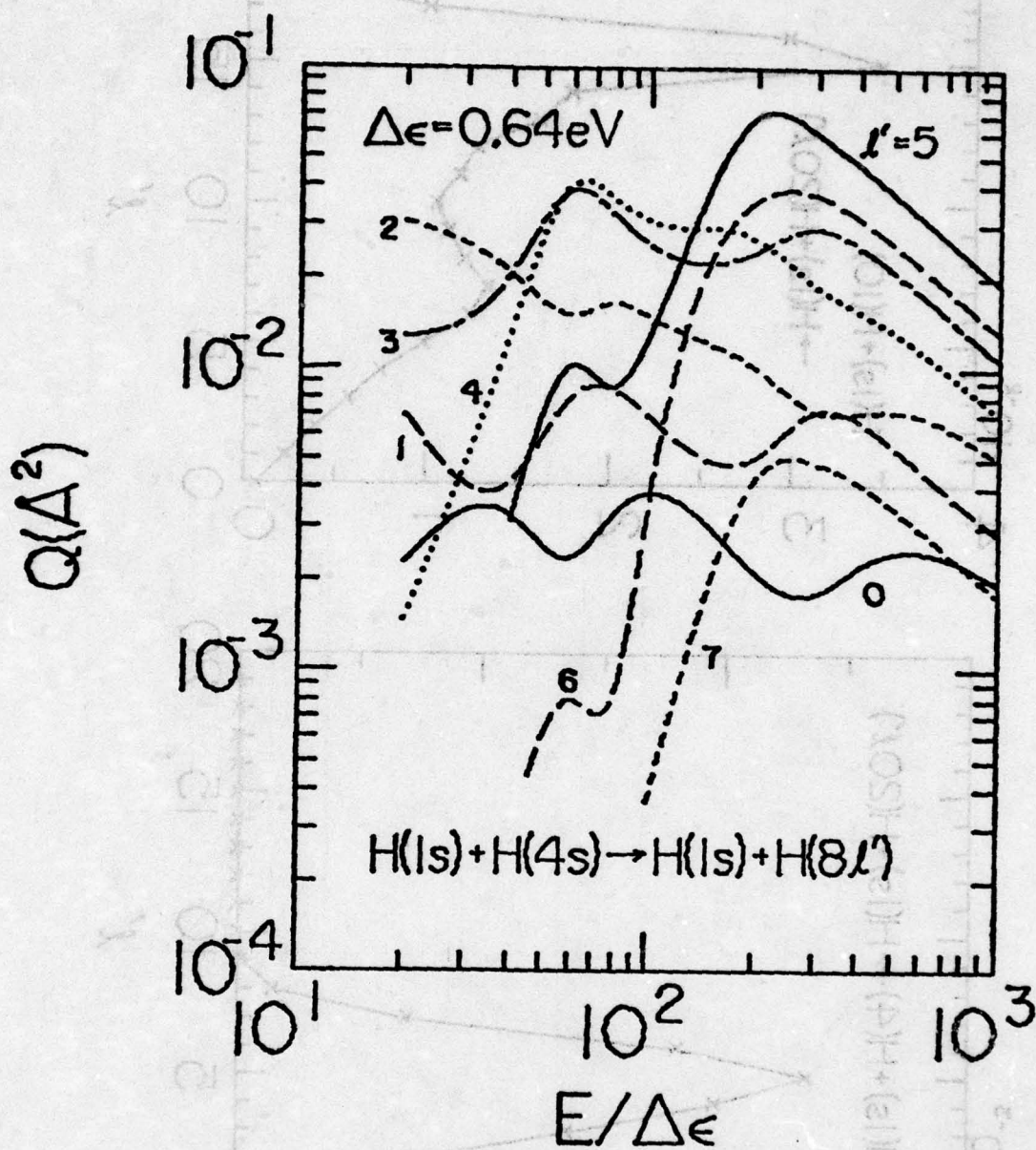


Figure 16

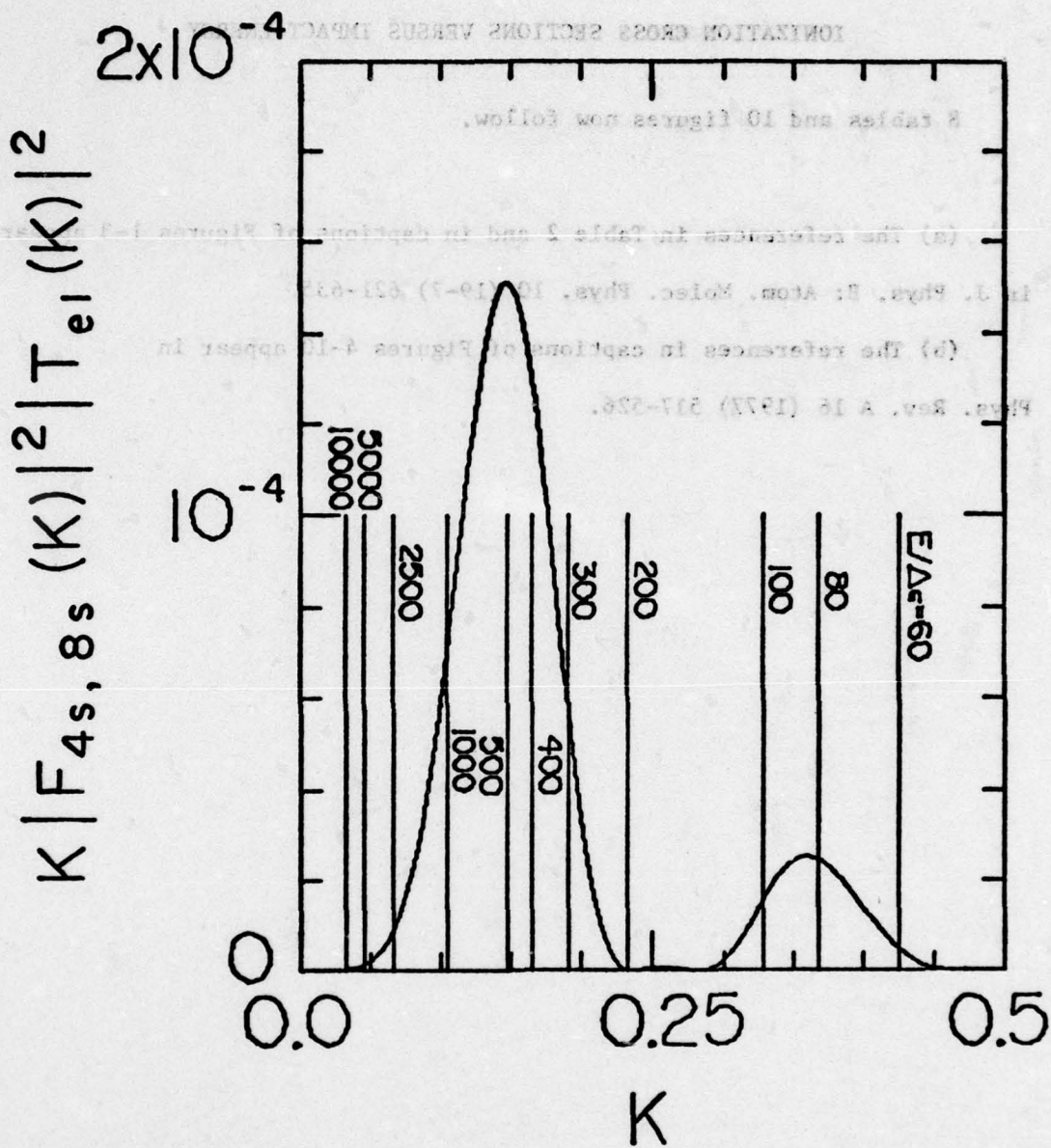


Figure 17

SECTION VIII

FINAL RESULTS: TABLES AND FIGURES OF THE RELEVANT EXCITATION AND IONIZATION CROSS SECTIONS VERSUS IMPACT-ENERGY

8 tables and 10 figures now follow.

(a) The references in Table 2 and in captions of Figures 1-3 appear in J. Phys. B: Atom. Molec. Phys. 10 (19-7) 621-635.

(b) The references in captions of Figures 4-10 appear in Phys. Rev. A 16 (1977) 517-526.

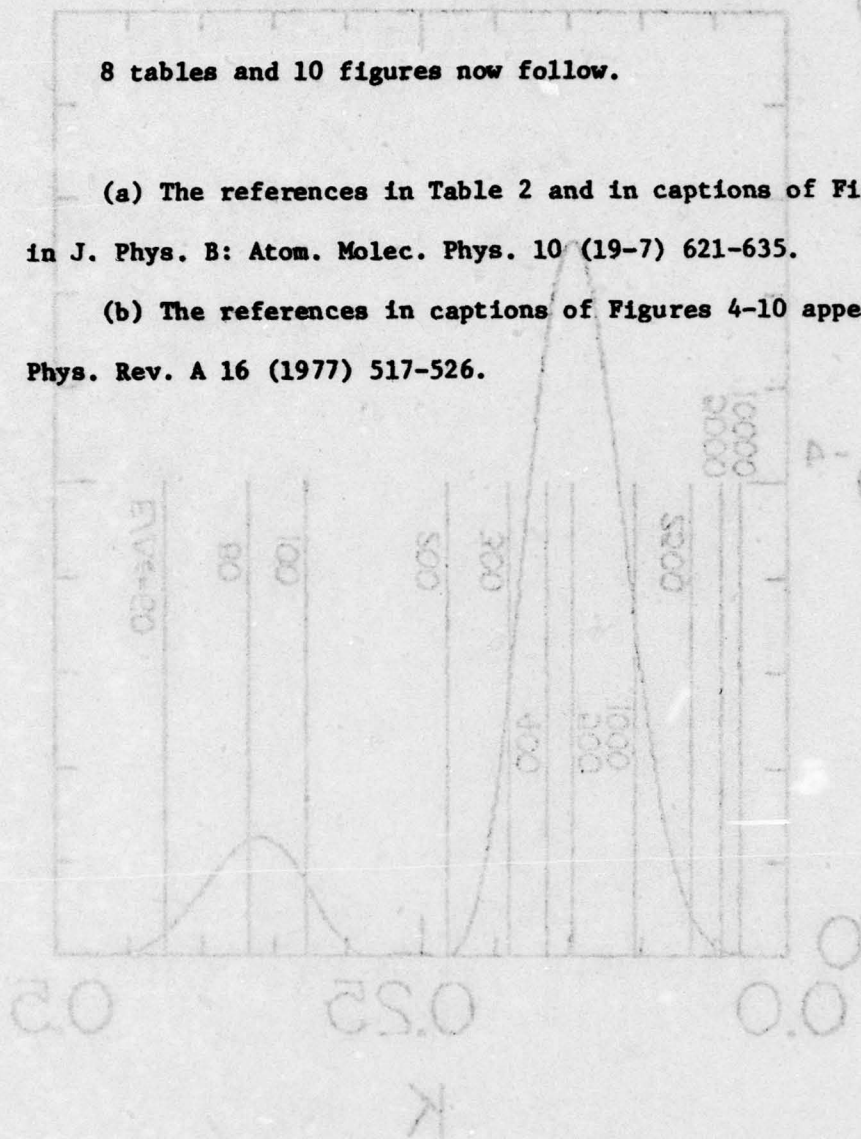


Table 1: Potentials I_0 and I_1 for Ionization of the ns Outer-shell and the (n-1) p^5 Inner-shell of Metastable Rare Gas Atoms

$X^* (1s^2, 2s^2 \dots (n-1) p^5, ns)$		
$X^* (ns)$	$I_0 (eV)$	$I_1 (eV)$
Ne* (3s)	4.95	32.13
Ar* (4s)	4.21	20.88
Kr* (5s)	4.09	18.16
Xe* (6s)	3.44	15.41

Table 2: Transition Energies ΔE (eV) and Born Cross Sections (πa_0^2) for the ($2^3S - n^3L$) Collisional Excitations of Helium by Electrons of Energy E (eV).

n^3L	2^3P	3^3S	3^3P	3^3D	4^3S	4^3P	4^3D	4^3F	5^3S	5^3P	5^3D	5^3F	5^3G
ΔE													
exp (a)	1.145	2.899	3.187	3.254	3.774	3.888	3.916	3.917	4.152	4.208	4.223	4.223	4.223(c)
derived (b)	1.184	2.875	3.177	3.230	3.749	3.868	3.891	3.892	4.126	4.186	4.198	4.198	4.198
n^3L	2^3P	3^3S	3^3P	3^3D	4^3S	4^3P	4^3D	4^3F	5^3S	5^3P	5^3D	5^3F	5^3G
E (eV)													
5	1.97+2 [†]	4.67 [†]	1.42 [†]	8.25 [†]	7.84-1	3.37-1 [†]	1.89	3.19-1	2.59-1	1.26-1	7.10-1	1.67-1	7.66-3
10	1.24+2	3.14	1.04	6.05	6.21-1	2.78-1	1.52	2.51-1	2.34-1	1.18-1	6.22-1	1.47-1	6.19-3
20	7.48+1	1.75	8.51-1	3.46	3.52-1	2.46-1	8.60-1	1.35-1	1.34-1	1.11-1	3.50-1	7.93-2	3.22-3
30	5.46+1	1.20	7.27-1	2.39	2.43-1	2.15-1	5.93-1	9.14-2	9.24-2	9.79-2	2.41-1	5.35-2	2.15-3
40	4.35+1	9.17-1	6.37-1	1.83	1.85-1	1.90-1	4.51-1	6.88-2	7.05-2	8.70-2	1.83-1	4.03-2	1.62-3
50	3.64+1	7.41-1	5.69-1	1.48	1.49-1	1.71-1	3.64-1	5.52-2	5.69-2	7.82-2	1.48-1	3.23-2	1.29-3
70	2.77+1	5.35-1	4.72-1	1.07	1.08-1	1.42-1	2.63-1	3.95-2	4.11-2	6.54-2	1.07-1	2.31-2	9.24-4
100	2.06+1	3.77-1	3.80-1	7.56-1	7.61-2	1.15-1	1.85-1	2.77-2	2.90-2	5.30-2	7.51-2	1.62-2	6.47-4
200	1.15+1	1.90-1	2.40-1	3.82-1	3.84-2	7.35-2	9.35-2	1.38-2	1.46-2	3.36-2	3.78-2	8.11-3	3.24-4
300	8.15	1.27-1	1.80-1	2.56-1	2.57-2	5.51-2	6.25-2	9.22-3	9.78-3	2.52-2	2.53-2	5.40-3	2.16-4
400	6.37	9.56-1	1.45-1	1.92-1	1.93-2	4.46-2	4.69-2	6.92-3	7.34-3	2.04-2	1.90-2	4.05-3	1.62-4
500	5.25	7.65-2	1.23-1	1.54-1	1.54-2	3.77-2	3.76-2	5.53-3	5.88-3	1.73-2	1.52-2	3.24-3	1.29-4
600	4.48	6.38-2	1.07-1	1.28-1	1.29-2	3.28-2	3.13-2	4.61-3	4.90-3	1.50-2	1.27-2	2.70-3	1.08-4
1000	2.87	3.83-2	7.16-2	7.70-2	7.73-3	2.20-2	1.88-2	2.77-3	2.94-3	1.01-2	7.61-3	1.62-3	6.47-5

(a) From Moore (1949)

(b) From method B in text.

(c) Extrapolated from 5^3P .

[†] From Kim and Inokuti (1969), Flannery et al. (1975).

Exponent gives power of ten by which entry is to be multiplied.

Table 3: Cross Sections (10^{-16} cm^2) for the $2^1\text{S}-n^1\text{L}$ Transitions in Helium by Collisions with Electrons of Energy $E(\text{eV})$ Obtained from the Ten-Channel Eikonal Treatment

$n^1\text{L}$	5	10	15	20	21.5	25	50	100
1^1S	1.29(-1)	7.59(-2)	5.08(-2)	4.54(-2)	5.08(-2)	4.36(-2)	2.56(-2)	1.51(-2)
2^1P_0	5.02(1)	3.53(1)	2.09(1)	9.25(0)	6.20(0)	1.17(0)	8.74(-1)	2.27(-1)
$2^1\text{P}_{\pm 1}$	1.08(2)	1.07(2)	9.76(1)	8.46(1)	7.95(1)	7.20(1)	4.95(1)	2.78(1)
2^1P	1.58(2)	1.43(2)	1.18(2)	9.38(1)	8.57(1)	7.32(1)	5.04(1)	2.81(1)
3^1S	5.21(0)	3.51(0)	2.60(0)	2.15(0)	2.13(0)	1.95(0)	1.05(0)	5.53(-1)
3^1P_0	9.50(-1)	7.39(-1)	7.65(-1)	8.10(-1)	8.34(-1)	8.50(-1)	4.02(-1)	1.58(-1)
$3^1\text{P}_{\pm 1}$	3.27(-1)	6.48(-1)	8.52(-1)	9.85(-1)	9.95(-1)	1.05(0)	1.20(0)	8.97(-1)
3^1P	1.28(0)	1.39(0)	1.62(0)	1.79(0)	1.83(0)	1.90(0)	1.60(0)	1.06(0)
3^1D_0	2.40(0)	2.67(0)	2.17(0)	1.35(0)	1.09(0)	6.67(-1)	4.13(-1)	2.06(-1)
$3^1\text{D}_{\pm 1}$	5.77(0)	6.30(0)	5.12(0)	3.17(0)	2.60(0)	1.66(0)	7.88(-1)	2.01(-1)
$3^1\text{D}_{\pm 2}$	1.57(0)	3.42(0)	3.72(0)	3.02(0)	2.90(0)	2.50(0)	1.69(0)	8.97(-1)
3^1D	9.76(0)	1.24(1)	1.10(1)	7.53(0)	6.58(0)	4.82(0)	2.89(0)	1.30(0)

The number in parenthesis indicates the power of 10 by which the entry is to be multiplied.

Table 4: Cross Sections (10^{-16} cm^2) for the $2^3\text{S} + n^3\text{L}$ Transitions in Helium by Collisions with Electrons of Energy E(eV) Obtained from the Multichannel (9) Eikonal Treatment

	E(eV)	5	10	15	20	21.5	25	50	100
3^3L									
2^3P_0		2.70(1)	2.09(1)	1.57(1)	1.16(1)	1.03(1)	8.08(0)	1.99(0)	1.44(0)
$2^3\text{P}_{\pm 1}$		4.07(1)	4.87(1)	4.76(1)	4.08(1)	3.95(1)	3.58(1)	2.47(1)	1.47(1)
2^3P		6.77(1)	6.96(1)	6.32(1)	5.24(1)	4.98(1)	4.38(1)	2.67(1)	1.61(1)
3^3S		1.72(0)	1.51(0)	1.28(0)	1.10(0)	9.97(-1)	8.79(-1)	5.44(-1)	2.82(-1)
3^3P_0		5.65(-1)	3.33(-1)	2.28(-1)	2.13(-1)	2.09(-1)	2.08(-1)	2.29(-1)	2.176(-1)
$3^3\text{P}_{\pm 1}$		8.34(-2)	2.85(-1)	3.37(-1)	3.02(-1)	2.86(-1)	2.61(-1)	2.36(-1)	1.58(-1)
3^3P		6.48(-1)	6.18(-1)	5.65(-1)	5.15(-1)	4.95(-1)	4.69(-1)	4.65(-1)	3.34(-1)
3^3D_0		1.18(0)	1.51(0)	1.27(0)	7.30(-1)	5.92(-1)	3.34(-1)	2.47(-1)	1.91(-1)
$3^3\text{D}_{\pm 1}$		1.66(0)	2.82(0)	2.57(0)	1.62(0)	1.32(0)	8.26(-1)	5.59(-1)	2.21(-1)
$3^3\text{D}_{\pm 2}$		3.40(-1)	1.23(0)	1.46(0)	1.24(0)	1.21(0)	1.08(0)	7.52(-1)	4.76(-1)
3^3D		3.18(0)	5.56(0)	5.30(0)	3.59(0)	3.12(0)	2.24(0)	1.56(0)	8.89(-1)

The number in parenthesis indicates the power of 10 by which the entry is to be multiplied.

Table 5: Born (full-range BF and half-range BH) and Binary Encounter

(BE) Cross Sections (10^{-16} cm^2) for the Ionization of $\text{He}(2^{1,3}\text{S})$ by Electrons with Energy $E(\text{a.u.})$.

$E(\text{a.u.})$	2^3S			2^1S		
	BF	BH	BE	BF	BH	BE
0.25	4.35	3.04	5.59	8.07	5.69	10.51
0.50	7.16	5.70	7.81	9.05	7.36	10.38
0.75	6.15	5.33	6.49	7.39	6.47	8.45
1.00	5.25	4.65	5.48	6.22	5.59	7.02
1.5	4.03	3.67	4.16	4.75	4.35	5.16
2.0	3.18	3.00	3.35	3.72	3.54	4.05
2.5	2.66	2.55	-	3.11	2.99	-
3	2.29	2.26	2.39	2.68	2.65	2.81
4	1.80	1.76	1.87	2.10	2.06	2.15
5	-	1.46	1.53	-	1.71	1.74
6	-	1.25	1.29	-	1.46	1.46
7	-	1.11	-	-	1.29	-
8	-	0.98	0.99	-	1.14	1.11

Table 6: Born (full-range BF and half-range BH) and Binary encounter (BE) cross sections (10^{-16} cm^2) for the ionization of the outer-shell of metastable $\text{Ne}^* (2p^5 3s)$ and $\text{Ar}^* (3p^5 4s)$ by electrons with energy $E(\text{a.u.})$. The cross sections BEI include additional inner-shell contributions as determined from the binary-encounter approximation.

$E(\text{a.u.})$	Ne^*				Ar^*			
	BF	BH	BE	BEI	BF	BH	BE	BEI
0.25	4.56	3.14	4.73	4.73	7.98	5.53	8.73	8.73
0.30	6.46	4.65	6.61	6.61	9.79	7.18	9.87	9.87
0.35	7.34	5.45	7.39	7.39	10.67	8.05	10.11	10.11
0.40	7.68	5.84	7.59	7.59	10.79	8.37	9.99	9.99
0.50	7.46	5.98	7.35	7.35	10.34	8.33	9.46	9.46
0.75	8.82	5.22	6.18	6.18	8.21	7.17	7.94	7.94
1.25	4.13	3.77	4.55	4.57	5.44	5.07	5.71	7.05
2.	2.75	2.57	3.25	3.74	3.59	3.38	3.90	6.40
3.	1.90	1.83	2.34	3.26	2.44	2.40	2.73	5.35
4.	1.46	1.41	1.81	2.92	1.88	1.84	2.13	4.47
6.	-	.971	1.24	2.47	-	1.25	1.52	3.31
8.	-	.741	.949	2.06	-	.951	1.20	2.64

Table 7: Born (full-range BE and half-range BH) and Binary encounter (BE) cross sections (10^{-16} cm^2) the ionization of the outer-shell of metastable $\text{Kr}^* (4p^5 5s)$ and $\text{Xe}^* (5p^5 6s)$ by electrons with energy $E(\text{a.u.})$. The cross sections BEI include additional inner-shell contributions as determined from the binary-encounter approximation.

$E(\text{a.u.})$	Kr^*				Xe^*			
	BF	BH	BE	BEI	BF	BH	BE	BEI
0.25	9.54	6.69	9.48	9.48	13.19	9.56	11.09	11.09
0.30	10.99	8.26	10.46	10.48	14.70	11.38	11.85	11.85
0.35	11.67	9.12	10.66	10.66	14.86	12.03	11.95	11.95
0.40	11.74	9.19	10.50	10.50	14.61	12.02	11.77	11.77
0.50	11.11	9.11	9.96	9.96	13.56	11.32	11.09	11.09
0.75	8.82	7.81	8.34	8.60	10.44	9.37	9.08	10.40
1.25	5.85	5.45	5.91	8.35	6.83	6.32	6.25	10.41
2.	3.91	3.63	4.01	7.44	4.47	4.23	4.25	8.74
3.	2.63	2.58	2.84	5.97	3.02	2.97	3.07	6.81
4.	2.01	1.97	2.24	4.89	2.32	2.26	2.43	5.63
6.	-	1.31	1.60	3.64	-	1.52	1.71	4.29
8.	-	1.02	1.25	2.96	-	1.17	1.31	3.48

Table 8: Electron-impact ionization cross sections (10^{-16} cm^2)

(Binary encounter method) for the ionization processes

1(a) - 1(c).

E(a.u.)	(a)	(b)	(c)
0.35	---	0.098	0.187
0.4	0.0016	0.32	0.49
0.5	0.21	0.82	1.13
0.75	0.89	1.92	2.41
1.	1.43	2.69	3.17
1.5	2.06	3.51	3.74
2.5	2.31	3.68	3.53
4.	2.	3.09	2.79
6.	1.54	2.36	2.09

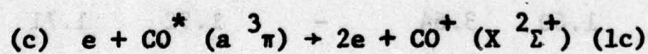
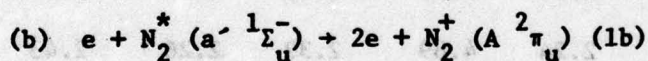
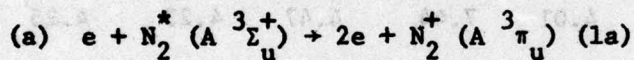


Figure Captions

Fig. 1. Comparison of present binary-encounter treatments of the cross sections for outer-shell ionization of $\text{He}(2^{1,3}\text{S})$ with different orbital-velocity distributions as determined: from methods A and B in text, and from Hartree-Fock functions C of Cohen and McEachran (1967a,b). V are results of Vriens (1964) using the exponential distribution of Gryzinski (1965). The associated numerals 1 and 3 refer to 2^1S and 2^3S targets respectively. The circles (open and full) are measurements of Dixon et al. (1976a) for the sum of all electron-impact processes leading to single (but not double) ionization of a predominantly $\text{He}(2^3\text{S})$ target.

Fig. 2. Comparison of present Born cross sections (F and H) for outer-shell ionization of $\text{He}(2^{1,3}\text{S})$ by electron-impact, with F and H denoting respective integrations over the full and the lower-half ranges of energy of the ejected electron. The associated numerals 1 and 3 refer to 2^1S and 2^3S targets respectively. The circles are measurements, as in figure 1.

Fig. 3. Cross sections for electron-impact ionization of $\text{He}(2^{1,3}\text{S})$. F and C are the full-range Born and binary encounter treatments respectively. Numerals 1 and 3 refer to 2^1S and 2^3S targets respectively. CI3 denotes the present binary encounter treatment of inner shell ionization of $\text{He}(2^3\text{S})$ and the C3 full curve includes this contribution. The circles are measurements, as in figure 1.

Figs. 4-7. Cross sections (10^{-16} cm^2) for collisional ionization of metastable (a) Ne^* , (b) A^* , (c) Kr^* and (d) Xe^* by electrons

with impact energy $E(\text{eV})$. BF and BH are the present Born results for outer-shell ionization obtained from integrations over the full and lower-half ranges of energy of the ejected electron i.e., $\alpha = 1$ and $1/2$ respectively in (7) of text. The binary encounter (quantal distribution) cross sections are denoted by BEO for outer-shell ionization, by BE1 for ionization of one of the electrons in the np^5 shell, by BE5 for the total ionization of the np^5 shell and by BE for the sum of BEO and BE5. Previous binary encounter (exponential distribution) results of Vriens are represented by V. o: measurements (Dixon, Harrison and Smith¹⁷).

Fig. 8. Bethe plots (cross section times collision energy E versus $\log_{10} E$) for electron-impact ionization of metastable (a) Ne^* , (b) A^* , (c) Kr^* and (d) Xe^* . Labeling of curves as in figure 1.

Fig. 9. Binary-encounter cross sections (10^{-16} cm^2), (a), (b) and (c), for the ionization of metastable N_2^* ($A^3\Sigma_u^+$), N_2^* ($a'^1\Sigma_u^-$) and CO^* ($a^3\Pi$) respectively by electrons with energy $E(\text{eV})$. The final state of the residual ion is indicated.

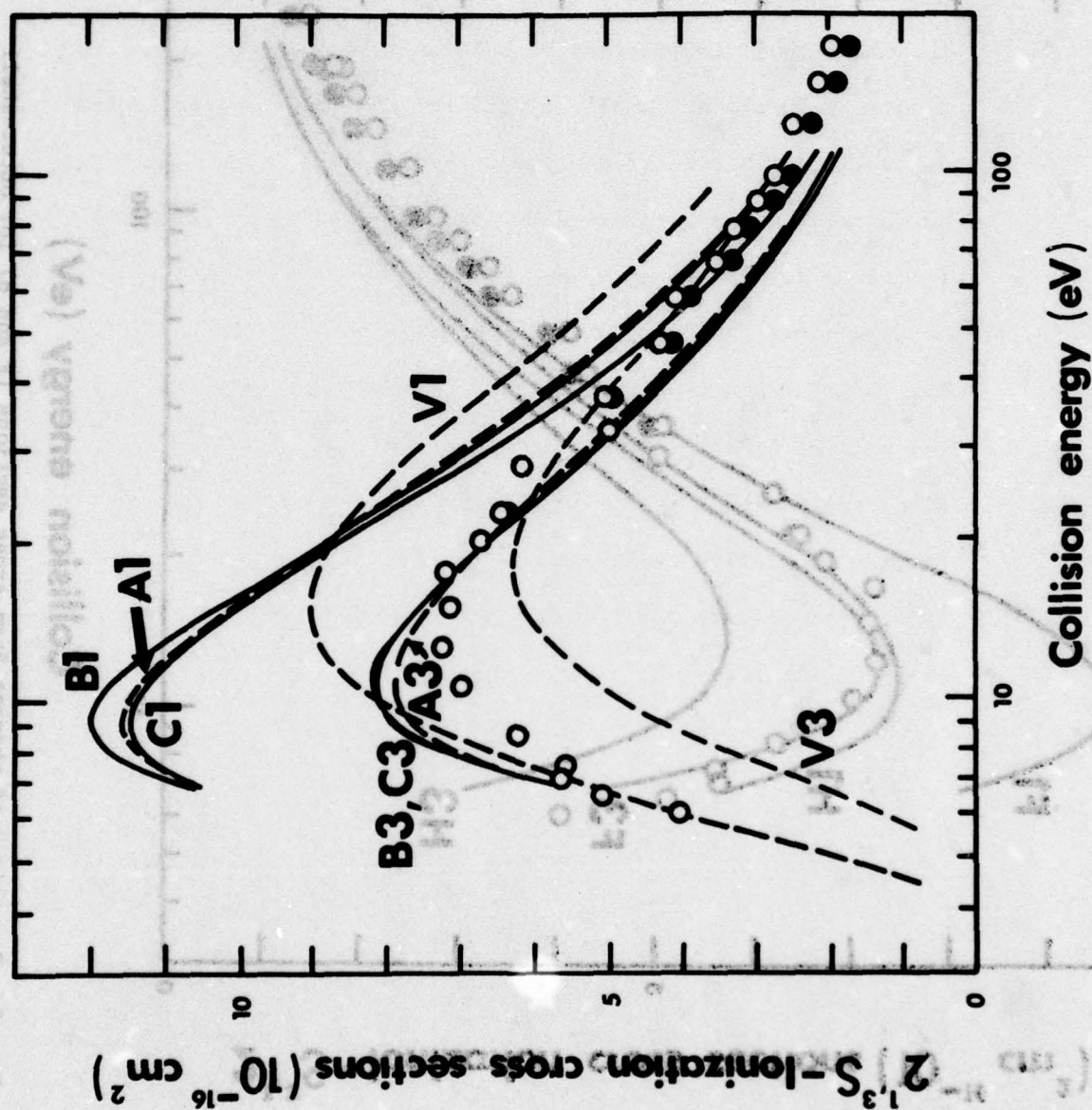


Fig. 1. Comparison of present binary-encounter treatments of the cross sections for outer-shell ionization of $\text{He}(2^1_3S)$ with different orbital-velocity distributions.

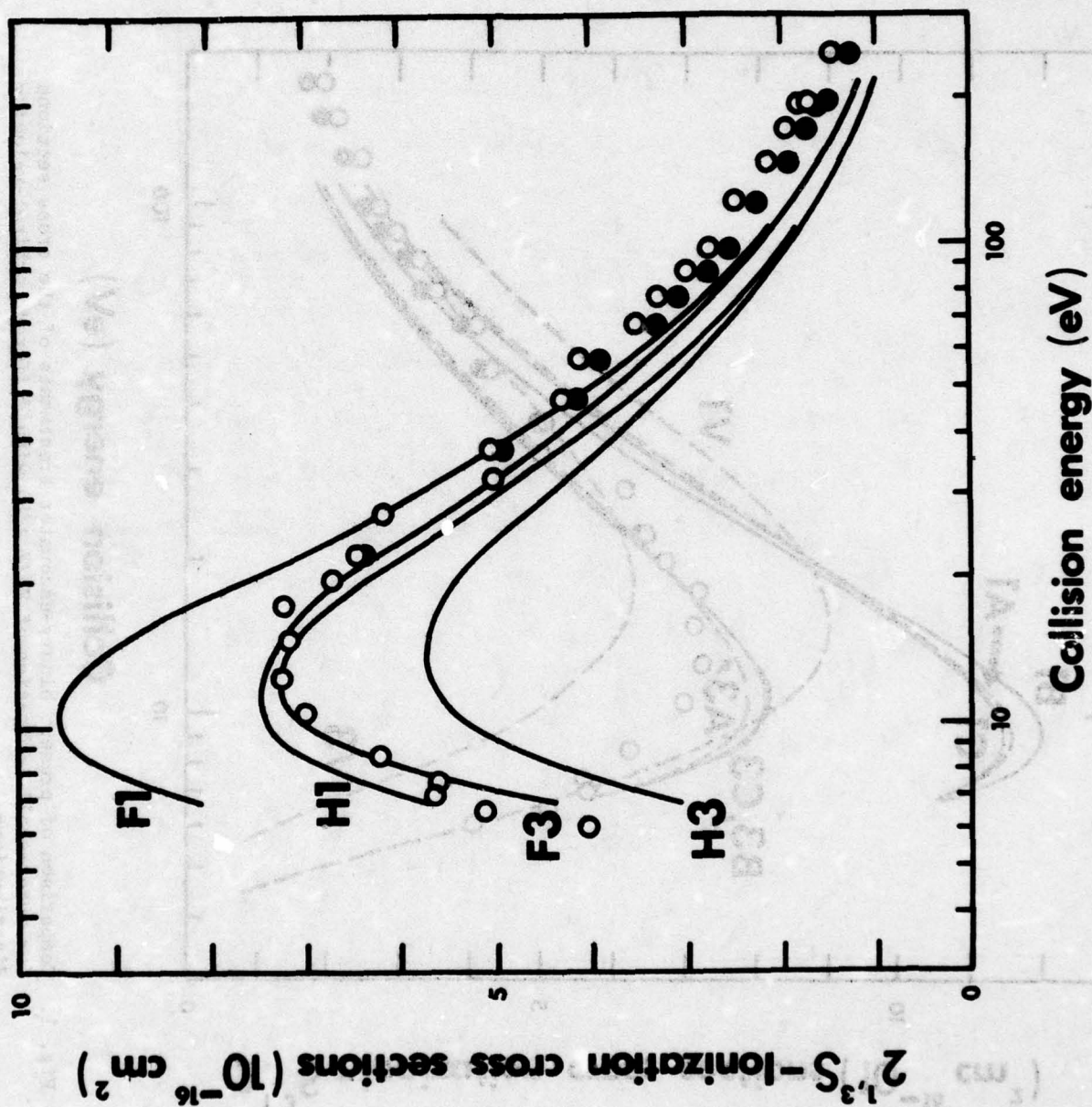


Fig. 2. Comparison of present Born cross sections (F and H) for outer-shell ionization of $\text{He}(2^1,3S)$ by electron-impact.

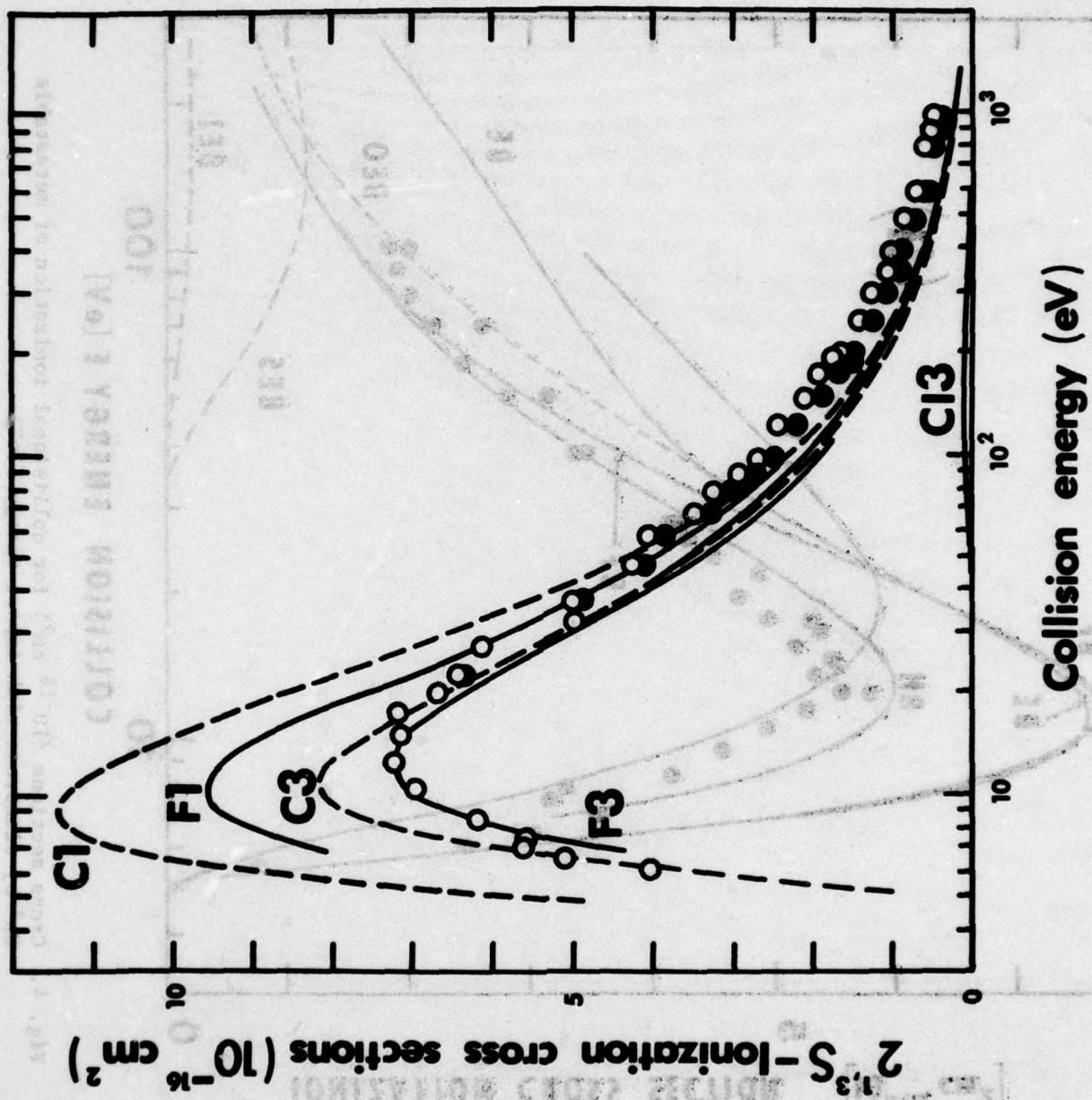


Fig. 3. Cross sections for electron-impact ionization of He($2^{1,3}S$).

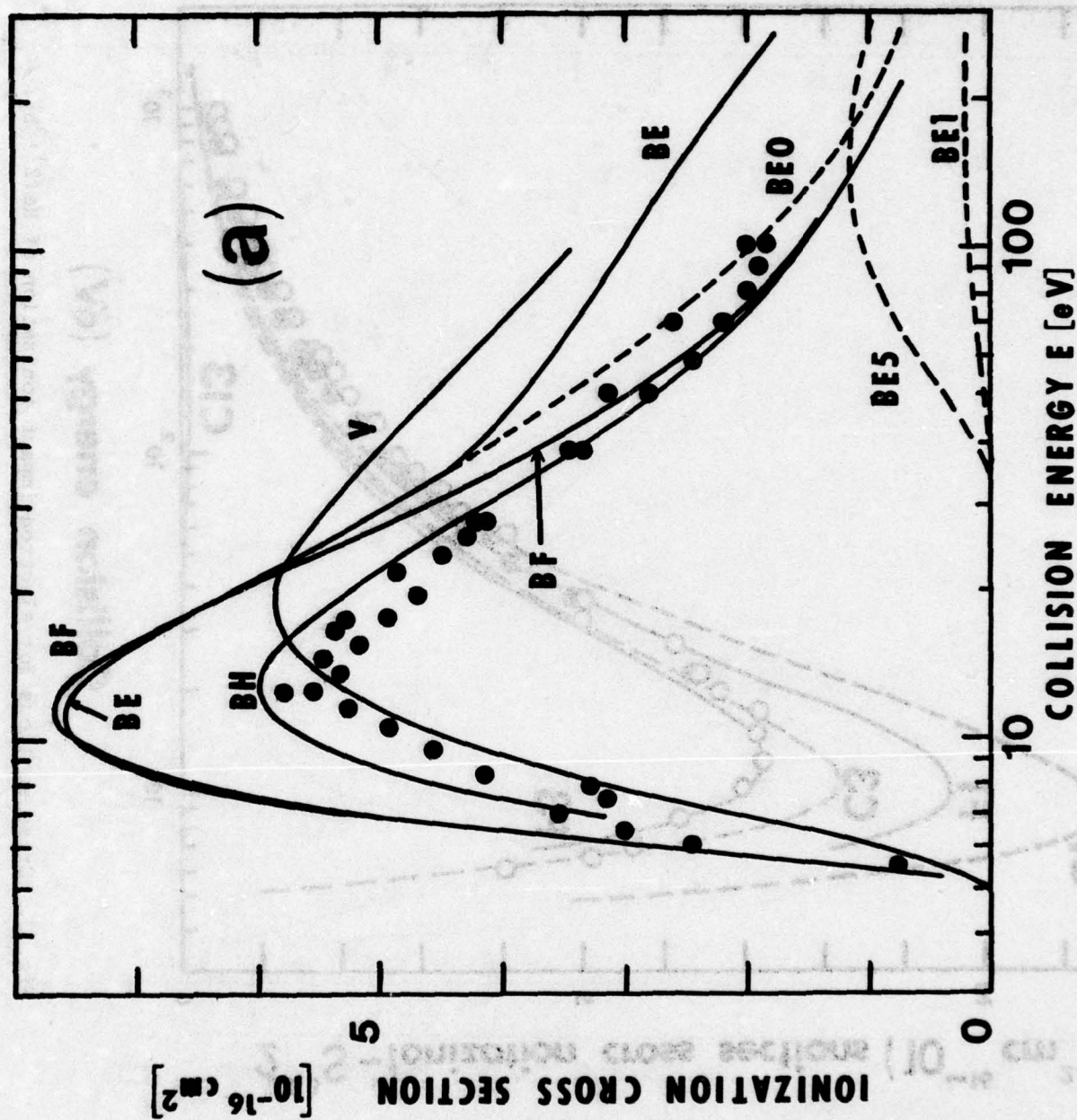


Fig. 4. Cross sections (10^{-16} cm^2) for collisional ionization of metastable Ne^* by electrons with impact energy E (eV).

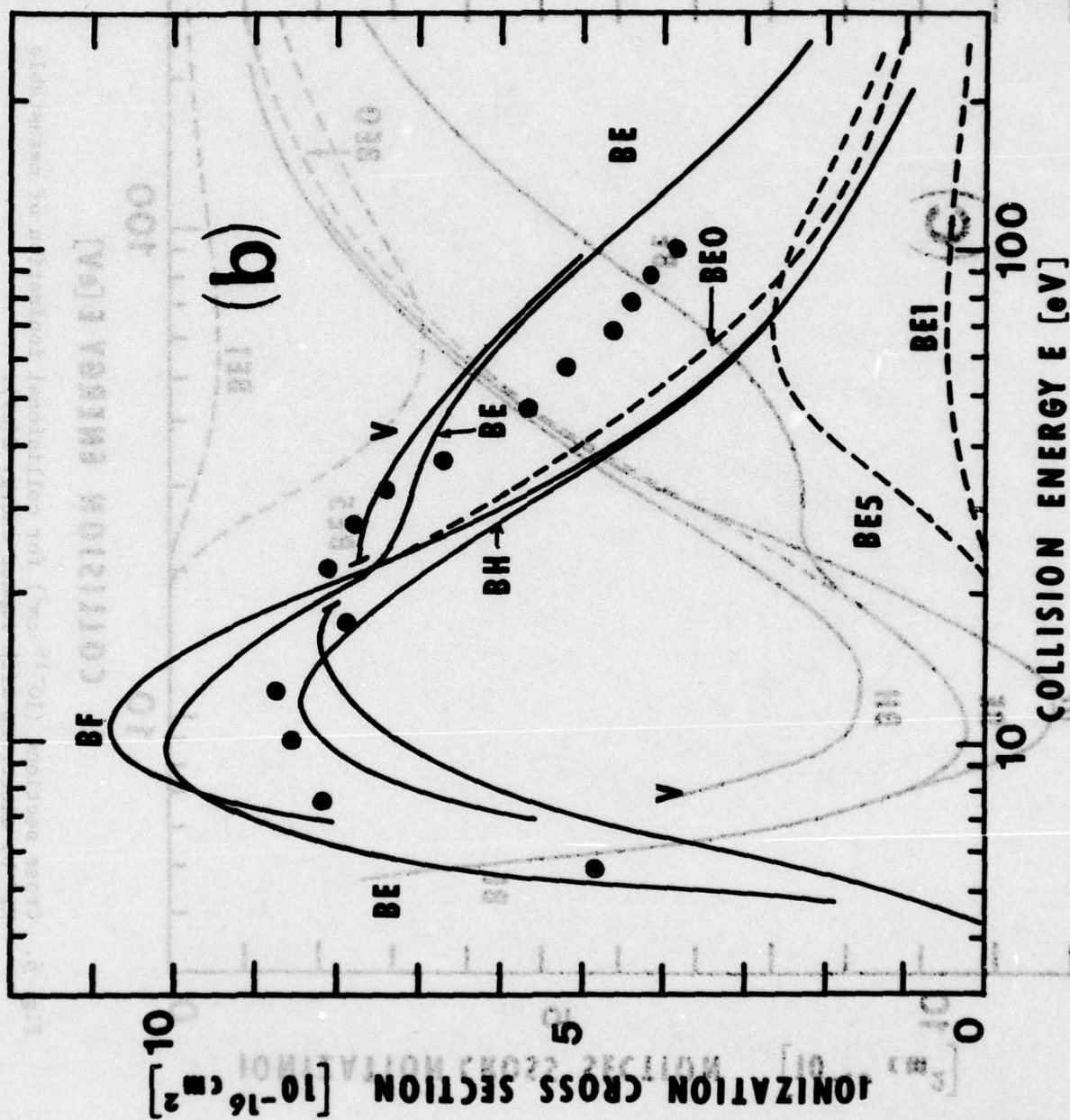


Fig. 5. Cross sections (10^{-16} cm^2) for collisional ionization of metastable A^* by electrons with impact energy E (eV).

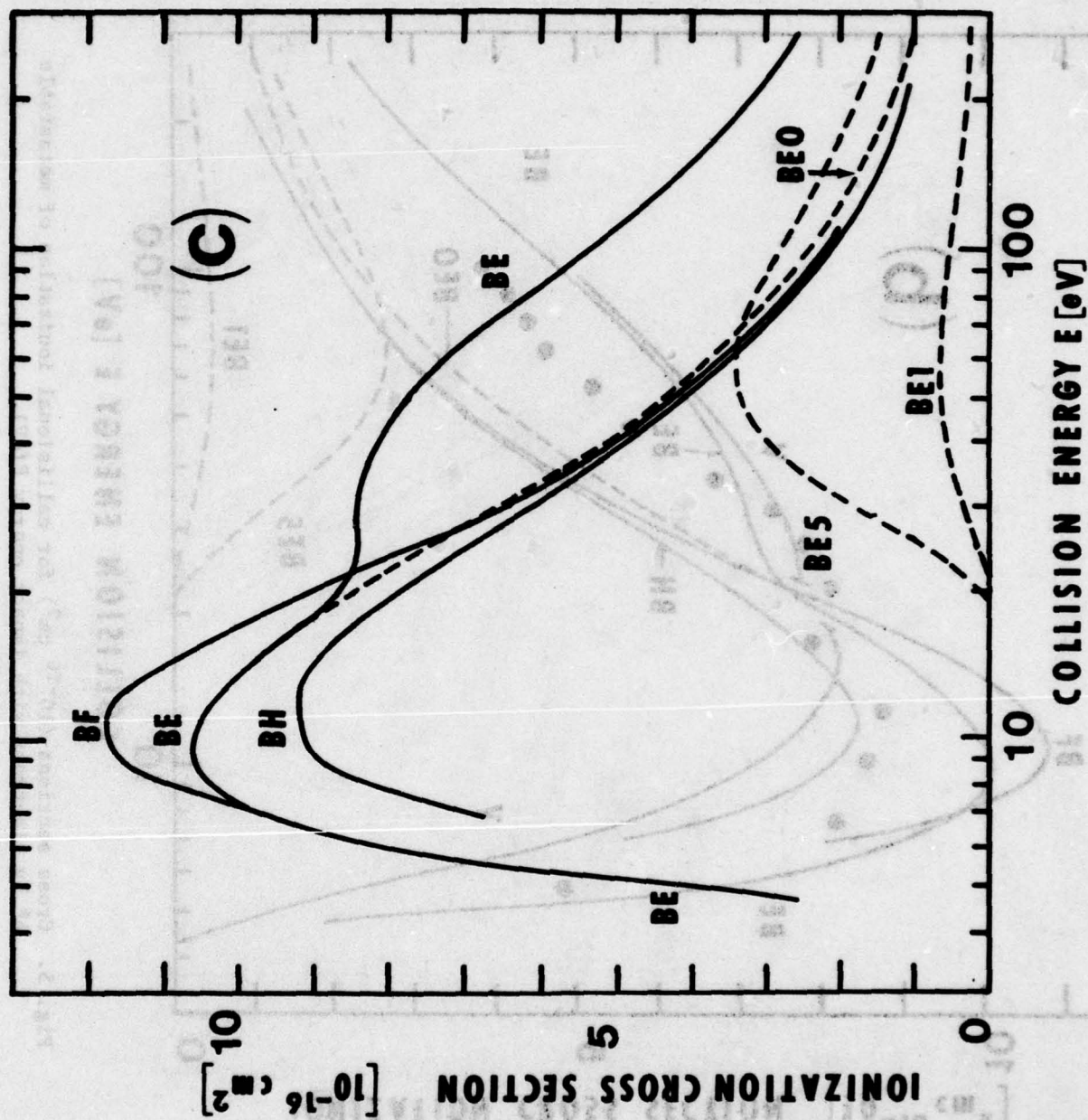


Fig. 6. Cross sections (10^{-16} cm^2) for collisional ionization of metastable Kr^* by electrons with impact energy E (eV).

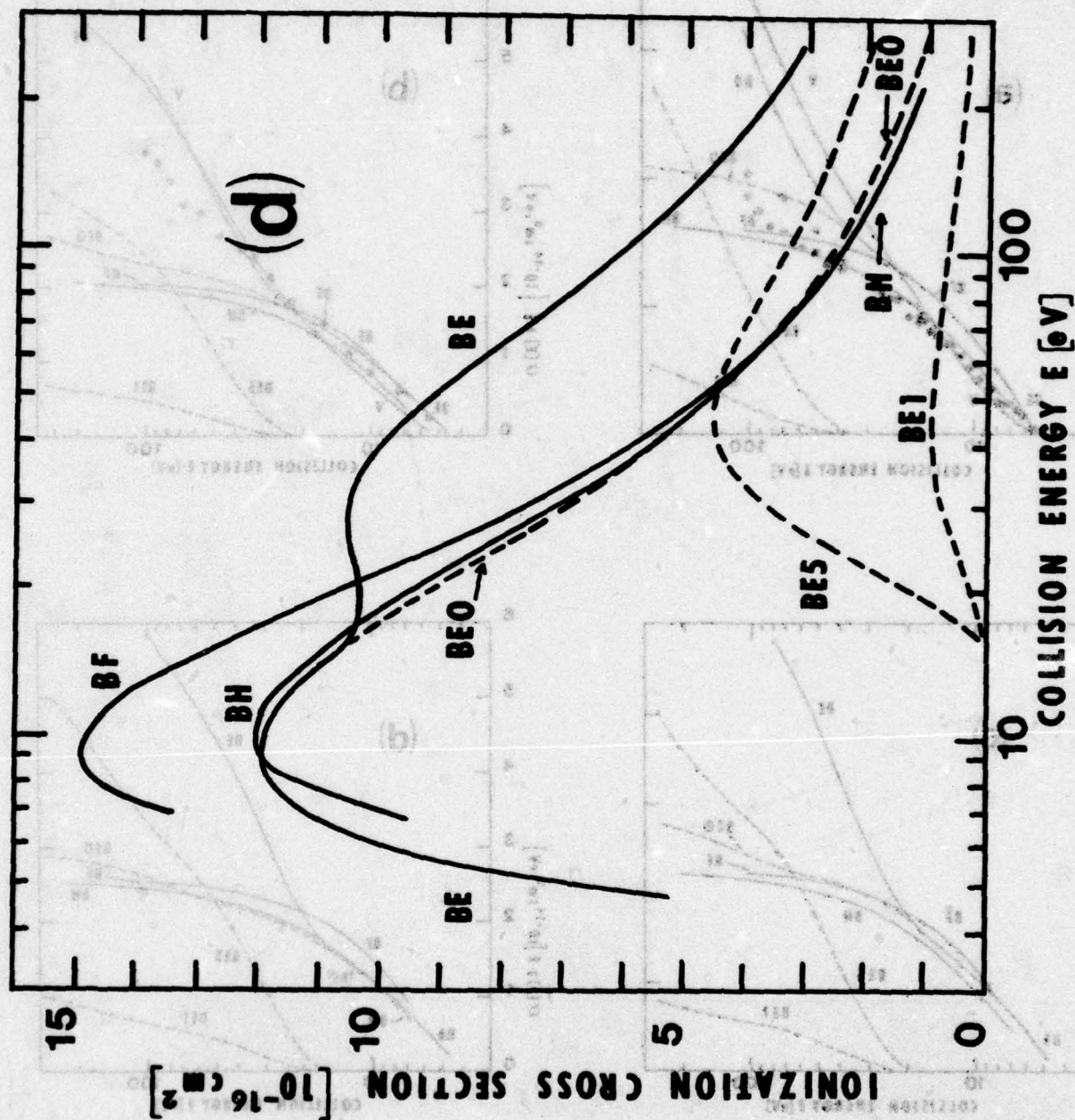


Fig. 7. Cross sections (10^{-16} cm^2) for collisional ionization of metastable Xe^* by electrons with impact energy E (eV).

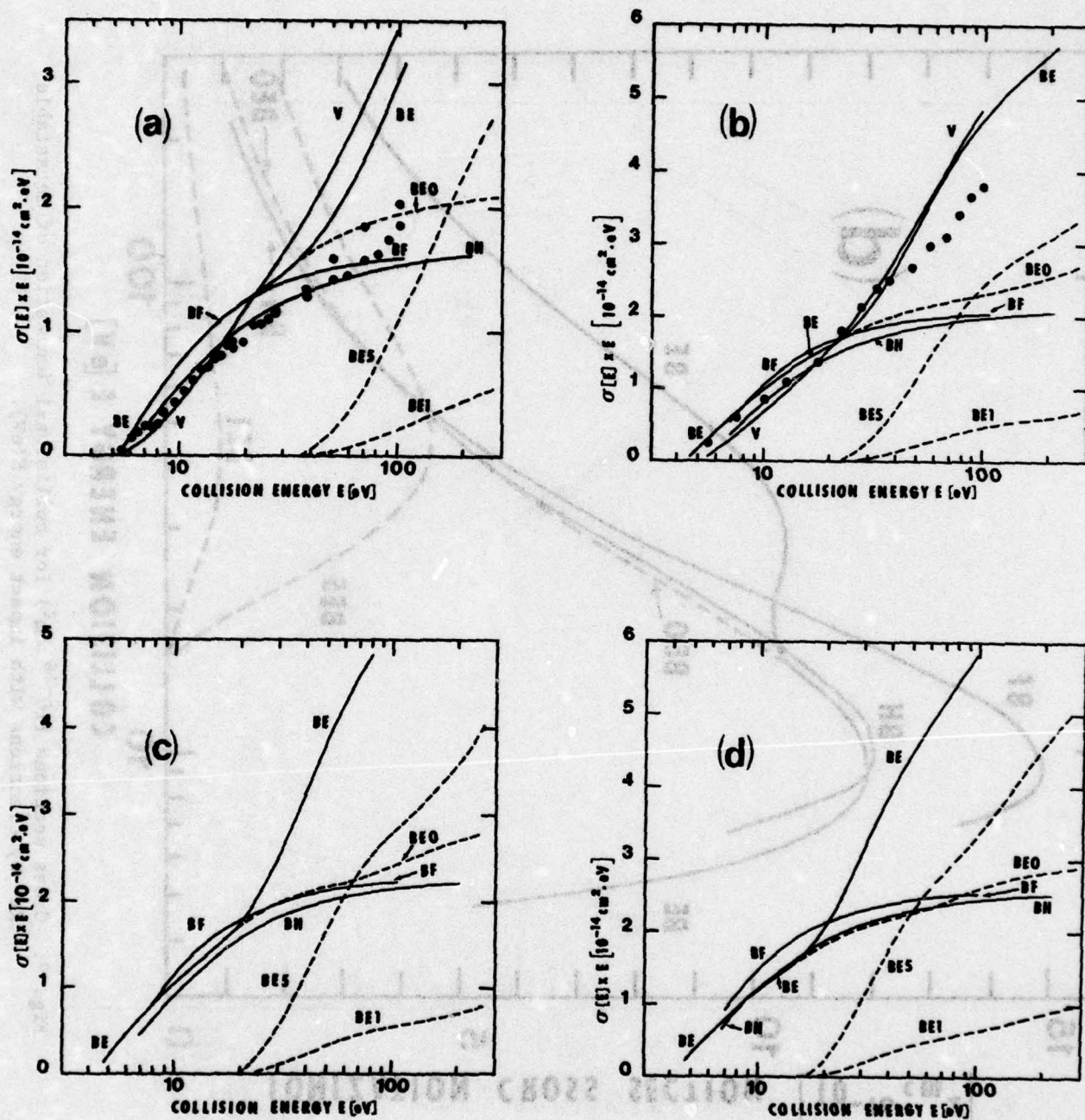


Fig. 8. Bethe plots (cross section times collision energy E versus $\text{Log}_{10} E$) for electron-impact ionization of metastable (a) Ne^* , (b) A^* , (c) Kr^* and (d) Xe^* . Labeling of curves as in figure 1.

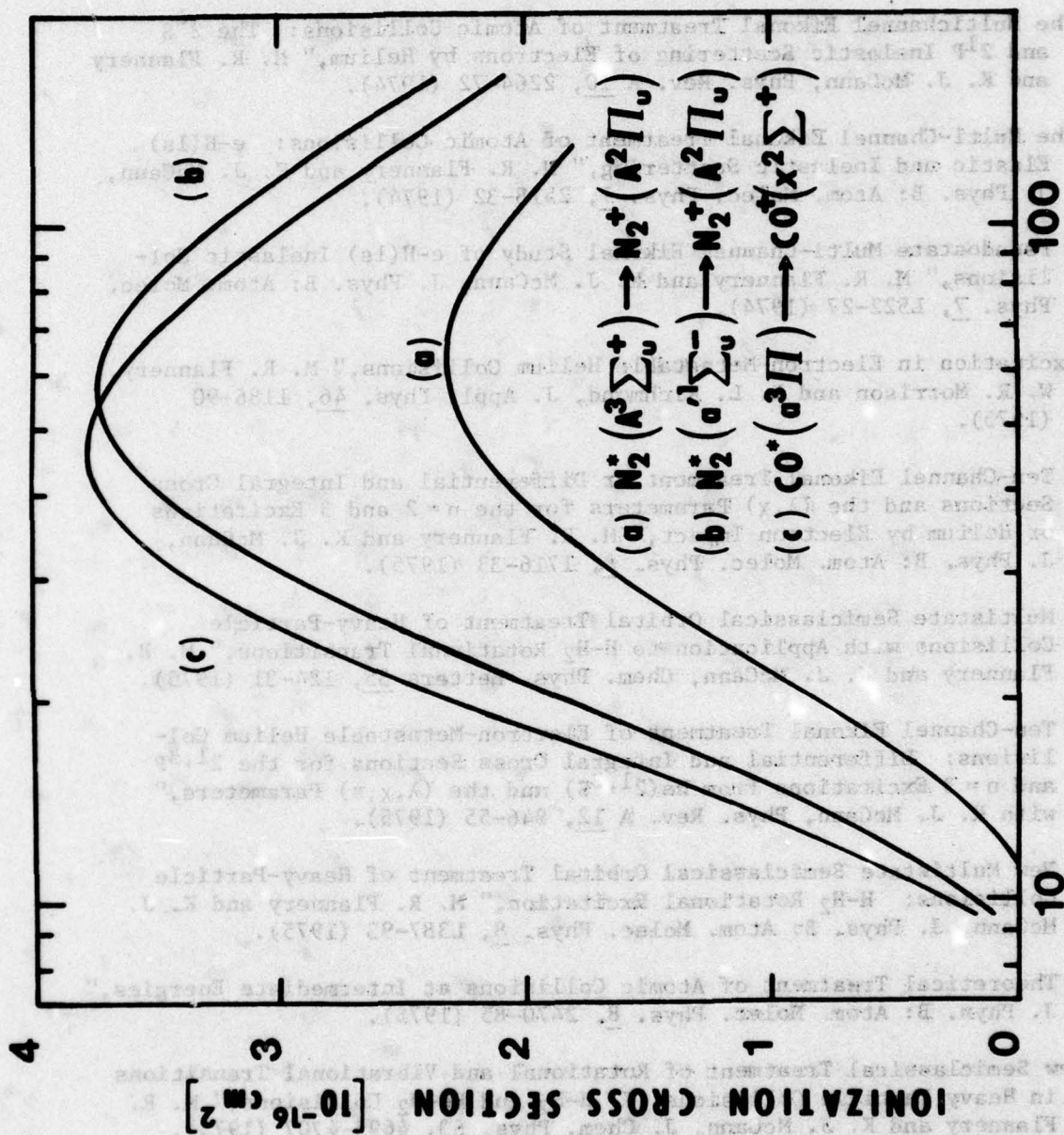


Fig. 9. Binary-encounter cross sections (10^{-16} cm^2), (a), (b) and (c), for the ionization of metastable $\text{N}_2^*(\text{A}^3\Sigma_u^+)$, $\text{N}_2^*(\text{a}'^1\Sigma_u^-)$ and $\text{CO}^+(\text{a}^3\Pi)$ respectively by electrons with energy E (eV). The final state of the residual ion is indicated.

SECTION IX

LIST OF PUBLICATIONS OF RESEARCH SPONSORED BY THE PRESENT AIR FORCE CONTRACTS F33615-74-C-4003 and F33615-76-C-2003

1. "The Multistate Eikonal Treatment of Electron-Atom Collisions," M. R. Flannery and K. J. McCann, J. Phys. B: Atom. Molec. Phys. 7, L223-27 (1974).
2. "The Multichannel Eikonal Treatment of Atomic Collisions: The 2^1S and 2^1P Inelastic Scattering of Electrons by Helium," M. R. Flannery and K. J. McCann, Phys. Rev. A 10, 2264-72 (1974).
3. "The Multi-Channel Eikonal Treatment of Atomic Collisions: e-H(1s) Elastic and Inelastic Scattering," M. R. Flannery and K. J. McCann, J. Phys. B: Atom. Molec. Phys. 7, 2518-32 (1974).
4. "A Pseudostate Multi-Channel Eikonal Study of e-H(1s) Inelastic Collisions," M. R. Flannery and K. J. McCann, J. Phys. B: Atom. Molec. Phys. 7, L522-27 (1974).
5. "Excitation in Electron-Metastable Helium Collisions," M. R. Flannery, W. R. Morrison and B. L. Richmond, J. Appl. Phys. 46, 1186-90 (1975).
6. "A Ten-Channel Eikonal Treatment of Differential and Integral Cross Sections and the (λ, χ) Parameters for the $n=2$ and 3 Excitations of Helium by Electron Impact," M. R. Flannery and K. J. McCann, J. Phys. B: Atom. Molec. Phys. 8, 1716-33 (1975).
7. "A Multistate Semiclassical Orbital Treatment of Heavy-Particle Collisions with Application to H-H₂ Rotational Transitions," M. R. Flannery and K. J. McCann, Chem. Phys. Letters 35, 124-31 (1975).
8. "A Ten-Channel Eikonal Treatment of Electron-Metastable Helium Collisions: Differential and Integral Cross Sections for the $2^1, 3P$ and $n=3$ Excitations from He($2^1, 3S$) and the (λ, χ, π) Parameters," with K. J. McCann, Phys. Rev. A 12, 846-55 (1975).
9. "A New Multistate Semiclassical Orbital Treatment of Heavy-Particle Collisions: H-H₂ Rotational Excitation," M. R. Flannery and K. J. McCann, J. Phys. B: Atom. Molec. Phys. 8, L387-93 (1975).
10. "A Theoretical Treatment of Atomic Collisions at Intermediate Energies," J. Phys. B: Atom. Molec. Phys. 8, 2470-85 (1975).
11. "New Semiclassical Treatment of Rotational and Vibrational Transitions in Heavy Particle Collisions. I. H-H₂ and He-H₂ Collisions," M. R. Flannery and K. J. McCann, J. Chem. Phys. 63, 4695-4707 (1975).

- SECTION 2
12. "The Multichannel Eikonal Treatment of Electron-Atom Collisions," M. R. Flannery and K. J. McCann, in Electron and Photon Interactions with Atoms, H. Kleinpoppen and M. R. C. McDowell, Eds., pp. 275-83 (1976).
 13. "Cross Sections for Excitation and Ionization in e-He($2^{1,3}S$) Collisions," M. R. Flannery, D. Ton-That and S. T. Manson, J. Phys. B: Atom. Molec. Phys. 10, 621-35 (1977).
 14. "Cross Sections for Ionization of Metastable Rare-Gas Atoms (Ne^*, A^*, Kr^*, Xe^*) and of Metastable N_2^* and CO^* by Electron Impact," M. R. Flannery and D. Ton-That, Phys. Rev. A 16, 517-26 (1977).

In addition, many invited papers on the above subject material were presented at national and international conferences.

SECTION X

PERSONNEL INVOLVED IN THE CONTRACT

- (1) Dr. M. R. Flannery is Principal Investigator.**
- (2) Dr. K. J. McCann and Dr. W. F. Morrison were originally graduate students and obtained their Ph.D.'s under this contract. Dr. McCann is at present research scientist in the contract.**
- (3) Dr. D. Ton-That fulfilled a three-year appointment 1973-1976 as a postdoctoral fellow under the contract.**
- (4) Mr. B. L. Richmond, graduate student.**

A. I. I. 1.11

SECTION XI

RELATED ADDITIONAL WORK PERFORMED UNDER THE CONTRACT

- 11.1 Appendix A: A theoretical treatment of atomic collisions at intermediate energies and highly excited states.
- 11.2 Appendix B: New semiclassical treatments of rotational and vibrational transitions in heavy-particle collisions.
I. H-H_2 and He-H_2 collisions.
- 11.3 Appendix C: The multichannel eikonal treatment of electron-atom collisions.

11.1 Appendix A

SECTION XI

RELATED ADDITIONAL WORK PERFORMED UNDER THE CONTRACT

- 11.1 Appendix A: A theoretical treatment of atomic collisions at intermediate energies and highly excited states.
- 11.2 Appendix B: New semiclassical treatments of rotational and vibrational transitions in heavy-particle collisions.
- 11.3 Appendix C: The multichannel formalism treatment of electron-atom collisions.

11.1 Appendix A

A theoretical treatment of atomic collisions at intermediate energies and highly excited states

M R Flannery

School of Physics, Georgia Institute of Technology, Atlanta, Georgia 30332, USA

Received 25 March 1975

Abstract. A theoretical description of transitions in electron-atom and heavy-particle collisions (with and without rearrangement) at intermediate energies is developed. The associated T matrices involve the solution of an integral equation describing elastic scattering by fixed centres. The solution, once determined, can be used to examine the full array of transitions for any given system. An effectively exact description of $e, H^+ - H(n)$ collisions is proposed. With certain simplifying assumptions the multiple scattering problem by fixed centres is solved, thereby providing a useful description of $A-H(n)$ collisions. Various approximate schemes capable of systematic improvement are constructed. The approach can also be applied to ionization problems.

1. Introduction

The theoretical description of atomic collisions at intermediate energies (ie beyond the ionization thresholds) is difficult. For low-energy collisions, when a few exit channels are open, the usual close-coupling expansion is, in principle, sound. However, the use of only a limited basis even with a pseudo-state modification prevents proper account of electronic excitation at intermediate energies and cannot naturally be applied to ionization, an instance for which schemes still need to be constructed that are capable of systematic improvement. The Born approximation, which has been applied extensively to high-energy collisions, is clearly inadequate for this intermediate energy region.

In an effort to bridge the energy gap, various approximate schemes have been proposed, mainly with electron-atom collisions in mind, eg distorted-wave approximations, second-order potential methods, multichannel eikonal treatments, eikonal Born series, many-body Green's function techniques, and have all met with varying degrees of success (cf reviews of Bransden 1973 and McDowell 1975).

Nevertheless, most of these methods, while performing in practice what the fully quantal close-coupling method formally suggests, are still based on a close-coupling concept which has inherent defects and obvious disadvantages when applied to collisions at intermediate energies. Experiment is achieving a fine precision for electron-atom collisions, ie the integral cross sections of eg Williams (1974) and of Donaldson *et al* (1972), differential cross sections of eg Trajmar (1973) and in particular the measurements of Eminyan *et al* (1974) of orientation and alignment parameters which are more basic to the collision, all provide independent assessment of the various theoretical models which still exhibit certain inadequacies (Bransden and Winters 1975, McDowell *et al* 1975, Flannery and McCann 1975).

In this paper a theoretical method designed particularly for atomic collisions at intermediate energies, with no obvious relationship to close-coupling prescriptions, is presented. As will be seen, the approach is effectively exact for e-H and atom A-excited-atom B(*n*) collisions, and is capable of application and systematic approximation for other collisions. It can also be applied to ionization problems. In the following sections, the theory is developed via operator formalism of scattering, thereby allowing greater transparency to the inclusion of various important effects and permitting the construction of the resulting equations in a form suitable for subsequent approximation.

2. Theory: the basic equations

The Lippmann-Schwinger operator equation describing the outgoing scattering of two atomic collision partners by their mutual interaction *V* is, in terms of the Green's resolvent *G* and transition operator *T* for the collision, given by

$$\Psi_i^+ = \Phi_i + G_0^+ V \Psi_i^+ = \Phi_i + G^+ V \Phi_i = \Phi_i + G_0^+ T \Phi_i \quad (1)$$

in the centre-of-mass system.

The basis set for the unperturbed A-B system with Hamiltonian \mathcal{H}_0 at infinite separation *R*, and associated Green's resolvent G_0^+ , is, for a fixed arrangement (*r*, *R*),

$$\Phi_i(r, R) = \psi_i(r) \phi_k(R) \equiv \psi_i(r) \exp(ik \cdot R) \quad (2)$$

a product of the eigenfunctions $\psi_i(r)$ of the internal Hamiltonian H_0 with eigenvalues ϵ_i for the motion of the internal electrons denoted collectively by *r* with respect to each parent nucleus, and $\phi_k(R)$, eigenstates of the free Hamiltonian K_0 with eigenenergies $\hbar^2 k^2 / 2\mu$ for the undistorted relative motion of A and B with wavevector *k* and reduced mass μ . Thus, Φ_i are eigenfunctions in the (direct) channel of $\mathcal{H}_0 = H_0(r) + K_0(R)$ with eigenenergy,

$$E_c = \frac{\hbar^2 k_i^2}{2\mu} + \epsilon_i = \frac{\hbar^2 k_n^2}{2\mu} + \epsilon_n \quad (3)$$

which is conserved throughout the collision. The spatial representation of the scattering function is,

$$\Psi_i^+(r, R) = \psi_i(r) e^{ik_i \cdot R} + \iint d\mathbf{r}' d\mathbf{R}' G_0^+(r, R; r', R') V(r', R') \Psi_i^+(r', R') \quad (4)$$

where the Green's function G_0^+ satisfies

$$(E_i - \mathcal{H}_0 + i\epsilon) G_0^+(r, R; r', R') = \delta(r - r') \delta(R - R') \quad (5)$$

and can therefore be expanded in terms of the complete set (2) of \mathcal{H}_0 as,

$$G_0^+(r, R; r', R') = \lim_{\epsilon \rightarrow 0^+} \frac{1}{(2\pi)^3} \frac{2\mu}{\hbar^2} \sum_n \psi_n^*(r) \psi_n(r') \int \frac{\exp[ik \cdot (R - R')] dk}{(k_n^2 - k^2 + i\epsilon)}. \quad (6)$$

For sufficiently energetic collisions when all excitations (*n*, *k*) and dominant ionizations (*ε*, *k*) are open, ie $k_n^2 > 0$ at incident energies well beyond the ionization thresholds

and much larger than the maximum energy range of ejection which contributes most to the energy spectrum ϵ of the ejected electron, (6) reduces to (cf Bransden 1970)

$$G_0^+(r, R; r', R') = -\frac{1}{4\pi} \frac{2\mu}{\hbar^2} \sum_n \frac{\exp(ik_n |R - R'|)}{|R - R'|} \psi_n^*(r) \psi_n(r'). \quad (7)$$

By considering the asymptotic ($R \rightarrow \infty$) behaviour of (7) in (4), the transition matrix T , and associated scattering amplitude f_{if} , can be defined with elements,

$$T_{fi} = \langle \Phi_f | T | \Phi_i \rangle = \langle \psi_f(r) \exp(ik_f \cdot R) | V(r, R) | \psi_i^+(r, R) \rangle = -\frac{4\pi\hbar^2}{2\mu} f_{if}(k_i, k_f). \quad (8)$$

Since, in general, exact solutions to (4) for use in (8) do not exist, various methods for constructing the T matrix (or Ψ_i^+ and G^+) as a perturbation expansion in the interaction V (assumed weak) give rise to close-coupling schemes, exact in principle but limited in practice to a restricted basis set. Moreover, the concept of close-coupling methods is alien to ionization, an instance for which schemes need to be designed which are capable of systematic improvement. There is however another alternative that involves the approximation of G_0^+ in (7) with respect to k_n , rather than G^+ in (1) with respect to V . In heavy-particle collisions and in electron-(excited) atom collisions at intermediate and high impact energies, for example, it is a good approximation to write $k_n \approx k_i$ in (7) which reduces, with the aid of the closure formula for the complete set of internal states n , including the continuum of H_0 ,

$$\sum_n \psi_n^*(r) \psi_n(r') = \delta(r - r') \quad (9)$$

to

$$G_0^+(r, R; r', R') = -\frac{1}{4\pi} \frac{2\mu}{\hbar^2} \frac{\exp(ik_i |R - R'|)}{|R - R'|} \delta(r - r') \quad (10)$$

with the result that the integration over r' in (4) can be performed. Thus this closure approximation, valid when the energy of the incident projectile is large compared to the internal energy-level spacings of the A-B system, replaces the many-particle Green's function in effect by the free-particle Green's function, with the result, the total scattering function is,

$$\Psi_i^+(r, R) = \psi_i(r) \exp(ik_i \cdot R) - \frac{1}{4\pi} \frac{2\mu}{\hbar^2} \int dR' \frac{\exp(ik_i |R - R'|)}{|R - R'|} V(r, R') \Psi_i^+(r, R') \quad (11)$$

a form which suggests the following substitution,

$$\Psi_i^+(r, R) = \psi_i(r) \chi_i^+(r, R) \quad (12)$$

where the new function χ_i^+ satisfies the integral equation

$$\chi_i^+(r, R) = \exp(ik_i \cdot R) - \frac{1}{4\pi} \frac{2\mu}{\hbar^2} \int dR' \frac{\exp(ik_i |R - R'|)}{|R - R'|} V(r, R') \chi_i^+(r, R'). \quad (13)$$

This equation (13) describes the *elastic* scattering of a *fictitious* projectile of original wavenumber k_i by a *fixed* multi-centred electrostatic interaction $V(r, R)$. The transition matrix (8) for the A-B collision is therefore,

$$T_{fi} = \langle \psi_f(r) \exp(ik_f \cdot R) | V(r, R) | \psi_i(r) \chi_i^+(r, R) \rangle \quad (14a)$$

which may be alternatively written as

$$T_{fi} = \langle \psi_f(r) | T_e(k_i, k_f; r) | \psi_i(r) \rangle_r \quad (14b)$$

where

$$T_e(k_i, k_f; r) = \langle \exp(ik_f \cdot R) | V(r, R) | \chi_i^+(r, R) \rangle_R \quad (15a)$$

the T matrix for scattering by the fixed structureless potential $V(r, R)$, is determined both on $(k_i = k_f)$ and off $(k_i \neq k_f)$ the energy shell. Thus (14) emphasizes directly the unique role of elastic scattering in inelastic collisions and involves, as the only known (15a) or alternatively the full solution to the equation,

$$\left[-\frac{\hbar^2}{2\mu} \nabla_R^2 + V(r, R) \right] \chi_i^+(r, R) = E_i \chi_i^+(r, R), \quad E_i = \hbar^2 k_i^2 / 2\mu \quad (15b)$$

subject to the usual outgoing scattering condition. Note that all the information obtained in general by numerical integration of (15b) is used in T_{fi} . The scheme is therefore efficient in that the work entailed in the solution χ_i^+ to (15b) is not redundant, as opposed to other methods based on perturbation series for which a solution is integrated out from the origin in an effort to obtain only its asymptotic behaviour. The full knowledge of χ_i^+ for all R is, of course, associated with the fact that the full T matrix (15a), with elements on and off the energy shell, is required (see appendix). Moreover, once $\chi_i^+(r, R)$ is obtained for a given scattering system, then it is preset for examination of all transitions within the system, ie χ_i^+ needs to be determined only once over the effective (r, R) range of a given system. Note that in the limit of zero V , χ_i^+ in (15b) is a plane wave and (14) reproduces the Born approximation.

3. Basis for systematic approximation: structureless projectiles

Thus, the (inelastic) scattering of composite structures is reduced to the solution of elastic scattering by fixed potential centres, in general multiple. For a structureless projectile at R incident on a target, centred at the origin and containing N -electrons at r_i ,

$$V(r, R) = V_0(R) + \sum_{i=1}^N V_i(r_i - R) \quad (16)$$

a series of two-body interactions. Structured projectiles are best treated by alternative procedures such as the one outlined in § 4.2. Although the following analysis can be immediately generalized so as to cover complex targets, assume for simplicity that the target is a one-electron atom ($N = 1$). Introduce

$$C_i^\pm = \phi_i + \frac{1}{E_i - K_0 \pm i\epsilon} V_0 C_i^\pm = \phi_i + \frac{1}{E_i - K_0 - V_0 \pm i\epsilon} V_0 \phi_i \quad (17)$$

the solution for elastic scattering by V_0 in (16) alone. With the aid of (17) and of

$$(E_i - K_0 + i\epsilon)^{-1} = (E_i - K_0 - V_0 + i\epsilon)^{-1} [1 - V_0(E_i - K_0 + i\epsilon)^{-1}] \quad (18)$$

the integral equation

$$\chi_i^+ = \phi_i + \frac{1}{E_i - K_0 + i\epsilon} (V_0 + V_1) \chi_i^+ \quad (19)$$

can be rewritten as,

$$\chi_i^+ = C_i^+ + \frac{1}{E_i - K_0 - V_0 + i\epsilon} V_1 \chi_i^+ \quad (20)$$

which, by further application of (18) with $K_0 \rightarrow K_0 + V_0$ and $V_0 \rightarrow V_1$, $V = V_0 + V_1$ can be alternatively written as

$$\chi_i^+ = C_i^+ + \frac{1}{E_i - K_0 - V + i\epsilon} V_1 C_i^+. \quad (21)$$

Hence, (14) is now exactly,

$$T_{fi} = \langle \psi_f(r) \phi_f(R) | V | \psi_i(r) C_i^+(R) \rangle + \langle \psi_f(r) \phi_f(R) | V | \psi_i(r) (E_i - K_0 - V + i\epsilon)^{-1} V_1 C_i^+(R) \rangle \quad (22)$$

in a form suitable for approximation. For example, when the effect arising from V_0 is much greater than the effect from V_1 then χ_i^+ in (21) is simply the extra scattering of C_i^+ by V_1 . When this additional scattering can be neglected, $\chi_i^+ = C_i^+$ and

$$T_{fi} \simeq T'_{fi} = \langle \psi_f(r) \phi_f(R) | V | \psi_i(r) C_i^+(R) \rangle \quad (23)$$

a formula analogous with the Coulomb-projected Born result of Geltman (1971) when V_0 is a Coulomb field and when the indices i and f are interchanged. Thus this approximation entirely neglects the second term of (22), a procedure valid only for very close encounters with the target nucleus.

Another alternative and exact form of (14) suitable for approximation is obtained with the aid of $\langle \phi_f |$ in (17) and of (20) in (14) to yield

$$T_{fi} = \langle \psi_f \phi_f | V_0 | \psi_i C_i^+ \rangle + \langle \psi_f C_f^- | V_1 | \psi_i \chi_i^+ \rangle \quad (24)$$

a two-potential scattering formula. Inserting (21) in the right-hand side of (24),

$$T_{fi} = \langle \psi_f \phi_f | V_0 | \psi_i C_i^+ \rangle + \langle \psi_f C_f^- | V_1 | \psi_i C_i^+ \rangle + \langle \psi_f C_f^- | V_1 | \psi_i (E_i - K_0 - V + i\epsilon)^{-1} V_1 C_i^+ \rangle \quad (25)$$

such that if V_1 is small then V_1^2 can be neglected with the result

$$T_{fi} \simeq T''_{fi} = \langle \psi_f \phi_f | V_0 | \psi_i C_i^+ \rangle + \langle \psi_f C_f^- | V_1 | \psi_i C_i^+ \rangle \quad (26)$$

which is the distorted Born-wave formula used for elastic scattering by $V(r, R)$ in an inelastic matrix element (14). The approximation T''_{fi} is obviously much more sophisticated than the customary DWBA to close-coupling formulae for which the distorted waves refer to distortion by the *static* interactions $\langle \psi_n | V | \psi_n \rangle$ of the initial and final channels and not as, in this case, to distortion by the full electrostatic interaction $V_0(R)$.

While only a few schemes suitable for approximation of (14) have been constructed above, there are several instances for which exact or effectively exact solutions can be obtained as follows.

4. Soluble models

4.1. Charged-particle-atom collisions

Consider collisions between structureless particles of charge Ze with atomic hydrogen. The function χ_i^+ is therefore the solution for elastic scattering by two *fixed* centres of

charge of opposite sign ($\pm Ze$), in general, or, in particular, by a fixed dipole, when distant encounters R are dominant, or by a Coulomb field when close collisions with the nucleus are important. In the general case (a situation analogous to the exact determination of the continuum orbital of H_2^+ by Bates *et al* (1953) and Flannery and Öpik (1965)), the introduction of the prolate spheroidal coordinates,

$$\begin{aligned}\lambda &= (R + |R - r|)/r, & 1 \leq \lambda \leq \infty \\ \mu &= (R - |R - r|)/r, & -1 \leq \mu \leq 1\end{aligned}\quad (27)$$

and Φ , the angle of rotation of R about the r axis, with the substitution,

$$\chi_i^+(r, R) = \Lambda(\lambda|r)M(\mu|r)e^{im\Phi} \quad (28)$$

permits the separation of the Schrödinger equation (15) into the following two second-order differential equations,

$$\frac{d}{d\lambda} \left[(\lambda^2 - 1) \frac{d\Lambda^{(m)}}{d\lambda} \right] + \left(A + p^2\lambda^2 - \frac{m^2}{\lambda^2 - 1} \right) \Lambda^{(m)}(\lambda) = 0 \quad (29a)$$

in which $p = \frac{1}{2}(k_1 r)$, and

$$\frac{d}{d\mu} \left[(1 - \mu^2) \frac{dM^{(m)}}{d\mu} \right] + \left(-A - p^2\mu^2 + 2rZ\mu - \frac{m^2}{1 - \mu^2} \right) M^{(m)}(\mu) = 0 \quad (29b)$$

coupled by a separation constant A . Equation (29a), which defines the radial spheroidal function, can be solved exactly as a linear combination of radial Bessel functions (cf Flammer 1956). Moreover, with the substitution,

$$\Lambda = (1 - \lambda^2)^{-1/2} \Omega(\lambda) \quad (30)$$

then (29a) reduces to

$$\frac{d^2 \Omega}{d\lambda^2} + \left(\frac{p^2 \lambda^2 + A}{\lambda^2 - 1} + \frac{1 - m^2}{(\lambda^2 - 1)^2} \right) \Omega(\lambda) = 0 \quad (31)$$

which is capable of direct numerical solution subject to $\Omega(1) = 0$, and to an appropriate asymptotic form, correctly normalized. To initiate the integration procedure, a series solution for small λ can be constructed to give,

$$\begin{aligned}\Omega^{(m)}(\lambda) &= (\lambda^2 - 1)^{\frac{1}{2}(m+1)} \left[1 - \frac{K(\lambda - 1)}{2(m+1)} + \frac{1}{4} \left(K - 2p^2 + \frac{K^2}{2m+1} \right) \frac{(\lambda - 1)^2}{m+2} + \dots \right], \\ K &= A + p^2 + m(m+1).\end{aligned}\quad (32)$$

In the limit as $r \rightarrow 0$, (29b) reduces to the equation for the associated Legendre functions $P_n^m(\mu)$ and a series solution to (29b) can be obtained with the form,

$$M^{(m)}(\mu) = \sum_{s=0}^{\infty} d_s^{(m)}(p, r) P_{m+s}^m(\mu) \quad (33)$$

where the coefficients $d_s^{(m)}$ satisfy certain recursion relations. Hence, the full solution χ_i^+ which contains all the information on distortion, is known, but must first be transformed from the coordinate axis in which r is fixed to a space-fixed frame so that the transition matrix,

$$T_{fi} = \left\langle \psi_f(r) \exp(ik_f \cdot R) \left| \frac{Ze^2}{R} - \frac{Ze^2}{|R - r|} \right| \psi_i(r) \mathcal{T}_r \Lambda(\lambda|r) M(\mu|r) e^{im\Phi} \right\rangle \quad (34)$$

can be evaluated exactly (although, not too easily), where \mathcal{T}_r denotes the appropriate rotation operator.

When distant encounters are important to the elastic scattering, eg through small angles, then χ_i^+ corresponds to elastic encounters with a fixed dipole with interaction

$$V(r, R) \sim + \frac{Ze^2}{R^2} r \cdot \hat{R}. \quad (35)$$

For point-dipoles Mittleman and von Holdt (1965) obtained exact solutions in terms of combinations of spherical (radial) Bessel and angular Legendre functions, and Shimizu (1963) has investigated scattering by dipoles of finite size.

Large-angle elastic scattering results primarily from close encounters with the nucleus with the result that

$$\chi_i^+(r, R) \simeq \psi_c^+(R) = \exp(-\frac{1}{2}\pi\alpha)\Gamma(1-\alpha)\exp(ik_i \cdot R)_1 F_1(\alpha; 1; -ik_i R_i - ik_i \cdot R) \quad (36)$$

the Coulomb function with $\alpha = Z(e^2\mu/\hbar^2)k_i$.

4.2. Neutral-(excited) atom collisions

For A-B collisions, an effectively exact solution to χ_i^+ , the fictitious wavefunction describing in general, multiple elastic scattering of A by N fixed targets within B can be achieved under certain conditions to be later determined. The eventual aim is to incorporate within the theoretical solution the asymptotic scattering amplitudes (or on-the-energy-shell T -matrix elements, assumed known) for two-body interactions between the projectile A and each particle n of B, ie A is regarded as being a *point particle* whose response to the target particles n is to be acknowledged by the possible use of elastic or inelastic scattering amplitudes describing two-body A- n scattering. Thus, the A-B interaction V is, in general, a sum of 'two-body' interactions $V_n(R, r_n)$ between projectile A and each particle n within target B, and hence,

$$\chi_i^+ = \phi_i + G_0 \left(\sum_{n=1}^N V_n \right) \chi_i^+ = \phi_i + G_0 V \phi_i + G_0 V G_0 V \phi_i + \dots, \quad (37)$$

where $G_0 \equiv (E - K_0 + i\epsilon)^{-1}$, a one-particle Green's operator for free motion of energy E , propagates the effect of each interaction V_n . This equation can be solved by 'recycling', as indicated on the right-hand side, in powers of V , a procedure, while generating the customary Born series, is nonetheless lacking in a simple physical interpretation needed for further approximation in the present instance. The Born series above can however be rearranged so that all terms which involve the scattering of A by each target n of B are combined together, thereby permitting the natural separation of two-body from individual higher-order multiple scattering effects. Each term $(j+1)$ of the Born series is

$$V_n(G_0 V_n)(G_0 V_n) \dots \equiv V_n \left(\frac{1}{E - K_0} V_n \right)^j \quad (38)$$

and hence by following Watson (1953) or Goldberger and Watson (1964) the exact solution can be written as,

$$\chi_i^+ = \phi_i + \frac{1}{E - K_0 + i\epsilon} \sum_{n=1}^N t_n \chi_n \quad (39)$$

a superposition of wavelets χ_n emitted by each target n and given as the solution of

$$\chi_n = \phi_i + \frac{1}{E - K_0 + i\epsilon} \sum_{m \neq n}^N t_m \chi_m \quad (40)$$

a set of coupled integral equations in which the two-body transition operators

$$t_n = V_n + V_n \frac{1}{E - K_0 + i\epsilon} t_n \quad (41)$$

correspond, in this case of *fixed* potentials, to scattering by an isolated target particle n free from interaction with other particles m . All details of the binding in the A-B collision have already been acknowledged by (14).

Thus, χ_i^+ is the unperturbed function ϕ_i together with wavelets which can be generated by 'recycling' (40) to yield

$$\begin{aligned} \chi_n &= \phi_i + G_0 \sum_{m \neq n} t_m \left[\phi_i + G_0 \sum_{r \neq m} t_r \left(\phi_i + G_0 \sum_{s \neq r} t_s (\phi_i + \dots) \dots \right) \dots \right] \\ &= \phi_i + G_0 \sum_{m \neq n} t_m \phi_i + G_0 \sum_{m \neq n} t_m G_0 \sum_{r \neq m} t_r \phi_i \\ &\quad + G_0 \sum_{m \neq n} t_m G_0 \sum_{r \neq m} t_r G_0 \sum_{s \neq r} t_s \phi_i + \dots \end{aligned} \quad (42)$$

which represents a truly sequential multiple scattering series in which each term corresponds to the arrival mode of the incident particle i on m , eg the first term in t_m refers to direct arrival while the second term corresponds to the arrival at m of a wave once scattered previously elsewhere, etc. In contrast the terms $\sum_n V_n G_0 \sum_n V_n \phi_i$ in the Born series above include to all orders the important successive interactions with the same particle. Thus (39)–(41) render the key quantity χ_i^+ in a form suitable for approximation to be used in (14).

The only assumption so far is $k_n \simeq k_i$ in the many-body Green's function (7), for the direct channel, which entails, from (3),

$$k_i - k_n = \frac{2\mu (\epsilon_n - \epsilon_i)}{\hbar^2 (k_i + k_n)} \simeq 0 \quad (43)$$

such that the averaged initial and final relative energy be much less than the internal energy level spacing, a weak-binding approximation *only* to that part of (7) which describes the relative motion. This assumption causes the introduction of an artificial χ_i^+ , for elastic scattering by *fixed* multicentre charges. Conversely, the scattering centres have no mechanism for recoil, can be regarded as infinitely heavy and hence binding between the charges will have no effect on the scattering (cf equation (29)). Thus, the free-particle transition operators t_n which emerge in (41) are properties only of the individual scatterer n (and projectile).

Additional Assumptions. (i) The impact energy must be uniquely defined between scattering events so that the mean free path λ_M must be much greater than the de Broglie wavelength λ_i of relative motion and hence,

$$\lambda_M \simeq (\rho \pi f_n^2)^{-1} \gg \lambda_i = k_i^{-1} \quad (44)$$

where ρ is the number density $N/\frac{4}{3}\pi R^3$ of N particles within the 'volume' of B assumed

spherical with radius R , and f_n is an effective range for A- n collisions. (ii) The aim is to use elastic scattering data on A- n collisions, ie knowledge of only the 'on-the-energy-shell' matrix elements of t_n is assumed. The momentum representation of (39) is

$$\chi_i^+ = \phi(k_i) + \frac{1}{(2\pi)^3} \frac{2}{\hbar^2} \sum_{n=1}^N m \int \frac{\langle k_a | t_n | k_i \rangle \chi_n(k_a) dk_a}{k_i^2 - k_a^2 + i\epsilon} \quad (45)$$

where m is the reduced mass of the A- n system.

As is shown in the appendix, the contribution $\chi_{i(0)}^+$ to (45) arising from 'on-the-energy-shell' T matrices with $k_a = k_i$ is

$$\chi_{i(0)}^+(r, R) = \chi_i^+(r, R) \quad R > R_{0n}, \quad r \text{ fixed} \quad (46)$$

where R_{0n} is a range beyond which V_n vanishes. Thus the use of the associated scattering amplitudes

$$f_n(k_a, k_i) = -\frac{1}{4\pi} \frac{2m}{\hbar^2} \langle k_a | t_n | k_i \rangle, \quad k_a = k_i \quad (47)$$

in (45) entails the condition,

$$f_n \lesssim r_{nm} \quad (48)$$

where r_{nm} is the (n, m) inter-particle spacing within B. Hence,

$$\lambda_m \approx \frac{\max(r_{nm}^3)}{N f_n^2} \gtrsim \frac{f_n}{N} \quad (49)$$

For H(1s)-H(p) collisions at speed v , $f_n \sim 1 a_0 \lesssim p^2$, and $\lambda_m \approx p^2 a_0 \gg 10^{-3}/v$ and thus (44) and (48) are valid for $v \gg 10^{-3}/p^2$ au, an easy accomplishment even for $p = 1$. Although, electron-atom collisions can be formally excluded because of their long Coulombic ranges, the conditions (44) and (48) are not too restrictive to an approximate treatment.

Therefore, in the spatial representation of (39),

$$\chi_i^+ \approx \chi_{i(0)}^+ = \exp(ik_i \cdot R) + \sum_{n=1}^N \int dR' dR'' G_0(R', R'') t_n(R', R'') \chi_n(R'') \quad (50)$$

with

$$t_n(R', R'') \equiv \langle R' | t_n | R'' \rangle = \frac{1}{(2\pi)^6} \int \langle R' | k' \rangle dk' \langle k' | t_n | k'' \rangle dk'' \langle k'' | R'' \rangle \quad (51)$$

where $\phi_i(R) \equiv \langle R | k_i \rangle = \exp(ik_i \cdot R)$. Hence, for a short-range interaction V_n located as a delta function about position r_n of particle n , (51) reduces to

$$t_n(R', R'') = -4\pi \frac{\hbar^2}{2m} f_n \delta(R' - r_n) \delta(R'' - r_n) \quad (52)$$

where f_n is the scattering amplitude associated with the short-range interaction V_n . For example, in collisions between ground-state neutrals A and atoms B(p) in highly excited Rydberg levels p , the interaction V_n (polarization, at most) between the valence electron n and the neutral has much shorter range than the Coulombic interaction between n and its parent ionic core, and may be regarded as fairly localized relative to the characteristic size $\sim p^2 a_0$ of B. This approach has already been successfully exploited in semi-quantal treatments elsewhere (Flannery 1970, 1973) and yields

encouraging results for ionization, even for the most extreme case $p = 1$. Therefore with the aid of explicit G_0 and (52),

$$\chi_i^+ = \exp(ik_i \cdot R) + \sum_{n=1}^N \frac{\exp(ik_i |R - r_n|)}{|R - r_n|} f_n \chi_n(r_n) \quad (53)$$

where, by a similar argument with (40),

$$\chi_n(r_n) = \exp(ik_i \cdot r_n) + \sum_{m=1}^N \frac{\exp(ik_i |r_n - r_m|)}{|r_n - r_m|} \chi_m(r_m), \quad n = 1, 2, \dots, N \quad (54)$$

a set of N algebraic (rather than integral) equations for the numbers $\chi_n(r_n)$.

For $N = 2$, the equations can be solved exactly to give

$$\chi_1(r_1) = \exp(ik_i \cdot r_1) \left\{ \left[1 + f_2 \left(\frac{\exp(ik_i r_{12})}{r_{12}} \right) \exp(-ik_i \cdot r_{12}) \right] \left[1 - \frac{f_1 f_2}{r_{12}^2} \exp(2ik_i r_{12}) \right]^{-1} \right\} \quad (55)$$

and a similar expression for χ_2 with $r_1 \leftrightarrow r_2$, to yield an explicit result for $\chi_i^+(r_1, r_2, R)$ to be used in (14).

The first term of (55) is the undistorted wavelet emerging from r_1 , the second term arises from the reception at 1 of the wavelet emitted by 2, and the denominator of (55) represents the shuttling back and forth. The expansion of (55) for small $f_{1,2} \ll r_{12}$ yield the customary multiple scattering sequence.

Hence, with the knowledge of e-A elastic scattering data, and with (53), and (54) in (14), the general A-H(n) elastic and excitation collisions for all n can effectively be solved exactly subject to the (certain) validity of (43), (44) and (48). Foldy (1945) and Brueckner (1953) originally applied (55) to the scattering of sound waves by two fixed centres, and to the scattering of pi mesons by deuterons, respectively. The present treatment (37)-(54) has presented the generalized form for χ_i^+ with atomic collisions in mind, and stresses the overall validity for subsequent use in (14) pertinent to A-B collisions.

5. Simple approximations

I. As previously noted, the Born approximation and the Coulomb-projected Born approximation (for charged particles) to the transition matrix T_{fi} in (14) are reproduced when the elastic scattering function χ_i^+ of (15) is associated either with no interaction V or else with a strong interaction V_0 only with the nucleus, respectively. For V weak, however, a perturbation treatment of (15) yields,

$$\chi_i^+(r, R) = \phi_i(R) + \frac{2\mu}{(2\pi)^3 \hbar^2} \int \frac{\langle \phi_{k_a}(R) | V(r, R) | \phi_{k_i}(R) \rangle}{k_i^2 - k_a^2 + i\epsilon} \phi_a(k_a) dk_a + \dots \quad (56)$$

which, for the charged particle-atom interaction,

$$V(r, R) = V_0 + V_1 = Ze^2 \left(\frac{1}{R} - \sum_{n=1}^N \frac{1}{|R - r_n|} \right) \quad (57)$$

reduces, with the aid of Bethé's integral to,

$$\chi_i^+(r, R) = \exp(ik_i \cdot R) \left(1 - \frac{8\pi Ze^2 \mu}{(2\pi)^3 \hbar^2} \int \frac{\exp(-iK_a \cdot R) [1 - \sum_{n=1}^N \exp(iK_a \cdot r_n)] dK_a}{K_a^2 (K_a^2 - 2k_i \cdot K_a)} \right),$$

$$K_a = k_i - k_a \quad (58)$$

to first order, in which the integral can be explicitly evaluated by contour integration. Moreover for charged particle-(highly) excited atom collisions for which $r_n \gg R$, then (57) is approximately

$$V(r, R) \simeq Ze \left(\frac{e}{R} + \sum_{n=1}^N \frac{(-e)}{r_n} \right) \quad (59)$$

with the result that,

$$\chi_i^+(r, R) = \psi_c^+(R) \prod_{n=1}^N \psi_c^+(r_n) \quad (60)$$

products of Coulombic functions (36).

Also, for neutral-neutral collisions A-B when multiple scattering effects can be neglected, (53) yields,

$$\chi_i^+(r, R) = \exp(ik_i \cdot R) + f_+ \frac{\exp(ik_i R)}{R} + f_- \sum_{n=1}^N \frac{\exp(ik_i |R - r_n|)}{|R - r_n|} \exp(ik_i \cdot r_n) \quad (61)$$

where f_{\pm} are the elastic scattering amplitudes (in the forward direction) for free H^+ -A and e-A collisions respectively. It is very apparent that a variety of other approximations, even semi-classical, to (15) exist for use in (14), eg use of the eikonal approximation to (15b) reproduces the Glauber approximation.

II. A different set of approximations may be generated by considering the contribution to T_{fi} in (14b) that arises from only 'on-the-energy-shell' matrix elements T_{ei} , ie

$$k_f = k_i \hat{k}_f \equiv k'_f$$

in T_e of (15a). Thus,

$$T_{fi} = \langle \psi_f(r) | T_{ei}(k_i, k'_f; r) | \psi_i(r) \rangle, \quad k_i = k'_f \quad (62)$$

in terms of an averaged amplitude for elastic scattering of the projectile by the fixed potential $V(r, R)$, ie the asymptotic behaviour of χ_i^+ in (15b) is only required. Equation (62) yields the adiabatic approximation suggested by Chase (1956) from a continuum analogue of the Born-Oppenheimer approximation to bound molecular states and used exclusively for rotational and vibrational excitation. The present derivation shows its applicability to electronic transitions. The Born approximation to T_{ei} for interaction (16) is

$$T_{ei}^{(B)} = \int V_0(R) \exp(iK \cdot R) dR + \sum_{n=1}^N \exp(iK \cdot r_n) \int V_n(R) \exp(iK \cdot R) dR,$$

$$K = k_f(\hat{k}_i - \hat{k}_f) \quad (63)$$

for use in (62). For Coulomb interactions (57), this procedure yields,

$$T_{fi}^{(B)} = \frac{4\pi}{K^2} [\delta_{fi} - F_n(K)] \quad (64)$$

a form similar to the Born approximation to T_{fi} in terms of the generalized form factor

$$F_{fi}(K) = \left\langle \psi_f(r_1, r_2, \dots, r_N) \left| \sum_{n=1}^N \exp(iK \cdot r_n) \right| \psi_i(r_1, r_2, \dots, r_N) \right\rangle \quad (65)$$

as a function of K in (63). Also, for rotational transitions by a pure dipole field, (63) in (62) reproduces the Born result for non-forward scattering. Hence (62) provides a basis for approximation schemes more accurate than the Born with $k_f \simeq k_i$.

The cross section for excitation of all states $f \neq i$ is proportional to,

$$S \equiv \sum_{f \neq i} |T_{fi}|^2 = S' \langle \psi_i(r) | T_e^*(k_i, k_f; r) | \psi_f(r) \rangle \langle \psi_f(r) | T_e(k_i, k_f; r) | \psi_i(r) \rangle \quad (66)$$

which reduces, with the aid of closure (9) and of 'on-the-energy-shell' matrices T_{ei} to the following initial-state average,

$$S = \langle \psi_i(r) | T_{ei}(k_i, k_f; r)^2 | \psi_i(r) \rangle - |\langle \psi_i | T_{ei} | \psi_i \rangle|^2 \quad (67)$$

in which the second term is due to elastic scattering alone (cf equation (62)).

On using (63) for the Coulomb interactions (57), the Born approximation with $k_f \simeq k_i$,

$$S^{(B)} = \left(\frac{4\pi}{K^2} \right)^2 [1 - |F_{ii}(K)|^2], \quad K = k_i(\hat{k}_i - \hat{k}_f) \quad (68)$$

follows from (67), which therefore can be used as a basis for a more refined description.

III. Approximations to T_e rather than to T_{ei} may be obtained directly. For target atoms in highly excited states, the interaction between the projectile and the Rydberg electron controls energy changes such that on neglecting the interaction with the core of the target,

$$\begin{aligned} T_e(k_i, k_f; r) &= \langle \exp(ik_f \cdot R) | V(R-r) | \chi_i^+(r, R) \rangle_R = \exp(iK \cdot r) \langle \exp(ik_f \cdot R') | V(R') | \tilde{\chi}_i^+(R') \rangle_{R'} \\ &= \exp(iK \cdot r) T_e(k_f, k_i) \end{aligned} \quad (69)$$

in which $\tilde{\chi}_i^+$ is $\exp(-ik_i \cdot r) \chi_i^+$ and describes elastic scattering by the central potential $V(R')$ with $R' = R - r$. Hence (14b) with (69) yields

$$T_{fi} = \langle \psi_f(r) | \exp(iK \cdot r) | \psi_i(r) \rangle_r T_e(k_i, k_f) \equiv F_{fi}(K) T_e(k_i, k_f) \quad (70)$$

a product of the form factor for the transition of the valence electron and the T -matrix elements (on and off the energy shell) for potential scattering of the projectile. Equation (70) is similar to, but not identical to, the basic formula of the impulse approximation (cf Newton 1966).

All of the foregoing procedures for the evaluation of χ_i^+ or T_e within (14) can be applied of course equally well to ionization as to excitation. However, within the assumption $k_n \simeq k_i$, the theoretical formulation in § 2 is exact for direct excitation, but not for ionization. This shortcoming (present also in all previous descriptions of ionization) arises by noting that the 'two-body' Green's function G_0^+ in (6) describes exactly the channel $a + (b, c)_n, \dots, a + (b + c)$ which includes states of excitation $(b, c)_n$ and of dissociation $(b + c)$ only for c in the field of b . The ionization states $(a + b + c)$ belong to a true three-body channel which is only approximately described by the above G_0^+ . The dissociative states $a + (b + c)$ do not actually belong to, nor do they bear any simple

relation to, the free states of any physical channel (direct, rearrangement and three-body). They do, however, contain certain projections onto these channels. The projection of the dissociative states in Ψ_i^+ is apparently lost by use of the closure relation (9) since Ψ_i^+ tends to zero as $r \rightarrow \infty$. However, equation (15) for χ_i^+ must be solved for the full (r, R) range such that χ_i^+ and hence Ψ_i^+ does contain some information, as in (56), (58) and (60), on the dissociative states.

In spite of this, however, the present formulation when applied to ionization does represent considerable improvement over previous theoretical approaches, eg the Born and related approximations assume χ_i^+ given by the first term of (56), a term containing no information on the three-body channel at all, while the close-coupling method assumes for Ψ_i^+ a limited basis set which because of practical difficulties contains no states of dissociation of the system. Moreover, the previous development can be easily generalized so as to include rearrangement or reaction channels, as follows.

6. Rearrangement channels

The Hamiltonian for the collision system is,

$$\mathcal{H} = \mathcal{H}_{0d} + V_d = \mathcal{H}_{0x} + V_x \quad (71)$$

where previously defined quantities associated with either direct channels d or rearranged channels x now contain, for identification purposes, an additional index d or x, respectively. The free Hamiltonians and corresponding eigenfunctions (which include translational phase factors) and eigenenergies of the collision system in the absence of the interactions V_d and V_x are respectively

$$\begin{aligned} \mathcal{H}_{0d} &= H_0(r_d) + K_0(R) \\ \Phi_{id}(r_d, R) &= \psi_{id}(r_d) \exp(ik_{id} \cdot R); \quad E_i^{(d)} = \epsilon_i^{(d)} + \frac{\hbar^2 k_{id}^2}{2\mu_d} \end{aligned} \quad (72)$$

and

$$\begin{aligned} \mathcal{H}_{0x} &= H_0(r_x) + K_0(s) \\ \Phi_{ix}(r_x, s) &= \psi_{ix}(r_x) \exp(ik_{ix} \cdot s); \quad E_i^{(x)} = \epsilon_i^{(x)} + \frac{\hbar^2 k_{ix}^2}{2\mu_x} \end{aligned} \quad (73)$$

where r_d and r_x denote respectively the internal coordinates of the isolated collision partners in the direct channel and in the channel for which the rearrangement $R \leftrightarrow s$ has occurred between the incident projectile at R with an atomic electron at s . The wavefunction for the total system therefore simultaneously satisfies,

$$\Psi_i^+ = \Phi_{id} + (E_i^{(d)} - \mathcal{H}_{0d} + i\epsilon)^{-1} V_d \Psi_i^+ \quad (74)$$

with its built-in boundary condition and

$$(E_i^{(x)} - \mathcal{H}_{0x}) \Psi_i^+ = V_x \Psi_i^+ \quad (75)$$

subject to an outgoing spherical wave alone as $s \rightarrow \infty$. The free-particle Green's

function for the open channels of (75) is

$$G_0^+(r_x, s; r'_x, s') = -\frac{1}{4\pi} \frac{2\mu_x}{\hbar^2} \sum_n \psi_{nx}(r_x) \psi_{nx}(r'_x) \frac{\exp(ik_{nx}|s-s'|)}{|s-s'|} \quad (76)$$

with the result that the transition matrix $T_{fi}^{(n)}$ for rearrangement can be extracted from the asymptotic form of (76) in (75) to yield

$$T_{fi}^{(n)} = \langle \psi_{fx}(r_x) \exp(ik_f \cdot s) | V_x(r_x, s) | \Psi_i^+ \rangle. \quad (77)$$

Since Ψ_i^+ is given by (74) solved so as to provide an incoming plane wave and an outgoing spherical wave at $R \rightarrow \infty$, then the analysis of § 2 is applicable with the result that,

$$T_{fi}^{(n)} = \langle \psi_{fx}(r_x) \exp(ik_f \cdot s) | V_x(r_x, s) | \psi_{id}(r_d) \chi_i^+(r_d, R) \rangle \quad (78)$$

a form analogous to (14a) for direct collisions. It is therefore apparent that the analysis previously developed in §§ 3-6 for the solution χ_i^+ is directly applicable to the determination of the T matrix for rearrangement collisions.

7. Summary and conclusions

A theoretical description of transitions in atomic and molecular collisions at intermediate energies has been presented. The method involves the basic approximation that $k_n \simeq k_i$ in only that part of the Green's function associated with the relative motion. This approach is effectively exact for e and H^+ collisions with $H(n)$ at intermediate energies since, in this instance, the basic premise (which represents the point of departure from following close-coupling techniques) that the incident energy be large compared to the energy-level spacings in $H(n)$ is well justified for high n in the case of electron impact and for much lower n (~ 2) for proton impact. In these cases the problem involves the solution of two second-order differential equations which can be solved by standard techniques. An attractive feature of the method is that the solution, once determined, can be used to examine the full array of transitions in any given system.

The application to A-B(n) collisions involves the solution of a multiple scattering problem, a solution greatly facilitated by the following two additional assumptions that the de Broglie wavelength of relative motion is small compared to the mean free path and that the effective range of interactions between A and the N fixed particles m of B be smaller than, or of comparable magnitude to, the interspacing between the N particles. The coupled integral equations then reduce to a set of coupled algebraic equations involving as parameters the scattering amplitudes for the A- m isolated collisions. As is easily apparent, the present approach to A-B(n) collisions is much more rigorous than the previous semi-quantal descriptions of Flannery (1970, 1973) in that multiple scattering events are included, and in that excitation (and not only ionization) can also be described.

Moreover the method provides a useful description of ionization, one which is capable of systematic improvement and which represents considerable improvement of Born's approximation. It certainly would be of interest, however, to apply this approach to e-He elastic and inelastic collisions at intermediate energies, a case which is currently receiving serious theoretical and experimental attention (cf McDowell

1975). Since the applications are obviously numerous, it is intended that future studies will include detailed investigations of certain illustrative atomic and molecular collision processes.

Acknowledgment

This research was sponsored by the Air Force Aerospace Research Laboratories, Air Force Systems Command, United States Air Force, Contract F33615-74-C-4003.

Appendix. The implication of using on-the-energy-shell T -matrix elements alone

The wavefunction for potential scattering by a fixed potential $V(R)$ is, in channel α ,

$$\psi_{\alpha}^{+}(R) = \phi_{\alpha}(R) + \int G_0^{+}(R, R') V(R') \psi_{\alpha}^{+}(R') dR' \quad (A.1)$$

$$= \phi_{\alpha}(R) + \frac{1}{(2\pi)^3} \frac{2\mu}{\hbar^2} \int \frac{T_{\gamma\alpha} \phi_{\gamma}(R) dk_{\gamma}}{k_{\alpha}^2 - k_{\gamma}^2 + i\epsilon} \quad (A.2)$$

with customary notation. Include in (A.2) only on-the-energy-shell matrix elements $T_{\gamma\alpha}$ with $k_{\gamma} = k_{\alpha} = k$ and expand the plane wave,

$$\phi_{\gamma}^{(*)}(R) = \exp(\pm i k_{\gamma} \cdot R) = \frac{1}{kR} \sum_{l=0}^{\infty} (\pm i)^l (2l+1) F_l(k, R) P_l(\hat{k}_{\gamma} \cdot \hat{R}) \quad (A.3)$$

in terms of the Legendre polynomials P_l and the Recatti-Bessel functions F_l which are, given by (Newton 1966),

$$F_l(kR) = (\frac{1}{2}\pi kR)^{1/2} J_{l+\frac{1}{2}}(kR) = (kR) j_l(kR) \xrightarrow{kR \gg 1} \sin(kR - \frac{1}{2}l\pi) \quad (A.4)$$

where $J_{l+\frac{1}{2}}$ and j_l are the Bessel and spherical Bessel functions respectively. By contour integration, the resulting integral in (A.2) is

$$\frac{1}{(2\pi)^3} \int \frac{\exp(i k_{\gamma} \cdot R) \exp(-i k_{\alpha} \hat{k}_{\gamma} \cdot R') dk_{\gamma}}{k_{\alpha}^2 - k_{\gamma}^2 + i\epsilon} = -\frac{1}{4\pi k R R'} \sum_{l=0}^{\infty} (2l+1) H_l^{+}(kR) F_l(kR') P_l(\hat{R} \cdot \hat{R}') \quad (A.5)$$

where the Recatti-Hankel function H_l^{+} in terms of the Recatti-Bessel functions F_l and G_l of the first and second kinds respectively, is (Newton 1966)

$$H_l^{+}(kR) = G_l(kR) + i F_l(kR) = i k R (j_l + i \eta_l) \xrightarrow{kR \gg 1} \exp[i(kR - \frac{1}{2}l\pi)] \quad (A.6)$$

in which η_l is the spherical Neumann function (or spherical Bessel function of the second kind).

The outgoing Green's function G_0^{+} in (A.1) can be expanded as

$$G_0^{+}(R, R') = -\frac{1}{4\pi k R R'} \frac{2\mu}{\hbar^2} \sum_{l=0}^{\infty} (2l+1) P_l(\hat{R} \cdot \hat{R}') \begin{cases} F_l(kR) H_l^{+}(kR'), & R < R' \\ H_l^{+}(kR) F_l(kR'), & R > R'. \end{cases} \quad (A.7)$$

Hence by comparing (A.5) in (A.2) and (A.7) in (A.1), it is seen that the contribution to $\psi_{a(o)}^+$ in (A.2) that arises from 'on-the-energy-shell' T -matrix elements is related to (A.1) by

$$\psi_{a(o)}^+(R) = \psi_a^+(R), \quad R > R_0 \quad (\text{A.8})$$

where R_0 is some radius beyond which $V(R)$ vanishes. Similar arguments can be applied to (45) and hence (46) holds. Conversely, full information on the scattering function within R_0 entails full knowledge of the T matrix, knowledge which cannot be provided experimentally.

References

- Bates D R, Öpik U and Poots G 1953 *Proc. Phys. Soc. A* **66** 1113-23
 Bransden B H 1970 *Atomic Collision Theory* (New York: Benjamin) p 135
 — 1973 *Proc. 8th Int. Conf. on Physics of Electronic and Atomic Collisions* (Belgrade: Institute of Physics) Invited Lectures and Progress Reports pp 400-16
 Bransden B H and Winters K H 1975 *J. Phys. B: Atom. Molec. Phys.* **8** 1236-44
 Brueckner K A 1953 *Phys. Rev.* **89** 834-8
 Chase D M 1956 *Phys. Rev.* **104** 838-42
 Donaldson F G, Hender M A and McConkey J W 1972 *J. Phys. B: Atom. Molec. Phys.* **5** 1192-210
 Eminyan M, MacAdam K B, Slevin J and Kleinpoppen H 1974 *J. Phys. B: Atom. Molec. Phys.* **7** 1519-42
 Flammer C 1957 *Spheroidal Wave Functions* (Stanford: University Press)
 Flannery M R 1970 *Ann. Phys., NY* **61** 465-87
 — 1973 *Ann. Phys., NY* **79** 480-517
 Flannery M R and McCann K J 1975 *J. Phys. B: Atom. Molec. Phys.* **8** 1716-33
 Flannery M R and Öpik U 1965 *Proc. Phys. Soc. A* **86** 491-500
 Foldy L L 1945 *Phys. Rev.* **67** 107-19
 Geltman S 1971 *J. Phys. B: Atom. Molec. Phys.* **4** 1288-98
 Goldberger M L and Watson K M 1964 *Collision Theory* (New York: Wiley) p 750
 McDowell M R C 1975 *Proc. Int. Symp. on Electron and Photon Interactions with Atoms* ed M R C McDowell and H Kleinpoppen (New York: Plenum)
 McDowell M R C, Morgan L A and Myerscough V P 1975 *J. Phys. B: Atom. Molec. Phys.* **8** 1053-72
 Mittleman M H and von Holdt R E 1965 *Phys. Rev.* **140** 726-9
 Newton R G 1966 *Scattering Theory of Waves and Particles* (New York: McGraw-Hill) p 38, 587
 Shimizu M 1963 *J. Phys. Soc. Japan* **18** 811-9
 Trajmar S 1973 *Phys. Rev. A* **8** 191-203
 Watson K M 1953 *Phys. Rev.* **89** 575-87
 Williams J F 1974 *J. Phys. B: Atom. Molec. Phys.* **7** L56-60

AD-A062 163

GEORGIA INST OF TECH ATLANTA SCHOOL OF PHYSICS
CALCULATION OF ELECTRON IMPACT CROSS SECTIONS FROM METASTABLE S--ETC(U)
AUG 78 M R FLANNERY

F/G 7/4

F33615-74-C-4003

UNCLASSIFIED

3 OF 3
AD
A062163

AFAD1 -TD-7A-5A

NI



END
DATE
FILMED
3-79
DDC

11.2 Appendix B

New semiclassical treatments of rotational and vibrational transitions in heavy-particle collisions. I. H-H and H-He collisions

K. J. MOSEMAN and M. R. J. JANSSEN

School of Physics, Georgia Institute of Technology, Atlanta, Georgia 30332
(Received 12 July 1975)

Two new semiclassical methods—the adiabatic channel treatment and the multiphonon channel treatment—are proposed for the description of rotational and vibrational transitions in heavy-particle collisions. The first method, which is based on the adiabatic channel treatment, is applied to the description of rotational transitions in H-H and H-He collisions. The second method, which is based on the multiphonon channel treatment, is applied to the description of vibrational transitions in H-He collisions. Both methods are shown to be in good agreement with the results of exact calculations. The adiabatic channel treatment is shown to be particularly useful for the description of rotational transitions in H-H collisions, while the multiphonon channel treatment is particularly useful for the description of vibrational transitions in H-He collisions.

1. INTRODUCTION

Recently, there has been considerable activity in the theoretical description of rotational and vibrational transitions in heavy-particle collisions. Theoretical approaches all based on the Born-Oppenheimer approximation have been proposed. Classical approaches have also been proposed. The following discussion is based on the Born-Oppenheimer approximation.

(i) The extraction of differential cross sections from the exact impact parameter treatment (IPT) is not immediately obvious since the resulting two-body scattering cross section is not a function of the impact parameter. The following discussion is based on the Born-Oppenheimer approximation.

(ii) The consequent use of a semiclassical treatment for the relative motion, required for the Born-Oppenheimer approximation, is clearly quite useful for rotational transitions which involve large angular momentum. It is also required for vibrational transitions.

(iii) While elastic scattering is usually treated by the Born-Oppenheimer approximation, it is also possible to treat inelastic scattering by the Born-Oppenheimer approximation.

tion and the internal structure by an expansion in eigenstates of the isolated species. Janssen and Moseman have recently developed a multiphonon channel treatment (MCT) which reduces to the Born-Oppenheimer approximation in the weak-coupling limit and to the Born-Oppenheimer approximation in the strong-coupling limit. The MCT is shown to be in good agreement with the results of exact calculations. The MCT is particularly useful for the description of rotational transitions in H-H collisions, while the multiphonon channel treatment is particularly useful for the description of vibrational transitions in H-He collisions.

Rotational transitions are, however, quite different in that coupled channel calculations are required for H-H collisions and for rotational scattering by rigid diatomic molecules. Rather than modifying the MCT as is done in the present paper, we propose, in this paper, a new semiclassical treatment of rotational transitions in H-H collisions. This new treatment is based on the Born-Oppenheimer approximation and is shown to be in good agreement with the results of exact calculations.

(1)

$$W_{\text{rot}}(J_f, J_i) = \frac{1}{2\pi} \int_0^{2\pi} d\phi \exp(i\phi(J_f - J_i)) \left[\frac{1}{2} (W_{\text{rot}}(J_f, J_i) + W_{\text{rot}}(J_i, J_f)) + \frac{1}{2} (W_{\text{rot}}(J_f, J_i) - W_{\text{rot}}(J_i, J_f)) \right]$$

Internal and differential cross sections for these collisions as a function of scattering angle θ will be investigated. It is worth noting that the present series of rotational transitions has been studied from various aspects.

New semiclassical treatments of rotational and vibrational transitions in heavy-particle collisions. I. H-H₂ and He-H₂ collisions*

K. J. McCann and M. R. Flannery

School of Physics, Georgia Institute of Technology, Atlanta, Georgia 30332
(Received 23 July 1975)

Two new semiclassical methods—the multistate orbital treatment and the multichannel eikonal treatment—are proposed for the description of rotational and vibrational excitation in heavy-particle collisions. The first method includes appropriate trajectories determined from a certain optical potential designed to couple the response of the internal structure, which is described by a quantal multistate expansion, to the orbit for the relative motion and vice versa. While this approach is, in general, valid when the quantal imprecision in the classical trajectories is small (as for heavy particles) the second method based on the use of a straight-line eikonal for the relative motion, of different local momenta in the various channels and of a multistate expansion for the internal motions, is valid for scattering mainly about the forward direction. These procedures are applied to representative rotational transitions in H-H₂ and He-H₂ collisions at 0.25–1.5 eV and yield angular distributions and integral cross sections in very close accord with corresponding quantal results. The methods are particularly valuable at higher impact energies when the inclusion of the resulting many rotational and vibrational channels by full quantal treatments is prohibitively difficult. Various approximate schemes—the perturbed-rotating-atoms approximation and the effective potential method—are also investigated.

I. INTRODUCTION

Recently, there has been considerable activity^{1–6} in theoretical descriptions of rotational excitation by approximate schemes all based on the full quantal close-coupling treatment.⁷ Classical studies have also been presented.⁸ The following difficulties have, however, prevented corresponding progress in finding adequate semiclassical descriptions of rotational excitation.

(i) The extraction of differential cross sections from the usual impact-parameter treatment (IPT) is not immediately obvious since the resulting first-order coupled equations⁹ naturally follow from the Dirac method of variation of constants,⁹ a time-dependent formulation.

(ii) The consequent use of a straight-line trajectory for the relative motion, adopted for the needed space-time transformation, is clearly quite invalid for rotational excitation which mainly occurs at large scattering angles θ due to the required repulsive close-encounters, particularly for neutral-neutral collisions.

(iii) While elastic scattering is mainly about the forward direction ($\theta \leq 40^\circ$), and while reasonable integral elastic cross sections can be obtained from the usual classical potential-scattering formulas,¹⁰ the elastic distributions, particularly at the larger scattering angles θ , can be affected appreciably by inelastic effects.

By appeal to a stationary-state representation of an A-B collision in which the relative motion appropriate to each channel is described by an eikonal approxima-

tion and the internal structure by an expansion of eigenstates of the isolated species, Flannery and McCann have recently developed^{11,12} a multichannel eikonal treatment (MET) which reduced to the Born-wave approximation in the weak-coupling limit and to the customary impact-parameter (IP) equations⁹ in the heavy-particle/high-energy limit. When compared with measurements and other theoretical results, this treatment achieved notable success¹¹ for *e*-H and *e*-He inelastic collisions at intermediate energies for which the dominant contribution to the integral cross sections arose from scattering through small angles $\theta \leq 40^\circ$, where electron exchange was negligible. Electronic excitation in heavy-particle collisions at keV energies, which involved only small scattering angles $\theta \leq 5^\circ$, was also described,¹² although lack of experiment and of full quantal calculations prevented complete assessment of the resulting angular distributions.

Rotational excitation is, however, quite different in that detailed quantal results are available^{5,6} for H-H₂ collisions and that inelastic scattering by angles $\theta \geq 90^\circ$ is significant. Rather than modifying MET so as to properly include the different physical trajectories for appropriate interactions, we propose, in this paper, a corresponding generalization to the heavy-particle limit of MET, i.e., to the impact-parameter prescription. The accuracy of the resulting time-dependent multistate orbital treatment, while applicable to heavy-particle collisions in general, will be assessed by comparison with the detailed quantal treatments of the collision processes^{1,5,6}

$$\left. \begin{matrix} \text{H}(1s) \\ \text{He}(1s^2) \end{matrix} \right\} + \text{H}_2(X^1\Sigma_g^+, v=0, J) - \left. \begin{matrix} \text{H}(1s) \\ \text{He}(1s^2) \end{matrix} \right\} + \text{H}_2(X^1\Sigma_g^+, v=0, J'); \quad J, J' = 0, 2, 4, 6. \quad (1)$$

Integral and differential cross sections for these collisions as a function of scattering angle θ will be investigated. It is worth noting that the present status of rotational excitation has been studied from various aspects

of molecular collisions in several recent reviews,¹³ an acknowledgment of the increased theoretical interest in this subject. In this paper, we present new developments and very recent progress in theoretical, semiclassical descriptions of rotational (and vibrational) excitation.

These treatments are termed semiclassical in that the relative motion of the collision partners is initially treated separately or decoupled from the internal structure. The classical Hamilton-Jacobi equation (i.e., the Schrödinger equation in the $\hbar \rightarrow 0$ limit) or Hamilton's equations, eikonal, JWKB, or even Born approximations describe the decoupled relative motion in the static field. This motion is then coupled to the motion of the internal degrees of freedom which are described by full quantal procedures.

II. THEORY

We propose here two new descriptions of atomic and molecular collisions—the multistate orbital treatment, valid when classical trajectories can be accurately defined (with small quantal imprecision), and the multichannel eikonal treatment, valid for scattering mainly in the forward direction and which includes different local momenta in the various excitation channels. The overlap of the two methods is difficult to assess without resort to detailed calculation.

A. The multistate orbital treatment

The time-dependent response of the internal structure of collision partners A and XY with unperturbed Hamiltonian \mathcal{H}_0 and associated eigenstates and eigenenergies ϕ_n and ϵ_n , respectively, to the mutual A-XY electrostatic interaction $V(R(t), \mathbf{r})$, with time dependence generated by variation of the channel coordinate $R(X, Y, Z)$ with time t , can be described in atomic units by

$$\Psi(\mathbf{r}, t) = \sum_n a_n(t) \phi_n(\mathbf{r}) \exp(-i\epsilon_n t), \quad (2)$$

where \mathbf{r} denotes the collective coordinates associated with the internal degrees of freedom relative to each parent center. Substitution of (2) into the time-dependent Schrödinger equation,

$$H\Psi = [\mathcal{H}_0(\mathbf{r}) + V(R(t), \mathbf{r})] \Psi = i(\partial\Psi/\partial t), \quad (3)$$

results in the following set of first-order coupled differential equations for the transition amplitudes:

$$i \frac{\partial a_n(t)}{\partial t} = \sum_k a_k(t) V_{nk}(R(t)) \exp(i\epsilon_{nk} t), \quad (4a)$$

$$\epsilon_{nk} = \epsilon_n - \epsilon_k \quad n=1, 2, \dots, \quad (4b)$$

in which the interaction matrix elements are

$$V_{nk}(R(t)) = \langle \phi_n(\mathbf{r}) | V(R(t), \mathbf{r}) | \phi_k(\mathbf{r}) \rangle. \quad (4b)$$

The customary procedure⁹ in this description then adopts a straight-line (SL) trajectory

$$R(t) = \rho + \mathbf{v}_0 t \quad (5)$$

in terms of the impact parameter $\rho(X, Y)$ and incident velocity \mathbf{v}_0 , taken constant, and directed along the Z axis (say), so as to effect the transformation $Z = v_0 t$ in

(4a), which can then be solved for the (asymptotic) transition probabilities $|a_f^{(SL)}(\rho, Z=\infty)|^2$ by standard numerical procedures to give

$$\sigma_f(v_0) = \int_0^\infty \int_0^{2\pi} |a_f^{(SL)}(\rho, \infty)|^2 d\rho \quad (6)$$

for the integral cross section for excitation of state f . By appeal to a stationary-state (rather than to a time-dependent) description of the collision, it can be shown that the heavy-particle limit to the multichannel eikonal treatment (to be discussed in Sec. II.B) yields, in terms of these $a_f^{(SL)}$,

$$\frac{d\sigma_{if}}{d\Omega} = \frac{k_f}{k_i} \left| \int_0^\infty J_\Delta(k_f \rho \sin\theta) [a_f^{(SL)}(\rho, \infty) - \delta_{if}] \rho d\rho \right|^2 \quad (7)$$

for the differential cross section for scattering through small angles θ , where k_i and k_f are the initial and final wavenumbers of relative motion, and J_Δ are Bessel functions of integral order $M_f - M_i$, the change in azimuthal quantum number of the internal structures. In the high-energy limit $k_i \approx k_f \gg 1$ and for small angle collisions (7), when integrated over all solid angles Ω reproduces the excitation cross section (6). For larger-angle scattering, a major improvement, proposed here, is based on the use of Hamilton's equations¹⁰

$$\left. \begin{aligned} \partial q_j / \partial t &= \partial \bar{\mathcal{H}} / \partial p_j \\ \partial p_j / \partial t &= -\partial \bar{\mathcal{H}} / \partial q_j \end{aligned} \right\} j=1, 2, 3 \quad (8)$$

to determine the actual variation with time t of the generalized coordinates q_j and associated conjugate momenta p_j of a particle of mass μ with the "averaged" Hamiltonian

$$\bar{\mathcal{H}} = \sum_{j=1}^3 \frac{p_j^2(t)}{2\mu} + \langle \Psi(\mathbf{r}, t) | \mathcal{H}_0(\mathbf{r}) + V(R(t), \mathbf{r}) | \Psi(\mathbf{r}, t) \rangle, \quad (9)$$

where the first term in the rhs is the kinetic energy of A-XY relative motion, $p^2(t)/2\mu$, and the second term, the expectation energy of internal motions under the interaction V at time t , is, with (2) inserted,

$$V(R(t), t) = \sum_n [|a_n|^2 \epsilon_n + \sum_k a_k^*(t) a_n(t) V_{nk}(R) e^{i\epsilon_{nk} t}], \quad (10)$$

an averaged Hamiltonian or optical potential \mathcal{U} designed to couple the response (2) of the internal A-XY structure to the perturbation V back to the relative motion and vice versa. Thus, the relative motion of the collision partners (A, XY) is coupled at all times t to the A-XY internal motions and is given by the classical solution of a particle moving under the "optical" potential \mathcal{U} instantaneously generated at time t by the internal structure averaged over its degrees of freedom. The uncoupled limit neglects this \mathcal{U} , and from (8) p_j is therefore constant, such that (5) is recovered. With this effective Hamiltonian (9), Eq. (8) therefore yields the set of additional coupled equations

$$\partial q_j / \partial t = p_j(t) / \mu, \quad j=1, 2, 3 \quad (11a)$$

and

$$\begin{aligned} \frac{\partial p_j}{\partial t} &= -\frac{\partial \mathcal{U}(R, t)}{\partial q_j}, \quad j=1, 2, 3 \\ &= -\sum_n \sum_k a_k^*(t) a_n(t) \frac{\partial V_{nk}(R(t))}{\partial q_j} \exp(i\epsilon_{nk} t) \end{aligned} \quad (11b)$$

whose solutions are coupled at all times t to the solution of (4a). For central potentials, scattering is in a plane (XZ, say), and when N eigenstates are used in (2), this procedure effectively increases the number of coupled equations from N to $N+4$. Hence, (4) and (11) are solved for the column matrix $\mathbf{a}(t) = \{a_n\}$ subject to the initial ($t=0$) boundary conditions that $X(0)=\rho$, $Z(0)=-\infty$, $(dX/dt)(0)=0$, $(dZ/dt)(0)=v_i$, and $a_n(0)=\delta_{ni}$, where i denotes the initial state.

An essential feature of the method is that the "effective" Hamiltonian \mathcal{H} is time independent. Thus, total energy is conserved and is continually being redistributed between the relative motion and the internal degrees of freedom, i.e., the time derivative

$$\frac{d\mathcal{H}}{dt} = \sum_{j=1}^3 \frac{p_j \dot{p}_j}{\mu} + \sum_{n,n'} \left[\dot{a}_n^* a_n + a_n^* \dot{a}_n + i \epsilon_{nn'} a_n^* a_n \right] H_{nn'} \times \exp(i\epsilon_{nn'} t) + \sum_{j=1}^3 \frac{\partial \mathcal{H}}{\partial q_j} \dot{q}_j, \quad H_{nn'} = \epsilon_n \delta_{nn'} + V_{nn'} \quad (12)$$

with the aid of (8) and (11a) reduces to $\partial \mathcal{H} / \partial t$, which in turn vanishes by subsequent use of (4a) for \dot{a}_n and \dot{a}_n^* .

For an incident flux of N particles/cm²/sec, a number $|a_f|^2 N d\rho$ are scattered in channel f within solid angles $d\Omega$, related to $d\rho$ by

$$d\rho = (d\sigma/d\Omega)_e d\Omega, \quad (13)$$

where $(d\sigma/d\Omega)_e$, the Jacobian of the (ρ, Ω) transformation, is the classical differential cross section for elastic scattering by the optical potential U determined previously from the solutions $\mathbf{a}(t)$ in (10). Hence

$$\frac{d\sigma_{if}}{d\Omega} = |a_f(X, Y, Z = \infty)|^2 \left[\frac{d\sigma(\mathbf{a})}{d\Omega} \right]_e \times \frac{p(t=\infty)}{p(t=0)} \quad (14)$$

is the differential cross section for $i \rightarrow f$ transitions in this time-dependent orbital method. In a one-channel case ($N=1$), the classical formulas¹⁰ for potential scattering by $V_{ii}(\mathbf{R}(t))$ are recovered. Hence this treatment is the natural semiclassical generalization of classical potential scattering to include inelastic processes.

Thus, (7) and (14) are complementary, in the sense that (7) pertains only to small angle scattering while (14) is strictly valid for well-defined trajectories \mathbf{R} , i.e., when the angular uncertainty $\delta\theta \approx (k_i R)^{-1}$ is much less than either the scattering angle $\theta \approx 2\mu V_{ii}(\mathbf{R})/k_i^2$,

when small, or unity, otherwise. Thus (14) will eventually fail in a range of very small θ , a range which is covered by the multichannel eikonal treatment (7). The angular range of overlap between the above two treatments, (7) and (14), is difficult to assess without resort to explicit calculation.

B. The multichannel eikonal treatment

In an effort to clarify more fully the basis of this method, and in the interest of providing full semiclassical descriptions of collisions involving rotational transitions, we develop in this section the present multichannel eikonal treatment by a method alternative to that previously described.¹ The wavefunction for the mutual scattering of an atom (or ion) A and a molecular species XY, in general, by their mutual interaction $V(\mathbf{r}, \mathbf{R})$ at nuclear separation $\mathbf{R}(X, Y, Z)$ is, in the cm frame,

$$\Psi_i(\mathbf{r}, \mathbf{R}) = \psi_i(\mathbf{r}) e^{i\mathbf{k}_i \cdot \mathbf{R}} + \iint d\mathbf{r}' d\mathbf{R}' G_0^+(\mathbf{r}, \mathbf{R}; \mathbf{r}', \mathbf{R}') \times V(\mathbf{r}', \mathbf{R}') \Psi_i(\mathbf{r}', \mathbf{R}'), \quad (15)$$

where the two-particle Green's function G_0^+ , appropriate to \mathcal{H}_0 , the Hamiltonian of the unperturbed system of energy E_i at infinite \mathbf{R} , satisfies

$$(E_i - \mathcal{H}_0 + i\epsilon) G_0^+(\mathbf{r}, \mathbf{R}; \mathbf{r}', \mathbf{R}') = \delta(\mathbf{r} - \mathbf{r}') \delta(\mathbf{R} - \mathbf{R}'), \quad (16)$$

in which the composite internal coordinates are denoted by \mathbf{r} relative to each parent nucleus. The free particle Green's function, which propagates the effect of the interaction V at $(\mathbf{r}', \mathbf{R}')$ to (\mathbf{r}, \mathbf{R}) , can be expanded in terms of the complete set of eigenfunctions of \mathcal{H}_0 as

$$G_0^+(\mathbf{r}, \mathbf{R}; \mathbf{r}', \mathbf{R}') = \lim_{\epsilon \rightarrow 0^+} \frac{1}{(2\pi)^3} \frac{2\mu}{\hbar^2} \sum_n \psi_n(\mathbf{r}) \psi_n^*(\mathbf{r}') \int \frac{e^{i\mathbf{k} \cdot (\mathbf{R} - \mathbf{R}')}}{(k_n^2 - k^2 + i\epsilon)} d\mathbf{k}, \quad (17a)$$

where $\psi_n(\mathbf{r})$ describes the internal structure at infinite nuclear separation \mathbf{R} , where the relative motion is planar with propagation vector $\mathbf{k}(k_x, k_y, k_z)$. For heavy-particle collisions and for electron-atom inelastic collisions at intermediate and high impact energy, scattering about the forward direction contributes most to the total cross section,^{11,12} and it is therefore a good approximation to assume that the major contributions to the propagator (17a) arises only from those waves at $Z' < Z$ with $k^2 \approx k_n^2$ such that

$$G_0^+(\mathbf{r}, \mathbf{R}; \mathbf{r}', \mathbf{R}') = \lim_{\epsilon \rightarrow 0^+} \frac{1}{(2\pi)^3} \frac{2\mu}{\hbar^2} \int_{-\infty}^{\infty} e^{i\mathbf{k}_z \cdot (\mathbf{R} - \mathbf{R}')} d\mathbf{k}_z \int_{-\infty}^{\infty} e^{i\mathbf{k}_\perp \cdot (\mathbf{R} - \mathbf{R}')} d\mathbf{k}_\perp \sum_n \psi_n(\mathbf{r}) \psi_n^*(\mathbf{r}') \left[\int_{-\infty}^{\infty} \frac{e^{i\mathbf{k}_\perp \cdot (\mathbf{R} - \mathbf{R}')}}{k_n^2 - k_\perp^2 + i\epsilon} d\mathbf{k}_\perp \right] H(Z - Z'), \quad (17b)$$

where $H(Z - Z')$ is the Heaviside step function (unity for $Z' < Z$ and zero otherwise). Hence, by contour integration and with introduction of the impact parameter $\rho(X, Y)$,

$$G_0^+(\mathbf{r}, \mathbf{R}; \mathbf{r}', \mathbf{R}') = \frac{i\mu}{\hbar^2} \sum_n \frac{e^{i\mathbf{k}_n \cdot (\mathbf{R} - \mathbf{R}')}}{k_n} \delta(\rho - \rho') H(Z - Z') \psi_n(\mathbf{r}) \psi_n^*(\mathbf{r}'). \quad (17c)$$

The reduction of (17a) to (17c) can also be obtained by the method of stationary phase (cf. Schiff¹⁴). The multichannel eikonal approximation follows by setting

$$\Psi_i(\mathbf{r}, \mathbf{R}) = \sum_m A_m(\rho, Z) \psi_m(\mathbf{r}) e^{iS_m(\mathbf{R})}, \quad (18)$$

where the eikonal S_m for the relative motion in excitation channel m under the static interaction

$$V_{mm}(\mathbf{R}) = \langle \psi_m(\mathbf{r}) | V(\mathbf{r}, \mathbf{R}) | \psi_m(\mathbf{r}) \rangle, \quad (19)$$

the diagonal elements of 4(b), satisfies

$$(\nabla S_n)^2 - i\hbar(\nabla^2 S_n) = k_n^2 - \frac{2\mu}{\hbar^2} V_{nn} = \kappa_n^2(R) \quad (20)$$

$$\Psi_i = \psi_i(r) e^{iS_i(R)} - \frac{i\mu}{\hbar^2} \sum_n \int_{R'} \frac{e^{i\kappa_n(R-R')}}{\kappa_n} \psi_n(r) \delta(\rho - \rho') H(Z - Z') \sum_{m,n} A_m(\rho', Z') V_{nm}(R') e^{iS_m(R')} d\rho' dZ'. \quad (21)$$

The projection of (21) onto the orthonormal set $\psi_n(r)$ is

$$(A_n e^{iS_n} - \delta_{ni} e^{iS_i}) e^{-i\kappa_n R} = -\frac{i\mu}{\hbar^2} \int_{R'} \frac{e^{-i\kappa_n R'}}{\kappa_n(\rho, Z')} \sum_m A_m(\rho, Z') V_{nm}(\rho, Z') e^{iS_m(\rho, Z')} dZ', \quad (22)$$

which, on differentiation, yields

$$\frac{\partial}{\partial Z} [A_n e^{i(S_n - \kappa_n Z)}] = -\frac{i\mu}{\kappa_n \hbar^2} \sum_m A_m(\rho, Z) V_{nm}(R) e^{i(S_m - \kappa_n Z)}. \quad (23)$$

Ignore the second term of the lhs of (20) and assume a straight-line trajectory along the Z axis, i.e., $|\nabla S_n| \approx \partial S_n / \partial Z \approx \kappa_n$, and $\partial \kappa_n / \partial Z \approx 0$ [equivalent to the neglect of $\nabla^2 S_n$ in (20)] such that (23) becomes

$$\frac{i\hbar^2}{\mu} \kappa_n \frac{\partial A_n}{\partial Z} = \sum_m A_m(\rho, Z) V_{nm}(R) e^{i(S_m - S_n)}, \quad (24)$$

a set of first-order coupled differential equations to be solved for A_n . Thus, for a finite number of states $n=1, 2, \dots, N$, the direct transition matrix element T_{fi} or its associated scattering amplitude f_{if} can be evaluated from

$$T_{fi} = \langle \psi_f(r) e^{iS_f(R)} | V(r, R) | \sum_n A_n \psi_n(r) e^{iS_n(R)} \rangle_{n,R} \\ = -4\pi \frac{\hbar^2}{2\mu} f_{if}(k_i, k_f) \quad (25a)$$

$$= \sum_n \langle e^{iS_f(R)} | V_{fn}(R) | A_n(\rho, Z) e^{iS_n(R)} \rangle_{\rho,Z}, \quad (25b)$$

the basis of the *multichannel eikonal treatment*. The transition matrix for rearrangement collisions between the projectile at R and a target particle at r_i is obtained from (25a) by the $R \leftrightarrow r_i$ interchange in the wavefunction for the final state f .

The above derivation therefore shows that the multichannel eikonal treatment is based on the following three assumptions: (a) the Green's function (17c); (b) $|\nabla S_n| \approx \kappa_n$; and (c) a straight-line trajectory, all included within a restricted basis set of N target states. This treatment can be immediately generalized, so that the eikonal S_n in (20) is the integral of κ_n along the actual

classical trajectory s_n appropriate to V_{nn} , with the result that the coupled set (24) are then obtained with Z replaced by s_n .

The basic formula (25a) for the scattering amplitude can be further reduced for two-particle interactions for which $V_{fn}(R) = V_{fn}(\rho, Z) \exp(i\Delta\Phi)$, where Δ is $(M_i - M_f)$, the change in azimuthal quantum number. This property permits the following definition of a phase Φ -independent transition amplitude B_f :

$$B_f(\rho, Z) = A_f(\rho, Z) \exp(-i\Delta\Phi) \exp i \int_{-\infty}^Z (\kappa_f - k_f) dZ. \quad (26)$$

After some algebraic manipulation, the scattering amplitude in (25a) can be expressed as

$$f_{if}(\theta, \phi) = -i^{M_i+1} \int_0^\infty J_\Delta(K'\rho) [I_1(\rho, \theta) - iI_2(\rho, \theta)] \rho d\rho, \quad (27)$$

where J_Δ are Bessel functions of integral order $(M_i - M_f)$, and K' is the XY component $k_f \sin \theta$ of the momentum change $K = k_i - k_f$. The collision functions

$$I_1(\rho, \theta; \alpha) = \int_{-\infty}^\infty \kappa_f(\rho, Z) \left[\frac{\partial B_f(\rho, Z)}{\partial Z} \right] \exp(i\alpha Z) dZ \quad (28)$$

and

$$I_2(\rho, \theta; \alpha) = \int_{-\infty}^\infty \left[\kappa_f(\kappa_f - k_f) + \frac{\mu}{\hbar^2} V_{ff} \right] B_f(\rho, Z) \exp(i\alpha Z) dZ \quad (29)$$

contain a dependence on the scattering angle θ via

$$\alpha = k_f(1 - \cos \theta) = 2k_f \sin^2 \frac{1}{2} \theta, \quad (30)$$

the difference between the Z component of the momentum change K and the minimum change $k_i - k_f$ in the collision. The coupling (phase Φ -independent) amplitudes B_f are solutions of the following set of N -coupled differential equations

$$\frac{i\hbar^2}{\mu} \kappa_f(\rho, Z) \frac{\partial B_f(\rho, Z)}{\partial Z} + \left[\frac{\hbar^2}{\mu} \kappa_f(\kappa_f - k_f) + V_{ff}(\rho, Z) \right] B_f(\rho, Z) = \sum_{n=1}^N B_n(\rho, Z) V_{fn}(\rho, Z) \exp i(k_n - k_f)Z, \quad f=1, 2, \dots, N \quad (31)$$

solved subject to the asymptotic boundary conditions $B_f(\rho, -\infty) = \delta_{if}$.

We note that in the absence of all couplings, except that directly connecting the initial and final channels, i.e., $B_f = \delta_{if}$, either (25b) or (27) yields

$$f_{if}(\theta, \phi) = -\frac{1}{4\pi} \frac{2\mu}{\hbar^2} \int V_{fi}(R) \exp(iK \cdot R) dR, \quad (32)$$

which is the Born-wave scattering amplitude. Obviously, that the Eqs. (28)-(31) then reduce to

$$k_f = k_i - \frac{\epsilon_{fi}}{\hbar v_i} \left(1 + \frac{\epsilon_{fi}}{2\mu v_i^2} + \dots \right) \quad \epsilon_{fi} = \epsilon_f - \epsilon_i, \quad \hbar k_i = \mu v_i, \quad (33)$$

$$f_{if}(\theta, \phi) = -i^{2\alpha+1} k_i \int_0^{\Delta} J_{\Delta}(K\rho) [C_f(\rho, \infty) - \delta_{if}] \rho d\rho, \quad (34a)$$

where $K'^2 = K^2 - \epsilon_{f,i}^2/\hbar^2 v_i^2$, and the amplitudes C_f satisfy

$$i\hbar v_i \frac{\partial C_f}{\partial Z} = \sum_{n=1}^N C_n(\rho, Z) V_{fn}(\rho, Z) \exp\left(\frac{i\epsilon_{fn}Z}{\hbar v_i}\right). \quad (34b)$$

We note on the adoption of the space-time transformation $Z = v_i t$ that the set of coupled equations (34b) is identical with (4a), which followed from a *time-dependent formulation*. Also, when the impact energy is sufficiently high ($k_i \approx k_f$) and when the scattering is into small angles θ such that $K'^2 \approx K^2 \approx 2k_i^2(1 - \cos\theta)$ can be used in (34a) together with

$$\int_{k_i - k_f}^{k_i + k_f} J_{\Delta}(K\rho) J_{\Delta}(K\rho') K dK \approx \frac{1}{\rho} (\rho - \rho') \quad (35)$$

such that (6) for the excitation cross section can be recovered¹¹ from (34a) when squared and integrated over all solid angles.

C. Interaction potentials

H-H₂ system. In order to directly compare the above semiclassical treatments with the detailed quantal results of Chu and Dalgarno,⁸ we adopt the same interaction as proposed by Wolken *et al.*¹⁵ for the H-H₂ system in the ground electronic state, i.e., the Porter-Karplus (PK) semiempirical short-range potential surface¹⁶ joined to the correct¹⁷ long-range van der Waals R^{-6} interaction. The PK surface was expanded according to¹⁵

$$V^{PK}(r, R, \theta) = \sum_{\lambda=0}^{\infty} v_{\lambda}^{PK}(r, R) P_{\lambda}(\cos\theta), \quad \cos\theta = \hat{r} \cdot \hat{R}, \quad (36)$$

where r and R are, respectively, the nuclear separation vector of H₂ and the relative channel vector. For the pure rotation transitions in (i), the interaction averaged over the ground vibrational level to give

$$V^{PK}(R, \theta) = \sum_{\lambda=0}^{\infty} v_{\lambda}^{PK}(R) P_{\lambda}(\cos\theta), \quad (37)$$

where the coefficients $v_{\lambda}(R)$ have been tabulated¹⁵ for $\lambda = 0, 2, \dots, 12$. Chu and Dalgarno⁸ have shown that the first two terms of (37) dominate the scattering and are sufficient for an accurate determination of the rotational transitions in (1).

The short-range PK contribution (37) is joined to the following correct long-range interactions¹⁷ (in eV):

$$v_0^L(R) = 511.088 \exp(-1.9R) - 251.546/R^6 \text{ (eV)}, \quad (38a)$$

$$v_2^L(R) = 346.664 \exp(-2R) - 27.8767/R^6 \text{ (eV)}, \quad (38b)$$

with R in a_0 . Thus the H-H₂ interaction, adopted here and in the full quantal treatment,⁸ has the following form:

$$V(R, \theta) = \sum_{\lambda=0}^2 v_{\lambda}^{PK}(R) P_{\lambda}(\cos\theta) \quad R \leq 4.6 a_0, \quad (39a)$$

$$V(R, \theta) = v_0^L(R) + v_2^L(R) P_2(\cos\theta) \quad 4.6 a_0 \leq R \leq 7 a_0, \quad (39b)$$

$$V(R, \theta) = v_0^L(R) + v_2^L(R) P_2(\cos\theta) \quad R \geq 7 a_0, \quad (39c)$$

where $4.6 a_0$ and $7 a_0$ are the respective intersections of v_0^L with v_0^{PK} and of v_2^L with v_2^{PK} . We note, however, that the slopes are discontinuous at the intersection points, with the result that a nonphysical rainbow effect will be evident in the semiclassical cross sections (14).

In order to compare also with the detailed quantal results of Hayes *et al.*,⁵ we also use the H-H₂ interaction of Tang,¹⁸ i.e., (37) with

$$v_0(R) = (90.2/R^4) \exp(-0.617R + 1.234) - 251.546/R^6 \text{ (eV)} \quad (40a)$$

and

$$v_2(R) = 92.04 \exp(-1.87R) - 12.92 \exp(-0.26R^2 - 0.39R) \text{ (eV)}. \quad (40b)$$

Although this potential is weaker and less anisotropic than (39) and hence will yield smaller elastic and inelastic cross sections, it is nevertheless continuous, such that no nonphysical rainbow will be evident. So as to ensure that the calculations are internally consistent, the energy levels¹⁵ used with (39) and (40) are those associated with the Morse curve.¹⁵

Matrix elements. Since H₂ is a linear molecule in the $1^1\Sigma_g^+$ ground electronic state, the eigenfunctions for the rotational state (J, M) are therefore given by the pure spherical harmonics $Y_{JM}(\hat{r})$. With the aid of (36), the interaction matrix elements (4b) appropriate for rotational transitions reduce to

$$\langle JM | V | J_0 M_0 \rangle = \sum_{\lambda=0}^{\infty} \frac{4\pi}{2\lambda+1} v_{\lambda}(R) \sum_{\mu} Y_{\lambda\mu}^*(\hat{R}) \times \int Y_{JM}^*(\hat{r}) Y_{\lambda\mu}(\hat{r}) Y_{J_0 M_0}(\hat{r}) d\hat{r}, \quad (41)$$

where

$$\int Y_{JM}^*(\hat{r}) Y_{\lambda\mu}(\hat{r}) Y_{J_0 M_0}(\hat{r}) d\hat{r} = \left[\frac{(2J_0+1)(2\lambda+1)}{4\pi(2J+1)} \right]^{1/2} \langle J_0 \lambda 0 0 | J 0 \rangle \langle J_0 \lambda M_0 \mu | J M \rangle \quad (42)$$

in terms of the Clebsch-Gordan coefficients $\langle j_1 j_2 m_1 m_2 | JM \rangle$ and where $Y_{JM}^* = (-1)^M Y_{J, -M}$ defines the phase convention. The inclusion of an extra rotational level J in the basis expansion (2) therefore implies an additional $(J+1)$ degenerate substates such that the number of coupled equations to be solved grows rapidly with each addition of J . Rabitz¹⁹ has, however, introduced an effective potential method which eliminates the M dependence in (41), thereby permitting considerable reduction in the number of equations that require solution. Thus, the orientation dependent interaction (41) is replaced by¹⁹

$$\langle J | V_{\text{eff}} | J_0 \rangle = (-1)^J [2J+1] [2J_0+1]^{1/2} \times \sum_{\lambda=0}^{\infty} \frac{v_{\lambda}(R)}{(2\lambda+1)^{1/2}} \begin{pmatrix} J & \lambda & J_0 \\ 0 & 0 & 0 \end{pmatrix}, \quad (43)$$

where

$$\eta = \frac{1}{2} (|J_0 - J| + J_0 + J) = \max(J, J_0), \quad (44)$$

and the $3j$ -symbol is either

$$\begin{pmatrix} J & \lambda & J_0 \\ 0 & 0 & 0 \end{pmatrix} = (-1)^J \left[\frac{(2g-2J)!(2g-2\lambda)!(2g-2J_0)!}{(2g+1)!} \right]^{1/2} \frac{g!}{(g-J)!(g-\lambda)!(g-J_0)!} \quad (45)$$

for integral $g = \frac{1}{2}(J + \lambda + J_0)$, or zero otherwise. Thus the use of the effective potential (43) causes a reduction, in a case where $J=0, 2, 4, 6$ rotational levels (with 16 substates) are included, from 20 coupled equations [(4a), (11a), (11b)] to 8. We also note that this procedure provides a spherical symmetric optical potential for (10) such that the solution of (11) becomes more simple than that involved with orientation-dependent interactions.

The above suggestion of Rabitz will, however, be tested in this paper by performing both explicit 16-state and four-level semiclassical calculations with the use of (41) and (43), respectively. In addition, the accuracy of the present semiclassical procedures will be assessed by direct comparison of the resulting integral and differential cross sections for various rotational transitions in the $\text{H}-\text{H}_2$ collision system at several impact energies, with the quantal results of Hayes *et al.*⁵ (who closely coupled the substates of the $J=0$ and 2 levels) and of Chu and Dalgarno⁶ [who used (43) within a quantal treatment which closely coupled the $J=0, 2, 4$, and 6 levels].

He- H_2 system. For direct comparison with the full quantal results of McGuire and Kouri,¹ the hypersurface determined by Krauss and Mies²⁰ is adopted for the He- H_2 interaction. Hence, for H_2 remaining in the ground vibrational state, the He- H_2 interaction in eV is given by (39) with v_0^{PK} and v_2^{PK} replaced by¹

$$v_0^{\text{KM}}(R) = 0.806 \exp[-3.49(R-1.6)] \text{ (eV)} \quad (46a)$$

$$v_2^{\text{KM}}(R) = 0.157 \exp[-3.47(R-1.6)] \text{ (eV)} \quad (46b)$$

for all R measured in Å.

Direct comparison with the quantal results¹ also necessitates the use of a corresponding semiclassical analogue to the " j_z -conserving method."¹ During a *slow* collision, there is a natural tendency, especially for intermediate encounters with impact parameter ρ in the range $\rho_1 < \rho < \rho_2$, for the quantization axis of each collision partner, which is fixed in the treatments developed in Secs. II.A and II.B, to follow the rotation of the internuclear vector R . This effect is acknowledged theoretically²¹ by

the "perturbed rotating-atom approximation." Hence, if the direction of R is taken as the axis of quantization of the collision species, the matrix elements, (46) in (41), are greatly simplified by setting

$$Y_{LM}(R) = Y_{L0}(R) \delta_{M0} = \left[\frac{2L+1}{4\pi} \right]^{1/2} \delta_{M0} \quad (47)$$

in (41), thereby causing a reduction in the number of coupled equations that require solution.

However, this tendency of the quantization axis to follow R becomes less for distant collisions $\rho > \rho_2$ because the perturbation is then not sufficiently strong to separate the degenerate magnetic substates, and also for close collisions, $\rho < \rho_1$, since the quantization axis of each collision partner is reluctant to follow the rapid rotation of R . These effects are, of course, theoretically acknowledged by including couplings between the M substates but are ignored in the perturbed rotating atom approximation (PRA). Therefore, the PRA approximation (or its quantal equivalent, the j_z -conserving method) is expected to be invalid (a) for distant encounters in small-angle scattering, and (b) for very close encounters in large-angle scattering, and (c) for cases involving sufficiently high relative speeds so that the quantization axis cannot adjust itself to the rapid rotation of R . The PRA approximation will be investigated further by direct calculation for He- H_2 collisions.

III. RESULTS AND DISCUSSION

A computer program was written for the solution of the coupled equations (4), (11), and (34) by the Burlish-Stoer rational extrapolation technique,²² which provided great accuracy and efficiency. A cubic spline interpolation routine was used for the interpolation of both the Porter-Karplus surface and of $(dp/d\theta)$. Multistate orbital treatments (MOT) and multichannel eikonal treatments (MET) developed previously in Secs. II.A and II.B, respectively, are applied to the following collision processes:

$$\left. \begin{matrix} \text{H}(1s) \\ \text{He}(1s^2) \end{matrix} \right\} + \text{H}_2(X^1\Sigma_g^+, v=0, J) \rightarrow \left. \begin{matrix} \text{H}(1s) \\ \text{He}(1s^2) \end{matrix} \right\} + \text{H}_2(X^1\Sigma_g^+, v=0, J') \quad J, J' = 0, 2, 4, 6 \quad (48)$$

at several impact energies E (eV), the interactions and approximations being chosen so as to provide direct comparison with corresponding full-quantal treatments carried out previously^{1,5,6} for these processes.

H- H_2 collisions: Figure 1 displays differential cross sections for $0 \rightarrow 0$ elastic collisions at 1 eV determined from (a) a four-level ($J=0, 2, 4, 6$) optical-potential orbital treatment MOT, (b) a one-state pure classical orbital description ($|a_i|=1$), and (c) a four-channel eikonal

treatment MET, together with (d) the corresponding multi-channel quantal results Q of Chu and Dalgarno⁶ (who used the technique of Rabitz¹⁹). The influence of inelastic effects on elastic scattering is manifested quite clearly by the difference between (a) and (b). Thus, while essential agreement exists at small angles between (a) and (b), inelastic effects become increasingly important with larger scattering angles θ , as expected, since rotational excitation primarily results from close encounters. Comparison between (a) and (d) demon-

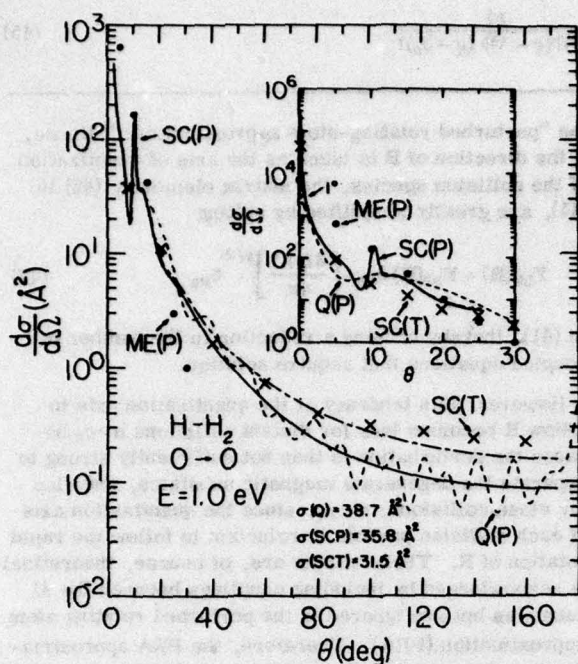


FIG. 1. Differential cross section ($\text{\AA}^2/\text{sr}$) vs scattering angle θ° for $\text{H}-\text{H}_2$ ($J=0$) elastic collisions at 1 eV. —: Present four-state ($J=0, 2, 4, 6$) orbital treatment SC; ---: one-state classical treatment; ---: Quantal treatment Q; four-state eikonal treatment ME: (P) or (T) denotes use of Porter-Karplus surface¹⁵ or of interaction of Tang,¹⁸ respectively.

states that inclusion of inelasticity, as in (a), is required so as to preserve accord with the full quantal results (d) for the "background" scattering (i.e., with

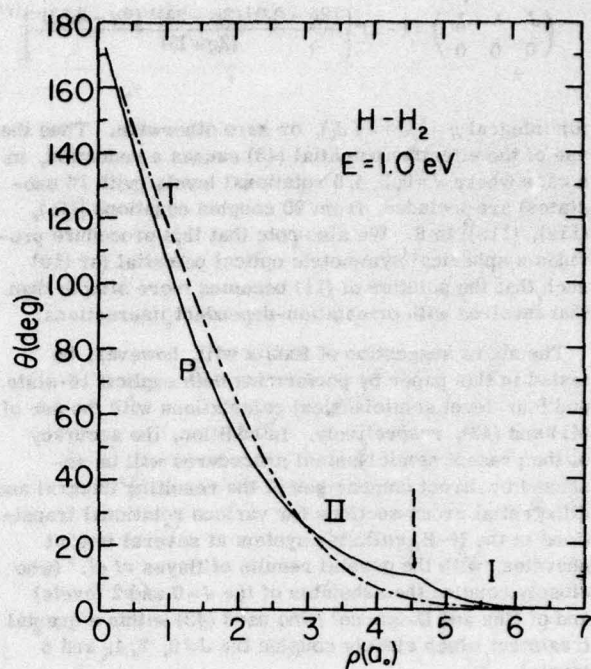


FIG. 3. Asymptotic impact-parameter ρ vs θ for $\text{H}-\text{H}_2$ scattering at 1 eV determined from Tang potential T and from potential P explained in text. Region I refers to contribution from long-range portion of P and II refers to the short-range Porter-Karplus surface. Nonphysical rainbow indicated by arrow.

quantal oscillations, due to phase-shift interference, removed) for $\theta > 30^\circ$. Also, in spite of the validity in describing large-angle scattering, a one state pure classical orbit is therefore inadequate, e.g., calcula-

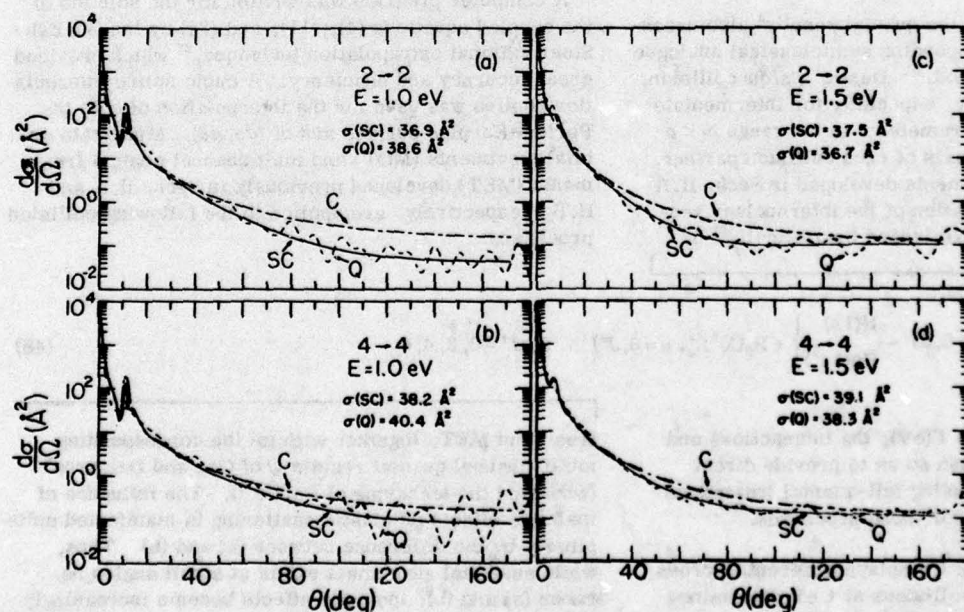


FIG. 2. Differential cross sections ($\text{\AA}^2/\text{sr}$) for the 2→2 and 4→4 elastic transitions in $\text{H}-\text{H}_2$ collisions at energies indicated. SC: present four-state semiclassical treatment; C: one-state classical treatment; Q: Quantal results.⁶ Interaction P and effective potential method¹⁵ used. Integral cross sections $\sigma(M)$ for a given treatment M.

TABLE I. Integral cross sections (\AA^2) for $\text{H} + \text{H}_2(J) \rightarrow \text{H} + \text{H}_2(J')$ at impact energies $E(\text{eV}) = 0.5, 1, \text{ and } 1.5$.

$E(\text{eV})$ $J \rightarrow J'$	0.5			1.0			1.5		
	(A)	(B)	(C)	(A)	(B)	(C)	(A)	(B)	(C)
0-0	37.2	39.0	41.2	35.8	37.7	38.7	36.7	37.3	37.1
2-2	39.8	40.8	41.3	36.9	38.4	38.6	37.5	39.0	36.7
4-4	41.9	43.7	43.3	38.2	39.9	40.4	39.1	39.6	38.3
6-6	41.6	43.1	45.4	40.2	41.7	42.6	41.8	42.4	40.4
0-2	4.37	4.17	4.02	5.16	5.04	5.00	4.58	4.51	4.44
2-0	0.81	0.85	0.88	1.00	1.02	1.05	0.90	0.91	0.92
2-4	1.07	0.96	0.83	1.86	1.76	1.75	1.78	1.72	1.70
4-2	0.60	0.66	0.45	1.04	1.09	1.01	0.99	1.02	1.03
4-6	0.26	0.22	0.014	0.85	0.78	0.48	0.96	0.91	0.83
6-4	0.18	0.21	0.018	0.587	0.631	0.43	0.66	0.69	0.63
0-4	0.228	0.192	0.104	0.507	0.468	0.437	0.375	0.356	0.344
4-0	0.020	0.023	0.017	0.054	0.058	0.055	0.041	0.043	0.043
2-6	0.014	0.010	0.0004	0.086	0.074	0.046	0.082	0.075	0.068
6-2	0.005	0.006	0.0004	0.033	0.037	0.024	0.031	0.034	0.030
0-6	$2.1 \cdot 10^{-4}$	$1.32 \cdot 10^{-4}$	$4.2 \cdot 10^{-5}$	0.013	0.011	0.007	0.010	0.009	0.008
6-0	$1.0 \cdot 10^{-4}$	$1.3 \cdot 10^{-4}$	$8.5 \cdot 10^{-5}$	0.001	0.001	0.001	$7.0 \cdot 10^{-4}$	$8.0 \cdot 10^{-4}$	$1.0 \cdot 10^{-3}$

Column (A): Present semiclassical four-level^b orbital treatment MOT ($J=0, 2, 4, 6$).

Column (B): Elastic scattering. Four-level^b eikonal approximation MET ($0 \leq \theta \leq 20^\circ$) combined with MOT for $\theta \geq 20^\circ$.

Column (B): Inelastic scattering. Present semiclassical MOT cross sections $\times (k_f/k_i)$.

Column (C): Corresponding four-level^b quantal treatment^a Q .

^aExponent gives power of 10 by which entry is to be multiplied.

^bEffective potential method¹⁹ used in all treatments.

tion shows that the probability for H_2 remaining rotationless at $\theta > 80^\circ$ is ~ 0.5 , rather than unity, as in (b).

Figure 2, a display of the 2-2 and 4-4 transitions at two impact-energies, shows again that inclusion of inelasticity is needed to introduce harmony with the quantal distributions. The inelastic effects are controlled by the variation with θ and E of the cross sections for rotational excitation. The semiclassical and integral cross sections given in Fig. 2 show good agreement.

However, the one oscillation observed in the semiclassical distributions, in both Figs. 1 and 2, at $\sim 10^\circ$ arises directly from a nonphysical rainbow effect introduced by the artificial graft of the short-range potential (37), to yield (39) as the full interaction P . Figure 3 isolates this rainbow, by exhibiting an infinite $(dp/d\theta)$ in the variation of p vs θ for $\text{H}-\text{H}_2$ collisions at 1 eV. The rainbow angle (at which $dp/d\theta \rightarrow \infty$) decreases with increase of E . Figure 3 also shows that this nonphysical rainbow vanishes on using the Tang interaction T , Eq. (40), which is continuous. The full quantal values based on p and θ given at 5° intervals in Figs. 1 and 2 also contain this effect, although in contrast to the semiclassical results, all angular momenta (or p) contribute here to a given θ , thereby causing an averaged and suppressed effect, evident in the inset of Fig. 1. Because of this peculiarity, strict comparison between (a) MOT, (b) MET, and (d) the quantal results are precluded in the angular range $5^\circ \leq \theta \leq 20^\circ$ about the rainbow angle. The inset in Fig. 1 illustrates the very slow divergence of the semiclassical MOT results for scattering in the forward direction. With the aid of Fig. 3, the quantal imprecision to scattering by small angles $\sim (k_i R)^{-1} \sim 1^\circ$ at 1 eV.

In order to obtain the actual inelastic cross sections σ from those $\bar{\sigma}$ determined directly from the effective po-

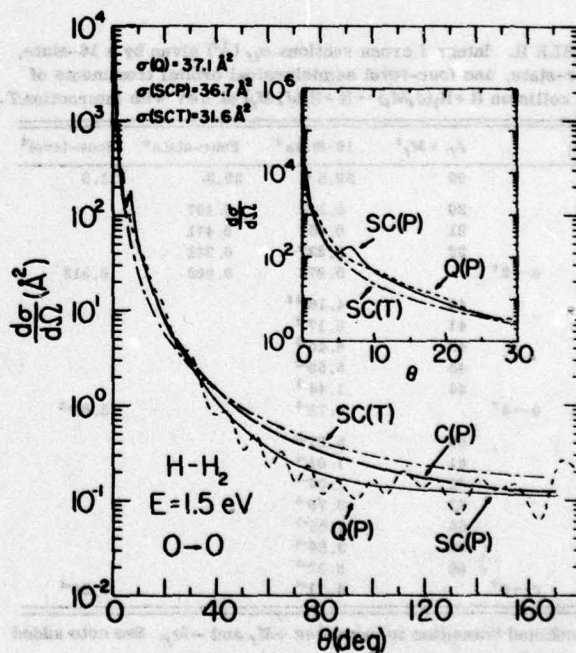


FIG. 4. Differential cross sections ($\text{\AA}^2/\text{sr}$) for $J=0 \rightarrow 0$ elastic $\text{H}-\text{H}_2(J)$ collisions at 1.5 eV. SC(P), SC(T): Present four-state ($J=0, 2, 4, 6$) orbital treatment simplified by effective potential method R of Rabitz¹⁹ and determined from interactions P^{15} and T^{15} , respectively. C(P): Present one-state pure classical treatment with interaction P . Q(P) corresponding quantal results determined from interaction P within method R .

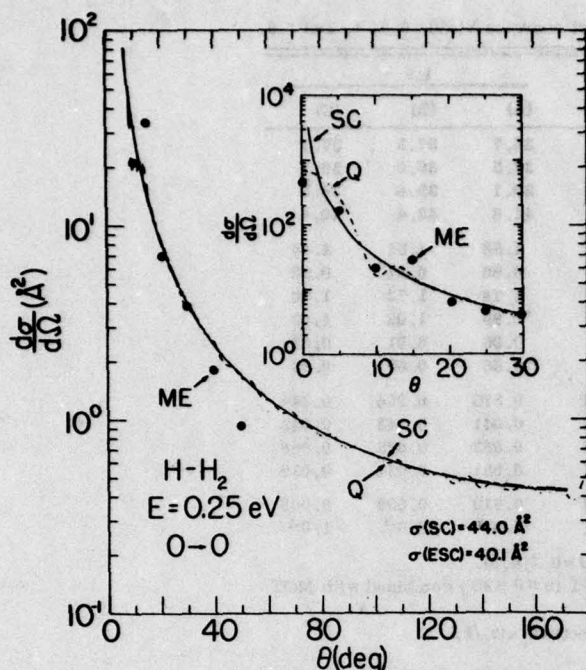


FIG. 5. Differential cross sections ($\text{\AA}^2/\text{sr}$) for $J=0 \rightarrow 0$ elastic $\text{H}-\text{H}_2(J)$ collisions at 0.25 eV. SC: Present four-state ($J, \pm M = 0, 0; 2, 0; 2, 1; 2, 2$) orbital treatment. ME: Present four-state eikonal treatment. Q: corresponding quantal results.⁵ $\sigma(\text{SC})$: integral SC cross section. $\sigma(\text{ESC})$: integral cross section determined from combination of ME for $0 \leq \theta \leq 30^\circ$ and of SC for $\theta > 30^\circ$.

TABLE II. Integral cross sections σ_{if} (\AA^2) given by a 16-state, four-state, and four-level semiclassical orbital treatments of the collision $\text{H} + \text{H}_2(J_i M_i) \rightarrow \text{H} + \text{H}_2(J_f M_f)$ at 1 eV with interaction T.

$J_i M_i$	$J_f, \pm M_f^a$	16-State ^b	Four-state ^c	Four-level ^d
00	00	39.5	39.5	31.5
00	20	0.165	0.197	
00	21	0.451	0.471	
00	22	0.237	0.241	
	0-2 ^e	0.873	0.909	0.913
00	40	4.16×10^{-3}		
00	41	8.17×10^{-3}		
00	42	8.40×10^{-3}		
00	43	5.59×10^{-3}		
00	44	1.44×10^{-3}		
	0-4 ^e	2.78×10^{-2}		2.03×10^{-2}
00	60	5.01×10^{-5}		
00	61	1.04×10^{-4}		
00	62	1.02×10^{-4}		
00	63	9.70×10^{-5}		
00	64	7.55×10^{-5}		
00	65	3.54×10^{-5}		
00	66	6.92×10^{-6}		
	0-6 ^e	4.71×10^{-4}		2.26×10^{-4}

^aCombined transition to substates $+M_f$ and $-M_f$. See note added in proof.

^bInclusion of all substates $\pm M$ of $J=0, 2, 4$, and 6 rotational levels.

^cInclusion of all substates of $J=0$ and 2 rotational levels.

^dInclusion of $J=0, 2, 4$, and 6 levels within effective potential method¹⁹ of Rabitz.

^eTransition between rotational levels specified.

^fExponent gives power of 10 by which entry is to be multiplied.

tential method,¹⁹ the following transformation²³ was adopted:

$$\frac{d\sigma}{d\Omega}(J_1 \rightarrow J_2) = \left[\frac{2J_2 + 1}{2J_1 + 1} \right]^{1/2} \frac{d\sigma}{d\Omega}(J_1 \rightarrow J_2), \quad J_2 > J_1. \quad (49)$$

In Table I we present values of the integral cross sections

$$\sigma_{if} = \int |a_f|^2 \frac{d\sigma(a)}{d\Omega} d\Omega = 2\pi \int_0^\infty |a_f|^2 \rho d\rho \quad (50)$$

and of $(k_f/k_i)\sigma_{if}$ for all the elastic and inelastic transitions in (48). Although the ratio (k_f/k_i) does not follow exactly from the present semiclassical treatment, its inclusion nonetheless introduces even better accord of the semiclassical cross sections with the full quantal results. The agreement is very good for the elastic and the stronger inelastic transitions ($\Delta J=2$) and is improving for the weaker $\Delta J=4$ transitions as E increases ~ 1.5 eV.

Figure 4, a display of the angular distribution in $\text{H}-\text{H}_2$ collisions at 1.5 eV, confirms that the nonphysical rainbow present with interaction P vanishes on using the continuous interaction T (see also Fig. 1). It also shows that the uncertainty in the $\text{H}-\text{H}_2$ interaction, as evidenced by the differences entailed in using P and T , introduces error greater than the neglect of inelastic effects. Potential T is (a) less anisotropic than P , such that inelastic effects are reduced and elastic scattering is therefore enhanced at large θ , and is also (b) weaker

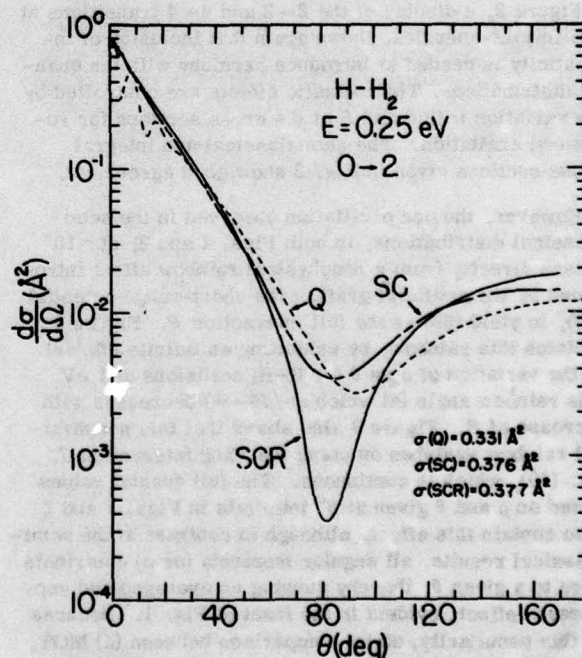


FIG. 6. Differential cross sections ($\text{\AA}^2/\text{sr}$) for the $J=0 \rightarrow 2$ inelastic transition in $\text{H}-\text{H}_2(J=0)$ collisions at 0.25 eV. SC: present four-state ($J, \pm M=0, 0; 2, 0; 2, 1; 2, 2$) orbital treatment. SCR: present two-state ($J=0, 2$) orbital treatment simplified by use of effective potential method of Rabitz.¹⁹ Q: quantal results⁵ corresponding to SC. $\sigma(T)$: integral cross sections given by each of the above three treatments T .

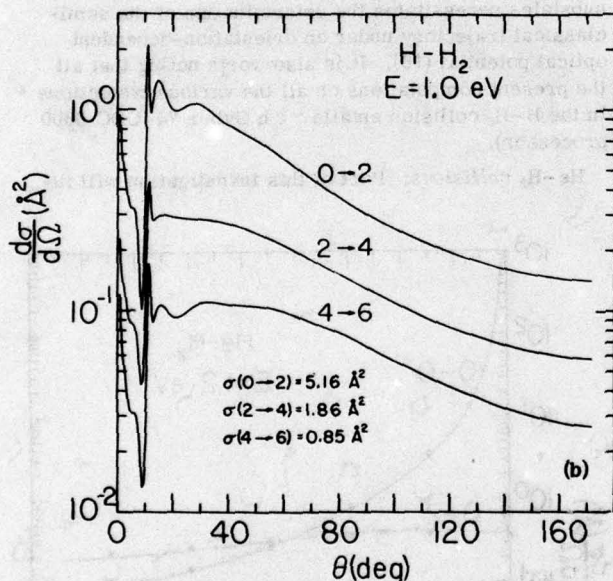
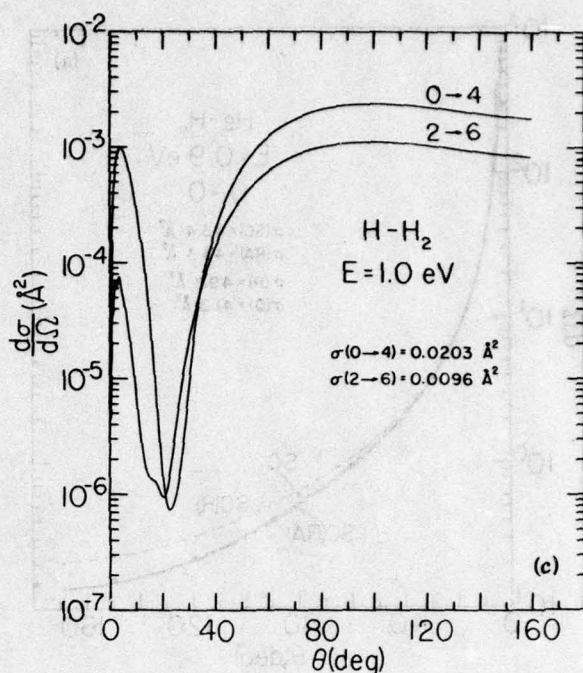
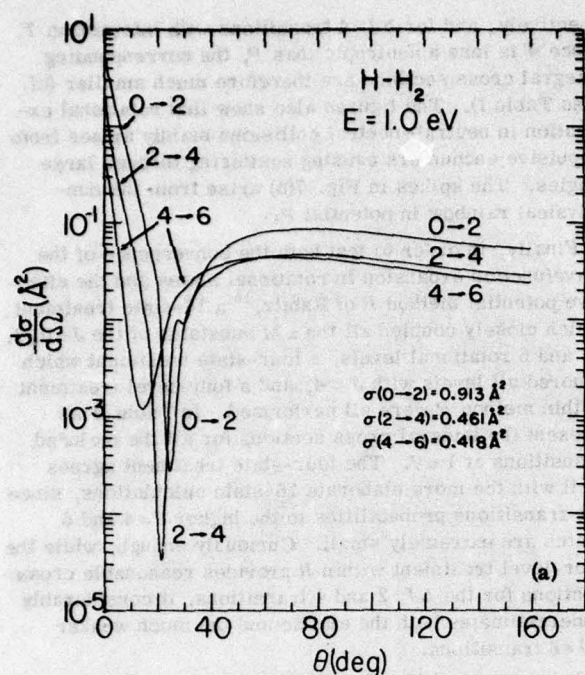


FIG. 7(a). Present differential cross sections for rotational excitation in $\text{H}-\text{H}_2$ collisions at 1 eV. Transitions $J \rightarrow J'$ indicated on each distribution. $\sigma(J \rightarrow J')$: Integral cross sections. Interaction T used within R method.¹⁹ (b) Present four-state orbital treatment of differential cross sections for 0-2, 2-4, 4-6 rotational transitions in $\text{H}-\text{H}_2$ collisions at 1 eV. Interaction P used within R method.¹⁹ (c) Present four-state orbital treatment of differential cross sections for 0-4 and 2-6 transitions in $\text{H}-\text{H}_2$ collisions at 1 eV. Interaction T used within R method.¹⁹

at large distances with, consequently, less elastic scattering by $\theta \leq 20^\circ$ which provides most of the integral cross section which is therefore reduced.

Figure 5 exhibits the impressive agreement of the quantal differential cross sections of Hayes *et al.*⁵ (who used potential T) at 0.25 eV with both the corresponding four-state eikonal and four-state orbital treatments, in which the substates $(J, \pm M) = (0, 0)$, $(2, 0)$, $(2, 1)$, and $(2, 2)$ are closely coupled. The eikonal treatment successfully describes scattering by $\theta < 30^\circ$, while the orbital description is excellent for $\theta > 5^\circ$.

Figure 6 shows that the differential cross sections for

the $J=0 \rightarrow 2$ rotational transition in H_2 by H impact at 0.25 eV are much smaller than those for the elastic case, in accord with the small inelastic effects evident in Fig. 4 when interaction T is used. The present semiclassical results are finite for scattering in the forward direction (since a_r tends to zero for these distant encounters) and are in general harmony with the quantal distribution¹ Q . While the procedure of Rabitz¹⁹ introduces a deeper minimum in the angular distribution, the integral cross sections are essentially unaffected. The semiclassical integral cross sections $\sigma(\text{SC})$ displayed in Fig. 6 are calculated from (12) alone; multiplication of (12) by the ratio (k_f/k_i) yields $\sigma(\text{SC}) = 0.34 \text{ Å}^2$, in closer

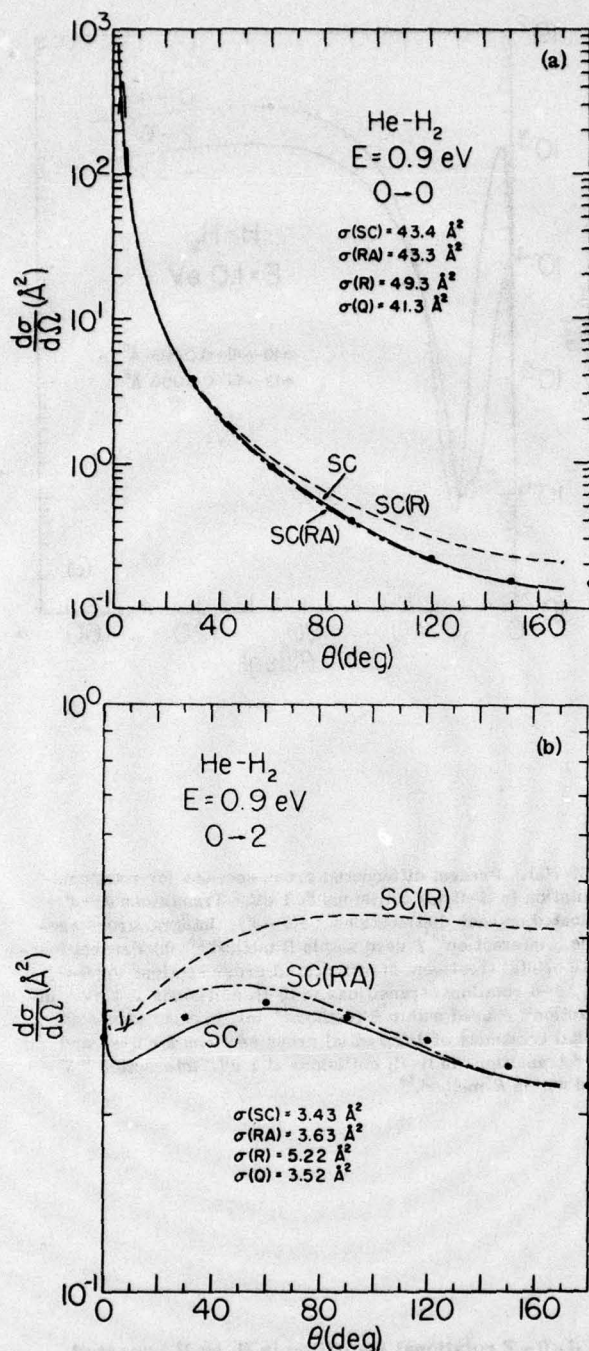


FIG. 8. Differential cross sections ($\text{\AA}^2/\text{sr}$) (a) for elastic scattering and (b) $J=0 \rightarrow 2$ transitions in He-H₂ ($J=0$) collisions at 0.9 eV. SC: Present nine-state orbital treatment alone, with rotating axis approximation RA, or with effective potential method¹⁹ R. σ : Corresponding integral cross sections obtained from ρ integration in (50). Q : \bullet , quantal j_z -conserving treatment.¹

accord with the quantal result.

Figures 7(a)-7(c) illustrate differential cross sections for $\Delta J=2$ transitions with interactions T and P , re-

spectively, and for $\Delta J=4$ transitions with interaction T . Since T is less anisotropic than P , the corresponding integral cross sections are therefore much smaller (cf. also Table I). The figures also show that rotational excitation in neutral-neutral collisions mainly arises from repulsive encounters causing scattering through large angles. The spikes in Fig. 7(b) arise from the non-physical rainbow in potential P .

Finally, in order to test both the convergence of the wavefunction expansion in rotational states and the effective potential method R of Rabitz,¹⁹ a 16-state treatment which closely coupled all the $\pm M$ substates of the $J=0, 2, 4$, and 6 rotational levels, a four-state treatment which ignored all levels with $J \geq 4$, and a four-level treatment within method R were all performed. In Table II we present the integral cross sections for all the included transitions at 1 eV. The four-state treatment agrees well with the more elaborate 16-state calculations, since the transitions probabilities to the higher $J=4$ and 6 states are extremely small. Curiously enough, while the four-level treatment within R provides reasonable cross sections for the $\Delta J=2$ and 4 transitions, it considerably underestimates both the elastic and the much weaker $\Delta J=6$ transitions.

It is important to note that the inclusion of the M substates necessitates the determination of the semi-classical trajectory under an orientation-dependent optical potential (10). It is also worth noting that all the present computations on all the various transitions in the H-H₂ collision entails ~ 1 h Cyber 74 (CDC 6600 processor).

He-H₂ collisions: Part of this investigation will in-

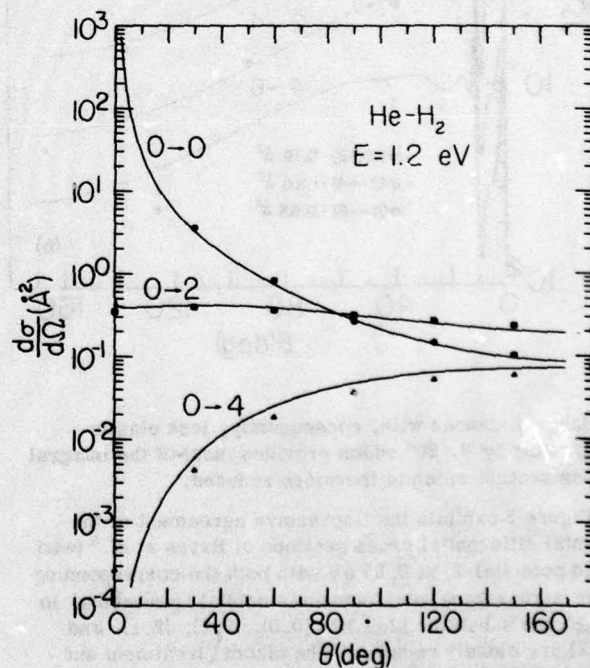


FIG. 9. Differential cross sections ($\text{\AA}^2/\text{sr}$) for $J=0 \rightarrow 0$, $0 \rightarrow 2$, and $0 \rightarrow 4$ transitions in He-H₂ ($J=0$) collisions at 1.2 eV. \bullet , Δ : corresponding quantal results.¹

volve direct comparison with the full quantal results of McGuire and Kouri,¹ who closely coupled the $J=0, 2$, and 4 rotational levels within the j_s -conserving method and who adopted the interaction (46) determined from that given by Krauss and Mies.²⁰ The accuracy of the rotating axis approximation PRA will also be assessed.

In Table III we present differential cross sections for elastic scattering in He-H₂ ($J=0$) collisions at 0.9 eV determined from the following three semiclassical schemes: (a) the present multistate orbital treatment MOT with all the substates ($J, \pm M=0, 0; 2, 0; 2, 1; 2, 2; 4, 0; 4, 1; 4, 2; 4, 3; 4, 4$) closely coupled, (b) MOT with the (0, 0) (2, 0) and (4, 0) substates closely coupled within the PRA approximation, and (c) MOT with the $J=0, 2$, and 4 levels closely coupled within the effective potential method. Columns 2-4 in Table III illustrate the effect of the above approximations (a)-(c), respectively, the accuracy of which can be assessed by comparing with the full quantal results (d) and (e) in columns 5 and 6, which are the respective quantal analogues of approximations (a) and (b). The agreement between (a) and (d) and between (b) and (e) can be considered as excellent. We note that the PRA approximation (b) is somewhat inadequate for small-angle scattering, i.e., distant encounters, as expected. Its closeness with (a) for large-angle scattering simply indicates that the required repulsive encounters are not sufficiently close to cause breakdown of this approximation. The PRA approximation which causes some decrease in the scattering through small angles is therefore apparently successful in describing elastic collisions at 1 eV, since here both the distant and close encounters, at which it fails, are not important. On the other hand, the effective potential method¹⁹ consistently overestimates the cross section.

Table IV presents similar findings for the 0-2 rota-

TABLE III. Differential ($\text{\AA}^2/\text{sr}$) and integral cross sections $\sigma(\text{\AA}^2)$ given by various treatments of He-H₂ ($J=0$) elastic scattering at 0.9 eV.

θ	Multistate orbital treatment			Quantal treatment	
	a (Nine-state)	b (PRA)	c (R)	d (cc)	e (cs)
0	(9.12) ^f	(9.12) ^g	(1.54) ^h	8.45 ⁱ	8.45 ^j
30	3.601	3.561	3.714	3.61	3.58
60	0.941	0.906	1.062	0.960	0.935
90	0.394	0.382	0.507	0.414	0.398
120	0.212	0.209	0.306	0.227	0.219
150	0.148	0.147	0.224	0.157	0.152
165	0.136	0.135	0.207	0.145	0.140
$\sigma(\text{\AA}^2)^k$	43.4	43.3	49.3	41.3	41.1

^aPresent nine-state ($J, \pm M=0, 0; 2, 0; 2, 1; 2, 2; 4, 0; 4, 1; 4, 2; 4, 3; 4, 4$) orbital treatment.

^bThree-state (0, 0; 2, 0; 4, 0) rotating-atom orbital treatment.

^cThree-level ($J=0, 2, 4$) orbital treatment within effective potential method.¹⁹

^dNine-state close-coupling quantal method.¹

^e j_s -Conserving quantal method.¹

^fExponent gives power of 10 by which entry is to be multiplied. Parentheses denote values at 0.6° which are closest to the quantal values at 0° scattering.

^gObtained from θ integration in (50).

TABLE IV. Differential ($\text{\AA}^2/\text{sr}$) and integral cross sections $\sigma(\text{\AA}^2)$ given by various treatments of the $J=0-2$ rotational transition in He-H₂ ($J=0$) collisions at 0.9 eV.

θ	a (Nine-state)	b (PRA)	c (R)
0	2.62 ^d	2.89	5.76
30	2.78	3.20	3.56
60	3.02	3.29	4.18
90	2.87	2.99	4.38
120	2.55	2.60	4.31
150	2.32	2.31	4.19
165	2.26	2.24	4.14
$\sigma(\text{\AA}^2)^e$	3.41	3.61	5.19
Quantal	3.33 ^g	3.52 ^f	...

^aPresent nine-state ($J, \pm M=0, 0; 2, 0; 2, 1; 2, 2; 4, 0; 4, 1; 4, 2; 4, 3; 4, 4$) orbital treatment.

^bThree-state (0, 0; 2, 0; 4, 0) rotating-atom orbital treatment.

^cThree-level ($J=0, 2, 4$) orbital treatment within effective potential method.¹⁹

^dAll the entries for the differential cross sections are to be multiplied by 0.1.

^eNine-state close-coupling quantal method.¹

^f j_s -Conserving quantal method.¹

^gObtained from θ integration in (50).

tional excitation except that the PRA approximation enhances all scattering but through the largest angles. The agreement of (a) and (b) with the corresponding quantal integral cross sections is very good.

Figure 8 exhibits quite clearly the effect of the various approximations. Finally, Figure 9 illustrates the relative importance of the $\Delta J=0, 2$, and 4 transitions in He-H₂ collisions at 1.2 eV and shows excellent agreement between the present semiclassical and quantal angular distributions.

In conclusion, two new semiclassical treatments of rotational transitions in heavy-particle collisions have been presented and their accuracy assessed by comparison with the detailed quantal angular distributions and integral cross sections. These methods would prove particularly valuable for high-energy collisions when the inclusion of the many rotational and vibrational channels, which is prohibitively difficult and time consuming in full quantal treatments, is relatively straightforward. Moreover, as mentioned in the introduction and in Sec. II.B, the multichannel eikonal treatment can be generalized so as to include appropriate trajectories with the result that electron-molecule collisions can be described. Also, preliminary semiclassical treatments of other collisions, e.g., the Li⁺-H₂, Li⁺-N₂, and H-HF systems for which the interactions are stronger, have longer range and are more anisotropic than those evident in the present neutral-neutral collisions, reveal that the present procedures are extremely successful when compared with full quantal treatments.^{4,24}

Note added in proof: For a given rotational level J , the associated $(2J+1)$ substates M are explicitly acknowledged in the basis set expansions (2) and (18). The

$\frac{1}{2}(J^* + 1)(J^* + 2)$ coupled equations (4a) and (31) resulting from such an expansion which included $J = 0, 2, 4, \dots, J^*$ levels were, in the present study, reduced by parity arguments, to $\frac{1}{2}(J^* + 2)^2$ coupled equations with explicit account taken of nonzero couplings between all the M sublevels.

*This research was sponsored by the Air Force Research Laboratories, Air Force Systems Command, United States Air Force, Contract F 33615-74-C-4003.

¹P. McGuire, and D. J. Kouri, *J. Chem. Phys.* **60**, 2488 (1974).

²H. Rabitz and G. Zarur, *J. Chem. Phys.* **61**, 5076 (1975).

³M. H. Alexander, *J. Chem. Phys.* **61**, 5167 (1975).

⁴J. Schaefer and W. A. Lester, Jr., *J. Chem. Phys.* **62**, 1913 (1975).

⁵E. F. Hayes, C. A. Wells, and D. J. Kouri, *Phys. Rev. A* **4**, 1017 (1971).

⁶S.-I. Chu and A. Dalgarno, *Astrophys. J.* **199**, 637 (1975).

⁷A. M. Arthurs and A. Dalgarno, *Proc. R. Soc. London Ser. A* **256**, 540 (1960).

⁸R. La Budde and R. B. Bernstein, *J. Chem. Phys.* **59**, 3687 (1973).

⁹D. R. Bates, *Quantum Theory. Elements I* (Academic, New York, 1961), pp. 251-297.

¹⁰H. Goldstein, *Classical Mechanics* (Addison Wesley, Reading, MA, 1965), pp. 217-221.

¹¹M. R. Flannery and K. J. McCann, *J. Phys. B* **7**, 2518 (1974); **7**, L522 (1974); **8**, 1716 (1975): ϵ -atom inelastic scattering.

¹²M. R. Flannery and K. J. McCann, *Phys. Rev. A* **8**, 2915 (1973); **9**, 1947 (1974); *J. Phys. B* **7**, 840 (1974); **7**, 1349 (1974); **7**, 1558 (1974): atom-atom and ion-atom elastic and inelastic scattering.

¹³Reviews: W. A. Lester, *Adv. Quantum Chem.* **9**, 211 (1975); W. H. Miller, *Adv. Chem. Phys.* **25**, 63 (1974); H. Rabitz, *Mod. Theor. Chem.* (to be published).

¹⁴L. I. Schiff, *Phys. Rev.* **103**, 443 (1956).

¹⁵G. Wolken, W. H. Miller, and M. Karplus, *J. Chem. Phys.* **56**, 4930 (1972).

¹⁶R. N. Porter and M. Karplus, *J. Chem. Phys.* **40**, 1105 (1964).

¹⁷A. Dalgarno, R. J. W. Henry, and C. S. Roberts, *Proc. Phys. Soc. London* **88**, 611 (1966).

¹⁸K. T. Tang, *Phys. Rev.* **187**, 122 (1969).

¹⁹H. Rabitz, *J. Chem. Phys.* **57**, 1718 (1972).

²⁰M. Krauss and F. Mies, *J. Chem. Phys.* **42**, 2703 (1965).

²¹D. R. Bates, *Proc. R. Soc. London Ser. A* **240**, 437 (1957).

²²R. Burlisch and J. Stoer, *Numerische Math.* **8**, 1 (1966).

²³G. Zarur and H. Rabitz, *J. Chem. Phys.* **60**, 2057 (1974).

²⁴L. A. Collins and N. F. Lane, *Phys. Rev.* (to be published).

The Multichannel Eikonal Treatment of Electron-Atom Collisions

M. R. FLANNERY AND K. J. MCCANN

A multichannel treatment of atomic collisions is presented and applied to the excitation of atomic hydrogen and helium by electrons with incident energy above the ionization threshold. The calculated cross sections compare very favourably with other refined theoretical procedures and with various experiments.

Introduction

A variety of methods have been proposed for the theoretical description of electron-atom collisions at low and intermediate energies. The close-coupling expansion with its pseudostate modifications (Burke and Webb, 1970) and the polarized-orbital distorted-wave model of McDowell *et al.* (1973) are among those that follow from the full wave treatment of the collision. Other methods, termed semiclassical—the eikonal approximations of Bates and Holt (1966), Callaway (1968), Byron (1971), and of Chen *et al.* (1972), the impact parameter approach (Bransden and Coleman, 1972), and the Glauber approximation (cf. Tai *et al.*, 1972)—all essentially separate the relative motion of the incident electron (described by an eikonal-type or Born wave function for the electron in a static field) from the internal electronic motions of the atomic system which is described by a multistate expansion. In this paper, a new generalization of the eikonal approximation to multichannel scattering is presented.

M. R. FLANNERY and K. J. MCCANN • School of Physics, Georgia Institute of Technology
Atlanta, Georgia 30332, U.S.A.

Theory

Consider the collision of a particle B of mass M_B and incident velocity v_i along the Z axis with a one-electron atomic system (A + e) of mass ($M_A + m$). The subsequent analysis can be immediately generalized so as to cover multielectron systems. Let \mathbf{R} , \mathbf{R}_B , \mathbf{r} , and \mathbf{r}_e denote the A-B, B-(Ae) center of mass, e-(AB) center of mass, and e-A separations, respectively. In the (ABe) center-of-mass reference frame, the scattering amplitude for a direct transition between an initial state i and a final state f of the collision system, of reduced mass μ , is

$$f_{if}(\theta, \varphi) = -\frac{1}{4\pi} \frac{2\mu}{\hbar^2} \langle \Psi_f(\mathbf{k}_f; \mathbf{r}, \mathbf{R}) | V(\mathbf{r}, \mathbf{R}) | \Psi_i^+(\mathbf{k}_i; \mathbf{r}, \mathbf{R}) \rangle_{\mathbf{r}, \mathbf{R}} \quad (1)$$

in which $V(\mathbf{r}, \mathbf{R})$ is the instantaneous electrostatic interaction between the collision species, and where the scattering is directed along the final relative momentum $\hbar\mathbf{k}_f$ ($1, \theta, \varphi$). The final stationary state of the isolated atoms in channel f is Ψ_f , and Ψ_i^+ is the solution of the time-independent Schrödinger equation,

$$\left[-\frac{\hbar^2}{2\mu} \nabla_{\mathbf{R}}^2 + H_e(\mathbf{r}) + V(\mathbf{r}, \mathbf{R}) \right] \Psi_i^+(\mathbf{r}, \mathbf{R}) = E_i \Psi_i^+(\mathbf{r}, \mathbf{R}) \quad (2)$$

solved subject to the asymptotic boundary condition

$$\Psi_i^+(\mathbf{r}, \mathbf{R}) \xrightarrow{\text{large } R} \sum_n \left[e^{i\mathbf{k}_n \cdot \mathbf{R}_B} \delta_{ni} + f_{in}(\theta, \varphi) \frac{e^{i\mathbf{k}_n \cdot \mathbf{R}_B}}{R_B} \right] \varphi_n(\mathbf{r}_e) \quad (3)$$

in which $\varphi_n(\mathbf{r}_e)$ are eigenfunctions of the Hamiltonian $H_e(\mathbf{r}) \approx H_e(\mathbf{r}_e)$ for the isolated atomic system (A + e) with internal electronic energy ϵ_n such that the total energy E_i in channel i is $\epsilon_i + \hbar^2 k_i^2 / 2\mu$, which is conserved throughout the collision.

The Multichannel Eikonal Approximation

The eikonal approximation to (2) sets

$$\Psi_i^+(\mathbf{r}, \mathbf{R}) = \sum_n A_n(\rho, Z) \exp i S_n(\rho, Z) \varphi_n(\mathbf{r}_e) \exp \left\{ i \left(\frac{m}{M_A + m} \mathbf{k}_n \cdot \mathbf{r}_e \right) \right\} \quad (4)$$

where the nuclear separation $\mathbf{R} \equiv (R, \Theta, \Phi) \equiv (\rho, \Phi, Z)$ in spherical and cylindrical coordinate frames respectively. The eikonal S_n in (4) is the characteristic-function solution of the classical Hamiltonian-Jacobi equation (i.e., the Schrödinger equation in the $\hbar \rightarrow 0$ limit) for the A-B relative motion

under the static interaction $V_{nn}(\mathbf{R}) = \langle \varphi_n | V | \varphi_n \rangle$, and is therefore given by

$$S_n(\rho, Z) = k_n Z + \int_{-\infty}^Z [\kappa_n(\mathbf{R}) - k_n] dZ \quad (5)$$

in which the local wave number $\kappa_n(\mathbf{R})$ of relative motion at \mathbf{R} is

$$[\kappa_n^2 - (2\mu/\hbar^2)V_{nn}(\mathbf{R})]^{1/2}$$

and where dZ is an element of path length along the trajectory, which, at present, is taken as a straight line. For electron-atom collisions, κ_n is always real. The use of the actual classical trajectory with its "built-in" turning point is therefore not as essential as, for example, in positron-atom collisions, where κ_n becomes imaginary for sufficiently close rectilinear encounters. The general problems associated with the choice of classical trajectory within a multichannel framework are at present unresolved, although the force-common-turning-point, two-state procedure of Bates and Crothers (1970) is attractive.

On assuming that the main variation of Ψ_i^+ on ρ is contained in S_n , i.e., provided $V_{nn}(\mathbf{R})$ varies slowly over many wavelengths $2\pi/\kappa(\mathbf{R})$ of relative motion, and the coefficients $A_n(\rho, Z)$ therefore vary primarily along Z , substitution of (4) in (2) yields the set of coupled differential equations

$$\begin{aligned} \frac{i\hbar^2}{\mu} \kappa_f \frac{\partial B_f(\rho, Z)}{\partial Z} + \left[\frac{\hbar^2}{\mu} \kappa_f (\kappa_f - k_f) + V_{ff}(\mathbf{R}) \right] B_f(\rho, Z) \\ = \sum_{n=1}^N B_n(\rho, Z) V_{fn}(\mathbf{R}) \exp \{i(k_n - k_f)Z\}, \quad f = 1, 2, \dots, N \end{aligned} \quad (6)$$

a set of N coupled equations to be solved for

$$B_f = A_f \exp \left\{ i \int_{-\infty}^Z (\kappa_f - k_f) dZ \right\},$$

subject to the asymptotic condition $B_f(\rho, -\infty) = \delta_{fi}$, which ensures that $\Psi_i \sim \varphi_i(\mathbf{r}_a) \exp \{ik_i Z\}$ as $Z \rightarrow -\infty$. The scattering amplitude (1), with the undistorted final wave $\Psi_f = \varphi_f(\mathbf{r}_a) \exp \{ik_f \cdot \mathbf{R}\}$ inserted, is therefore

$$f_{if}(\theta, \varphi) = -\frac{1}{4\pi} \frac{2\mu}{\hbar^2} \int \exp \{i\mathbf{K} \cdot \mathbf{R}\} d\mathbf{R} \sum_{n=1}^N B_n(\rho, Z) V_{fn}(\mathbf{R}) \exp \{i(k_n - k_i)Z\} \quad (7)$$

where \mathbf{K} is the momentum change $\mathbf{k}_i - \mathbf{k}_f$ caused by the collision. Since the electrostatic interaction $V(\mathbf{r}, \mathbf{R})$ is composed of central potentials,

$$V_{fi} = \langle \varphi_f | V | \varphi_i \rangle = V_{fi}(\mathbf{R}, \Theta) \exp \{i\Delta\Phi\},$$

where $\Delta = M_i - M_f$ is the change in the azimuthal quantum number of

the atom. Hence, with the substitution

$$C_f(\rho, Z) = B_f(\rho, Z) \exp \{-i\Delta\Phi\},$$

the set of phase Φ -independent equations

$$\begin{aligned} \frac{i\hbar^2}{\mu} \kappa_f(\rho, Z) \frac{\partial C_f(\rho, Z)}{\partial Z} + \left[\frac{\hbar^2}{\mu} \kappa_f(\kappa_f - k_f) + V_{ff}(\rho, Z) \right] C_f(\rho, Z) \\ = \sum_{n=1}^N C_n(\rho, Z) V_{fn}(\rho, Z) \exp \{i(k_n - k_f)Z\} \end{aligned} \quad (8)$$

is obtained, solved subject to the boundary condition $C_f(\rho, -\infty) = \delta_{if}$. On completion of the Φ -integration in (7), the scattering amplitude reduces to

$$f_{if}(\theta, \varphi) = -i^{\Delta+1} \int_0^\infty J_\Delta(K'\rho) [I_1(\rho, \theta) - iI_2(\rho, \theta)] \rho d\rho \quad (9)$$

where K' is the XY component $k_f \sin \theta$ of \mathbf{K} and where J_Δ are Bessel functions of integral order. Both the functions

$$I_1(\rho, \theta; \alpha) = \int_{-\infty}^\infty \kappa_f(\rho, Z) \left[\frac{\partial C_f(\rho, Z)}{\partial Z} \right] \exp \{i\alpha Z\} dZ \quad (10)$$

and

$$I_2(\rho, \theta; \alpha) = \int_{-\infty}^\infty \left[\kappa_f(\kappa_f - k_f) + \frac{\mu}{\hbar^2} V_{ff} \right] C_f(\rho, Z) \exp \{i\alpha Z\} dZ \quad (11)$$

contain a dependence on the scattering angle θ via

$$\alpha = k_f(1 - \cos \theta) = 2k_f \sin^2 \frac{\theta}{2} \quad (12)$$

the difference between the Z component of the momentum change \mathbf{K} and the minimum momentum change $k_i - k_f$ in the collisions. Equations (8)–(12) are the basic formulas given by the present multichannel eikonal description for the scattering amplitude, and they can be easily generalized so as to cover collisions involving multielectron systems. It is apparent that a variety of approximations readily follow. Note that in the absence of all couplings except that connecting the initial and final channels, i.e., $C_n = \delta_{ni}$, either (7) or (9) directly yields

$$f_{if}(\theta, \varphi) = -\frac{1}{4\pi} \frac{2\mu}{\hbar^2} \int V_{ff}(\mathbf{R}) \exp \{i\mathbf{K} \cdot \mathbf{R}\} d\mathbf{R} \quad (13)$$

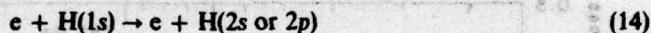
which is the Born-wave scattering amplitude.

Moreover, it can be shown (Flannery and McCann, 1974) by successive approximation that the above equations can reproduce (a) the customary one-channel eikonal expression (cf. Bransden, 1970) for elastic scattering and (b) the distorted-Born-wave expression of Chen *et al.* (1972). Also, in the heavy-particle or high-energy limit the usual impact-parameter and Glauber formulas are recovered.

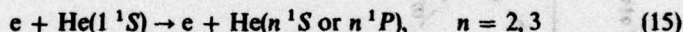
In summary, the present method (i) has defined a scattering amplitude rather than an excitation probability, the key quantity occurring in time-dependent impact-parameter treatments; (ii) has acknowledged different local momenta of relative motion in various channels; and (iii) has automatically included an infinite number of partial waves, via the eikonal in (4), which are distorted by the static interactions associated with the various channels and which in turn are coupled to the internal electronic motions via A_n in (4).

Results and Discussion

As examples of the preceding analysis, the full eikonal equations (8)–(12) are now applied to the examination of the excitation processes



and



in which the initial and all final channels with the same n are closely coupled. Note that the resulting set of coupled equations in which exchange is neglected are *not* the semiclassical analogues or even approximations to the actual coupled differential equations obtained from the full close-coupling method (cf. Burke and Webb, 1970).

In Figures 1–3 are displayed the total cross sections, labeled FE,

$$\sigma_f(E_i) = 2\pi \frac{k_f}{k_i} \int_0^\pi |f_{if}(\theta, \varphi)|^2 \sin \theta d\theta \quad (16)$$

computed as functions of electron-impact energy E_i , together with various theoretical results and experimental measurements, as referenced in the captions. For process (14), curve EB is an approximation to FE in which $\kappa_n = k_n$ and I_2 in (9) and the term in square brackets in (8) are ignored. For (15), two sets of orthogonal wave functions for He ($n = 2$) are used. The cross sections labeled FE1 and FE2 refer to calculations performed with the analytical wave functions respectively given by Flannery (1970)

and the multiparameter Hartree-Fock frozen-core set of McEachran and Cohen (1969) and Crothers and McEachran (1970).

The figures provide an indication of the overall ability of the present method, and very little need be said. The situation appears rather encouraging.

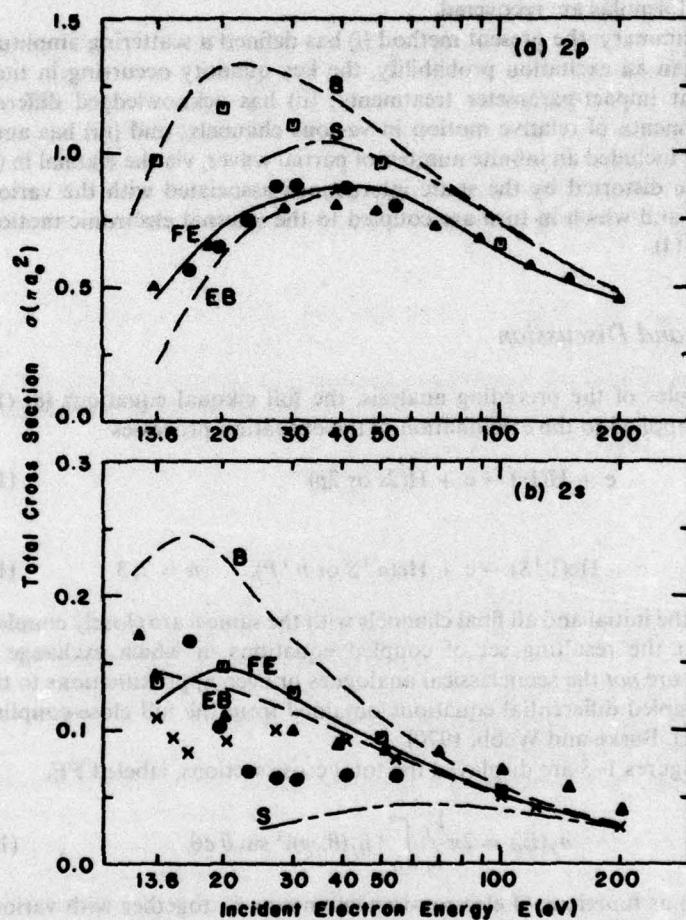


Figure 1. Cross sections for (a) the 2p and (b) the 2s excitations of H(1s) by electron impact. *Theory*: FE, full eikonal treatment; EB, eikonal approximation ($\kappa_s = k_s$); S, second-order potential method (Sullivan *et al.*, 1972); B, Born approximation; ●, pseudostate method (Burke and Webb, 1970); x, polarized-orbital distorted-wave model (McDowell *et al.*, 1974); □, four-state impact-parameter method. *Experiment*: ▲ (a) Long *et al.* (1968); (b) Kauppila *et al.* (1970).

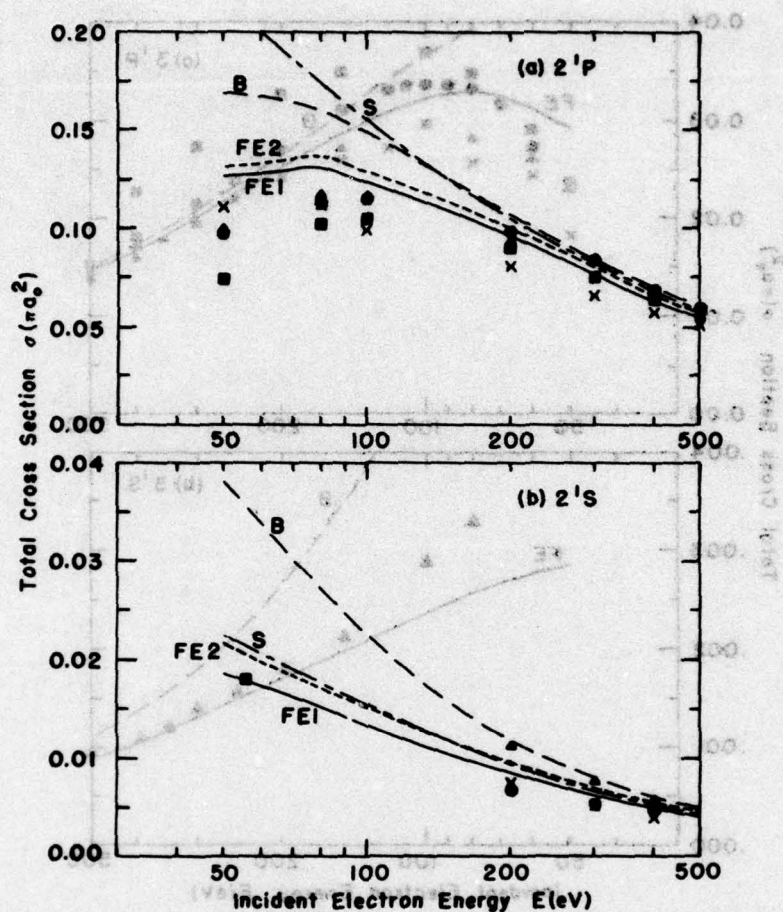


Figure 2. Total cross sections for (a) the 2^1P and (b) the 2^1S excitations of $\text{He}(1^1S)$ by electron impact. Theory: FE1: Four-channel eikonal treatment with first set of atomic wave functions; FE2: Four-channel eikonal treatment with second set of atomic wave functions; S: Second-order potential method with first set of atomic wave functions (Berrington *et al.*, 1973); B: Born approximations (Bell *et al.*, 1969). Experiment: [2^1P] \blacktriangle : Donaldson *et al.* (1972); \blacksquare : Jobe and St. John (1967); \times : Moustafa-Moussa *et al.* (1969); \bullet : van Eck and de Jongh (1970); [2^1S] \blacktriangle : Lassettre *et al.* (1970); \times : Miller *et al.* (1968); \bullet : Vriens *et al.* (1968).

This research was sponsored by the Air Force Research Laboratory, Air Force Systems Command, United States Air Force, Contract F33612-74-C-4002.

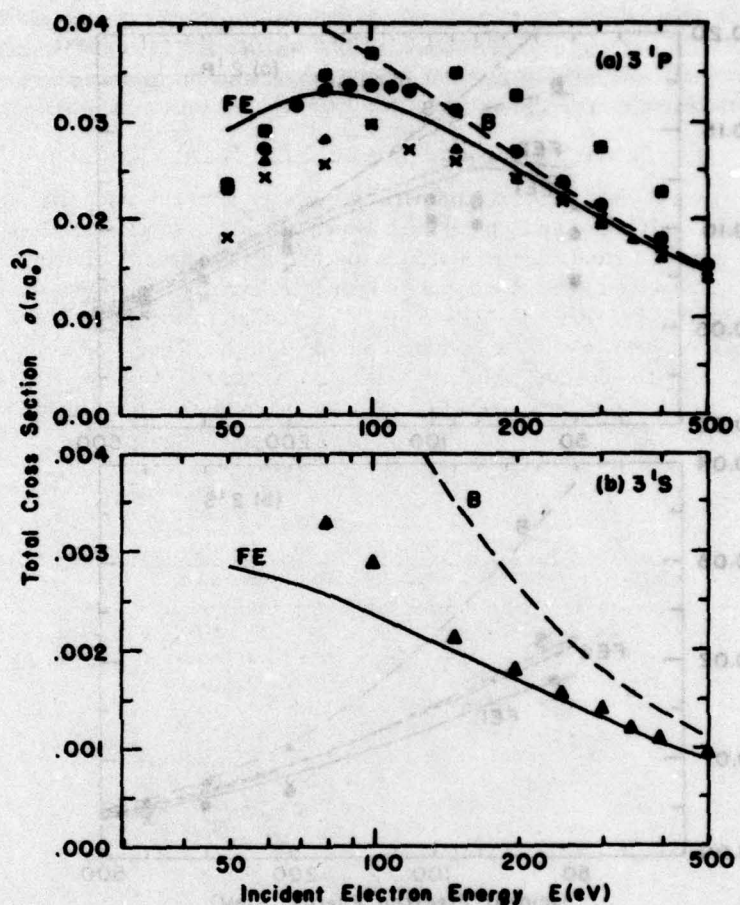


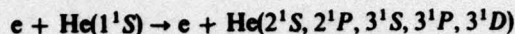
Figure 3. Total cross sections for (a) the 3^1P and (b) the 3^1S excitations of $\text{He}(1^1S)$ by electron impact. Theory: FE: Four-channel eikonal treatment with Hartree-Fock frozen core wave functions; B: Born approximation (Bell *et al.*, 1969). Experiment: \bullet : Donaldson *et al.* (1972); \blacktriangle : Moustafa-Moussa *et al.* (1969); \times van Eck and de Jongh (1970); \blacksquare : St. John *et al.* (1964).

Acknowledgment

This research was sponsored by the Air Force Aerospace Research Laboratories, Air Force Systems Command, United States Air Force, Contract F 33615-74-C-4003.

Note Added in Proof

We have recently presented in *J. Phys. B.*, 8, 1716 (1975) a more elaborate ten-channel treatment of differential and integral cross sections for the excitation processes



This work also includes comparison with experiment and theoretical predictions of the λ and χ parameters which provide, as functions of θ and E , the orientation and alignment vectors together with the circular polarization fractions of the radiation emitted from the n^1P levels. We have also recently reported [*Phys. Rev. A.*, 12, 846 (1975)] a similar treatment of the $n = 3$ excitation and $n = 1$ de-excitation arising in $e - \text{He}(2^{1,3}S)$ collisions. Finally, a pseudostate and seven-state eikonal treatment of the $2s$, $2p$, $3s$, and $3p$ excitations in $e - \text{H}(1s)$ collisions is presented in *J. Phys. B.*, 7, L522 (1974).

References

- Bates, D. R., and Crothers, D. S. F. (1970). *Proc. Roy. Soc. A*, 315, 465.
Bates, D. R., and Holt, A. R. (1966). *Proc. Roy. Soc. A*, 292, 168.
Bell, K. L., Kennedy, D. J., and Kingston, A. E. (1969). *J. Phys. B.*, 2, 26.
Berrington, K. A., Bransden, B. H., and Coleman, J. P. (1973). *J. Phys. B.*, 6, 436.
Bransden, B. H. (1970). *Atomic Collisions Theory*, New York: Benjamin, Inc., p. 82.
Bransden, B. H., and Coleman, J. P. (1972). *J. Phys. B.*, 5, 537.
Burke, P. G., and Webb, T. G. (1970). *J. Phys. B.*, 3, L1313.
Byron, F. W. (1971). *Phys. Rev.* 4, 1907.
Callaway, J. (1968). In *Lectures in Theoretical Physics*. Eds. S. Geltman, K. T. Mahanthappa, and W. E. Brittin, 11C, p. 119. New York: Gordon and Breach.
Chen, J. C. Y., Joachain, C. J., and Watson, K. M. (1972). *Phys. Rev.*, 5, 2460.
Crothers, D. S. F., and McEachran, R. P. (1970). *J. Phys. B.*, 3, 976.
Donaldson, F. G., Hender, M. A., and McConkey, J. W. (1972). *J. Phys. B.*, 5, 1192.
Flannery, M. R. (1970). *J. Phys. B.*, 3, 306.
Flannery, M. R., and McCann, K. J. (1974). *J. Phys. B.*, 7, 2518.
Jobe, J. E., and St. John, R. M. (1967). *Phys. Rev.*, 164, 117.
Kauppila, W. E., Ott, W. R., and Fite, W. L. (1970). *Phys. Rev.*, 141, 1099.
Lassettre, E. N., Skerbele, A. and Dillon, M. A. (1970). *J. Chem. Phys.*, 52, 2797.
Long, R. L., Cox, D. M., and Smith, S. J. (1968). *J. Res. Nat. Bur. Standards*, 72A.
Miller, K. J., Mielczarek, S. R., and Krauss, M. (1968). *J. Chem. Phys.*, 51, 945.
McDowell, M. R. C., Morgan, L. A., and Myerscough, V. P. (1973). *J. Phys. B*, 6, 1435.
McDowell, M. R. C., Myerscough, V. P., and Narain, U. (1974). *J. Phys. B.*, 7, L195.
McEachran, R. P., and Cohen, M. (1969). *J. Phys. B.*, 3, 976.
Moustafa-Moussa, H. R., de Heer, F. J., and Schulten, J. (1969). *Physics*, 40, 517.
St. John, R. M., Miller, F. L., and Lin, C. C. (1964). *Phys. Rev.*, A134, 888.
Sullivan, J., Coleman, J. P., and Bransden, B. H. (1972). *J. Phys. B.*, 5, 2061.
Tai, H., Bassel, R. H., Gerjuoy, E., and Franco, V. (1970). *Phys. Rev.*, A1, 1819.
Van Eck, J., and de Jongh, J. P. (1970). *Physics*, 47, 141.
Vriens, L., Kuyatt, C. E., and Mielczarek, S. K. (1968). *Phys. Rev.*, 165, 7.

AFAPL/ POD
WRIGHT-PATTERSON AFB, OH 45433

UNITED STATES AIR FORCE
OFFICIAL BUSINESS